The recent launch of NASA's Gamma Ray Observatory will increase interest in gamma-ray astronomy. This book, which is a fully updated and new edition of the authors' earlier volume published in 1986, will prove invaluable in providing the background science to this important field. In assessing the current state-of-the-art, the book also indicates the exciting basis from which new discoveries will be made.

Gamma-ray astronomy gives us a view of the Universe through the most recent window to have been opened. The emphasis in this account is firmly on the astronomy and astrophysics of known sources of cosmic gamma-rays outside the solar system. The authors first introduce the mechanisms for the production and absorption of gamma-rays. The gamma-ray line astronomy of the interstellar medium, the Galactic Centre and various discrete sources is then discussed. Gamma-ray bursts are treated in considerable detail in Chapter 3, and the final two chapters describe medium energy and ultra high energy gamma-rays. The supernova SN 1987A continues to provide data of interest to gamma-ray astronomers, and the results achieved so far have been included in this edition. The book includes comprehensive references to the primary literature, together with many figures and tables.

The concentration on phenomenology makes this book a fine introduction to gamma-ray astronomy. It will be of use to all those, students and professional astronomers alike, who are working in this developing field.

Cambridge astrophysics series

Editors: R.F. Carswell, D.N.C. Lin *and* J.E. Pringle

Gamma-ray astronomy

Titles available in this series

1 Active Galactic Nuclei
edited by C. Hazard and S. Mitton

2 Globular Clusters
edited by D.A. Hanes and B.F. Madore

3 Low Light-level Detectors in Astronomy
by M.J. Eccles, M.E. Sim and K.P. Tritton

5 The Solar Granulation
by R.J. Bray, R.E. Loughhead and C.J. Durrant

6 Interacting Binary Stars
edited by J.E. Pringle and R.A. Wade

7 Spectroscopy of Astrophysical Plasmas
by A. Dalgarno and D. Layzer

10 Quasar Astronomy
by D.W. Weedman

11 X-ray Emission from Clusters of Galaxies
by C.L. Sarazin

12 The Symbiotic Stars
by S.J. Kenyon

13 High Speed Astronomical Photometry
by B. Warner

14 The Physics of Solar Flares
by E. Tandberg-Hanssen and A.G. Emslie

15 X-ray Detectors in Astronomy
by G.W. Fraser

16 Pulsar Astronomy
by A. Lyne and F. Graham-Smith

17 Molecular Collisions in the Interstellar Medium
by D. Flower

18 Plasma Loops in the Solar Corona
by R.J. Bray, L.E. Cram, C.J. Durrant and R.E. Loughhead

19 Beams and Jets in Astrophysics
edited by P.A. Hughes

20 The Observation and Analysis of Stellar Photospheres
by David F. Gray

21 Accretion Power in Astrophysics 2nd Edition
by J. Frank, A.R. King and D.J. Raine

22 Gamma-ray Astronomy 2nd Edition
by P.V. Ramana Murthy and A.W. Wolfendale

23 The Solar Transition Region
by J.T. Mariska

GAMMA-RAY ASTRONOMY

SECOND EDITION

POOLLA V. RAMANA MURTHY FNA
Professor of Physics, Tata Institute of Fundamental Research, Bombay

ARNOLD W. WOLFENDALE FRS
Professor of Physics, University of Durham, and Astronomer Royal

CAMBRIDGE
UNIVERSITY PRESS

Published by the Press Syndicate of the University of Cambridge
The Pitt Building, Trumpington Street, Cambridge CB2 1RP
40 West 20th Street, New York, NY 10011-4211, USA
10 Stamford Road, Oakleigh, Melbourne 3166, Australia

First published 1986
Second edition 1993

Printed in Great Britain at the University Press, Cambridge

A catalogue record for this book is available from the British Library

Library of Congress cataloguing in publication data

Ramana Murthy, P. V.
Gamma-ray astronomy / Poolla V. Ramana Murthy, Arnold W. Wolfendale.—2nd ed.
p. cm.—(Cambridge astrophysics series ; 22)
Includes bibliographical references and index.
ISBN 0-521-42081-4
1. Gamma ray astronomy. I. Wolfendale, A. W. II. Title.
III. Series.
QB471.R36 1993
522'.6862—dc 20 92-16465 CIP

ISBN 0 521 42081 4 hardback

KW

To Subhadra and Audrey

Contents

Preface to the first edition

Gamma-ray astronomy comprises the view of the Universe through what is essentially the last of the electromagnetic windows to be opened. All other windows from radio right through to X-rays have already been opened wide, and as is well known their respective astronomies are quite well developed – and the views there are very rich. Gamma-ray astronomy promises to be likewise; the strong link of γ-rays to very energetic processes and the considerable penetration of the γ-rays see to that.

Admittedly one deals with a small number of photons in this new window and yet a considerable amount of progress has already been made; hopefully this progress will shine through in what follows.

It is usually necessary to make a selection of topics when writing a book, and the present one is no exception. The selection made here reflects both the interests of the authors (both of whom are cosmic ray physicists) and the perceived needs of the subject. The authors' interests and, no doubt, biases show through in the areas in which they have themselves contributed (Chapters 4 and 5). There appears to be a contemporary need for a comprehensive review of γ-ray bursts and this is the reason for an extended Chapter 3. We have not included in Chapter 2 any material relating to γ-ray lines in solar flares – a very important subject in its own right – as we felt that it was outside the character of this book, dealing as it does with source regions exclusively beyond the solar system. Furthermore, we have not reproduced many formulae, tables or graphs concerning γ-ray production mechanisms; we touch upon them only briefly. The mechanisms have a character of unchangeability associated with them; nor has anything significantly new been added in recent years. Reference is therefore made in the text to some of the books and original articles where detailed information on the subject can be found. Similarly, we have not elaborated on the detectors used in the experiments, but confined ourselves only to a cursory description of a few of them. Rather we have devoted much of the book to a presentation of experimental facts and what one makes of them at the current stage of development.

While undergraduates may find the present book useful as a supplement to earlier publications, it is the authors' view that it will be more useful to graduate students and young researchers who have spent a few years carrying out research in the area.

Hopefully, the book will also be of value to the wide fraternity of astronomers

who work in the other regions of the electromagnetic spectrum. Already gamma-ray astronomy is having something of interest to say about all these regions, as well as requiring information from them, and the general astronomical value of the subject will no doubt increase over the next few years.

We have benefited considerably from discussions with many colleagues and fellow workers in the field, too numerous to mention individually, and our thanks go out to them.

Mention must be made, however, of a number of friends who contributed specifically to the production of the manuscript of the book. Mrs Pauline Russell drew the diagrams, and the typing was carried out by Mrs Margaret Chipchase, and we are grateful to them for their effort and expertise. Mrs C. V. Raisinghani and Mr H. Fernandez are also thanked for their help with word processing.

Special thanks must go to Dr Chaman L. Bhat, himself a noted worker in the γ-ray field, for his painstakingly reading, correcting and improving the manuscript. His contribution went far beyond the usual proof-reader's work and we are most grateful to him.

P. V. Ramana Murthy is also grateful to the Director of the Tata Institute of Fundamental Research, Professor B. V. Sreekantan, for his support.

Preface to the second edition

The popularity of the subject of gamma-ray astronomy has led to the need to update the material presented in the first edition, and this we are pleased to do.

The subject is in an exciting state in the lower energy region, below some tens of GeV, with the successful launch of the Gamma Ray Observatory in April, 1991. Already, sufficient data have appeared to show that, barring unforseen accidents, the subject will march forward at these energies. It is unfortunate that the Soviet GAMMA 1 satellite did not meet its design specifications – a reminder of the difficulties still inherent in satellite experiments.

The supernova SN 1987A continues to provide data of interest to the gamma-ray astronomer, and the results achieved so far have been included in this edition.

At the higher energies, advances have been less spectacular; indeed, there is some disappointment that many of the claimed TeV and PeV sources have still not been confirmed. Our view is that time variability of genuine sources married with some spurious signals probably accounts for the situation. Nevertheless, the subject is so important that continued, indeed enhanced, effort is needed.

The rate of publications in the field of gamma-ray astronomy at all energies is several times higher now than in 1985, when the manuscript for the first edition was turned in to the editors. Although we have made every effort to make the presentation in the second edition up to date (till the end of July, 1991), we apologise for inadvertent omission of any important results prior to that date.

We again acknowledge the help of many colleagues who provided us with preprints and reprints of their work. We are grateful to Mrs Margaret Norman, Mrs C.V. Raisinghani and Mr G.P. Satyanarayana for their help with word processing.

P.V. Ramana Murthy is also grateful to the Director of the Tata Institute of Fundamental Research, Professor Virendra Singh, for his support, and thanks the Royal Society (UK), the Indian National Science Academy and the Trustees of the Cambridge Society Bombay Scholarship Fund for their generosity.

1

Production and absorption mechanisms

1.1 Introduction

In this chapter attention will be given to the various production and absorption mechanisms operating in the celestial settings. Although the value of the subject is bound up with these two topics – production is by way of a variety of very energetic processes, and the low absorption experienced by γ-rays allows us to 'see' regions not otherwise accessible – they are not treated in great detail here. The reason is that the processes are rather well known and have been described in detail by a number of authors. Specifically, the books of Stecker (1971), Chupp (1976) and Hillier (1984) give excellent treatments. Our own descriptions, then, are brief.

Starting with production mechanisms, a summary is given in Figure 1.1. Understandably, the relative importance of the various mechanisms depends on the properties of the production region: gas density, temperature, magnetic field, ambient radiation etc. It is often the determination of these conditions that is the end product of the analysis of the γ-ray observations.

1.2 Gamma-ray production mechanisms

1.2.1 Gamma-ray lines

γ-ray lines have been observed from a variety of regions: solar flares, the Galactic Centre, Galactic Plane and the object SS 433, and they exhibit a variety of temporal features, from time independence to rapid time variability.

The lines generated in solar flares are proving to be of considerable interest, but in view of our preoccupation with astronomical regions further afield we refer the reader to Ramaty and Lingenfelter (1981), Ramaty, Lingenfelter and Kozlovsky (1982) and references quoted therein.

γ-ray lines are produced in (*a*) e^+e^- annihilations, (*b*) neutron capture reactions, (*c*) the de-excitation of target nuclei struck by energetic protons and other particles, together with projectile nuclei excited by impact, or by virtue of the fact that they are the radioactive products of stellar ejecta, and (*d*) Landau transitions. These topics are described in turn.

(*a*) The best known line is the annihilation line at 511 keV resulting from an

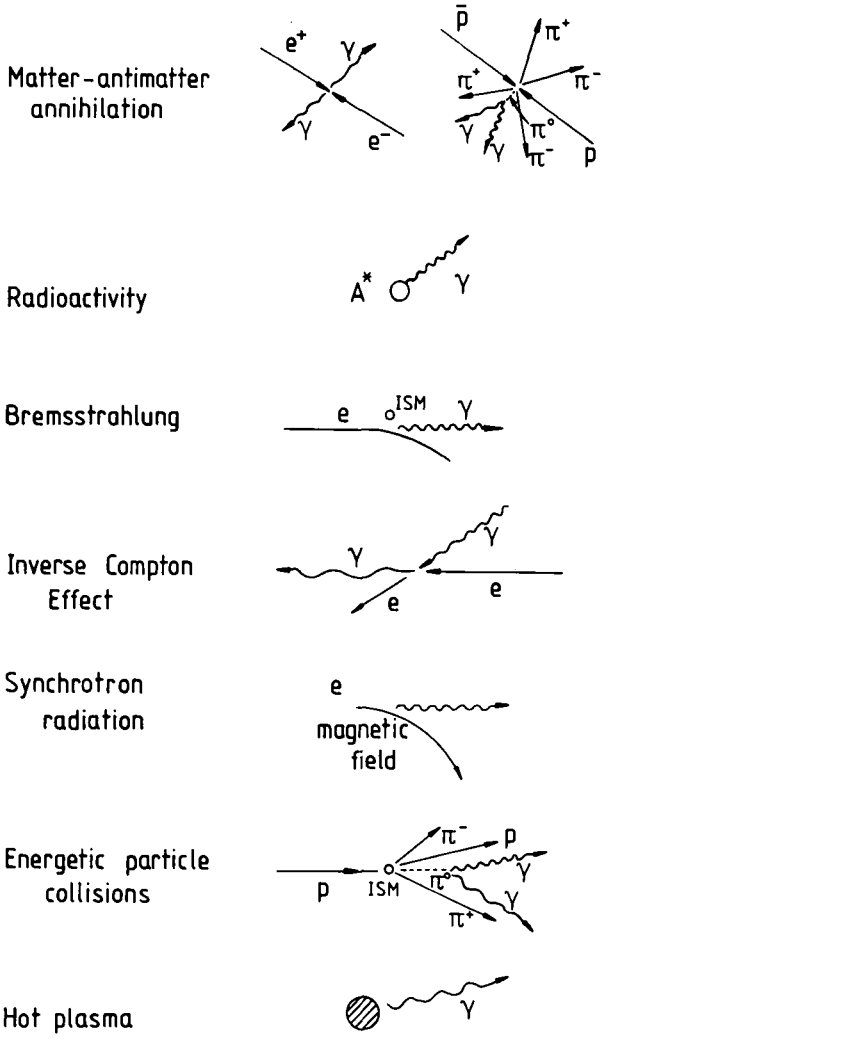

Figure 1.1. Summary of production mechanisms. A* represents an excited nucleus. The other symbols have their usual meanings.

e^+e^- collision at rest:

$$e^+ + e^- \rightarrow \gamma + \gamma \tag{1.1}$$

The annihilation can also take place while the particles are in flight (free annihilation), in which case the resulting γ-rays will have a continuous energy distribution instead of being a line (see Section 1.2.2 below). At low energies the e^+ and e^- first form positronium atoms, 25% of which are in the singlet $^1S_0$ state, decaying by the mode as shown in equation (1.1) with a mean lifetime of 1.25×10^{-10} s. The resulting γ-rays appear as lines at 511 keV. The remaining 75% of positronium atoms are in the triplet $^3S_1$ state and decay into three γ-rays

with a lifetime of 1.5×10^{-7} s; these γ-rays form a continuum with a maximum energy of 511 keV.

The γ-ray source strength is proportional to the product of the e^+ and e^- densities. The positrons themselves arise from β-decays of nuclides produced in nucleosynthesis processes or from $\pi^+ \rightarrow \mu^+ \rightarrow e^+$ decays, the parent pions having been produced in the interactions of energetic particles with ambient matter, or through $\bar{p}p$ annihilations. Positrons may also be produced in more exotic (but not necessarily unrealistic) processes going on near massive black holes (Blandford 1976, Lovelace 1976, Lingenfelter, Higdon and Ramaty 1978) or around mini-primordial black holes (Okeke and Rees 1980).

(*b*) Thermalised neutrons can produce γ-rays at 2.22 MeV by the capture reaction

$$n + {}^1H \rightarrow \gamma + {}^2H \tag{1.2}$$

the cross section for which is $7.3 \times 10^{-20}\, v^{-1}$ cm^2, where v is the velocity of the neutron in units of cm s^{-1}. The neutrons themselves originate in the interactions of energetic particles with the ambient matter, e.g. in reactions of the type ^{4}He (p, pn)^{3}He, ^{2}H(d, n)^{3}He and ^{3}H(d, n)^{4}He, and later become thermalised by repeated collisions with hydrogen. For reaction (1.2) to take place, the density of hydrogen must be greater than 10^{16} cm^{-3}, for otherwise the neutrons would decay before interacting. It is therefore likely that this mechanism operates in relatively dense regions such as in solar flares and accretion disks but not in the interstellar medium. Neutron capture by many nuclei gives rise to compound nuclei which decay by γ-emission, and are thus of interest; particularly relevant is the capture of neutrons by ^{56}Fe leading to excited states of ^{57}Fe which emit γ-rays at 7.632 and 7.646 MeV. The surface regions of neutron stars are believed to be rich in iron and these are potentially important sites for the above process to occur.

(*c*) Turning to the interesting area of cosmic-ray-induced lines, it is instructive to make an order of magnitude estimate of the expected flux of the line resulting from protons interacting with an important nuclear component of the ISM such as oxygen. The cross section for ^{16}O as a function of proton kinetic energy is given in Figure 1.2 (also shown is that for ^{12}C); it is seen that protons in the range 8–30 MeV are largely responsible, yielding a mean $\sigma \approx 100$ mb. The proton intensity in the ISM in this energy range is virtually unknown but we take 2 cm^{-2} s^{-1}sr^{-1} as illustrative. The cosmic abundance of ^{16}O is $\approx 7 \times 10^{-4}$ of hydrogen by number and the corresponding number of excited oxygen atoms produced for a region of the ISM, where the total gas density is 1 cm^{-3}, follows as $\approx 2 \times 10^{-27}$ cm^{-3} s^{-1}. If each excited oxygen atom were to de-excite by way of a γ-ray line then the line flux expected along a path length of 10 kpc would be 5×10^{-6} cm^{-2} s^{-1} sr^{-1}. This is clearly a very low flux, giving a counting rate of only ≈ 1 γ-ray per day in a detector of area 100 cm^2 and solid angle (1/60) sr (the γ-ray flux will be strongly collimated in the Galactic Plane). Detailed calculations in the above manner, but with much greater accuracy, have been made by Meneguzzi and Reeves (1975) and Ramaty, Kozlovsky and Lingenfelter (1979). The most conspicuous line expected appears to be the one at 6.129 MeV resulting

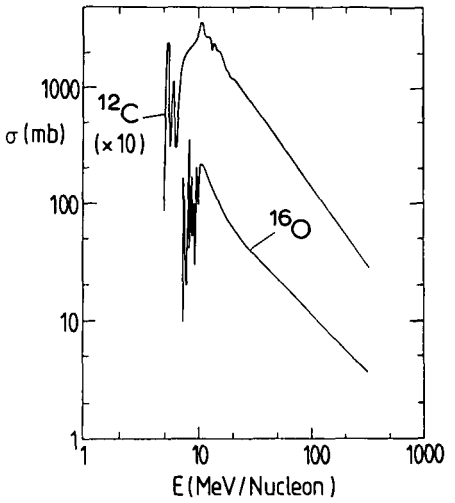

Figure 1.2. The interaction cross sections, leading to γ-ray emission, for protons on ^{12}C and ^{16}O as a function of proton kinetic energy (after Ramaty and Lingenfelter 1981).

from ^{16}O, but there are many others. The results of the calculations by Ramaty and Lingenfelter are given later in Figure 2.1.

An important feature is the line width, and this can be examined briefly. There will be Doppler broadening depending on the lifetime of the excited state and on the density and temperature of the medium, due to the kinetic energy imparted to the nuclide in the collision and the general Maxwell–Boltzmann distribution of the velocities of the nuclide. The line width from recoil often dominates, as can be seen simply from the considerations of the previous section. A 10 MeV proton has $\beta = 0.14$ and a recoil oxygen nucleus will have $\beta \approx 0.01$. If the oxygen nucleus is free in the ISM it will decay before being reduced to rest and the line width will be of order 1 %, i.e. 60 keV for a line at 6 MeV. An even larger line width will arise from those cosmic ray nuclei (carbon, oxygen etc.) which are excited by collision with ISM nuclei.

Much of the 'heavy material' (C, O etc.) in the ISM is in the form of grains, however, and here the struck nuclei will usually come to rest before decaying; the line widths then will be very narrow, less than the instrumental resolution (≈ 5 keV for a good detector). (Figure 2.2 shows these features.)

In addition to the ^{16}O line at 6.129 MeV, there are other important ones, notably 4.438 MeV from ^{12}C; 2.313 and 5.105 MeV from ^{14}N; 2.741, 6.917 and 7.117 MeV from ^{16}O; 1.634, 2.613 and 3.34 MeV from ^{20}Ne; 1.369 and 2.754 MeV from ^{24}Mg; 1.779 and 6.878 MeV from ^{28}Si; and 0.847, 1.238 and 1.811 MeV from ^{56}Fe. Long lived nuclides from supernova ejecta will also contribute (Clayton, Colgate and Fishman 1969, Ramaty and Lingenfelter 1981). Examples are the lines at 1.809 MeV from ^{26}Al; 0.847 and 1.238 MeV from ^{56}Co; 1.156, 0.076 and 0.068 MeV from ^{44}Ti; and 1.332 and 1.173 MeV from ^{60}Co.

(*d*) In regions where strong magnetic fields exist, cyclotron emission lines can

be produced from transitions between Landau levels. Transitions from the first such level result in the emission of a γ-ray line whose energy is given by

$$E_\gamma(\text{keV}) = heB/m_e c = 11.6B_{12} \tag{1.3}$$

where B_{12} is the magnetic field in units of 10^{12} G. The line may be seen in absorption or emission depending on the temperature of the ambient medium. The cyclotron lines were seen in Her X-1 (Trumper *et al.* 1978, Mihara *et al.* 1990) and in another X-ray binary object 4U 0115 + 63 (Wheaton *et al.* 1979) as well as in several γ-ray burst sources; see Section 3.4.2A. The lines are seen generally in the energy range 20–50 keV, which implies, according to equation (1.3), magnetic fields in the range (2–5) $\times$ 10^{12} G near the sources.

Before closing this discussion, we should examine a number of other possible causes of the displacement or energy smearing of γ-ray lines.

Although the decay of a neutral pion at rest results in two γ-rays of half the rest mass (i.e. 67.48 MeV) each, the π^0 are seldom produced at rest in the interactions of energetic particles with matter because of motion of the centre-of-mass in the laboratory frame. Consequently, the γ-ray 'line' has a broad hump around 67.5 MeV. Gravitational red-shift can also be very large: for example, a γ-ray of energy E_γ produced close to a neutron star can be gravitationally red-shifted by as much as $\Delta E_\gamma = (GM/R)(E_\gamma/c^2) \approx (0.1 \text{ to } 0.3)E_\gamma$; see the discussion in Sections 3.3.1 and 3.4.2B with reference to the Jacobson transient and the γ-ray burst of November 19, 1978, respectively. Furthermore, the cosmological red-shifts operating on γ-rays produced in the remote past and in distant regions of the Universe but reaching us now, may reduce the energy of the γ-ray considerably; see Stecker (1971, 1973). Finally, Doppler shifts due to the organised motion of the bulk of emitting nuclides can, of course, make the lines appear at lower *or* at higher energies than those at emission. Experimental evidence for such Doppler shifts of the 1.369 MeV line identified with ^{24}Mg from SS 433 has been presented by Lamb *et al.* (1983); see Section 2.4.2.

1.2.2 The gamma-ray continuum

1.2.2A Electrons

The particles responsible for the continuum are, principally, cosmic ray electrons and protons.

Starting with electrons, continuum γ-rays are produced by (*a*) annihilation in flight with positrons, (*b*) bremsstrahlung in the Coulomb fields of nuclei and electrons, (*c*) inverse Compton scattering against the ambient radiation, (*d*) synchrotron emission in magnetic fields, and (*e*) curvature radiation in the magnetospheres of pulsars.

(*a*) *Annihilation in flight.* The cross section for e^+e^- annihilation at extreme relativistic energies is given by

$$\sigma_A = \frac{\pi r_e^2}{\gamma}[\ln(2\gamma) - 1] \tag{1.4}$$

(see Stecker 1971 for details), where γ $(=E_e/m_ec^2)$ is the Lorentz factor of the positrons and $r_e(=e^2/m_ec^2 = 2.82 \times 10^{-13}$ cm) is the classical radius of the electron. Two-photon emission is the dominant result of annihilation, leading to a continuum of photon energies. At high positron energies, the photon emitted in the extreme forward direction has almost all the energy of the positron while the other photon has an energy of $m_ec^2/2 = 0.256$ MeV.

The cross section given by equation (1.4) is quite low; as an example, for a 100 MeV positron, $\sigma_A = 6 \times 10^{-27}$ cm^2, leading to a mean free path for annihilation of $1.6 \times 10^{26}/n_e$ cm, where n_e is the electron number density. Now, in the ISM, $n_e \approx 3 \times 10^{-2}$ cm^{-3} and the mean free path follows as $\approx 5 \times 10^{27}$ cm, i.e. nearly 2000 Mpc; in turn, the mean life of e^+ in the Galaxy would be 5×10^9 y. Other processes will clearly be more important in degrading the positron energy, although eventually, for those positrons which do not escape from the Galaxy but rather slow down to very low energy, the much higher annihilation cross section at these low energies will cause the positrons to disappear.

(*b*) *Bremsstrahlung.* The differential cross section for an electron of energy E_e to radiate a photon with energy between E_γ and $E_\gamma + dE_\gamma$ in the Coulomb field of a nucleus with charge Z is given by (Rossi 1952)

$$\sigma(E_e, E_\gamma)\, dE_\gamma = 4\alpha Z^2 r_e^2 \frac{dE_\gamma}{E_\gamma} F(E_e, v) \tag{1.5}$$

where

$$F(E_e, v) = [1 + (1 - v)^2 - \tfrac{2}{3}(1 - v)]\left[\ln\left(\frac{2E_e}{m_ec^2}\frac{1 - v}{v}\right) - \frac{1}{2}\right] \tag{1.6}$$

for the case of no screening (i.e. a bare nucleus); i.e. $E_e \ll 100m_ec^2[v/(1 - v)]Z^{-1/3}$, and

$$F(E_e, v) = [1 + (1 - v)^2 - \tfrac{2}{3}(1 - v)] \ln(183Z^{-1/3}) + \tfrac{1}{9}(1 - v) \tag{1.7}$$

for the case of complete screening; i.e. $E_e \gg 100m_ec^2[v/(1 - v)]Z^{-1/3}$. In equation (1.5) α is the fine structure constant and v $(=E_\gamma/E_e)$ is the fractional energy carried by the photon. The bremsstrahlung photons have the spectral shape $\sim 1/E_\gamma$, so that more photons are emitted at lower energies. For ionised hydrogen, obviously the case of no screening (equation 1.6) applies. Bremsstrahlung in the Coulomb field of the atomic electrons is included by replacing Z^2 by $Z(Z + 1)$ in equation (1.5). Bremsstrahlung in the field of the electron assumes importance when the numbers of $e^\pm$ are far higher than those of the nuclei as in regions where temperatures are in excess of 10^{10} K.

The mechanism of radiation loss is such that the electron falls in energy by a factor e in one radiation length; the radiation length in hydrogen is ≈ 61 g cm^{-2} and for the ISM, with a mean density 1 atom cm^{-3}, this length is about 10 Mpc. In turn, for an electron moving with $v \approx c$, the mean life for loss by bremsstrahlung

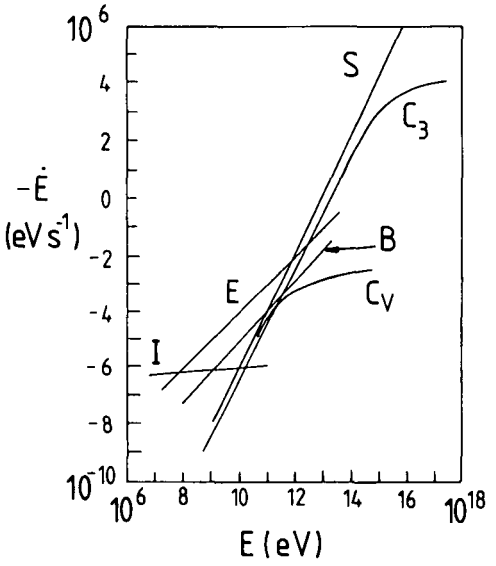

Figure 1.3. Rate of energy loss of electrons $-\dot{E}$ as a function of electron energy E (from the work of Ramaty 1974). Many of the processes involve the production of γ-rays (or X-rays when E is 'small'). S: synchrotron losses in a magnetic field of 4 μG; C_v: inverse Compton interactions with visible photons (energy density = 0.45 eV cm^{-3}); C_3: ditto with '3 K' microwave background; B: bremsstrahlung (gas density = 1 atom cm^{-3}); E: escape, with mean life in galaxy of 3.3×10^6 y; I: ionisation loss. (E and I do not involve γ-ray production.)

is $\approx 4 \times 10^7$ y. Figure 1.3 summarises the situation for loss of electron energy by bremsstrahlung and also some of the other processes to be described.

Stecker (1975) has shown that in the case of bremsstrahlung from electrons in the interstellar gas, the γ-ray emissivity, $q_b(E_\gamma)$, is given by

$$q_b(E_\gamma) = 4.3 \times 10^{-25} n I_e(>E_\gamma)/E_\gamma \text{ cm}^{-3} \text{ s}^{-1} \text{ MeV}^{-1} \tag{1.8}$$

where n is the number density of nuclei in the production region and $I_e(>E_\gamma)$ is the integral energy spectrum of the electrons. Equation (1.8) shows that the exponent of the bremsstrahlung γ-ray spectrum has the same value as that of the parent electron spectrum.

An order of magnitude calculation can be made for the typical path length of ~ 10 kpc and $n = 1$ atom cm^{-3} encountered in the Galactic Plane. Strong and Wolfendale (1981) have shown that $I_e(>100 \text{ MeV})$ is $\approx 5 \times 10^{-3}$ cm^{-2} s^{-1} sr^{-1}, yielding $q_b(100 \text{ MeV}) = 2 \times 10^{-27}$ cm^{-3} s^{-1} MeV^{-1} and $q_b(>100 \text{ MeV}) \approx 2 \times 10^{-25}$ cm^{-3} s^{-1}. In fact, as will be demonstrated later, a similar contribution comes from proton interactions. We see that the flux is about 100 times that expected for a (strong) γ-ray line (see Section 1.2.1) and, when it is appreciated that γ-ray detectors in the 100 MeV region can have a typical area of 500 cm^2, solid angle of 0.25 sr and detection efficiency of $\approx 10\%$, the expected counting rate

will now be 'reasonable': ≈ 500 γ-rays per day (multiplied by two to allow for proton-induced γ-rays).

(*c*) *Inverse Compton scattering.* An ambient photon of energy ε appears to be moving with an energy $\gamma\varepsilon$ in the rest system of a relativistic electron with Lorentz factor γ. In this inertial frame, the Compton scattered photon has an energy $\lesssim \gamma\varepsilon$ and, when transformed back to the laboratory system, an energy $\sim \gamma^2\varepsilon$. The energy of the Compton boosted photon is given by

$$E_\gamma \approx \varepsilon\gamma^2 \quad \text{when} \quad \gamma\varepsilon \ll m_e c^2 \tag{1.9}$$

and

$$E_\gamma \sim E_e \quad \text{when} \quad \gamma\varepsilon \gg m_e c^2 \tag{1.10}$$

This process is important when the density of ambient photons is high. It is also an efficient process in elevating photon energies to very high levels. Cross sections for the regions represented by equations (1.9) and (1.10) are given, respectively (Heitler 1960), by

$$\sigma_c = \sigma_T\left(1 - \frac{2\gamma\varepsilon}{m_e c^2}\right) \tag{1.11}$$

and

$$\sigma_c = \frac{3}{8}\sigma_T\left(\frac{m_e c^2}{\gamma\varepsilon}\right)\left[\ln\left(\frac{2\gamma\varepsilon}{m_e c^2}\right) + \frac{1}{2}\right] \tag{1.12}$$

Here $\sigma_T (= 8\pi r_e^2/3)$ is the Thomson cross section, having a numerical value of 6.65×10^{-25} cm^2.

The condition $\gamma\varepsilon \ll m_e c^2$ is commonly experienced in connection with the interaction of electrons with the 2.7 K background radiation. Here the mean value of ε, $\langle\varepsilon\rangle \approx 6 \times 10^{-4}$ eV and the condition is therefore satisfied for $\gamma < 10^9$, i.e. electron energies below about 5×10^{14} eV.

For such energies, the accurate relation between the mean γ-ray energy, $\langle E_\gamma\rangle$, and $\langle\varepsilon\rangle$ is

$$\langle E_\gamma\rangle = \tfrac{4}{3}\gamma^2\langle\varepsilon\rangle \tag{1.13}$$

Assuming that the differential energy spectrum of electrons is given by

$$I_e(E_e) = KE_e^{-\Gamma} \tag{1.14}$$

where K is a normalisation factor, Stecker (1975) has shown that the γ-ray emissivity, $q_c(E_\gamma)$, is given by

$$q_c(E_\gamma) = \tfrac{8}{3}\pi\sigma_T\rho_{ph}(m_e c^2)^{1-\Gamma}(\tfrac{4}{3}\langle\varepsilon\rangle)^{[(\Gamma-3)/2]}KE_\gamma^{-[(\Gamma+1)/2]} \tag{1.15}$$

Here ρ_{ph} is the energy density of the low energy photons (0.24 eV cm^{-3} for the microwave background) and all other quantities are as defined earlier. The

exponent of the γ-ray energy spectrum, given by $-(\Gamma + 1)/2$, is flatter than that of the parent electron spectrum for values of $\Gamma > 1$.

Insofar as the cosmic ray electron spectrum in the ISM has a power law spectrum satisfying this condition, the inverse Compton mechanism can be an important source of low energy γ-rays. For example, 1 MeV γ-rays will come from electrons of $\approx 2 \times 10^{10}$ eV (equation 1.13) and here $\Gamma \approx 3$.

Figure 1.3 includes the role of inverse Compton interactions in dissipating electron energy.

(*d*) *Synchrotron emission.* Photons are emitted when an electron (or positron) traverses a transverse magnetic field (see Ginzburg and Syrovatskii (1964) for an exhaustive treatment of the subject). In a homogeneous magnetic field of strength H an electron of energy E_e moving at an angle θ with respect to the field will emit synchrotron radiation of intensity (energy flux density per unit frequency interval) along the direction of observation given by

$$I_\nu = \frac{3^{1/2} e^3}{m_e c^2} N_e(\mathbf{K}) H \sin\theta \frac{\nu}{\nu_c} \int_{\nu/\nu_c}^{\infty} K_{5/3}(\eta)\, d\eta \tag{1.16}$$

Here e is the electron charge; $N_e(\mathbf{K})$ is the number of electrons per unit solid angle along the line of vision whose velocity vectors are towards the observer; $K_{5/3}$ is the modified Bessel function of the second kind; ν is the frequency of the emitted photon; and

$$\nu_c = \frac{3eH \sin\theta}{4\pi m_e c} \left(\frac{E_e}{m_e c^2}\right)^2 \tag{1.17}$$

The maximum emission occurs at a frequency given by

$$\nu_m = 1.2 \times 10^6 H_\perp \left(\frac{E_e}{m_e c^2}\right)^2 \tag{1.18}$$

or, equivalently, at an energy

$$E_{\gamma,m}(\text{eV}) = h\nu_m = 5 \times 10^{-9} H_\perp \left(\frac{E_e}{m_e c^2}\right)^2 \tag{1.19}$$

Here $H_\perp = H \sin\theta$ is in gauss. The energy of the electron is halved in a time $t_{1/2}$ given by

$$t_{1/2} = 5 \times 10^8 \left(\frac{m_e c^2}{E_e}\right) \left(\frac{1}{H_\perp(\text{G})}\right)^2 \text{ s} \tag{1.20}$$

and the corresponding rate of energy loss, for a particular magnetic field strength, is shown in Figure 1.3.

If the radiating electrons have a differential energy spectrum given by equation (1.14) the synchrotron photon *number* spectrum will be of the form

$$G_s(E_\gamma) \propto E_\gamma^{-[(\Gamma+1)/2]} \tag{1.21}$$

a form similar to that of the inverse Compton produced photons.

Attention must be drawn here to the fact that in other windows of the electromagnetic radiation spectra are usually expressed in terms of the power radiated. To find the exponent of the radiated power spectrum (W m^{-2} Hz^{-1}), one has to multiply the number spectrum equation (1.21) by E_γ, leading to the resulting synchrotron power spectrum:

$$J_s(E_\gamma) \propto E_\gamma^{-[(\Gamma-1)/2]} \tag{1.22}$$

(*e*) *Curvature radiation.* In the exceptionally strong magnetosphere of a pulsar, high energy electrons and positrons are constrained to move parallel to the magnetic field lines with an essentially zero pitch angle. Since the field lines themselves are curved, the particles radiate 'curvature' radiation in their direction of motion (Manchester and Taylor 1977). The characteristic energy of this radiation, E_c, is given by

$$E_c(\text{eV}) \approx \frac{3}{2}\frac{\hbar c\gamma^3}{\rho_c} = \frac{2.96 \times 10^{-5}\gamma^3}{\rho_c(\text{cm})} \tag{1.23}$$

Here ρ_c is the radius of curvature of the magnetic field line, $\hbar = h/2\pi$, and $\gamma = E_e/m_e c^2$. This process is important for very high energy electrons and positrons in the environs of pulsars. As an example, a 10^{13} eV electron moving along a field line with a curvature of 10^8 cm, typical for a pulsar, emits photons of energy $\approx$2.5 GeV.

1.2.2B Protons

High energy protons can, in principle, produce γ-rays by processes (*b*) to (*e*) listed in Section 1.2.2A for electrons. These mechanisms are, however, very inefficient because of the much higher mass-to-charge ratio for the proton ($m_p/m_e = 1836$). Protons can, on the other hand, generate π^0 mesons in inelastic collisions with matter either directly or indirectly and, less efficiently, through the decays of kaons and hyperons and through the annihilations of antinucleons (kaons, hyperons and antinucleons being produced in the inelastic collisions). Protons can also interact with ambient radiation, e.g. the microwave background, to produce π^0 mesons. These natural pions decay into γ-rays with a mean lifetime of γ_π 0.83 $\times$ 10^{-16} s, where γ_π is the Lorentz factor of the pion.

Interaction with matter. The threshold kinetic energy, T_{th}, for producing a particle with a mass m in a proton–proton collision is given by

$$T_{th} = 2mc^2(1 + m/4m_p) \tag{1.24}$$

where m_p is the proton mass. For a π^0 meson of mass 134.96 MeV/c^2, the threshold kinetic energy is 279.6 MeV. If the target is a heavy nucleus instead of a proton the threshold is lowered somewhat due to the Fermi motion of nucleons within the nucleus. The product of the production cross section, σ_{π^0}, and the neutral pion multiplicity, ζ_{m^0}, is shown as a function of proton energy in Figure 1.4. Folding this dependence on energy with the differential proton energy spectrum (Figure 1.5),

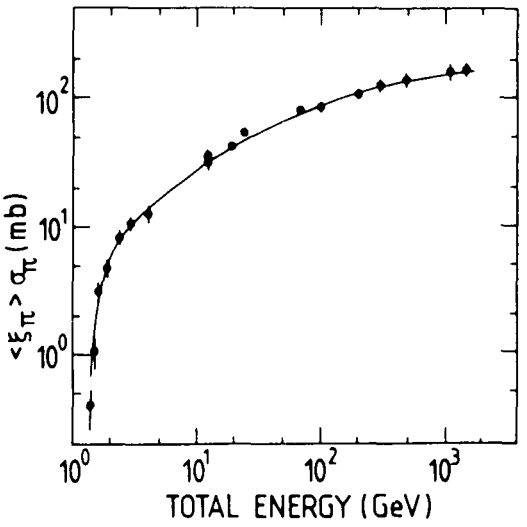

Figure 1.4. Product of cross section and multiplicity for neutral pion production in proton–proton collisions as a function of incident energy (after Stephens and Badhwar 1981).

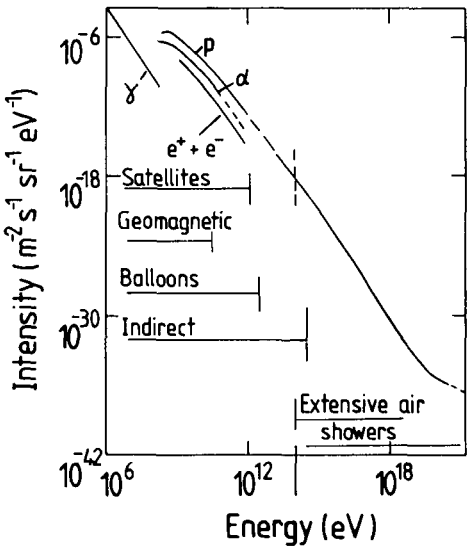

Figure 1.5. Energy spectrum of cosmic rays. In addition to the components shown, there are small fluxes of heavier nuclei. The mass composition above about 10^{14} eV becomes increasingly uncertain with a possible increase in the fraction of heavy nuclei; however, there is a general agreement that the particles are mainly protons above 10^{17} eV.

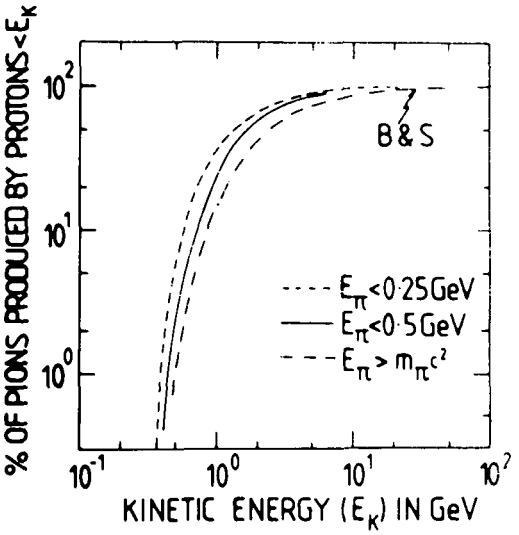

Figure 1.6. Percentage of neutral pions produced by protons of kinetic energy less than E_K as a function of E_K for various ranges of pion energy (E_π is the total pion energy). The graph is from Stephens and Badhwar (1981).

it is found that the bulk of the neutral pions are produced by protons having kinetic energies between 1 and 10 GeV. Quantitatively, the situation is as shown in Figure 1.6, which has been taken from extensive calculations by Stephens and Badhwar (1981). We note that only 10% of all pions are produced by protons of energies above 10 GeV. Also shown in Figure 1.6 are the percentages of pions produced with a low energy, namely below 0.25 and 0.5 GeV; here a significant fraction come from protons of kinetic energy below 1 GeV, a region of the spectrum where solar modulation causes uncertainty in the intensity estimates. Fortunately, however, most γ-ray measurements to be discussed later (in Chapter 4) are of too high energy to be affected in this way.

Many workers have calculated the energy spectra of photons per hydrogen atom in the ISM, and Figure 1.7 gives results from a summary by Stephens and Badhwar. We note the variety of predictions. It is the curve for p–p (i.e. cosmic ray protons on hydrogen in the ISM) that is derived from the total inclusive cross section for neutral pion production in Figure 1.4, the kinematics of $\pi^0 \rightarrow \gamma + \gamma$ and the cosmic ray energy spectrum. To this contribution must be added the results of proton collisions with nuclei in the ISM having $Z > 1$ and cosmic rays themselves with $Z > 1$ interacting with the ISM. All the contributions are included in the upper curves.

The division of γ-ray emissivity between the various components of the cosmic ray spectrum and the ISM can be seen from the complementary work of Dodds, Wolfendale and Wdowczyk (1976), shown in Table 1.1, which is essentially the integral of Figure 1.7, over all γ-ray energies (and above 100 MeV) but broken down into the constituents. Case A corresponds to a primary spectrum very similar to that of M_u in Figure 1.7.

Table 1.1. *Gamma-ray emissivities (after Dodds* et al. *1976)*

Photon energy	Contribution	Emissivity $\times 10^{-25}$ s^{-1}	
		A	B
All γ-rays	proton–hydrogen nucleus	2.17	1.60
	α–hydrogen nucleus	0.41	0.30
	$Z > 2$–hydrogen nucleus	0.22	0.16
	all CR on hydrogen nuclei	2.80	2.06
	all CR on ISM	3.90	2.88
γ-rays above 100 MeV	0.68 × emissivity for all CR on ISM	2.65	1.96

The interstellar spectra adopted are A = Fisk (1975); B = Bedijn, Burger and Swanenburg (1973).

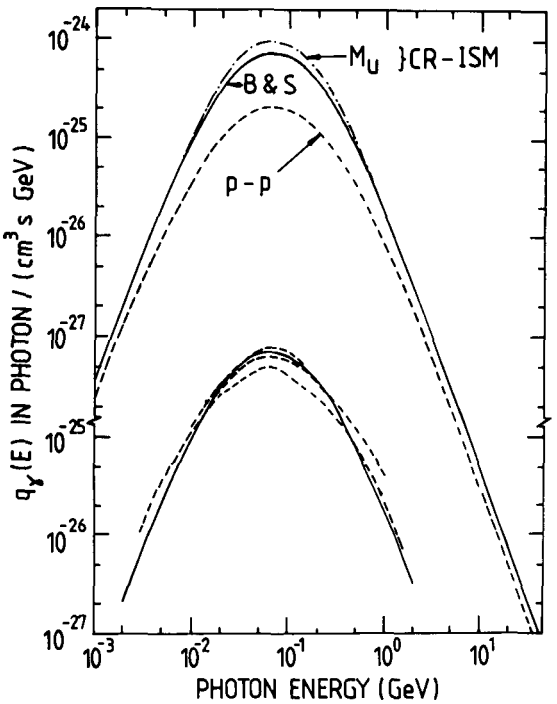

Figure 1.7. Differential production rate of γ-rays as a function of photon energy for a variety of possible cosmic ray spectra (after Stephens and Badhwar 1981). p–p relates to predictions for protons on interstellar hydrogen (using the spectrum). The remaining curves refer to all cosmic rays on all nuclei in the ISM (assuming $n_H = 1$ hydrogen atom cm^{-3}). M_u: upper spectrum adopted by Stephens and Badwhar; B & S: Badhwar and Stephens (1977). The full line in the lower set of spectra is the B & S spectrum. It is seen that there are significant differences in the predictions. A production rate intermediate between B & S and M_u is probably the best estimate at the present time.

Adopting the emissivity given in Table 1.1 for $E_\gamma > 100$ MeV we can make the standard calculation of the γ-ray intensity I_γ expected along a 10 kpc path through an ISM of 1 atom cm^{-3}. The result is $I_\gamma = 2.65 \times 10^{-25} \times 1/4\pi \times 3 \times 10^{22} = 5 \times 10^{-4}\ cm^{-2}\ s^{-1}\ sr^{-1}$. This result is, quite fortuitously, similar to the electron contribution for the same γ-ray energy threshold.

Moving to much higher γ-ray energies, the predicted spectral shape is much simpler and it can be represented by a power law of roughly constant exponent. Characterising the differential energy spectrum of cosmic rays at energies greater than a few GeV by

$$N(E_p) \propto E_p^{-\Gamma} \tag{1.25}$$

the multiplicity dependence as $\zeta_{\pi^0} \propto E_p^a$ and the dependence of the average π^0 energy as $\langle E_{\pi^0} \rangle \propto E_p^b$, the differential energy spectrum of the produced γ-rays has the form

$$q(E_\gamma) \propto E_\gamma^{-[(\Gamma + b - a - 1)/b]} \tag{1.26}$$

(Stecker 1973).

If one takes the values $\Gamma = 2.5$ and $a = \frac{1}{4}$, $b = \frac{3}{4}$ (Fermi model), the exponent of the γ-ray spectrum has a value -2.67. Although the Fermi model is not exactly applicable, as demonstrated by the accelerator experiments, the point is made that the exponent of the γ-ray energy spectrum is close to that of the parent cosmic ray spectrum.

Generation of ultra high energy γ-rays from proton interactions with radiation. An ambient low energy photon of energy ε, when seen in the rest system of a proton of energy $\gamma m_p c^2$, has an energy $\gamma\varepsilon$. If $\gamma\varepsilon$ exceeds the photomeson production threshold, it can lead to π^0 production and energy degradation of the primary proton, typically by about 10%. The threshold energy for this process is given by

$$m_{\pi^0}(1 + m_{\pi^0}/2m_p) = 144.7 \text{ MeV} \tag{1.27}$$

The 2.7 K microwave background, with photon number density of 400 cm^{-3}, forms an ambient photon field for this process to occur. The average energy of a 2.7 K photon is 6.4×10^{-4} eV, making the threshold γ as high as 2.3×10^{11}, i.e. the mechanism operates only at the extremely high proton energies of $\approx 10^{20}$ eV. Nevertheless, in the vast intergalactic distances, this process leads to energy degradation and hence to a steepening of the primary cosmic ray proton spectrum at $E_p \lesssim 10^{20}$ eV. (This is an area of active experimental investigation in cosmic ray research.) The produced photons have energies $\approx 10^{19}$ eV, and interact with the same microwave background photons to produce e^+e^- pairs. These particles in turn produce high energy γ-rays by inverse Compton scattering. The resulting electromagnetic cascade gives γ-rays of much lower energies; see Wdowczyk, Thackzyk and Wolfendale (1972) and Stecker (1973) for details.

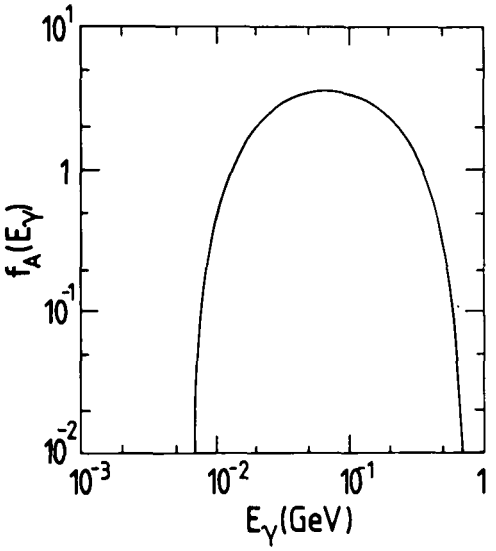

Figure 1.8. The normalised differential γ-ray spectrum from $\bar{p}p$ annihilation at rest (Stecker 1971).

1.2.2C $\bar{p}p$ annihilations

Neutral pions can be produced in the annihilations of protons with antiprotons. In principle, the antiprotons can arise from the interactions of energetic protons with matter, but the mechanism is too inefficient compared to the direct production of π^0 mesons during the interactions. If antimatter exists in its own right in significant quantities in the Universe, however, this process can add to others in producing neutral pions which subsequently decay into γ-rays. Stecker (1971) has calculated the differential γ-ray energy spectrum resulting from $\bar{p}p$ annihilations at rest; see Figure 1.8.

1.2.2D Black body radiation and thermal bremsstrahlung

Black body radiation is the radiation emitted by a body having a large optical depth at all frequencies. Its spectrum is given by the well known Planck formula

$$I_{BB}(\nu)\,d\nu = \frac{2\pi h\nu^3}{c^2}\left[\frac{1}{\exp(h\nu/kT)-1}\right]d\nu \text{ erg cm}^{-2}\text{ s}^{-1} \tag{1.28}$$

where the symbols have their usual meanings. The photon number spectrum (number of photons emitted per unit area of the source per unit time and energy interval) follows as:

$$N(E_\gamma) = 9.89 \times 10^{40} E_\gamma^2\left[\frac{1}{\exp(1.16 \times 10^{10}E_\gamma/T)-1}\right]$$
$$\text{photons cm}^{-2}\text{ s}^{-1}\text{ MeV}^{-1} \tag{1.29}$$

where T is the temperature in kelvin and E_γ is the energy of the γ-ray in MeV.

Characteristic black body energies are: the energy corresponding to the maximum in the wavelength distribution (i.e. Wien's law)

$$E_w(\text{MeV}) = 4.7 \times 10^{-10} T(\text{K})$$

and the average photon energy

$$\langle E \rangle(\text{MeV}) = 2.7kT = 2.3 \times 10^{-10} T(\text{K})$$

Clearly, temperatures of the order of 10^{10} K are needed before appreciable production of γ-rays above 1 MeV can occur. Such temperatures are rare and occur only in explosive phenomena (on the cosmic scale) and in hot Big Bang models of the early Universe. With respect to the latter, we note that the cosmological red-shift will displace the photon energies to considerably lower values.

Equations (1.28) and (1.29) refer to emission from optically thick media (i.e. the black body situation). For optically thin media, one has to multiply equation (1.29) by the absorption coefficient of photons in a hot plasma, and the resulting spectrum of thermal bremsstrahlung γ-rays is given by

$$N(E_\gamma) \propto \frac{n_e^2}{T^{1/2}} \frac{1}{E_\gamma} \exp(-E_\gamma/kT) \tag{1.30}$$

where n_e is the electron density and T is the temperature of the medium; for details see Ginzburg (1969) and Hayakawa (1969). Several examples of photon spectra from optically thin sources are presented in Section 3.4.1, which deals with the spectra of γ-ray bursts.

1.2.3 Summary of production mechanisms

A variety of γ-ray production mechanisms have been mentioned on the preceding pages. In any given astrophysical setting one or a few of them are more important than the others. To help appreciate the relative significances, we have listed in Table 1.2 the parameters relevant to the production of γ-rays of 1 MeV, 1 GeV and 1 TeV by the various processes.

1.3 Gamma-ray loss mechanisms

1.3.1 Introduction

It is the low loss of energy by γ-rays in penetrating a variety of astronomical environs that makes γ-rays such a powerful probe of these regions – and (the other side of the coin) that makes their detection so difficult. Hillier (1984) has given a good description of the various types of detectors and of the physical processes underlining their operation, together with the attendant problems of background γ-rays produced by unwanted processes, and the reader is referred to that book for details. Here we concentrate instead on the loss mechanisms which are operative in the astronomical environment. The topic can be divided into two parts: γ–matter interactions and γ–γ processes.

Table 1.2. *Gamma-ray production parameters*

Mechanism	$E_\gamma = 1$ MeV	$E_\gamma = 1$ GeV	$E_\gamma = 1$ TeV
Inverse Compton effect, formulae (1.13) and (1.10)	Against microwave background		
	$\varepsilon \sim 7 \times 10^{-4}$ eV	$\varepsilon \sim 7 \times 10^{-4}$ eV	$\varepsilon \sim 7 \times 10^{-4}$ eV
	$E_e \sim 1.7 \times 10^{10}$ eV	$E_e \sim 5.3 \times 10^{11}$ eV	$E_e \sim 1.7 \times 10^{13}$ eV
	Against starlight		
	$\varepsilon \sim 1$ eV	$\varepsilon \sim 1$ eV	$\varepsilon \sim 1$ eV
	$E_e \sim 4.4 \times 10^{8}$ eV	$E_e \sim 1.4 \times 10^{10}$ eV	$E_e \gtrsim 1$ TeV
	Against X-rays		
	$\varepsilon = 10$ keV	$\varepsilon = 10$ keV	$\varepsilon = 10$ keV
	$E_e \sim 4.4 \times 10^{6}$ eV	$E_e \gtrsim 1$ GeV	$E_e \gtrsim 1$ TeV
Synchrotron radiation, formula (1.19)	$B = 10^{-4}$ G		
	$E_e = 7.7 \times 10^{14}$ eV		
	$B = 1$ G	$B = 1$ G	$B = 1$ G
	$E_e = 7.2 \times 10^{12}$ eV	$E_e = 2.3 \times 10^{14}$ eV	$E_e = 7.2 \times 10^{15}$ eV
	$B = 10^{4}$ G	$B = 10^{4}$ G	$B = 10^{4}$ G
	$E_e = 7.2 \times 10^{10}$ eV	$E_e = 2.3 \times 10^{12}$ eV	$E_e = 7.2 \times 10^{13}$ eV
Bremsstrahlung	$E_e \gtrsim 2$ MeV	$E_e \gtrsim 2$ GeV	$E_e \gtrsim 2$ TeV
Curvature radiation, formula (1.23)	$\rho = 10^{8}$ cm	$\rho = 10^{8}$ cm	$\rho = 10^{8}$ cm
	$E_e = 7.7 \times 10^{11}$ eV	$E_e = 7.7 \times 10^{12}$ eV	$E_e = 7.7 \times 10^{13}$ eV
p–p inelastic collisions $\rightarrow \pi^0 \rightarrow 2\gamma$		$E_p \gtrsim 10^{10}$ eV	$E_p \gtrsim 10^{13}$ eV

1.3.2 Gamma-ray–matter interactions

General. The relative importance of the various γ–matter interactions can be seen by reference to Figure 1.9. If we define γ-rays as photons above 0.5 MeV then only the Compton and pair production processes are important; however, when we go to somewhat lower energies to provide an overlap with hard X-rays (an area of particular interest in connection with γ-ray transients), the photoelectric effect has importance, at least for modest values of Z. Nevertheless we will not describe any features of the photoelectric process here.

Compton effect. The well known theory of the Compton effect gives for the wavelength shift of the scattered photon the magnitude

$$\lambda' - \lambda = \frac{h}{m_e c}(1 - \cos\theta) \tag{1.31}$$

where λ' is the wavelength of the scattered photon, λ is the incident wavelength, θ is the angle of scatter, and the other symbols have their usual meanings.

The cross section for Compton scattering depends on the polarisation of the photon beam as well as on the other parameters. Following Heitler (1960) it can be written as

$$\frac{d\sigma_c}{d\Omega} = \frac{r_0^2}{4}\left(\frac{\nu'}{\nu}\right)^2\left(\frac{\nu}{\nu'} + \frac{\nu'}{\nu} - 2 + 4\cos^2\theta\right) \text{cm}^2\,\text{sr}^{-1}\,\text{electron}^{-1} \tag{1.32}$$

where ν' and ν are the corresponding photon frequencies and θ is the angle between the electric vectors of the two photons.

When the incoming photon is unpolarised, the corresponding expression is now,

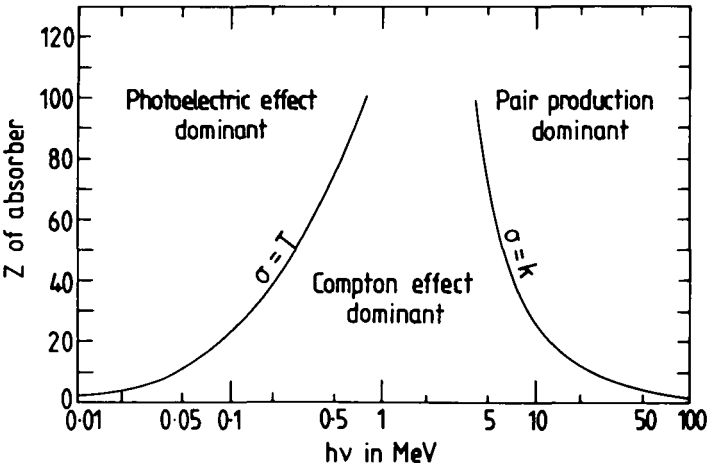

Figure 1.9. The relative importance of the major forms of γ–matter interaction as a function of γ-ray energy and atomic number of the material involved (after Evans 1955).

θ being the angle of scatter,

$$\frac{d\sigma_c}{d\Omega} = \frac{r_0^2}{2}\left(\frac{\nu'}{\nu}\right)^2\left(\frac{\nu}{\nu'} + \frac{\nu'}{\nu} - \sin^2\theta\right) \text{cm}^2\,\text{sr}^{-1}\,\text{electron}^{-1} \tag{1.33}$$

As is well known, the cross sections reduce to the Thomson cross section $(8\pi r_0^2/3)$ in the limit of very low frequency and when integrated over the whole solid angle. At high photon energies the fall off in $d\sigma_c/d\Omega$ with increasing ν (Klein–Nishina formula) is apparent.

Compton telescopes using the above process have been used quite extensively in γ-ray experiments, the telescopes being carried aloft by balloons. More sophisticated versions in which photons interact twice ('double-Compton' telescopes) are being used increasingly.

Figure 1.10 gives the corresponding mass attenuation coefficient for Compton scattering in hydrogen, and also for the other relevant processes. As an example we can consider the standard 10 kpc of ISM of density 1 atom cm^{-3}. At 1 MeV the mass attenuation coefficient is 0.13 $\text{cm}^2\,\text{g}^{-1}$, i.e. a mean free path of ≈ 8 g cm^{-2} hydrogen which, converting to units of length, is $8 \times (1.7 \times 10^{-24})^{-1}$ cm, i.e. ≈ 2 Mpc. The scattering in 10 kpc is thus quite negligible. The same situation does

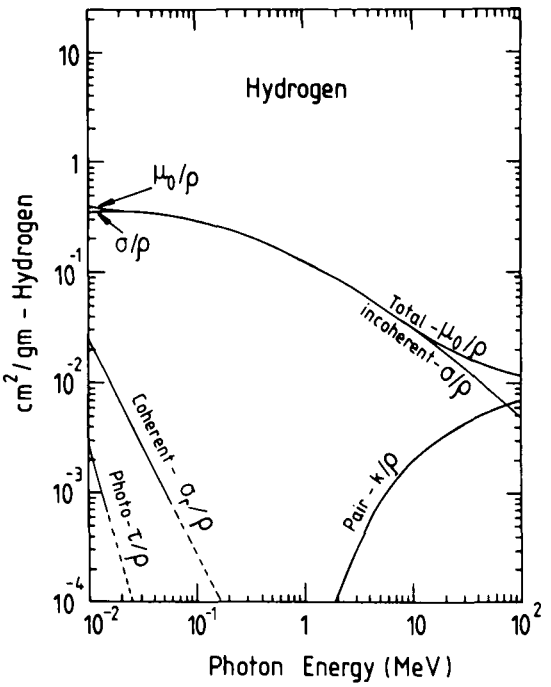

Figure 1.10. Mass attenuation coefficients for γ-rays in hydrogen for the more important processes (after Chupp 1976). The quantities μ, σ, k and τ are the linear attenuation coefficients so that each, divided by density ρ, is the mass attenuation coefficient.

not apply in dense plasmas, however, and here Compton scattering can be quite important.

Pair production. The threshold for this process is $2mc^2(1 + m/M)$, where M is the mass of the particle (usually a nucleus) in whose Coulomb field the pair of particles, each of mass m, is being produced. For creation of electrons on a nucleus the threshold is $2m_ec^2 = 1.022$ MeV, and for creation of electrons on an electron (a rare phenomenon) the threshold rises to $4m_ec^2 = 2.044$ MeV.

Straightforward forms can be given for the pair production cross sections in the limiting cases of no atomic screening and complete screening.

For no screening (relevant to $1 \ll h\nu/m_ec^2 \ll 1/\alpha Z^{1/3}$),

$$\sigma_{pp} = \bar{\sigma}Z^2\left(\frac{28}{9}\log\frac{2h\nu}{m_ec^2} - \frac{218}{27}\right)\text{cm}^2\text{ atom}^{-1} \tag{1.34}$$

following Marmier and Sheldon (1969).

When $h\nu/m_ec^2 \gg 1/\alpha Z^{1/3}$, there is the condition of complete screening and the increase of σ_{pp} with ν is suppressed. The form is then

$$\sigma_{pp} = \bar{\sigma}Z^2\left(\frac{28}{9}\log\frac{183}{Z^{1/3}} - \frac{2}{27}\right)\text{cm}^2\text{ atom}^{-1} \tag{1.35}$$

The form of the corresponding mass attenuation coefficient is given in Figure 1.10; above 100 MeV pair production dominates. As with the Compton effect, losses in the general ISM are negligible, but in dense plasmas, such as might be found near black holes, the process can become important.

1.3.3 Gamma–gamma interactions

A γ-ray of energy ε_1 colliding with another of energy ε_2 gives rise to a pair of particles, each of mass m, if ε_1 is greater than a threshold value, ε_t, given by

$$\varepsilon_t = \frac{2m^2c^4}{\varepsilon_2(1 - \cos\theta)} \tag{1.36}$$

where θ is the angle between the photon trajectories. Restricting attention to electrons and the case of head-on collisions, we have

$$\varepsilon_t = 0.26 \times 10^{12}/\varepsilon_2$$

where the energies are in eV.

Considering now collisions with astronomically important radiation fields, we have (with their mean energies in brackets)

2.7 K radiation	$(6 \times 10^{-4}$ eV), $\varepsilon_t \approx 4 \times 10^{14}$ eV
starlight	(2 eV), $\varepsilon_t \approx 10^{11}$ eV
X-rays	(1 keV), $\varepsilon_t \approx 3 \times 10^{8}$ eV

The corresponding cross section for the production of pairs of particles each of mass m in head-on collisions is

$$\sigma_1 = \pi r_e^2 \left(\frac{m}{\omega}\right)^2 \left[2 \ln\left(\frac{2\omega}{m}\right) - 1\right] \tag{1.37}$$

for $\omega \gg m$, i.e. in the extreme relativistic region, and

$$\sigma_2 = \pi r_e^2 \left(1 - \frac{m^2}{\omega^2}\right)^{1/2} \tag{1.38}$$

for ω close to m, i.e. in the classical region. In the expressions $\omega = (\varepsilon_1 \varepsilon_1)^{1/2}$ and r_e is the classical electron radius. (For further details see Jauch and Rohrlich 1955.)

Although the cross section is not small, photon–photon collisions are not generally frequent because the spatial density of target photons is not large. Nevertheless, even with low photon densities, such as encountered with the various extragalactic photon fields – $\approx 400\ \text{cm}^{-3}$ for the 2.7 K radiation and $\approx 5 \times 10^{-3}\ \text{cm}^{-3}$ for extragalactic starlight with an energy density of $\approx 10^{-2}$ eV cm^{-3} – the ensuing mean free paths for collision are such as to lead to a significant attenuation over typical extragalactic distances. Figure 1.11 shows the interaction lengths derived using expressions of the form given above but allowing for the geometry of the collisions and including the energy distribution of the target photons.

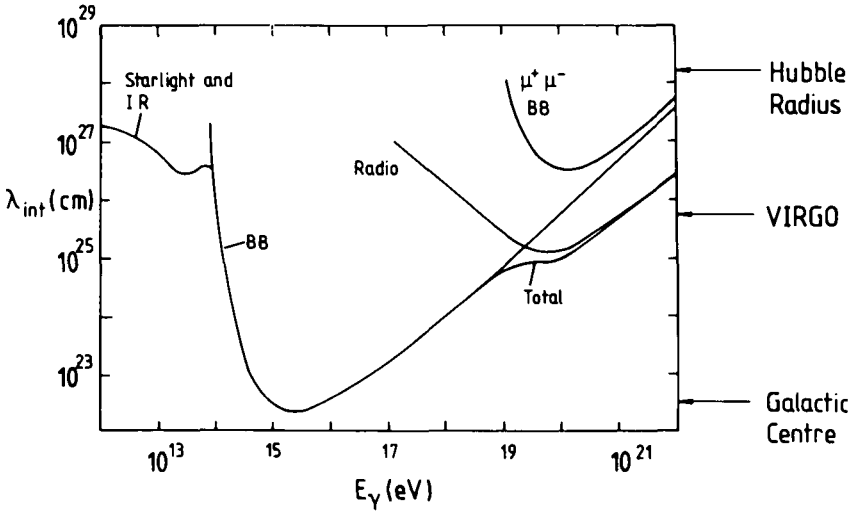

Figure 1.11. Interaction length of γ-rays on the various background radiation fields. Unless otherwise stated the process concerned is electron pair production. BB denotes the 2.7 K black body radiation (0.24 eV cm^{-3}, ≈ 400 photons cm^{-3}). Several important distances are indicated on the right-hand side; 'VIRGO' denotes the distance to the important cluster of galaxies at the centre of 'our' supercluster. The results are from the work of Wdowczyk *et al.* (1972).

The extent to which γ–γ collisions are important in attenuating γ-rays can be seen by reference to Figure 1.11. On the Galactic scale the flux received from sources as far away as the Galactic Centre, or further, will be reduced for γ-rays in the region of 10^{15} eV. It will be seen later (Chapter 5) that the loss is serious for the source Cygnus X–3, the distance of which appears to be about 11 kpc.

At the extragalactic level, it will be seen that attenuation is important at all energies in the range considered in Figure 1.11. In fact, the interaction length for γ-rays on starlight photons becomes greater than the Hubble radius just below 10^{12} eV so that there is an effective transparency of the Universe for $E_\gamma < 10^{12}$ eV.

The behaviour of very high energy photons, produced on a universal scale and propagating over extragalactic distances, is one of great interest and some complexity. Photon cascading occurs, with the electron pairs generated in γ–γ collisions themselves producing more photons by way of the inverse Compton interactions. Wdowczyk *et al.* (1972 and later papers) have considered this problem and derived the γ-ray energy spectrum to be expected from the injection of γ-rays of energy above 10^{19} eV such as might have come from the interaction of cosmic ray protons with the 2.7 K photons. The ensuing cascade gives a γ-ray cascade extending down to low energies, but the intensity predicted, corresponding to a γ/proton ratio of $\approx 10^{-6}$ at $E_\gamma = 10^{12}$ eV, is too low to be detected yet.

The foregoing has been concerned mainly with interactions of γ-rays and the background photons. In the immediate vicinity of various exotic objects the X-ray and harder photon fluxes can be so high that γ-rays in the GeV and even MeV regions are seriously affected. The steepening of the energy spectrum of γ-rays from quasars at about 2 MeV may be due to this cause (see Chapter 4).

2

Gamma-ray line astronomy

2.1 Introduction

The spectroscopy of γ-ray astronomy is, understandably, an area where important advances are to be expected, an expectation born of similar previous experience with other regions of the electromagnetic spectrum. Technical difficulties are considerable at present, however, due to low line fluxes aggravated by serious background problems; nevertheless, a promising start has been made and several interesting observations have already appeared.

As with astronomy in general, a distinction can be made between observations of 'discrete' objects (such as stars, supernovae, other galaxies, etc.) and signals from more extended regions, in particular the interstellar medium (ISM).

In the first category, γ-ray lines from the Sun – due to energetic protons and heavier nuclei interacting with the solar atmosphere – provide interesting and important information about a variety of solar phenomena. This subject of solar γ-ray spectroscopy is distant from the main stream of topics discussed here, and the reader is directed to a number of useful reviews by Ramaty and Lingenfelter (1981), Trombka and Fichtel (1982), Ramaty and Murphy (1987), and the books by Chupp (1976) and Hillier (1984).

In the non-solar region, which is of main concern here, only a few γ-ray lines have been detected from non-transient celestial sources so far. These include the lines at 1809 keV from the Galactic Equatorial Plane, the line at 511 keV from the Galactic Centre region and the one at 1369 keV from the object SS 433; these will be described in Sections 2.2, 2.3 and 2.4, respectively. Turning to transient sources, the most dramatic source has been the supernova in the Large Magellanic Cloud (SN 1987A), and a description of the results from this object will be given in Section 2.5. We will then briefly present in Section 2.6 the searches made for γ-ray lines from other extragalactic objects. Finally, in Section 2.7, there is a summary of the results obtained so far and a résumé of their implications.

2.2 Lines from the interstellar medium

2.2.1 Expectations

Chapter 1 dealt with the manner in which ISM lines are expected to be produced; here we given more details. Ramaty and Lingenfelter (1979) have made extended calculations of the lines expected from cosmic ray interactions in the

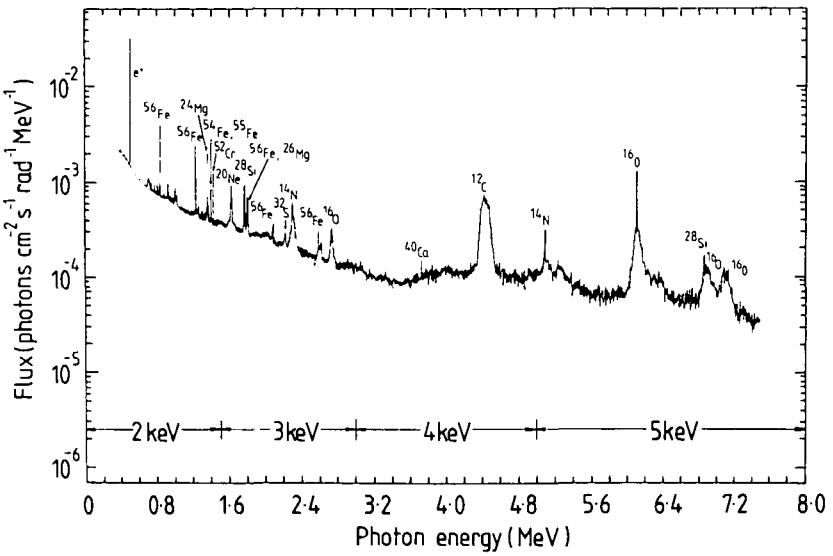

Figure 2.1. The expected γ-ray spectrum in the general direction of the Galactic Centre arising from cosmic ray interactions in the interstellar medium (after Ramaty and Lingenfelter 1979). The ranges marked '2 keV, 3 keV . . .' refer to the instrumental line widths assumed in the calculations and used to derive the indicated line fluxes. For example, the ^{16}O line at 6.13 MeV plotted with a flux, above background, of 1.2×10^{-3} cm^{-2} s^{-1} rad^{-1} MeV^{-1} would have a flux of 5×10^{-3} times this value, i.e. 6.0×10^{-6} cm^{-2} s^{-1} rad^{-1} when seen with a detector having a FWHM of 5 keV.

ISM, with the result shown in Figure 2.1. Two classes of lines can be identified: sharp and broad. The sharp lines come from interactions with interstellar dust, the recoil nuclei in the dust grains coming to rest before de-exciting. The broader lines are due to the ISM in gaseous form; to give a perspective, it is likely that about 15% of carbon and oxygen, for example, are in the gaseous ISM. The broad lines will also include a contribution from cosmic ray nuclei ($Z > 1$) rendered radioactive by collisions with the nuclei of the ISM.

Sharp lines from the dust–grain phase of the ISM are expected for the common elements in the ISM: oxygen (^{16}O), magnesium (^{24}Mg) and iron (^{54}Fe, ^{55}Fe, ^{56}Fe), as can be seen in Figure 2.1. Of these lines the ^{16}O line at 6.13 MeV is most conspicuous in view of the lack of other lines in its immediate neighbourhood.

It should be stressed that the estimates in Figure 2.1 are necessarily approximate because of uncertainty in both the distribution of cosmic ray intensity and in the heavy element abundances along the line of sight. The topic of cosmic-ray-intensity variations in the Galaxy is taken up in Chapter 4.

The positron annihilation line is also seen to be quite marked, the positrons having come from the $\pi^+ \rightarrow \mu^+ \rightarrow e^+$ chain and having slowed down to very low velocities before annihilating (the e^+e^- cross section for annihilation is high only at such low velocities). The predicted strength of the 511 keV line is

Table 2.1. *The decay chains from nucleosynthesis in supernovae (after Ramaty and Lingenfelter 1979)*

Decay chain	Mean life (y)	$Q/Q(^{56}Ni)$	Energy (MeV)	Positrons or photons per disintegration
$^{56}Ni \rightarrow {}^{56}Co \rightarrow {}^{56}Fe$	0.31	1	e^+	0.2
			0.847	1
			1.238	0.7
$^{57}Co \rightarrow {}^{57}Fe$	1.1	2×10^{-2}	0.122	0.88
			0.014	0.88
$^{22}Na \rightarrow {}^{22}Ne$	3.8	5×10^{-3}	e^+	0.9
			1.275	1
$^{44}Ti \rightarrow {}^{44}Sc \rightarrow {}^{44}Ca$	68	2×10^{-3}	e^+	0.94
			1.156	1
			0.078	1
			0.068	1
$^{60}Fe \rightarrow {}^{60}Co \rightarrow {}^{60}Ni$	4.3×10^5	1.5×10^{-4}	1.322	1
			1.173	1
			0.059	1
$^{26}Al \rightarrow {}^{26}Mg$	1.1×10^6	1.5×10^{-4}	e^+	0.85
			1.809	1

$\approx 7 \times 10^{-5}\,cm^{-2}\,s^{-1}\,rad^{-1}$, i.e. about $3 \times 10^{-5}\,cm^{-2}\,s^{-1}$ for a detector of resolution 0.2 sr (FWHM = 30°) centred on the Galactic Centre.

The possibility of detecting γ-ray lines from supernova remnants (SNRs) is one of great potential interest because of its relevance to the physics of supernova explosions and to the (likely) demonstration of continuing nucleosynthesis. The importance of this field seems to have been recognised first by Clayton *et al.* (1969); later calculations have been made by a variety of authors (e.g. Clayton 1973, Lingenfelter, Higdon and Ramaty 1978, Woosley, Axelrod and Weaver 1981). Short-lived radioactive nuclei will generate γ-rays which are unlikely to escape from the high density material around a very young supernova, but sufficient amounts of isotopes with longer mean life will survive until the SNR density is low enough to allow penetration. Nuclei with lifetimes longer than a few times 10^5 y will survive so long that the remnant will have merged into the general ISM, and after subsequent mixing these radioactive nuclei will add their γ-rays to the reservoir from cosmic ray interactions. The isotope ^{26}Al (mean life = 1.04×10^6 y) is of particular interest in this context because it is almost certainly produced largely in supernova and nova explosions and its study can allow inferences as to how much nucleosynthesis takes place in these explosive cosmic occurrences.

Ramaty and Lingenfelter (1979) give data (Table 2.1) for the more important isotopic decay chains associated with the nucleosynthesis reactions occurring in supernovae. The ensuing lines are indicated in Figure 2.2, superimposed on the 'ordinary' ISM lines. It will be noted in Figure 2.2 that the e^+ annihilation line

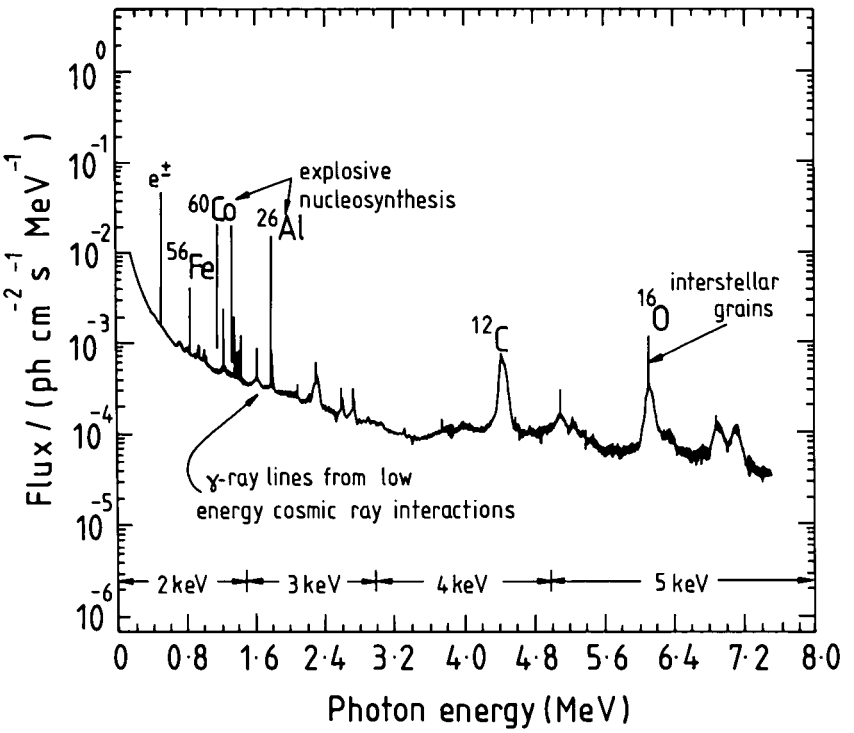

Figure 2.2. Diffuse γ-ray line emission from the interstellar medium, including contributions from explosive nucleosynthesis (after Ramaty and Lingenfelter 1979).

is higher in flux than for the ISM alone (Figure 2.1); this is because of the additional contribution of positron emitters produced during nucleosynthesis (Table 2.1).

2.2.2 Observations

One of the major lines to have been detected so far from the ISM is the ^{26}Al line at 1809 keV. The detection was achieved by way of observations with the HEAO-3 satellite by Mahoney *et al.* (1984*a*,*b*) and confirmation came from the observations of Share *et al.* (1985). The instrument consisted of a cluster of four cooled high purity germanium detectors in an active CsI(Na) shield, the shield defining a geometrical aperture of about 30° FWHM. Mahoney *et al.* (1980) have described the instrumentation in detail.

HEAO-3 was launched on September 20, 1979, and although the instruments worked well, a build up of radiation contamination occurred due to cosmic ray bombardment. Of specific importance to the search for narrow lines was the instrumental width of the lines – this increased from 3.5 keV (FWHM) just after launch to about 19 keV in the late spring of 1980 (Mahoney *et al.* 1980). A preliminary search (Mahoney *et al.* 1982) gave an indication of the ^{26}Al line at the 2.6σ level, and more recent analysis has confirmed the result at a higher level

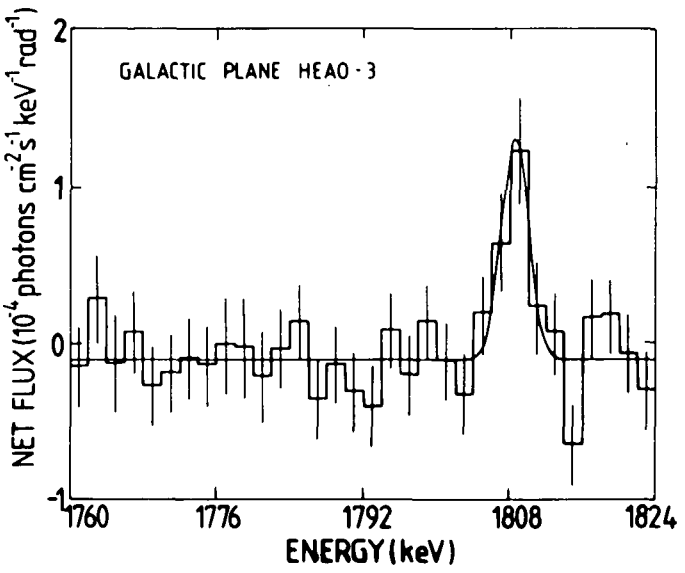

Figure 2.3. HEAO-3 results on the ^{26}Al line (Mahoney *et al.* (1984*a*,*b*). The data refer to the total net Galactic Plane emission near 1809 keV normalised to the direction of the Galactic Centre. The data are those of highest quality and were taken during autumn, 1979. The channel width is 2 keV and the solid curve is the best fit for a background plus an unresolved line at 1809 keV. The fit gives a line with an energy of 1808.49 $\pm$ 0.41 keV consistent with the expected 1808.65 $\pm$ 0.07 keV emission from ^{26}Al at rest. The width in the fit is consistent with the instrumental resolution and gives a 1σ upper limit of 3 keV FWHM for the intrinsic width of the line.

of significance. The analysis was performed with considerable difficulty because of the low signal strength, high background rate and poor angular resolution. Unfortunately, it was not possible to study the longitude distribution, which would have enabled the mode of production of the ^{26}Al line to be examined in some detail. Instead, a model longitude distribution was adopted and the appropriate average value fitted. The model taken assumed that the longitudinal dependence was the same as that of diffuse γ-rays (above 70 MeV) as measured by the SAS II and COS B satellites (see Chapter 4 for a full description of these results). Essentially, this distribution has a ratio of $\sim$4:1 for the Galactic Centre to Galactic Anti-Centre directions, the width of the broad excess towards the Galactic Centre is $\approx \pm 60°$ in longitude and the flux towards $l = 0°$ is about twice the mean flux.

The result of the fitting is to give a line flux of the ^{26}Al γ-rays towards the Galactic Centre of $(4.8 \pm 1.0) \times 10^{-4}$ cm^{-2} s^{-1} rad^{-1} with a line width of <3 keV (FWHM). Figure 2.3 summarises the results.

We shall first examine the significance of the line width. The lifetime of ^{26}Al is such that most of its nuclei will have reached equilibrium with the gas in the ISM and thus have velocities <10 km s^{-1}. A bigger contribution to velocity – and thus Doppler broadening – is from Galactic rotation, and this corresponds to a velocity

$v \lesssim 250$ km s^{-1}; the fractional line width will therefore be less than, approximately, $v/c = 2.5 \times 10^7/3 \times 10^{10}$, i.e. $<10^{-3}$, or, equivalently <2 keV for the 1809 keV line. There is seen to be no inconsistency with the results of Mahoney *et al.* (1982).

It is interesting to note that, although there have been a number of measurements by other workers since the pioneering studies of Mahoney *et al.*, the experimental situation is still not completely clear cut. The most serious problem concerns the angular size of the 'source'. Even the most recent detectors (Mallet *et al.* 1992 and Teegarden 1992) have $\sim 20°$ fields of view so that the intensity profile cannot be determined with any accuracy. It appears that the 'source' is not localised at the Galactic Centre and the profile could well occupy at least 10°–20° in longitude.

Concerning the predicted flux, Figure 2.2 indicates a value of $\approx 1.5 \times 10^{-2}$ cm^{-2} s^{-1} MeV^{-1} which, for a line width of 3 keV (the value assumed in drawing the spectrum), translates to 4.5×10^{-5} cm^{-2} s^{-1} rad^{-1} (allowing for the fact that the flux is roughly constant towards the Galactic Centre over about 1 rad). The measured value of 4.8×10^{-4} cm^{-2} s^{-1} rad^{-1} is thus an order of magnitude higher than expected. It seems likely, then, that some other source is important in providing ^{26}Al in the ISM besides the SNR considered in the derivation of Figure 2.2.

The mass of ^{26}Al in the ISM has been estimated by Mahoney *et al.* as follows. With flux $\bar{F}$ (cm^{-2} s^{-1} rad^{-1}) of ^{26}Al γ-rays from the Galactic Centre direction, the total number of γ-rays emitted by the Galaxy follows from the assumed radial distribution of radioactive nuclei ($\propto$ emissivity of medium energy γ-rays) as $Q = 10^{46}\bar{F}$. Thus, for $\bar{F} = 4.8 \times 10^{-4}$, $Q \approx 4.8 \times 10^{42}$ γ-rays s^{-1}. Multiplying by the mean life of ^{26}Al (3.28×10^{13} s) gives $\approx 1.6 \times 10^{56}$ atoms (i.e. $3M_\odot$, where $M_\odot$ denotes the mass of the Sun) for the contemporary mass of ^{26}Al in the ISM.

Returning to the question of the significance of the ^{26}Al observation, and the relevance to the contribution from supernovae and novae, the situation can be examined in a little detail. The important question is the relationship between the ratio of the average isotopic production ratio for explosive nucleosynthesis in supernovae: $(P_{26}/P_{27})_{SN}$, and the derived ^{26}Al content. Model calculations by Arnett and Wefel (1978), Truran and Cameron (1978), Arnould *et al.* (1980), and Woosley and Weaver (1980), give values in the range $(0.4–2.0) \times 10^{-3}$ for this ratio, and this range appears to be acceptable. However, the conversion depends on the ratio of the average Galactic metallicity to that of solar system matter $(A_G/A_\odot)$ and on the appropriate Galactic mass to adopt (M_G). Mahoney *et al.* (1984*a*,*b*) adopting $A_G/A_\odot = 2.3$ and $M_G = 2 \times 10^{11} M_\odot$ use the measured ^{26}Al content to derive $(P_{26}/P_{27}) \approx 4 \times 10^{-3}$, not far from expectation. Clayton (as described by Mahoney *et al.* 1984*a*,*b*) has pointed out that the values adopted for $A_G/A_\odot$ and M_G were inappropriate, however, and using the values ~ 1 and $7 \times 10^{10} M_\odot$, respectively, appropriate to Population I star material, which is the product of supernovae, P_{26}/P_{27} moves up to 30×10^{-3}, a factor of at least 15 above the expected value. This conclusion is consistent with that following from the calculations of Ramaty and Lingenfelter (1979) and given in Figure 2.2.

The question of the supernova contribution is still a live one, however. Woosley, in a long series of calculations of the various nucleosynthesis processes in Type II supernovae (SNII) has managed to produce up to $0.5M_\odot$ and conceivably $1M_\odot$ of ^{26}Al from these objects (Woosley 1992). The higher values than hitherto arise from the realisation that there should be enhanced pre-explosive production of ^{26}Al in the neon shell of high mass SNII ($>12M_\odot$) and that neutrino induced nucleosynthesis may well be significant. The extreme upper limit ($1M_\odot$) arises from taking the most optimistic values and also by extrapolating the enhanced production in the neon shell to even higher SNII masses.

There is a problem with invoking considerable steady state nucleosynthesis of ^{26}Al in that ^{44}Ti should also be produced and lines from this nucleus have not been observed. Specifically, ^{44}Ti generates a line at 1.16 MeV with 15 times the intensity of the 1.8 MeV ^{26}Al line, and this has not been seen (Von Ballmoos *et al.* 1987). It seems more likely that sources other than supernovae are important for the production of ^{26}Al.

Novae have been considered in detail by Mahoney *et al.* (1984*a*,*b*), and these authors have used the calculations of Hillebrandt and Thielemann (1982) to derive an expected mass of $\sim 1M_\odot$ of ^{26}Al in the Galaxy.

In addition to ^{26}Al, mention must also be made of the very recent detection of the 6.7 MeV iron-line emission by Koyama *et al.* (1989). This line is interpreted as due to the excitation of Galactic gas by SNRs.

Very massive Wolf–Rayet stars ($M > 0.25M_\odot$) have also been invoked, and Prantzos (1992) estimates a contribution here of $\sim 0.25M_\odot$ of ^{26}Al with an uncertainty of a factor of two.

Adding together the best estimates of the masses generated by the various stars we have a total of somewhat less than $1M_\odot$; it is doubtless not impossible to reach the $3M_\odot$ required but it is clear that there is little confidence in this procedure.

Considerable help will come from new observations (hopefully with the Gamma Ray Observatory) of the actual profile of the ^{26}Al emission line, although it will be appreciated that our knowledge of the spatial distribution of the likely originators: SNII, Wolf–Rayet stars, novae, is far from complete.

2.3 The 511 keV line from the Galactic Centre

2.3.1 The observations

The progress of research on the positron annihilation line from the Galactic Centre epitomises the whole subject of γ-ray astronomy. Early balloon observations gave tantalising evidence for a significant flux, but high backgrounds and an apparent variability of signal caused much scepticism. However, following more recent satellite observations it is generally agreed that there *is* a significant flux and that it *does* vary somewhat with time.

The first observation of a line in the region of 511 keV seems to have been made by Johnson and Haymes (1973) – the energy in fact being reported as ≈ 476 keV. Two years later, in a repeat experiment, Haymes *et al.* (1976) found a line again, although this time at ≈ 530 keV. Technical improvements – principally the use of

a cooled Ge(Li) detector – by Leventhal, MacCallum and Strong (1978) led to the detection of a line feature at 511 keV, with a resolution of 3.2 keV, the flux being $1.2 \times 10^{-3}\,\mathrm{cm}^{-2}\,\mathrm{s}^{-1}$.

Later observations by Leventhal *et al.* (1980) and Albernhe *et al.* (1981) confirmed the existence of the line, and significant results came from the Jet Propulsion Laboratory's γ-ray spectrometer on the HEAO-3 satellite (Riegler *et al.* 1981). The satellite data gave an energy of 510.9 ± 0.25 keV and a width less than about 3 keV for the line.

Most recently, the GRIS spectrometer (Leventhal *et al.* 1989) has given a FWHM of 2.9 ± 0.6 keV and a weighted average of the observations covering the period 1977 to 1989 give an energy of (510.91 ± 0.17) keV; such a value is consistent with the rest energy for positron annihilation of $m_e c^2 = 511.0$ keV.

As most of the detectors have angular apertures of 13° or greater, the exact location of the source is unclear; in fact it is almost certain that there is not one source but a mixture. A favoured model is that of Lingenfelter and Ramaty (1989) which has a variable 'point' source at or near the Galactic Centre together with a steady diffuse emission associated with the interstellar medium and thus distributed along the Galactic Plane. The evidence for the diffuse component and the details of the model will be considered later.

2.3.2 *The main features of the 511 keV line*

Figure 2.4 shows the signal from a 1979 Galactic Plane scan by HEAO-3 (Riegler *et al.* 1981); there can be no doubt about the statistical significance of the Galactic Centre line; the most recent observations by Leventhal *et al.* (1989) are very similar, the only difference being that the line is somewhat sharper, as already mentioned, and a small step in the continuum level – the flux below 510 keV being slightly higher than that above.

There are two remarkable features about this line: its magnitude and its time variability. Although the cosmic ray intensity at the Galactic Centre is probably higher than locally, and also there is an abundance of target gas (see Bhat *et al.* 1985), the contribution of cosmic-ray-generated positrons appears to be negligible. This fact follows from the lack of observation of other cosmic-ray-induced nuclear lines in the 1–2 MeV region from Mg, Si and Fe (Ramaty and Lingenfelter 1979) and the strong 4.4 MeV line emission from the de-excitation of ^{12}C. Matteson, Nolan and Peterson (1979) estimate that no more than about 20% of all the 511 keV line intensity could be due to cosmic rays of energy below about 100 MeV per nucleon. The preceding lines would have come from interactions not sufficiently energetic to produce pions. However, if positrons from the $\pi \rightarrow \mu \rightarrow$ e chain were to be responsible for the observed line, the ensuing γ-rays from the associated π^0 decays would be very intense. There is, in fact, evidence for a peak from the direction of the Galactic Centre in the 100 MeV region (as will be described later), but its flux is too low by a factor of at least 100 to be consistent with the 511 keV line if the γ-ray lines were produced by the annihilations of positrons resulting from the $\pi^+ \rightarrow \mu^+ \rightarrow e^+$ chain. Reverting to the actual magnitude of the line flux as observed in the 1979 observation (Figure 2.4) the corresponding source

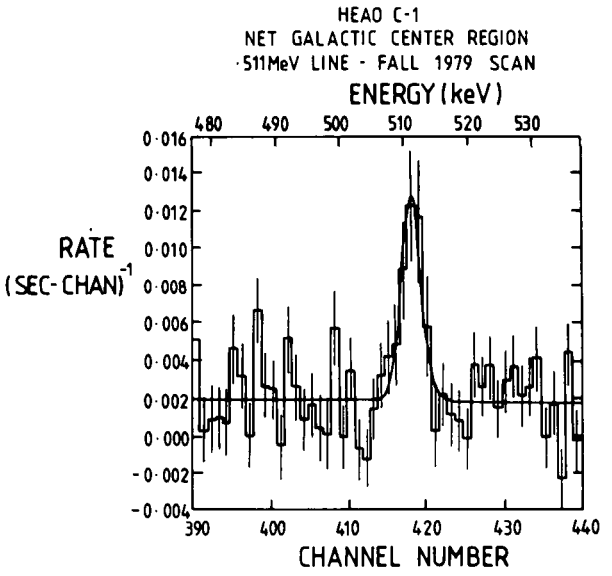

Figure 2.4. HEAO-3 observations of the 511 keV positron annihilation line from the 'Galactic Centre' (Riegler *et al.* 1981). The observations were taken in the autumn of 1979. The emission is centred on 510.90 ± 0.25 keV. The observed width is (3.13 ± 0.57) keV, to be compared with an instrumental resolution of 2.72 keV; the corresponding intrinsic width is 1.6 (+0.9 − 1.6) keV (all the widths are FWHM). (The latest measurements give a FWHM of 2.9 ± 0.6 keV.)

luminosity is $L \approx 1.4 \times 10^{37}\,\mathrm{erg\,s^{-1}}$ and the positron annihilation rate is $\approx 10^{43}\,\mathrm{s^{-1}}$ (adopting a value of 8.5 kpc for the Sun–Galactic Centre distance).

At this stage it is appropriate to mention that analysis by Riegler *et al.* (1983) indicated a continuum both below and above 511 keV from the Galactic Centre direction, and later observations have firmed up the results. Figure 2.5 shows the measurements made by the 1988 GRIS project (Gehrels *et al.* 1992).

The width of the spectral line at 511 keV is important from the standpoint of determining the relative fractions of γ-rays coming from direct e^+e^- annihilation. Although singlet state positronium yields two photons of energy 511 keV, the triplet state (formed three times as often) yields three photons of variable energy below 511 keV. It is possible to determine the relative fraction, f, of the 511 keV line, which has come by way of positronium compared with direct annihilation, by fits to the points in the plot of flux versus energy on a fine scale. Riegler *et al.* derived $f = 0.58 \pm 0.17$ at the 90% confidence level, a value somewhat smaller than the $f = 0.9$ quoted in the earlier experiment of Leventhal *et al.* (1978) but not inconsistent. The question of the expected value of f has been considered by Bussard, Ramaty and Drachman (1979) and later authors (e.g. Ramaty and Lingenfelter 1992), and it seems that the observed values are in the expected region in the sense that both the line width and the f values would be consistent with positrons annihilating and forming positronium in a warm, mildly ionised plasma,

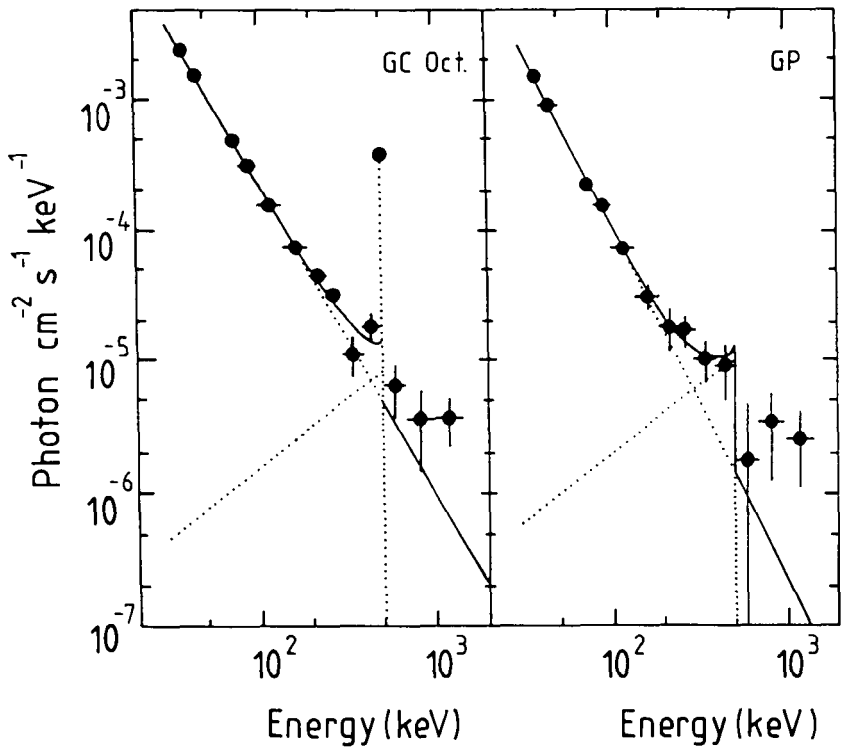

Figure 2.5. Energy spectra and model fits to the GRIS observations in 1988 of the Galactic Centre (GC) and the Galactic Plane (GP). After Gehrels *et al.* (1992).

a not unexpected environment for the Galactic Centre region. In fact, there are complications arising from the presence of the diffuse component, a component that will be discussed later.

Turning to the time variability, Figure 2.6 shows the situation. The variability, which seems quite genuine, suggests that the object is confined in space, presumably to less than about a light year (or, more precisely, the e^+e^- annihilation region is localised within this magnitude). It is interesting to note that a somewhat similar variability has been seen in the hard X-ray region.

The evidence for a diffuse component, associated with positrons annihilating in the ISM, comes from the observation that the detected fluxes are somewhat bigger for those detectors with bigger opening angles; see Share *et al.* (1988, 1990). These authors working with their detector of 130° aperture on the Solar Maximum Mission (SMM) satellite reported a flux of $(2.1 \pm 0.4) \times 10^{-3}\,\mathrm{cm}^{-2}\,\mathrm{s}^{-1}$, if attributed to a point source at the Galactic Centre. However, comparison of this SMM flux with upper limits ($< 5 \times 10^{-4}\,\mathrm{cm}^{-2}\,\mathrm{s}^{-1}$; see Figure 2.6) obtained with narrow aperture (15° FWHM) germanium spectrometers during contemporaneous balloon flights in 1981 and 1984 suggests that much of the radiation observed by SMM comes from an extended region.

There are many possible forms for the 511 keV line emission as a function of

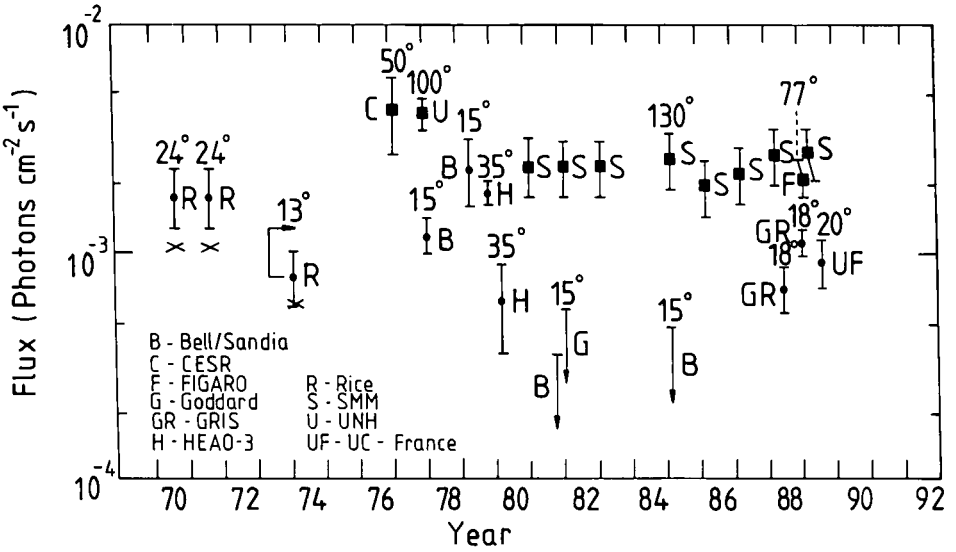

Figure 2.6. Time variability of the Galactic Centre 511 keV positron annihilation time (summarised by Gehrels *et al.* 1992).

position in the Galaxy, but of these the distribution of 'young objects' can be chosen as *a priori* likely. A good indicator is the measured CO distribution, and in this case the SMM observations yield a flux of $(1.6 \pm 0.3) \times 10^{-3}$ cm^{-2} s^{-1} rad^{-1} towards the Galactic Centre.

It seems likely that the Galactic output in annihilation γ-rays is roughly the same for the diffuse component and the Galactic Centre source, when the latter is active.

A recent significant advance in the observations of γ-ray lines has been made by a Franco–Soviet collaboration team. These authors (Sunayaev *et al.* 1992) have observed the Galactic Centre on three different occasions with their SIGMA telescope (angular resolution = 2′) aboard the GRANAT satellite, on March 24, April 8, and October 13/14, 1990. During the first two observations the authors found the X-ray source IE 1740.7-2942 to emit photons up to several hundred keV without any evidence for the 511 keV line emission. In their October observation, on the other hand, the authors found that the source emitted a strong 511 keV line. These observations not only identify the source ($\sim$100 pc away from the Galactic Centre) but confirm the variable nature of the source once again.

The models put forward to account for the above features will be discussed in the next section.

2.3.3 *Models for the origin of the 511 keV line*

A comprehensive study of models has been made by Lingenfelter and Ramaty in a number of publications (e.g. 1982, 1989) and their studies will be followed here.

A two-component nature for the emission from the Galactic Centre region appears very likely, as remarked already.

Starting with the discrete source (or possibly sources) at or near the Galactic Centre itself, most models involve the presence of a black hole. One idea is that γ–γ collisions are the source of the electron–positron pairs, the positrons then annihilating in the vicinity of the black hole to generate the detected 511 keV lines. The requirements indicate that the size of the photon–photon interaction region should be less than a few times 10^8 cm. Ramaty and Lingenfelter (1992) argue that a black hole mass of less than several hundred solar masses would suffice for this mechanism. Such a mass is much less than the $10^6 M_\odot$ or to sometimes invoked to explain various Galactic Centre phenomena (such as the origin of some of the energetic cosmic ray flux). The massive black hole has often been hypothesised to explain the 511 keV line too by way of photon–photon collisions in a narrow beam or by interactions of the beam with gas clouds. The choice between these possibilities has yet to be made – in fact it is not inconceivable that there are several black holes at the Galactic Centre.

The width of the line contains information about the nature of the medium in which the annihilations occur. Bhattacharya and Gehrels (1992) argue that one possibility is that the production is in a plasma of temperature $\simeq 10^5$ K; another possibility is that the annihilations are in a narrow disk orbiting the black hole in the plane of the observer. In the latter case it is the orbital motion of the region round the black hole that causes the observed line width.

A final remark that can be made about the Galactic Centre source is that it may be the X-ray source IE 1740.7-2942 as remarked already. This source is probably associated with a relativistic positron–electron plasma; again, a black hole is postulated in which an accretion disk is involved.

Turning now to the diffuse 511 keV line it would be surprising if there were not a significant distributed flux from the annihilation of the many positrons generated as β-decay products of unstable nuclei in the ISM. As with ^{26}Al, there are many sources of the radioactive nuclei: supernovae, novae, Wolf–Rayet stars, pulsars and cosmic rays. The detected level referred to earlier is not unreasonable. Many calculations have been made of the expected line shape, and these should be useful when the necessary precise measurements are available. A number of factors are relevant, most particularly the nature of the (extended) medium in which the annihilations occur: the different phases (hot and cold) of the ISM and their degrees of ionisation and the extent to which the positrons are able to penetrate the cold cores of gas clouds.

2.4 Gamma-ray lines from other Galactic objects

2.4.1 The Crab pulsar and nebula

Extensive measurements have been made of the Crab region at all wavelengths, from long radio waves to ultra high energy γ-rays. The situation with respect to γ-ray lines is not as clear cut as would have been hoped, with no measurement, as yet, being statistically very strong. However, there is some evidence for a line in the region 73–79 keV and another in the range 400–455 keV and these are significant enough for a description to be given.

A good review has been given recently by Owens (1992), and this will be followed. Starting with the range 73–79 keV the first detection is credited to Ling *et al.* (1979), the paper referring to balloon observations in 1974 (the long delay between observation and publication is indicative of the extraordinary care that is needed in data analysis in order to extract the small signal from the background). The mean photon energy was 73.3 ± 1 keV and the flux $3.8 \pm 0.9 \times 10^{-3}$ cm^{-2} s^{-1}.

From 1974 to 1990 (date of observation) five experiments have reported finite fluxes in the 73–79 keV range, all the observations being at the 3–4σ significance level. Other experiments have given upper limits below the claimed fluxes. If the signals are genuine it must be concluded that the output is variable – a not too unlikely result. Of considerable interest is an apparent slow increase in line energy, from $\sim$73 keV at the beginning of the period to $\sim$78 keV more recently.

The facts have given rise to a model in which the line represents cyclotron emission in the tera-gauss magnetic field of the Crab pulsar such that the emission region is moving radially outwards as time progresses. In consequence the gravitational red-shift falls with time and the γ-ray line energy increases. It can also be added that there is other evidence (Strickman, Kurfess and Johnson 1982) favouring involvement of the pulsar.

Turning to the 400–455 keV region, the subject started with the report by Leventhal, MacCallum and Watts (1977) of a line at 400 keV of width less than 3 keV (FWHM) and flux $2.24 \pm 0.65 \times 10^{-3}$ cm^{-2} s^{-1}, from a balloon experiment on May 10–11, 1976. This flux was higher than the 3σ upper limit of 1.7×10^{-3} cm^{-2} s^{-1} placed on the line some two years earlier by Ling *et al.* (1979).

An important search was made by Mahoney *et al.* (1984*a*,*b*) using the HEAO-3 detector. Although during normal operations the spin axis of the 'observatory' was pointed towards the Sun, during two periods in 1979 and 1980 its spin axis was oriented towards a Galactic Pole so that the C-1 instrument (γ-ray spectroscopy experiment) which was mounted perpendicular to the spin axis, scanned the Galactic Equatorial Plane. The Crab passed within 20° of the 'look axis' for 18 days in the autumn of 1979 (from September 23) and for 41 days in the spring of 1980 (from February 24). The data accrued therefore represent the best available to date.

The results showed no evidence for line emission from the Crab pulsar at an energy above 100 keV at the 3σ level of about 2×10^{-4} cm^{-2} s^{-1}, the value corresponding to an assumed incident line with an intrinsic width less than the energy resolution of the instrument.

Notwithstanding this important null result, a number of other observations have been made claiming signals at the 2–4σ level and covering the range 1×10^{-4} to 7×10^{-3}, together with upper limits, although none as low as the Mahoney *et al.* value. Again, time-variability must be claimed.

In a remarkably similar fashion to the case for the (73–79) keV line, there has been a steady upward drift in energy, from $\sim$400 keV in 1977 to $\simeq$450 keV in 1990.

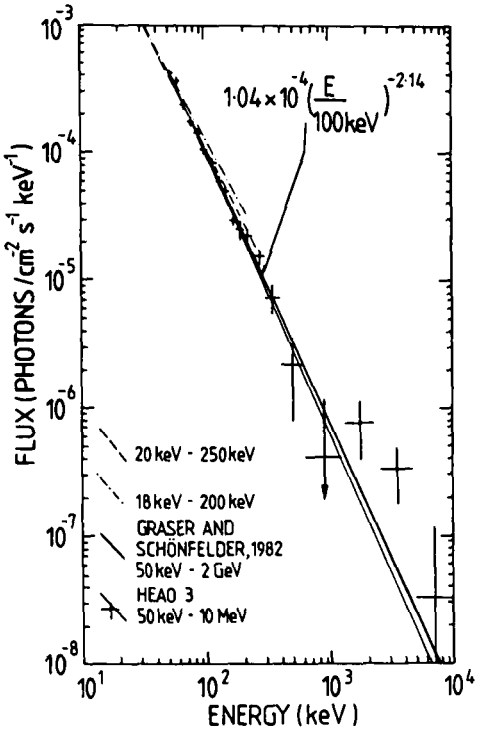

Figure 2.7. Energy spectrum of the Crab pulsar averaged over the whole phase, from the HEAO-3 experiment and other observations (after Mahoney *et al.* 1984*a,b*). Previous estimates are also shown. The heavy line is the best power law fit to the HEAO-3 data.

The usual explanation for this line is that it is an e^+e^- annihilation line gravitationally red-shifted because of the proximity of its production region to the pulsar surface. It seems that a drift in production region away from the pulsar surface as for the lower energy line would give a good explanation of the phenomenon.

Although not strictly relevant to the line problem, mention should be made of the rather precise measurement of the pulsed continuum γ-ray flux from the Crab pulsar with the HEAO-3 experiment. The phase-averaged spectrum was measured from 50 keV to 10 MeV and found to be consistent with a single power law, in agreement both in spectral index and intensity with the earlier analysis of Graser and Schonfelder (1982). Figure 2.7 shows the spectrum.

The 'light curve' of the γ-ray emission in this energy band is very similar to that at higher γ-ray energies, namely two main peaks of approximately equal intensity connected by strong interpeak emission. There was no significant change in the profile over the six months separating the observations, unlike the situation at higher energies (to be described in Chapter 4) where some variability has been reported in the observed light curve.

2.4.2 SS 433

SS 433 is a remarkable object, some 5.5 kpc away, which appears to comprise oppositely directed jets of relativistic material ($v \approx 0.26c$; see Abell and Margon 1979, Milgrom 1979), and it is an obvious candidate for γ-ray searches. HEAO-3 (Lamb *et al.* 1983) searched for emission from the direction of SS 433 and found a signal which is present at the 6σ level. The line in question was at 1.5 MeV and appeared variable by a factor of three on a time scale of days during the 46-day observation period. Figure 2.8 shows the result. In addition, the authors also saw a line at 1.2 MeV. Although there is no doubt about the veracity of the signal, the identification with SS 433 is somewhat uncertain in view of the poor angular resolution of the detector (FWHM 30°). Nevertheless, we proceed with the assumed identification in the following discussion.

The line near 1.5 MeV was detected at a level of $2–4\sigma$ in each of a series of three intervals, and it is the superposition of six such sets of data which gives rise to the results shown in Figure 2.8. Inspection of likely γ-ray line energies shows none at the energy detected, and Lamb *et al.* were thrown back on the hypothesis of red- or blue-shifted lines. Two stand out as candidates: a blue-shifted decay of the first excited state of ^{24}Mg at 1.369 MeV or a red-shifted decay of the first excited state of ^{28}Si at 1.779 MeV. Of these the workers chose ^{24}Mg as the more likely emitting isotope since there is also some evidence for a red-shifted ^{24}Mg line at 1.2 MeV, and this would be expected on the basis of the twin-jet model of SS 433. Although the precision is poor, there is also the suggestion of a change of line energy with time, such as would be expected from the model which explains the optical features, namely a precession of the axis of the jets with a 163.51-day period (Margon 1982). This feature increases confidence in the results somewhat.

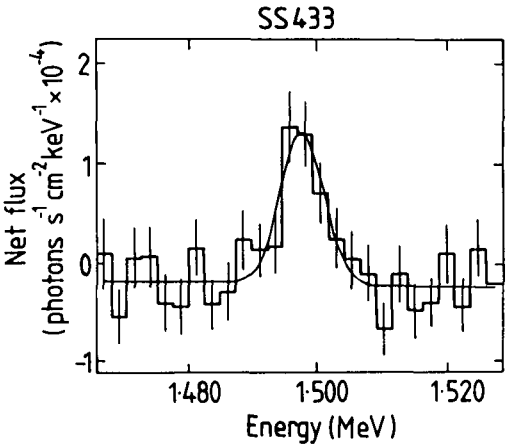

Figure 2.8. Averaged γ-ray flux from the region of SS 433 within ± 30 keV of the 1.5 MeV feature, as detected by HEAO-3 (Lamb *et al.* 1983). The centre of the 'line' is at 1.497 MeV and the shape is 'consistent with a Gaussian of FWHM $\approx$9 keV'.

The authors found no evidence for the unshifted 1.369 MeV line and placed a 3σ upper limit at 1×10^{-3} photons cm^{-2} s^{-1} for this line.

Turning to the energy involved, this is considerable. If the lines correspond to near isotropic emission (likely even though the particles initiating the γ-rays are collimated in two jets), a γ-ray line luminosity of 2×10^{37} erg s^{-1} results. This is about 250 times that emitted in the X-ray region from 2 to 10 keV.

The theoretical estimates of the particle beam kinetic energy are in the range 10^{38}–10^{41} erg s^{-1} (Begelman *et al.* 1980, Davidson and McCray 1980) so that the γ-rays may well represent a significant fraction of the beam energy.

Lingenfelter and Ramaty (1985) have argued that the fact that the γ-ray and optical Doppler shifts are similar implies that the Mg nuclei are moving essentially at the flow speed (0.26c) of the jets. If the Mg nuclei are excited in their inelastic collisions with the ambient protons, the velocity differential between the protons and the Mg nuclei must lie in a narrow range of 0.07c to 0.09c so that the protons have sufficient energy to excite the line but not too much energy to broaden it excessively. For further discussions on line-narrowing effects and Mg nuclei embedded in grains, the reader may refer to Lingenfelter and Ramaty (1985).

Despite the apparent reliability of the earlier measurements, there now seems to be some difficulty in accepting the reality of this line. Geldzahler *et al.* (1985) did not find the line with their γ-ray spectrometer on the SMM and placed an upper limit (99% confidence limit) of 2×10^{-4} cm^{-2} s^{-1}, averaging their observations over 360 days. This upper limit has to be compared with the detected intensity level of 10^{-3} cm^{-2} s^{-1} reported by Lamb *et al.* (1983). MacCallum *et al.* (1985) have also failed to detect the lines in an observation with a balloon-borne germanium detector. Time variability of the signal may be invoked to explain the result. In summary, the 1.369 MeV line emission from SS 433 needs to be confirmed in another observation.

The interesting topic of γ-ray lines from *transient* sources is taken up in Chapter 3.

2.5 SN 1987A

Although it is true to say that the most dramatic science to come from SN 1987A – the supernova that exploded in the Large Magellanic Cloud on February 23, 1987 – was the observation of the intense pulse of neutrinos, the detection of γ-ray lines came a close second. The γ-ray observations have proved without doubt that the fundamental tenet of the origin of most of the elements, by way of explosive nucleosynthesis, is basically correct.

The basic principle is that after core collapse following the exhaustion of the nuclear fuel, a shock wave propagates through the inner layers of the parent star and heats the material, which is enriched by heavy elements, to a temperature of order 5×10^9 K. The dominant end product is ^{56}Ni, which has a radioactive half-life of 6.1 days for decay via electron capture to ^{56}Co. This element is also unstable ($T_{1/2}$ = 77.1 days) against decay; other radioactive nuclei are also produced.

The γ-rays are emitted with an intensity dependent on the degree of absorption

in the shell, a quantity that will clearly depend on its clumpiness. The line shape will be affected by the velocity of the layers emitting the detected lines and one might hope to identify both forward and backward moving components.

The supernova shell is expected to remain optically thick to γ-rays for a period varying from months to years (the actual time being energy dependent). Initially a multiply scattered continuum will appear, but as the optical depth diminishes the fraction of γ-ray energy which emerges in the form of lines will be expected to increase. For the first 1000 days the principal lines are from the decay of ^{56}Co to ^{56}Fe (847, 1238 and 2599 keV) and at longer times ^{57}Co will dominate. At still longer times ^{44}Ti should take over.

Teegarden (1992) has recently summarised the results found for SN 1987A and his summary can be followed.

The progenitor star was a blue supergiant (SK-69202) with a main sequence mass of $\simeq 20M_\odot$, although at the time of the explosion mass loss appears to have reduced this to $\simeq 16M_\odot$. The star would have had a $6M_\odot$ helium core surrounded by a $10M_\odot$ envelope.

One does not expect to see the γ-rays for a few hundred days after the explosion because of the absorption in the overlying material. As the supernova expands, it must eventually become thin to the γ-rays emitted by the nuclear decays in its own centre. According to Woosley (1988*a*,*c*) the column depth in SN 1987A is $5 \times 10^4 t_6^{-2}$ g cm^{-2}, with t_6 being the age in units of 10^6 s. One can then expect to see γ-rays only after about a year has elapsed from the explosion. Before that time γ-rays are degraded to below 20 keV X-rays by Compton scattering and then totally absorbed due to the enormous photoelectric opacity. One expects that, for a year or so, γ-rays provide thermal energy which in turn powers the light curve of the supernova. The observations on the bolometric light curve of SN 1987A, showing an exponential decay with a half-life of 77.1 days, are indeed consistent with the decay of $0.075M_\odot$ of ^{56}Co powering the light curve. This fact in itself is a proof of nucleosynthesis taking place in supernova envelopes, leading to the production of ^{56}Ni decaying into ^{56}Co.

Surprisingly, X-rays from SN 1987A were seen as early as 100 days after the explosion; see Dotani *et al.* (1987). Very soon after this, γ-rays were seen. The fact that these signals come approximately 100 to 150 days earlier than anticipated has necessitated major modifications to the theory. The first observations of γ-ray lines were made by the SMM (Matz *et al.* 1988*a*,*b*) about 150 days after the explosion and confirmation followed from a number of balloon observations.

A summary of the data of the important 847 and 1238 keV lines is given in Figure 2.9. The rise time corresponding to a gradual thinning of the shell and the radioactive decay can be seen. It will also be noted that the errors are large – in all cases the signals have been extracted from rather large backgrounds.

The fact that γ-ray emission appeared as early as 150 days after the explosion showed that the emitting layers were not situated deep in the supernova shell but were mixed with the outer high velocity layers. Many studies have been made of the mixing process, and predictions have been made for a variety of scenarios. Agreement appears if it is assumed that the outermost material has a velocity of

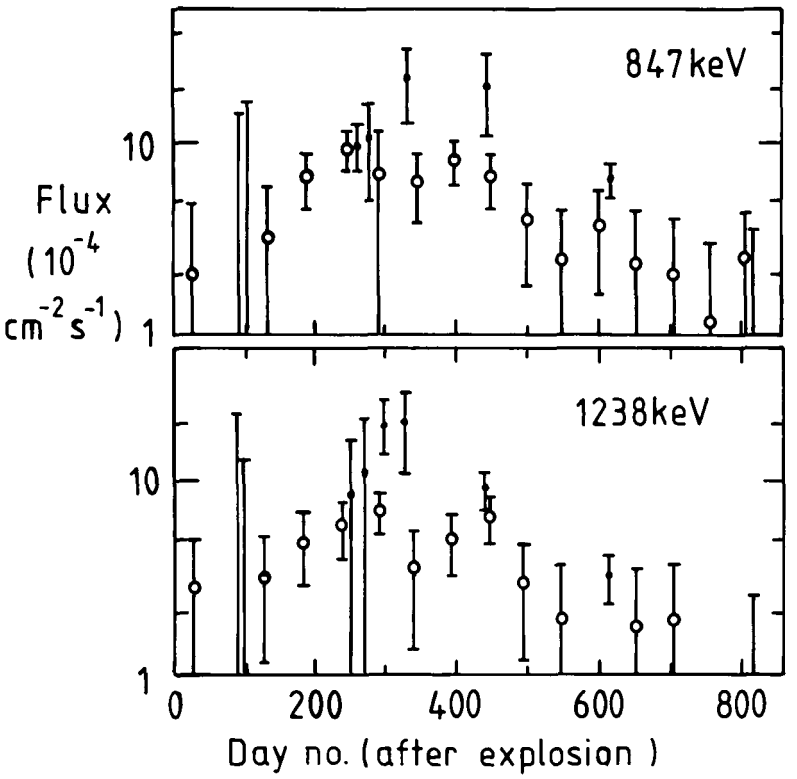

Figure 2.9. Summary of data on the fluxes of γ-ray lines at 847 and 1238 keV as a function of time (after Teegarden 1992).

3–4000 km s^{-1}, and a consequence is that the lines should be significantly broadened. In fact, the observed line width (after 300–600 days) is ~ 10 keV, some 5 keV wider than would be expected; furthermore, the expected 'blue-shift' at early times – due to material coming towards us providing more of the flux when the optical depth is high – has not been seen.

The most likely explanation of the results is that the shell of SN 1987A is clumpy so that the optical depth is small, in places, at earlier stages than would be appropriate for a constant density shell. Supporting evidence for this hypothesis comes from observations at both optical and infra-red wavelengths. The X-ray light curve shows an extended tail, again suggesting clumpiness, which means that even at long times part of the shell is optically thick. Finally, hydrodynamic theory suggests the presence of Rayleigh–Taylor instabilities for the conditions of the shell.

2.6 Gamma-ray lines from other galaxies

2.6.1 A search for lines from near-normal galaxies

The HEAO-3 satellite has been used by Marscher *et al.* (1984) to search for the 511 keV annihilation line from what the authors term 'mildly active

Table 2.2. *Expected flux and observed limits to the 511 keV line, from the work of Marscher* et al. *(1984)*

Expectation is based on a mean Galactic Centre flux of 1.3×10^{-3} cm^{-2} s^{-1} and the assumption that the line strength is proportional to the radio flux.

Galaxy	F_{511} (expected) (10^{-4} photons cm^{-2} s^{-1})	F_{511} (observed upper limit) (10^{-4} photons cm^{-2} s^{-1})
M81/M82	5.3	<2.4
NGC 4278	9.2	<3.5
M104	1.4	<3.9
NGC 6500	3.7	<2.8
NGC 2911	3.7	<2.2
NGC 262	4.6	<2.5

galaxies', in that these galaxies have somewhat active central regions similar to our own. On the basis of a simple model for the γ-ray line emission mechanism from the Galactic Centre in which γ-ray emission is related to radio emission, these workers estimate that five of the six galaxies studied should have detectable fluxes (see Table 2.2). In practice none was detected, and for these five the 98% upper limit was less than the expected flux.

The obvious conclusion to be drawn is that the model is inapplicable. A number of possibilities arise. For example, the Galactic Centre measurements may refer to an unusually 'high' period in its certainly variable output characteristic. Another obvious possibility is that the Galactic Centre γ-rays are beamed. A further idea is that the 'mildly active' galaxies do in fact have sufficient activity to eject part of the target gas from the region where the positrons would be expected to annihilate. Further Galactic Centre observations should help test at least the first hypothesis.

2.6.2 Gamma-ray lines from Centaurus A

γ-ray lines at 1.6 and 4.4 MeV have been reported by Hall *et al.* (1976), although the 511 keV line was not seen. Fabian *et al.* (1976) have put forward a possible explanation in terms of quasi-thermonuclear reactions near a black hole, where the absence of the 511 keV line could be due to the smearing effect of large Doppler broadening in the hot accretion gas. Clearly it would be wise to have confirmation of the lines before pushing conjecture too far.

It must be added that even the 1.6 and 4.4 MeV lines seen by Hall *et al.* (1976) were not seen in the observations made by Gehrels *et al.* (1984, 1987), Von Ballmoos *et al.* (1987) and Baity *et al.* (1981).

2.6.3 Gamma-ray lines from active galaxies

The Seyfert galaxy NGC 4151 has been detected in the MeV region by a number of authors. Although lines have not been claimed yet, the steepening of

the γ-ray spectrum above a few MeV (see Dean and Ramsden 1981 for summary) – which may well be a feature of Seyferts – *could* be due to a number of unresolved lines in the MeV region, thereby accentuating what would otherwise have been a gradual change of slope. This feature is relevant to the interpretation of the so-called diffuse flux of extragalactic X-rays and γ-rays (see Chapter 4).

Future plans for line measurements are considered in Chapter 4, and we shall see that the GRO has potential here.

2.7 Summary

It will be clear from what has been written that γ-ray line astronomy has started in earnest with a number of interesting and widely different phenomena.

At the lowest energies, there is the detection of the e^+e^- annihilation line from the Galactic Centre region. Although the linear dimension of the 'source' cannot be determined experimentally, the time variability over a period of years strongly suggests that the source is 'small' ($\lesssim 1$ pc); the time variability is also of importance because of its relevance to the mechanism of line formation and of the origin of the parent positrons. An exotic 'engine' generating these particles is indicated.

Moving to the interstellar medium, a strong line at 1809 keV, presumably due to ^{26}Al, has been detected. Its strength appears to be excessive in comparison with expectation for the ejecta of supernovae. The much more common novae may be contributing significantly.

Lines have also been detected from discrete celestial objects, specifically the Crab nebula and the remarkable object SS 433. Concerning the latter, there appears to be evidence for the Doppler shift in energy in line with the twin-jet model; this feature is an excellent example of how powerful γ-ray line studies will be for a whole collection of objects once measurements of adequate statistical precision are available.

Finally, the unexpected supernova in the Large Magellanic Cloud, SN 1987A, has produced a wealth of data; allied with data from the Crab pulsar the whole range of supernova/pulsar phenomena is now available for study.

3

Gamma-ray bursts

3.1 Introduction

The discovery of γ-ray bursts was serendipitous, as was that of pulsars, which were discovered at about the same time. Pulsars were first detected in 1967 in an experiment designed to study interplanetary scintillation of compact radio sources, and the discovery paper (Hewish *et al.* 1968) was subsequently published; the first γ-ray burst (GRB) was also seen in the year 1967 (although not reported until six years later; see Strong and Klebesadel 1976 for an account of the chronology) in a satellite-borne detector intended to monitor violations of the nuclear explosion test ban treaty. The publication of the discovery of GRBs was first made in 1973 by Klebesadel, Strong and Olson (1973). The detector comprised six caesium iodide scintillators, each of 10 cm^3, mounted on each of the four Vela series of satellites (5A, 5B, 6A and 6B), these vehicles being arranged nearly equally spaced in a circular orbit with a geocentric radius of $\sim 1.2 \times 10^5$ km. The detectors were sensitive to individual γ-rays in the approximate energy range 0.2–1.5 MeV and the detector efficiency ranged from 17 to 50%.* The scintillators had a passive shield around them; background γ-ray counting rates were routinely monitored. A statistically significant increase in the counting rates initiated the recording of discrete counts in a series of quasi-logarithmically increasing time intervals. The event time was also recorded. Data were telemetered down to the ground-based receiving stations. Unexpectedly large increases in the γ-ray counting rates that occurred nearly simultaneously in detectors on at least two different widely separated spacecraft heralded the discovery of the phenomenon of GRBs.

In their discovery paper, Klebesadel *et al.* (1973) reported the detection of 16 bursts during the three-year period July 1969 to July 1972. The time histories of one of the bursts (GRB 700822)† as seen by detectors on three separate spacecraft

* In many situations the term 'γ-rays' is applied only to quanta with energies greater than several hundred – perhaps 511 – keV. In the context of GRBs, it is customary to designate all quanta with energies of some 20 keV and above as 'γ-rays', for one finds a continuous spectrum of quanta all the way from 20 keV to several tens of MeV energies in the bursts, with the energy output reaching a maximum in the MeV region.

† It is customary to denote a GRB by the notation GB or GRB ijklmn, where ij, kl and mn refer to the year, the month and the date on which the burst occurred. If more than one burst was seen on a given date, an additional symbol a, b, c, ... is added in the order (in time) in which they occurred. If the source direction of a GRB is determined to an accuracy of better than 1°, the source is referred to as GBS ijklmn where ij, kl refer to right ascension (hours, minutes) and mn to declination (degrees).

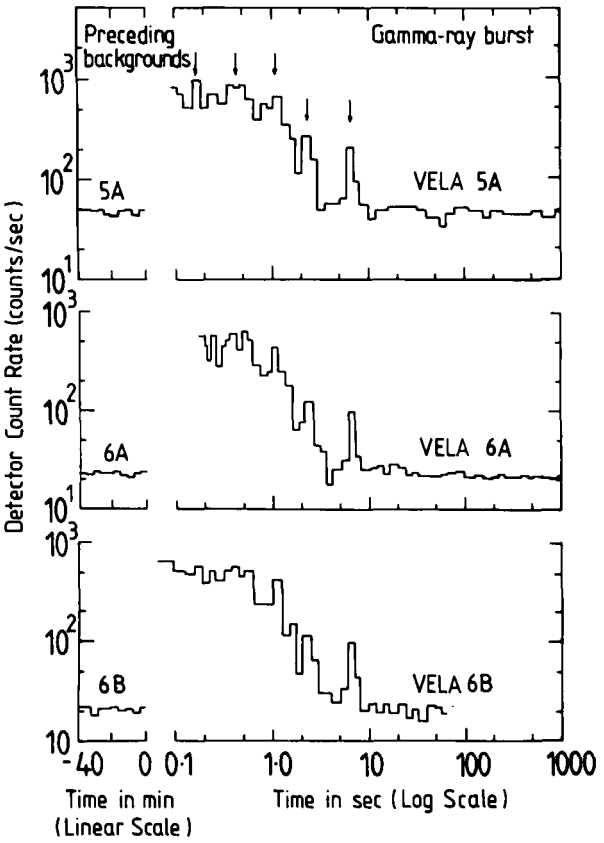

Figure 3.1. Count rate as a function of time for GRB 700822 as recorded at three VELA spacecraft by Klebesadel *et al.* (1973). Arrows indicate some of the common structure. Background rates immediately preceding the burst are also shown. VELA 5A count rates have been reduced by 100 counts s^{-1} (a major fraction of the background) to emphasise structure.

are shown in Figure 3.1. The near coincidence in the time of occurrence, of an order of magnitude increase in the counting rates, and similarities in burst profile features in more than one detector, left no doubt about the reality of the phenomenon. The burst shown in Figure 3.1 had an integrated flux density $\sim 8 \times 10^{-5}$ erg cm^{-2}. The arrival times of the event at different spacecraft were recorded to an accuracy of 0.05 s. From the finite differences in these times and the known positions of satellites in space, it was possible to deduce the arrival direction of the GRB by triangulation. From such knowledge, the Sun and Earth were ruled out as the sources of the 16 GRBs reported, though an additional burst from the direction of the Sun was seen. Colgate (1968) had predicted, before the discovery was announced, that intense emission of prompt γ-rays could occur during the initial stages of the development of supernovae; however, there does not seem to be any correlation between the GRBs and reported supernovae seen at optical wavelengths, and another mechanism is necessary.

Following the announcement of the discovery of GRBs, groups all over the world built dedicated instruments to study this exciting phenomenon, and these have since been flown in geocentric and heliocentric orbiting spacecraft and on planetary probes in order to have improved direction information.

To date more than 500 GRBs are positively known and several hundred more have probably also been detected, but we await their analysis and publication. For catalogues of GRBs listing their various characteristics, see Mazets *et al.* (1981*b*), Klebesadel *et al.* (1982), Baity *et al.* (1984), Atteia *et al.* (1987*a*), Golenetskii *et al.* (1987*a*) and Mitrofanov *et al.* (1989).

GRBs are highly individualistic, each being unlike any other in some features. Their time histories are much more disparate than their energy spectra, which can in themselves be quite distinctive. Any gross description of GRBs as a class has therefore to be necessarily crude. One such description follows: the size or 'fluence' (integral of flux over time) for most of the GRBs is in the range 10^{-7}–10^{-3} erg cm^{-2}. At a typical flux of 10^{-5} erg cm^{-2} s^{-1}, and a typical distance of 1 kpc, the luminosity ($\sim 10^{39}$ erg s^{-1}) surpasses for a brief time that of the diffuse background γ-radiation over the entire Galaxy. The duration of a GRB ranges from a few tens of milliseconds to several hundreds of seconds. Except in three cases (GRB 790305b, GRB 790107 and GRB 790324), there is no direct and strong evidence to show that they recur. These three recurrent sources are known as 'soft repeaters' (because of the soft energy spectrum of the γ-rays they emit) and are denoted as GBS 0526−66, GBS 1806−20 and GBS 1900+14, respectively. We will consider them in greater detail later in Section 3.3.4. Some of the bursts exhibit absorption (intensity lower than the continuum) or emission (intensity higher than the continuum) features in their energy spectra.

The single most remarkable GRB (GRB 790305b) occurred on March 5, 1979 (Mazets *et al.* 1979*a*,*b*). The question of whether it is truly unique or an extreme example of a class of bursts is not yet settled. This GRB merits a mention of a few of its features. It is the most intense GRB observed to date at a fluence of $> 10^{-3}$ erg cm^{-2} and has the smallest rise time ($\lesssim 0.25$ ms). An 8 s periodicity in emission following the impulsive phase was established by several groups, and a quasi-periodicity with a period of 23 ms has been claimed by one group (Barat *et al.* 1983). It was seen by no fewer than nine different detectors. Its source direction was the most precisely determined among all the GRBs, with an error box ~ 0.1 arc min^2 (Cline *et al.* 1982). Apparently it is associated with the SNR N49 in the Large Magellanic Cloud situated at a distance of 55 kpc (see the reviews by Cline 1980, 1982). The Leningrad* group, however, has persistently questioned this association (see, for example, Mazets and Golenetskii 1981*a* and Golenetskii, Ilyinkskii and Mazets 1984), arguing that, at source distances greater than 1 kpc, the Eddington luminosity limit is violated. If the association is true, it makes this object the only certain extragalactic GRB source detected so far. It must be remembered that a nearby neutron star, not detected at radio wavelengths, cannot

* To avoid confusion, we have retained the place names that were in use when the work was carried out. Hence, Leningrad (now St. Petersburg) is appropriate here.

be ruled out. This GRB source is also one of the three clear cut cases of recurrent bursts.

Although there was initially a plethora of potential models for GRB sources (see, for example, Ruderman 1975), the majority opinion today favours highly magnetised neutron stars as the GRB sources. The actual mechanism of γ-ray production is not yet agreed upon, but the basic energy source powering the burst is expected to be gravitational or nuclear binding energy.

References to much of the experimental and theoretical work on the subject can be found in papers published in the proceedings of the following conferences: (*a*) the 1979 Toulouse conference (France), *Astrophys. & Space Sci.* (1981) **75**, 5–224; (*b*) the 1980 Royal Society Meeting (UK), *Phil. Trans. Roy. Soc. Lond.* (1981), **A301**; (*c*) the 1981 La Jolla Conference (USA), *Am. Inst. Phys. Conf. Proc. 77* (1982) (Lingenfelter, R.E., Hudson, H.S. and Worrall, D.M., eds); (*d*) the 1982 Garching Conference (Germany), *Max Planck Institute Report 177* (1982) (Brinkmann, W. and Trumper, J., eds); (*e*) the 1983 Goddard Conference (USA), *Am. Inst. Phys. Conf. Proc. 101* (1983) (Burns, M.L., Harding, A.K. and Ramaty, R., eds); (*f*) the 1984 Santa Cruz Conference (USA), *Am. Inst. Phys. Conf. Proc. 115* (1984) (Woosley, S.E., ed.); (*g*) the Stanford Workshop (1986), *Am. Inst. Phys. Conf. Proc. 141* (1986) (Liang, E.P. and Petrosian, V., eds); and (*h*) the COSPAR Symposia Proceedings, which appeared in *Adv. Space Res.*, **6** (4) (1986) (Hurley, K. and Vedrenne, G., eds), **8** (2–3) (1988) (White, N.E. and Filipov, L.G., eds), and **10** (2) (1990) (Bleeker, J.A.M. and Hermsen, W., eds). The reader may also consult the reviews by Zdziarski (1987), Golenetskii (1988), Hartmann and Woosley (1988), Klebesadel (1988), Lamb (1988), Mazets (1988), Hurley (1989*a*,*b*), and Higdon and Lingenfelter (1990).

The subject of GRBs is one of the areas in astrophysics that is being pursued most vigorously both experimentally and theoretically. In the next section we will present a few details of the detectors that are employed in their study. Typical results on time histories and energy spectra are presented in Sections 3.3 and 3.4, respectively. Section 3.5 deals with efforts to identify GRB source objects with those seen at other wavelengths. This is followed by a presentation of the statistical distributions of GRBs (in intensity and in galactic coordinates) in Section 3.6. We will then present a discussion of source models in Section 3.7, before ending the chapter with a brief summary.

3.2 Detectors and instrumentation

The guiding principles in the design of the recent GRB detectors have been (i) to attain as low a detection threshold as possible, affording nearly bias-free statistical analysis of GRBs; (ii) to have a good energy resolution, allowing better delineation of spectral features; (iii) to have accurate event time information, resulting in a precise source direction determination; and (iv) to record many energy spectra over as short an integration time as possible to study fast spectral variability. Some of the detectors are mentioned below together with references where information can be found on them:

KONUS experiments of the Leningrad group (Mazets and Golenetskii 1981*b*);
SIGNE experiments of the Franco–Soviet collaboration (Barat *et al.* 1981, Boer *et al.* 1986);
ISEE-3, the International Sun–Earth Explorer experiment (Klebesadel, Evans and Laros 1981, Teegarden and Cline 1981);
SMM, the Solar Maximum Mission Experiment (Forrest *et al.* 1980);
HEAO-1 (Knight, Matteson and Peterson 1981);
PVO, the Pioneer Venus Orbiter Experiment (Evans *et al.* 1981);
GINGA, a Japanese satellite experiment (Murakami *et al.* 1989);
SIGMA, a French–Soviet high resolution detector (Paul *et al.* 1990);
BATSE, Burst and Transient Source Experiment (Fishman *et al.* 1985, 1989);
and a balloon-borne experiment (Fishman 1981), which was a prototype of BATSE on the GRO, which was launched in April, 1991.

This list is admittedly incomplete but hopefully representative.

3.2.1 Detector description

While referring the reader to the list of references given above, we elaborate here on just two detectors, chosen to illustrate the kind of instrumentation that is generally employed.

ISEE-3 Ge detector. The high resolution Ge detector (Teegarden and Cline 1981) was one of the several sensors aboard the ISEE-3 spacecraft launched in September, 1978, into a halo orbit about the Lagrangian point approximately 230 Earth radii radially inward towards the Sun. The high purity germanium crystal, 4.02 cm in diameter and 2.9 cm thick, is shielded from direct sunlight. It is also thermally insulated from the rest of the spacecraft and radiatively cooled, so that it remains at a constant temperature of 130 K. It has a resolution ~ 10 keV at 570 keV. The useful energy window is from 200 keV to 3 MeV. Instead of storing the number of counts in a succession of fixed time intervals, elapsed times for the occurrence of a ground commandable fixed number of counts (time-to-spill mode) are recorded with a command-selectable resolution of 0.12 to 1.0 ms. If time-to-spill does not exceed a ground-selectable value, a trigger is generated to initiate the data recording routines. Energy spectra are recorded with a time resolution of 8 ms. The 10-bit on-board memory, in which all this information is recorded, is dumped on to an earth station either automatically upon filling or, manually, on a ground command.

KONUS detectors. A block diagram of the sensors and instrumentation of the KONUS experiment (Mazets *et al.* 1983) aboard the spacecraft Venera 13 and Venera 14 is shown in Figure 3.2. There are six detectors on each spacecraft facing the six directions of a cartesian coordinate system. Each detector is a NaI(Tl) scintillator of diameter 8.0 cm, and of thickness 3.0 cm, and each has a passive

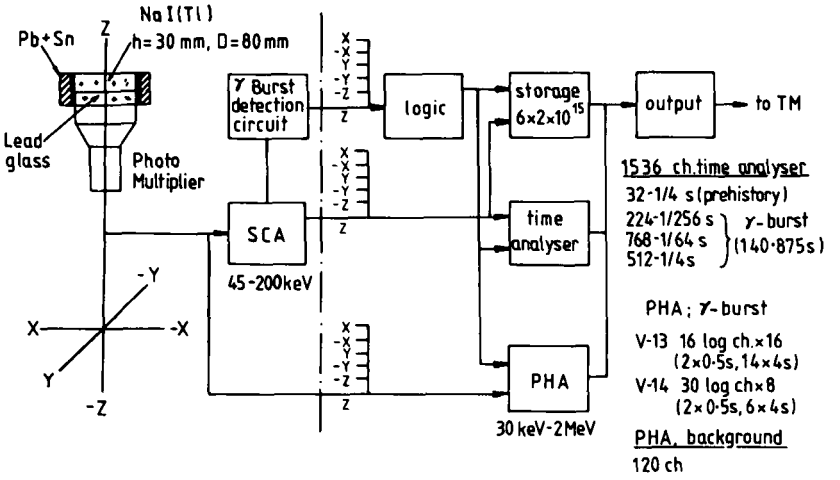

Figure 3.2. Block diagram of KONUS instrumentation for detectors aboard the spacecraft Venera 13 and 14 (Mazets *et al.* 1983).

shield on the sides made up of lead and tin. Background rates from each of the six sensors are monitored once in 20 min in the 45–200 keV energy range. When the counting rate over an integration time of 0.25 s significantly exceeds the average rate, a trigger is generated to initiate the processing of information from the six detectors. The time analyser stores the 8 s long prehistory with a resolution of 0.25 s, and measures the burst time profile for 0.875 s with a resolution of 1/256 s, then for the next 12 s with a resolution of 1/64 s, and finally for a further 128 s with a resolution of 1/4 s. Thus 8 s of prehistory and a total 140.875 s of post-trigger time profile on each GRB is recorded with a varying time resolution. γ-ray counting rates from each of the six detectors during the burst are recorded in 0.5 and 8 s time intervals. This information, when combined with the measured angle-dependent efficiency of each detector (which approximates to a $\cos\theta$ distribution, where θ is the angle of incidence of a GRB with respect to the normal to the detector face), yields information on the source direction. In order to have good statistics, and yet maintain correct energy assignment, the pulse height analysers (PHAs) are connected to the single detector that is most favourably oriented with respect to the burst source. The PHA on Venera 13 records 16 energy spectra over as many consecutive time intervals, two of 0.5 s and 14 of 4 s duration; each spectrum has 16 quasi-logarithmic energy bins. The 30 channel PHA on Venera 14 records eight consecutive energy spectra, two of 0.5 s and six of 4 s duration.

3.2.2 *Selection effects and observational biases*

Spurious events. First, there is the important problem of spurious events seen in only one detector that have nothing to do with the phenomenon of GRBs. For example, Mazets and Golenetskii (1981*a*) report several spurious bursts falling into this category. These are thought to be due to phosphorescence in the NaI(Tl)

crystal induced by high energy losses that occur in the detector when multiply charged cosmic rays pass through it or when nuclear spallation takes place (Fishman *et al.* 1978). In an experiment with two simultaneous balloon flights separated by several hundred kilometres, Cline *et al.* (1977) observed the occurrence of a wide variety of fluctuations in detectors on one balloon but not simultaneously on the other. These variations are presumably of magnetospheric origin and underline the need for a GRB to be seen by two or more detectors located far apart for it to be accepted as such.

Energy spectra. In any given experiment one actually records an energy loss spectrum, and this is related to the incident photon spectrum by the relation

$$N(E') = \int_{E'}^{\infty} F(E)P(E, E')\,\mathrm{d}E \tag{3.1}$$

where E' is the energy loss detected; E is the energy of the γ-ray; and $P(E, E')$ is the probability that a photon of energy E gives rise to an energy loss E' in the detector. The observed energy loss spectrum has to be deconvoluted to obtain the true photon spectrum on the basis of laboratory calibrations of the $P(E, E')$ matrix and a trial (assumed) photon spectrum, $F(E)$, for the GRB. It is of course the deconvoluted photon spectrum that forms the basis of any modelling.

Selection effects. Most of the experiments operate in the trigger mode; i.e. when the number of counts from a detector over a fixed integration time, τ, exceeds the background counts, $n_b\tau$, by a predetermined number, k, of standard deviations, a trigger is generated to initiate data recording. If the burst duration, T, is less than or equal to τ, then the detection threshold is given by

$$S_0 = k(n_b\tau)^{1/2} \tag{3.2}$$

If, on the other hand, the burst duration is much longer than τ (with no spikes in the burst) then the detection threshold becomes

$$S_T = S_0 T/\tau \tag{3.3}$$

i.e. it increases linearly with burst duration time T. Thus the detection threshold of a given experiment is a function of τ and k (which are experimenter settable) and T, and this introduces a selection effect. A moderately intense burst lasting for a very long time may never be recorded in an experiment because of this effect. Mazets and Golenetskii (1981*a*) have treated this problem mathematically and have found that, for a flat burst-duration distribution $\phi_T = 1/T_{max}$ for $0 \leq T \leq T_{max}$ the efficiency of recording a burst with a fluence S_0 is given by

$$\varepsilon(S_0) = \frac{\tau}{T_{max}}\left[3 - 2(\tau/T_{max})^{1/2}\right] \tag{3.4}$$

for a burst size distribution of the type $N(>S) \propto S^{-3/2}$ (see Section 3.6). For an S^{-1} distribution, the efficiency is given by

$$\varepsilon(S_0) = \frac{\tau}{T_{\max}}[1 + \ln(T_{\max}/\tau)] \tag{3.5}$$

Here $\varepsilon(S_0) = N_{\text{obs}}(S_0)/N_{\text{true}}(S_0)$. For example, if $\tau = 0.25$ s and $T = 3$ s, the detection efficiency for a burst with a fluence S_0 is 0.20 for $S^{-3/2}$ distribution and 0.29 for S^{-1} distribution. For very intense bursts, $S_0 \leq S \leq S_{\max}$, the detection efficiencies are likewise given by

$$\varepsilon(S) = \frac{S}{S_{\max}}[3 - 2(S/S_{\max})^{1/2}] \tag{3.6}$$

for an $S^{-3/2}$ distribution, and by

$$\varepsilon(S) = \frac{S}{S_{\max}}[1 + \ln(S_{\max}/S)] \tag{3.7}$$

for an S^{-1} distribution. When comparing data from different experiments, it is necessary to keep the above selection effects in mind. These effects obviously have a role to play in the interpretation of log N–log S curves (see Section 3.6).

3.3 Time histories

Time profiles provide important clues to understanding the nature of the GRB sources. As an illustration, it is well known that GRB 790305b exhibits an 8 s periodicity (Barat *et al.* 1979, Mazets *et al.* 1979*a,b*, Terrell *et al.* 1980, Cline, Desai and Teegarden 1981*a*). If this periodicity is due to the rotation of the burst source, one expects the centrifugal force at the surface of the source to be less than the gravitational force, which leads to a matter density of

$$\rho \geq 3\pi/GP^2 = 2.2 \times 10^6 \text{ g cm}^{-2} \tag{3.8}$$

where P is the period of rotation of the source object, and G is the gravitational constant. Densities in this range imply that the object has to be a white dwarf, a neutron star or an even more compact object. Furthermore, the very short risetime observed for this GRB ($\leq$0.25 ms) implies an emission region with linear dimensions $\gtrsim$100 km, which, when combined with a canonical solar mass, leads to densities $>10^{12}$ g cm^{-3}, leaving only neutron stars or higher density gravitationally collapsed objects as candidate sources for the GRB. Fast time scales also impose additional constraints on models in that they should adequately describe correspondingly fast energy transport to the emission regions. The implications of time histories for GRB source models are postponed to Section 3.7.

3.3.1 Burst profiles and durations

In discussing this topic we first emphasise that it is closely connected with the topic of energy spectra discussed in Section 3.4. As an example, Kuznetsov *et al.* (1987) have clearly demonstrated that the profile and duration of the burst

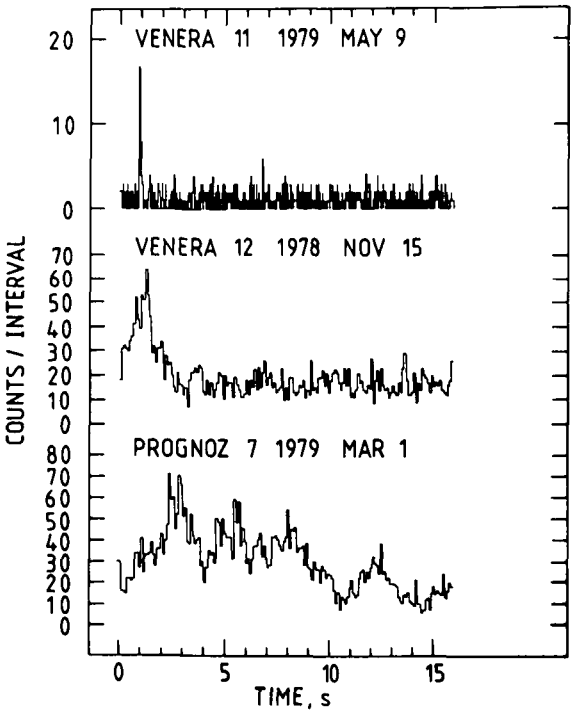

Figure 3.3. Three GRB histories from the Franco–Soviet SIGNE experiments, illustrating the three classes of bursts: very short (100 ms) events, long (1 s) events, and long complex events. The time histories are for the energy range 100–600 keV (Hurley 1983*a*).

GRB 830801b look different in different energy bands ranging from 39 to 7500 keV. This is clearly due to the variability of the energy spectrum. Also the delineation of time structure and duration depend on the size of the detector, data recording algorithms, memory size of the on-board data bank, and the distance to the source, besides, obviously, on the characteristics of the burst at production. At the moment efficiency of recording GRBs lasting for 20 ms is extremely low in most detectors. Likewise, most detectors cannot determine the exact duration of a GRB if it lasts for more than 200 s due to limitations in the data memory.

No two GRBs are completely alike in their time profiles. To illustrate this we present in Figure 3.3 profiles of three GRBs with three different burst durations (Hurley 1983*a*). In Figure 3.4 is shown the profile of a very short duration burst (Barat *et al.* 1984*a*). The time profile of GRB 790305b, shown in Figure 3.5, is unique. Note the very fast risetime (≤ 0.25 ms), the initial intense peak lasting for about 130 ms, and a series of pulsations following the impulsive peak. The peak intensity of this burst, at several times 10^{-3} erg cm^{-2} s^{-1}, is the highest recorded yet. Some of the GRBs have a precursor to the main burst, e.g. GRB 820331 (Mazets 1988) shows a small but clear peak 60 s prior to the onset of a multipeaked main burst. Whereas most GRBs exhibit multiple peaks in their light curves, some

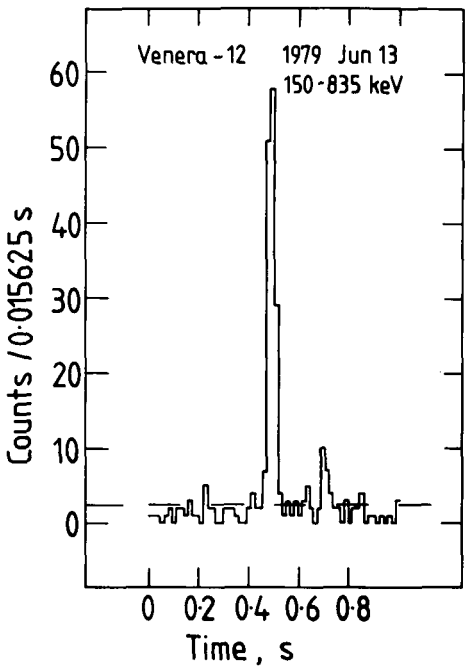

Figure 3.4. Time histories of GRB 790613 from the Franco–Soviet SIGNE experiments for the energy range 150–835 keV (Barat *et al.* 1984*a*).

(e.g. GRB 830801b) show a single peak. Laros *et al.* (1985*a*) have reported that the burst GRB 841215 exhibits sharpest (full width ≤ 5 ms) multipeaked structure and wondered if there is any substructure (undetected by them) in each of these sharp peaks.

A remarkable 20 min long γ-ray transient (the so-called Jacobson transient) was observed by Ling *et al.* (1982) in a balloon-borne detector on June 10, 1974. Four intense γ-ray lines at 0.413, 1.79, 2.2 and 5.9 MeV appeared in the background spectrum. The widths were all broader than the instrument resolution. No continuum emission was detected. Lingenfelter, Higdon and Ramaty (1978) suggested that the 0.413, 1.79 and 5.9 MeV lines are the red-shifted lines ($z = 0.20$–0.29) due to pair annihilation and neutron capture on hydrogen and iron, respectively, at and near the surface of neutron star accreting matter in a binary system. The 2.2 MeV line, on the other hand, was interpreted as the unshifted line from neutron capture on hydrogen in the atmosphere of the companion star. Subsequent searches failed to observe similar events. It is not clear what relationship, if any, exists between GRBs and the Jacobson transient.

Cline and Desai (1974) have pointed out that very brief, ~ 0.1 s, bursts form a class distinct from the long and highly structured bursts. Mazets *et al.* (1981*b*, 1982*b*) suggest that there is a distinct class of short duration bursts of which GRB 790305b is the prime example. Some of these short duration bursts are now recognised as soft gamma repeaters (SGRs), whereas all the others are denoted as

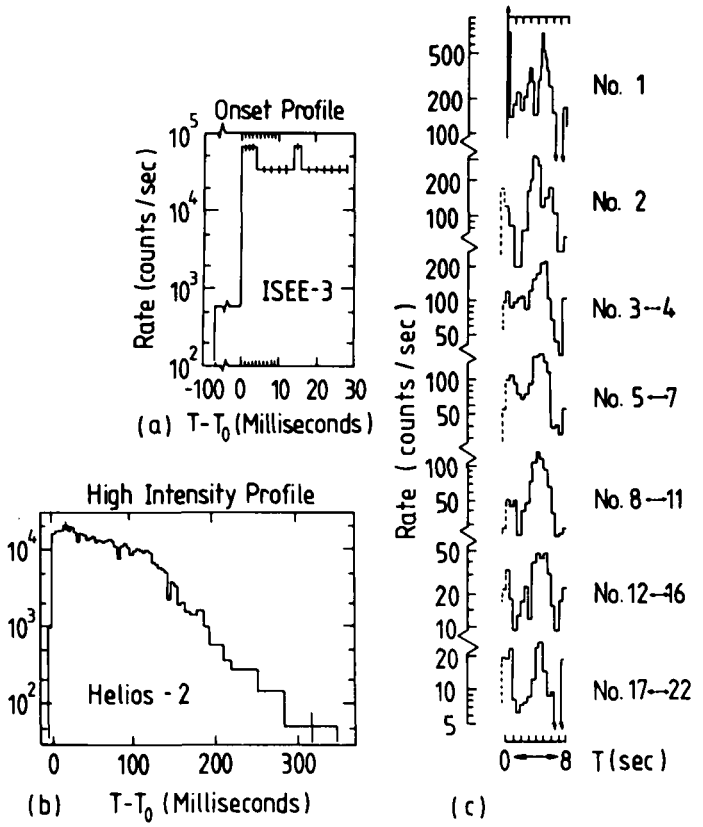

Figure 3.5. Time histories of GRB 790305b. (*a*) The onset of the high intensity portion of the burst showing the increase in count rate by two orders of magnitude within a resolving time of 1 ms (ISEE-3). (*b*) Details of the high intensity portion of the burst observed with HELIOS-2. (*c*) The first 22 cycles of the burst plotted on an 8 s period basis with the event onset chosen at zero of time folded with increasing number of cycles per plot. The initial peak remains at constant phase within 1 s yielding an average period of 8.0 ± 0.05 s (Cline *et al.* 1981*a*).

classical GRBs; we will elaborate on this distinction in Section 3.3.4. In Figure 3.6, we have shown the distribution of burst durations for the 216 GRBs observed by the Leningrad group (Mazets and Golenetskii 1981*b*, Golenetskii *et al.* 1987*a*) with detectors aboard Venera 11–14. We have also shown in Figure 3.6 the relative distributions of burst durations of one of the three SGRs, as given by Hurley (1989*a*). One can see that SGRs have durations of the order of 100 ms, whereas the classical GRBs are ~10 s long; there is admittedly an overlap between the two distributions. There is a suggestion that there is a break around 1 s in the distribution of the classical GRBs. Barat *et al.* (1984*a*) point out that there is a break at 600 ms in the burst duration distribution of single-peaked bursts. Norris *et al.* (1984), emphasising the importance of selection effects in recording short

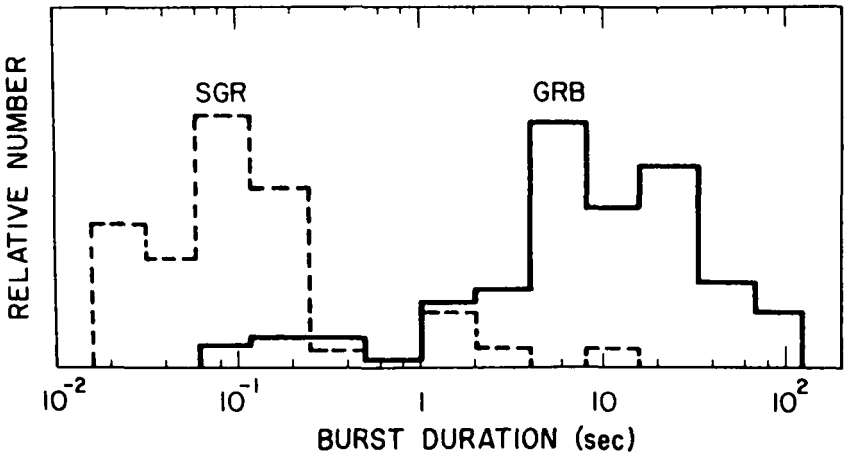

Figure 3.6. Distribution of 216 GRBs with respect to duration as obtained in the KONUS experiments on Venera 11–14 (Mazets *et al.* 1981*b*, Golenetskii *et al.* 1987*a*) and a sample of repeating bursts from one of the soft gamma repeaters (SGRs) (Hurley 1989*a*).

duration bursts, give figures ranging from 0.07 ± 0.02 to 0.29 ± 0.10 for the fraction of GRBs with $T \leq 1$ s among all the bursts.

Mazets *et al.* (1982*b*) point out that the short duration bursts have many properties in common; in particular, the authors point out that their energy spectra are all soft with $kT \sim 35$ keV. While this is certainly borne out by the observations on SGRs, there are, however, observations on classical bursts contradicting this; see Laros *et al.* (1981, 1982) and Barat *et al.* (1984*b*). Mazets and Golenetskii (1981*a*) and Golenetskii (1988) find that a positive correlation exists between the burst fluence and its duration; see Figure 3.7. This observation is corroborated by Barat *et al.* (1984*a*).

3.3.2 Burst risetimes

The well known GRB 790305b has the shortest detected risetime, $T \leq 0.25$ ms (Cline *et al.* 1981*a*). Barat *et al.* (1984*a*) have studied the distributions of risetimes, T_r, decay times, T_d, and peak fluxes of a selected sample of 20 short single-peaked GRBs. These authors suggest that the rise and decay times, being less subject to instrumental effects, are better parameters to describe a GRB than the burst duration, T. They find a correlation between T_r and T_d among the 20 GRBs, as shown in Figure 3.8. The distributions, both T_r and T_d, seem to be continuous, extending over several orders of magnitude, and suggest that there is nothing like a standard burst profile. A wide variety of physical conditions may therefore be present at or around the burst sites. It is difficult to know if time histories directly reflect processes at work at the site of energy release or whether, for example due to beaming, they carry a signature of conditions at a more distant

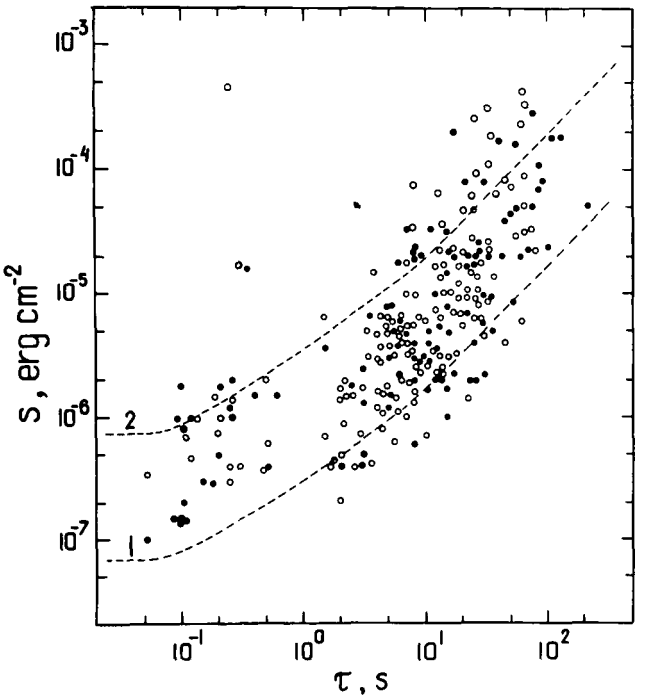

Figure 3.7. Intensity of GRBs as a function of their duration, as seen in the KONUS experiments on Venera 11 and 12 (open circles) and Venera 13 and 14 (filled circles). Dashed lines 1 and 2 show the calculated dependence of detection threshold in s on duration of bursts of simple rectangular shape for soft ($kT = 30$ keV) and hard ($kT = 2$ MeV), respectively (Golenetskii 1988).

site. Barat *et al.* (1984*a*) found that T_r and T_d when expressed in units of milliseconds are related by

$$T_r = 0.13 T_d^{1.25} \tag{3.9}$$

at $T_r > 70$ ms. In general, $T_r \sim T_d$ within a factor of two. One notable exception is GRB 790305b for which the risetime is two orders of magnitude smaller than that of both an average short duration burst and its own decay time. Barat *et al.* found that the mean risetimes are 17 ± 3 ms and 402 ± 40 ms and that the mean decay times are 19 ± 5 ms and 568 ± 56 ms for short (~ 100 ms) and long (~ 1 s) duration bursts, respectively. They also found that the peak flux during a burst is a decreasing function of risetime; see Figure 3.9. The authors noted that bursts with the following combinations of T_r and T_d (which could have been recorded) do not occur in nature: (i) short T_r, long T_d; (ii) long T_r, short T_d; and (iii) long duration bursts with short T_r and short T_d. One is cautioned, however, that the sample is small, limited to only 20 events, and that instrumental effects may also play a role.

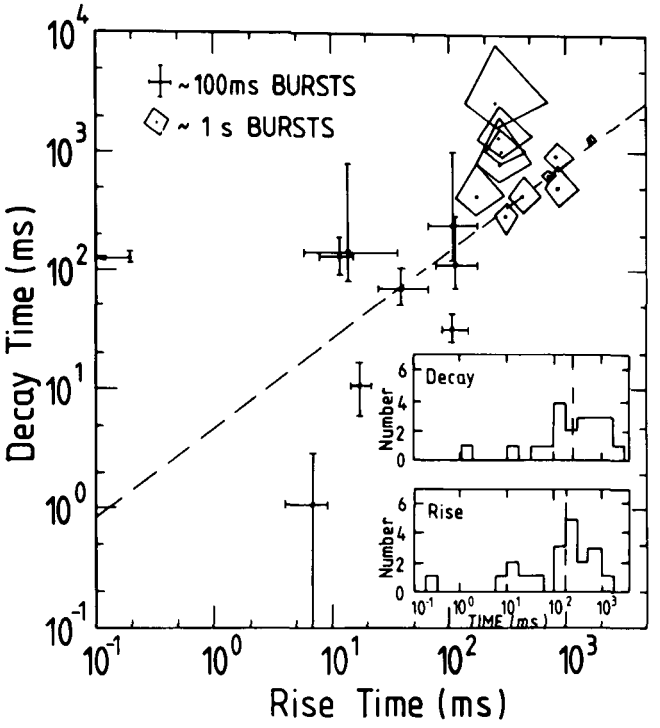

Figure 3.8. e-folding rise and decay times of the 20 single-peaked GRBs studied by Barat *et al.* (1984*a*). Error bars are for the 68% confidence level. Crosses are for shorter duration (~100 ms) bursts, and diamonds are for the longer bursts. Dashed line: $T_r = 0.13T_d^{1.25}$, where T_r is the risetime and T_d is the decay time. Insets are histograms of the numbers of events as a function of rise and decay times.

3.3.3 Burst periodicities and quasi-periodicities

As will be clear from the following, periodicity in a GRB is the exception rather than the rule.

The only convincing example of periodicity in GRB emission is the well known GRB 790305b. Mazets *et al.* (1979*a*,*b*) were the first to report a periodicity, the period being 8.1 ± 0.1 s; see Figure 3.10. This result was soon confirmed by Barat *et al.* (1979) with $P = 7.9 \pm 0.3$ s, by Terrell *et al.* (1980) with $P = 8.0 \pm 0.05$ s, and by Cline *et al.* (1981*a*) with $P = 8.0 \pm 0.05$ s. Cline *et al.* detected pulsations out to 172 s after the initial impulsive peak; see Figure 3.5(*c*). The initial impulsive peak occurred at a phase coincident with that of the interpulse at a phase of 0.5 (Mazets and Golenetskii 1981*a*). The latter authors found that pulsations ceased sometime prior to 360 s after the commencement of the burst. The exact point in time when an object ceases pulsating is doubtless governed by processes near the object itself. Its measurement, however, is dependent on the geometrical acceptance factor of the sensor in a given experiment, i.e. on its ability to distinguish the signal from fluctuations in the background noise and also on the capacity of the memory

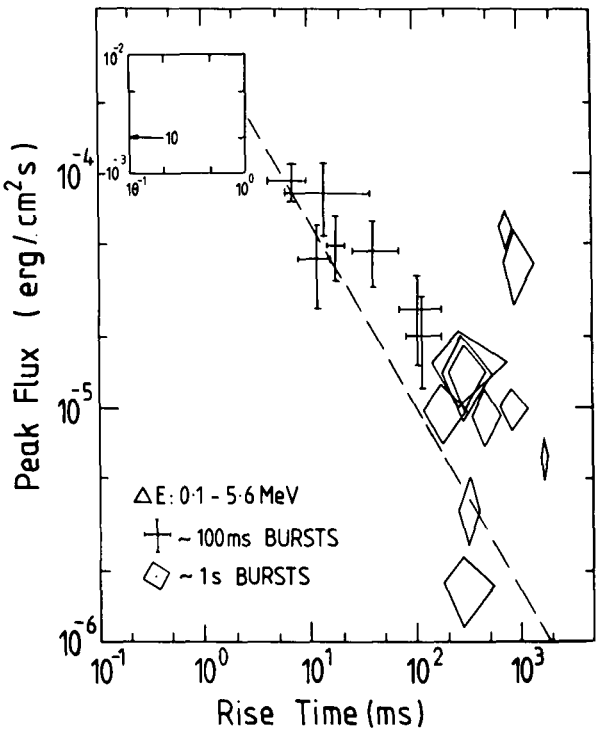

Figure 3.9. The peak fluxes are shown as a function of risetime for 19 of the single-peaked GRBs studied by Barat *et al.* (1984*a*). Dashed line: peak flux = $4 \times 10^{-4} T_r^{-0.5}$. The peak fluxes have been extrapolated to a common energy range 0.1–5.6 MeV.

bank aboard the spacecraft to hold a long and continuous data stream. Mazets *et al.* (1981*a*) found that during the first four periods the main pulse weakens in intensity whereas the interpulse stays at the same level. During the next three pulsations the situation is reversed.

There have been many other claims of detection of periodicity in a GRB. Wood *et al.* (1981) claimed to have detected a period of 4.2 ± 0.2 s in GRB 771029 over five or six cycles. Some other GRBs suspected to exhibit periodicities are: GRB 781104 ($P = 0.280$ s) and GRB 781023 ($P = 0.143$ s) by Chambon (1982); GRB 771029 ($P = 4$ s) by Pizzichini (1981); GRB 790113 ($P = 5.7$ s) by Barat *et al.* (1984*d*); GRB 781102 ($P \sim 15$ s) by Mazets *et al.* (1982*b*); and a few other cases by Loznikov and Kuznetsov (1982). Not all cases of reported periodicity are convincing, however. One must recognise here the experimental difficulty in demonstrating the existence of a periodicity when the length of the data stream is not much longer than the suspected period itself and there is but a single opportunity to observe the burst since the phenomenon by its very nature is transient.

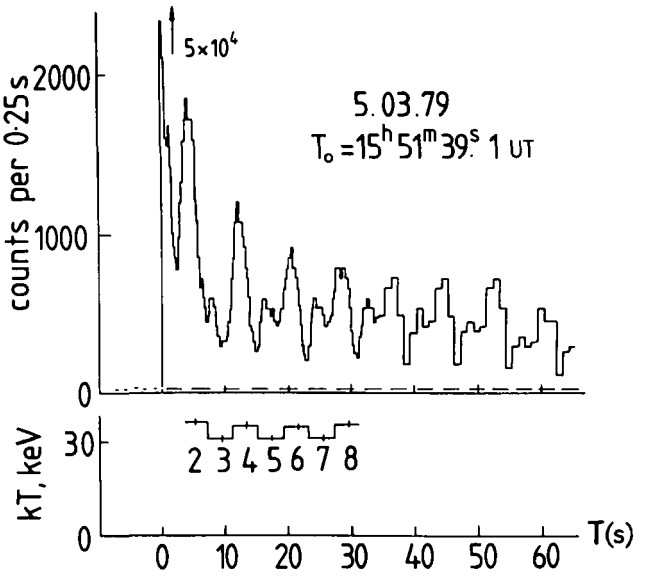

Figure 3.10. The pulsating phase of the time history profile of GRB 790305b as seen by the Leningrad group in the KONUS experiments. Top: time profile showing narrow initial pulse and pulsations with a resolution of 0.25 s. If the main pulse in the pulsations (i.e. the second big peak) is assigned zero phase, the narrow initial pulse has a phase 0.5. Bottom: temperature variations for the thermal bremsstrahlung spectra (integrated over 4 s) in the pulsating stage of the burst, $I \propto \exp(-E/kT)$ (from Mazets *et al.* 1982*b*).

Barat *et al.* (1983) suggest that GRB 790305b may also be exhibiting a periodicity of 23 ms (Figure 3.11) on the basis of power spectral and superimposed epoch analyses of their data on the time history of the burst. Following Brecher (1982), one can think of 23 ms as the rotation period of the neutron star (the source object of GRB 790305b) and 8 s its precession period.

Schaefer and Desai (1988) have carried out Monte Carlo calculations to assess the significance of reported periodicities in 20 cases of GRB light curves and have concluded that the claim for an 8.1 s periodicity in GRB 790305b is the only significant one; in all other cases random events are probably mimicking the claimed periodicity.

3.3.4 Burst recurrences

Since more and more GRBs are being detected as time progresses, the problem of chance superposition of source directions within the error boxes is becoming worse. It is therefore imperative to determine burst source directions rather precisely to be able to say unequivocally if a particular source is recurrent or not. To date there are only three sources known to be recurrent: GBS 0526−66, GBS 1806−20 and GBS 1900+14. Sometimes a GBS is also referred to as an SGR.

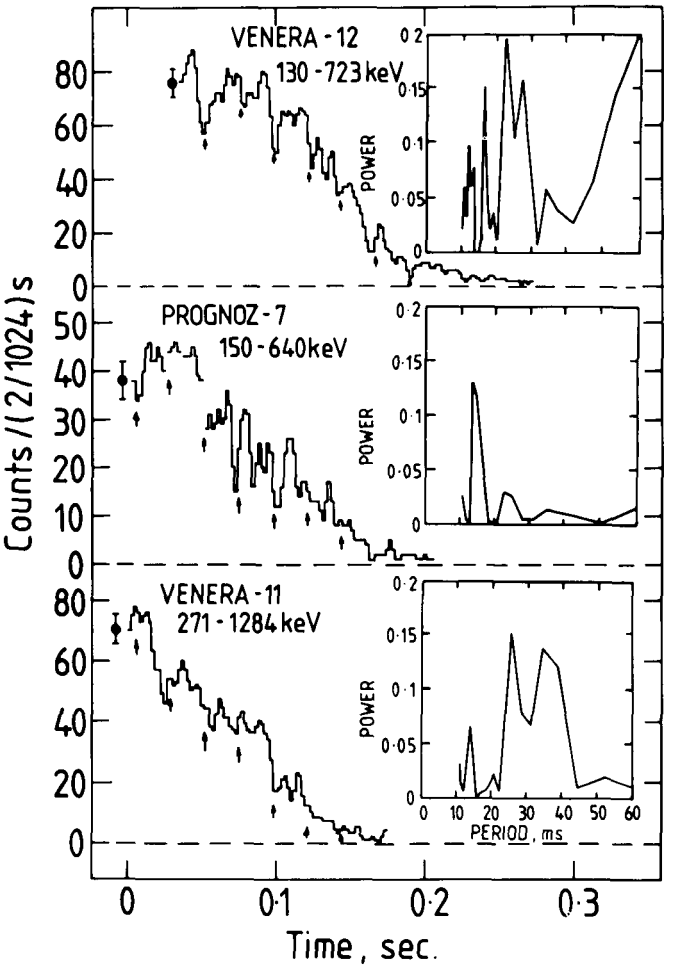

Figure 3.11. Time profiles of GRB 790305b during the first 200 ms observed with 2 ms time resolution by identical detectors aboard the Prognoz 7, Venera 11 and Venera 12 spacecraft (Barat *et al.* 1983). Dashed line: background levels; arrows: 23 ms period. Insets show spectral power in counts^2 Hz^{-1} as a function of period. These spectra result from a power spectral analysis of the residuals of the raw data.

3.3.4A Soft gamma repeaters (SGRs)

Time profiles of SGRs are of simple shape and short duration (100 ms). The energy spectra are soft with $kT \sim 30$ keV and are constant in time.

GBS 0526−66. The first burst from this source, GRB 790305b, was detected by ten different experiments. An examination of Venera 11 and 12 data by Mazets *et al.* (1979*a*,*b*) suggested that GRB 790305b showed itself again on March 6, April 4, and April 24, 1979. Later, the same group (see Golenetskii *et al.* 1984 and Golenetskii *et al.* 1987*b*) presented evidence for 13 more recurrences from this

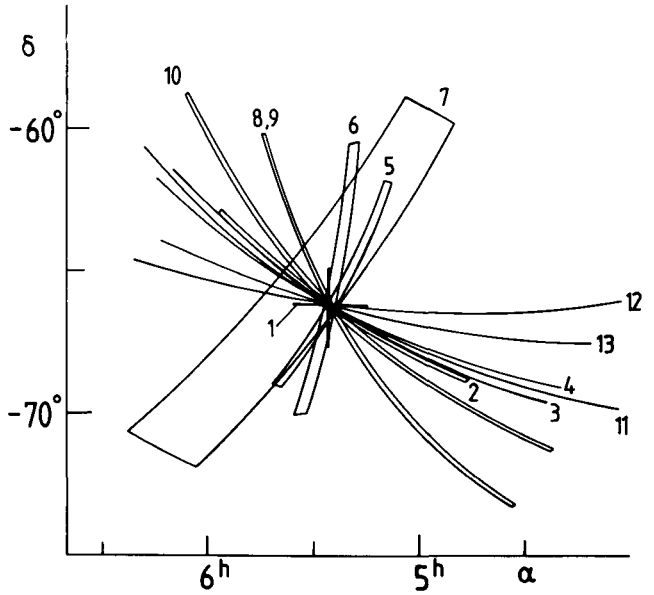

Figure 3.12. GRB recurrences of the source of the famous GRB 790305b, as seen by the Leningrad group (Golenetskii *et al.* 1984). The localisation error band is shown for each recurrence. Numbers 1 to 13 on the bands refer to the events on March 5, March 6, April 4, April 24, 1979, December 1, 1981, January 2, February 15, April 23 *a* and *b*, May 10, May 30, July 8 and December 31, 1982, respectively.

source based on Venera 13 and 14 data. Intersection of the error bands for the source direction in the first 13 events at the same position, as shown in Figure 3.12, leaves no doubt about the identity of the source. The published recurrences of this burst source (RA = 05 h 25 m 55 s, Decl. = $-66°07'$) occurred during the time spans from March, 1979, to January, 1980 (Venera 11 and 12) and from December, 1981, to April, 1983 (Venera 13 and 14), with a break in observations of about 22 months. If the source recurred during this break, it almost certainly did not have a very intense impulsive peak at the beginning of the burst as it had on March 5, 1979; otherwise, such an intense burst would have been detected by other experiments. Indeed the 16 recorded recurrences of the burst source were never seen in other experiments and were three orders of magnitude lower in intensity than in its very first detected appearance on March 5, 1979.

The fluence, in units of 10^{-6} erg cm^{-2}, was 450 at its first appearance and generally in the range 0.15 to 7 during the subsequent appearances. The energy spectra were all soft with $kT \sim 35$ keV, except on March 5, 1979, when the spectrum exhibited a harder component as well, with $kT = 520 \pm 100$ keV. The burst durations were in the range 100 ms–3.5 s, and, except during its first appearance, it did not show any pulsations. The mean time between recurrences appears to be 38.6 d with the least and the highest intervals being 12.8 h and 100 d, respectively. There does not seem to be any correlation between the time interval between two consecutive recurrences and the corresponding fluence values. The

direction of this GBS is coincidental with that of the supernova remnant N49 in the direction of the Large Magellanic Cloud; see Section 3.5.2. At a distance corresponding to that of the Large Magellanic Cloud (~ 55 kpc), the typical peak flux $\sim 2 \times 10^{-6}$ erg cm^{-2} s^{-1} of the recurrent bursts implies a luminosity of $\sim 6 \times 10^{41}$ erg s^{-1} during the burst, if the association of the GBS with N49 is true.

Rothschild and Lingenfelter (1984) have noted a pattern in the recurrence times of these bursts, showing an apparent period of 164 d. The pattern is that their recurrence time (time elapsed since the previous burst) keeps progressively increasing and then becomes very small, giving a saw-tooth curve with a period of 164 d. The authors suggest that the pattern reflects periodic accretion on to a neutron star from a binary companion in a highly eccentric orbit ($e \approx 0.9$).

GBS 1806−20. The first GRB from this source, GRB 790107, was detected by Mazets *et al.* (1982*b*). The source direction ($l \sim 9\overset{\circ}{.}8$ and $b \sim -0\overset{\circ}{.}24$) lies close to that of the Galactic Centre. Later, Laros *et al.* (1986, 1987) and Atteia *et al.* (1987*b*) have observed 110 repetitions over an eight-year period with more than half of them occurring within just a two-week period. The recurrences were observed in an experiment on the International Cometary Explorer in the energy band 5–100 keV. Although it was possible to localise 18 of the recurrences with additional information from the other experiments, the remaining 92 recurrences were identified on the basis of energy spectra and burst profile shapes. It is clear that the recurrences were spread in time very unevenly. The peak intensities varied by nearly a factor of 30, in contrast to the situation in the other two SGRs. The spectra were quite soft, with $kT \sim 35$ keV. The peak intensities were as high as 4×10^{-5} erg cm^{-2} s^{-1}. If one assumes that the source lies close to the Galactic Centre, the peak intensity corresponds to a peak luminosity of 4×10^{41} erg s^{-1}, a value close to the one deduced in the case of GBS 0526−66.

GBS 1900+14. This source was observed solely by the KONUS detectors on Venera 11 and 12 (Golenetskii *et al.* 1979, Mazets *et al.* 1979*a,b*, Mazets *et al.* 1981*a*). The first detection (GRB 790324) was on March 24, 1979, and within three days two more bursts were seen (GRB 790325a and GRB 790327a). Coincidences within the errors in the spatial direction and similarities in the energy spectra led the authors to claim that the bursts were recurrent. Peak intensities were nearly the same, $\sim 2 \times 10^{-5}$ erg cm^{-2} s^{-1} in the three recurrences. The burst location, corresponding to $l \sim 47°$ and $b \sim 4°$, leads to the belief that it is a Galactic disk object and is probably several kpc away. If this is so, the peak luminosity in this SGR too comes close to a few times 10^{41} erg s^{-1}.

Although Kouvelitou *et al.* (1987) have suggested a similarity between the SGR and Type II X-ray bursters, the two populations may be distinct because the X-ray bursters have (i) much longer risetimes (~ 1 s), (ii) black body spectra with $kT \sim 1.5$ keV, (iii) regular recurrence intervals ($\sim$six months), and (iv) intensities correlated with time between recurrences; see Lewin and Joss (1983).

Terrell *et al.* (1980) are of the view that the recurrences of GRB sources are related to the neutron star itself such as an internal restructuring or a critical

accumulation of accreted material and not due to the improbable recurrent collisions with incoming solid objects such as comets or asteroids.

3.3.4B Classical gamma-ray bursts

In contrast with SGRs, the classical GRBs have multipeaked complex profiles and are of much longer duration (~ 10 s). Generally the energy spectra are harder than in the case of SGRs and become softer with time.

There is no observational evidence to show that any of the classical GRBs recur.

Among the 40 burst sources precisely localised by the International Network (HELIOS-2, SIGNE, PVO and ISEE-3), no recurrent bursts were observed over a period of ~ 1.5 y (Vedrenne 1983). Taking the solid angle of coverage into account, Vedrenne states that the recurrence time for a GRB is more than one year. Atteia *et al.* (1987*a*) looked for directional coincidences among 84 bursts occurring over a 17-month period. The authors have concluded that whatever coincidences they observed were consistent with random sky positions leading to a 3σ lower limit of 8 y for the mean recurrence time for bursts above the detection threshold.

While the observations set a lower limit in the range 1–10 y to the mean recurrence time, model dependent calculations set upper limits in the range 10^2–10^6 y for the same. Hurley (1989*a*) has assumed that there are 10^8 neutron stars in the Galaxy and ~ 40 GRBs occur each year that can be said to be originating at neutron stars. If each neutron star bursts only once in its lifetime, the neutron star population can account for GRBs only for $10^8/40 \approx 2.5 \times 10^6$ y. Thus one can qualitatively say that the maximal recurrence time is ~ 2.5 million years. In a similar qualitative calculation, Higdon and Lingenfelter (1990) have assumed that the nearby neutron star density in space is $\sim 10^{-3}$ pc^{-3} and that the sources of the GRBs are distributed isotropically within a distance of ~ 200 pc, which is less than the scale height of the Galactic disk. The number of potential neutron stars that can generate a GRB is, then, $\sim 10^{-3} \times (200)^3 \sim 3 \times 10^4$. With the observed GRB rate of 300 y^{-1} (all of them assumed to be originating in a neutron star), one deduces a maximal recurrence time of $3 \times 10^4/300 \sim 100$ y.

3.4 Energy spectra

As noted in Section 3.2.2, what is measured by a detector is not the energy of an incident photon but its energy loss in the detector. One has to deduce the photon energy spectrum from the measured energy loss spectrum by making use of detector calibrations and an assumed trial spectrum of the incident photons. This procedure sometimes makes some conclusions based on energy spectra contentious. We illustrate the general features in the energy spectra of both the SGRs and classical GRBs in Figure 3.13, taken from Hurley (1989*a*). Whereas the SGRs exhibit soft spectra with $kT \sim 35$ keV without any features, the classical GRBs generally exhibit two different shapes of continuum at low and at high energies on which the absorption and emission features are superimposed. We must add that the GBS 0526–66 (GRB 790305b) is an exception, being the only

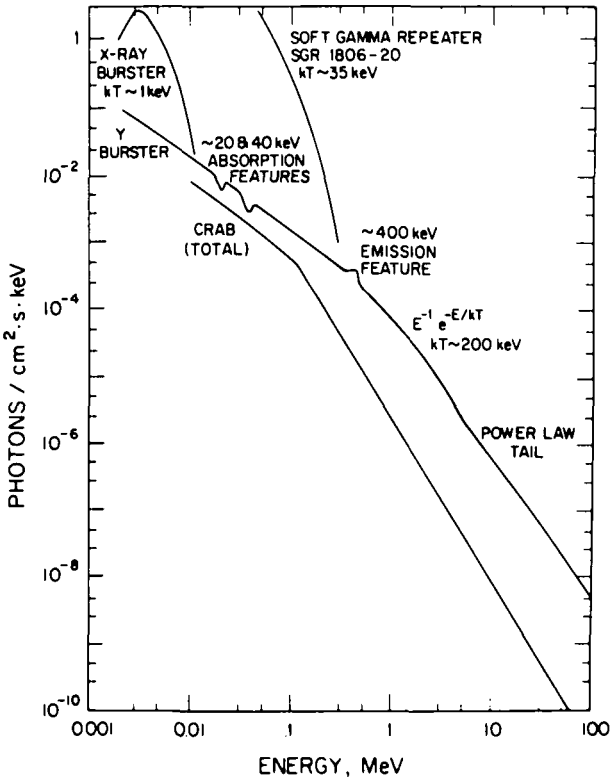

Figure 3.13. Typical GRB differential photon spectrum, a composite illustrating some of the important features seen in the various observations. Also shown are spectra from an X-ray burster (black body, $T \sim 1$–2 keV), from the Crab nebula and pulsar (total) and from the soft gamma repeater SGR 1806−20 (Hurley 1989*a*).

SGR to have exhibited emission features, that being only once when it was first detected on March 5, 1979.

3.4.1 *Spectral measurements and fits*

We first mention that the spectra from SGRs are all soft (with the exception of GRB 790305b, which exhibited an additional hard component) with $kT \sim 30$ keV; e.g., see the spectra of GBS 1806−20 reported by Atteia *et al.* (1987*b*). The rest of the discussion in this subsection relates mostly to the classical GRBs.

Early results on the energy spectra of GRBs were given by Cline *et al.* (1973) based on their IMP-6 data. These spectra could all be fitted with a simple exponential of the type

$$\frac{dN}{dE} = I_0 \exp(-E/E_0) \text{ photons cm}^{-2}\text{ s}^{-1}\text{ keV}^{-1} \tag{3.10}$$

where $E_0 \sim 150$ keV. Later, Cline and Desai (1975) represented the data from IMP-7 by the original 150 keV exponential modified by a power law of the type

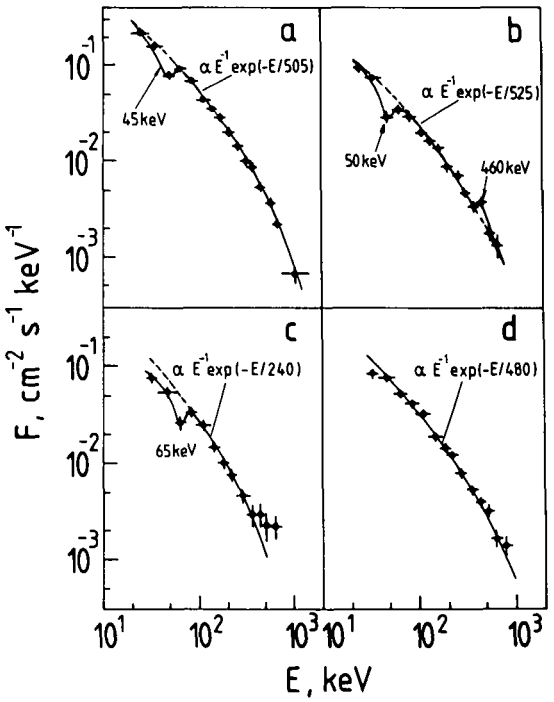

Figure 3.14. Typical γ-ray lines recorded in the energy spectra in the KONUS experiments (Mazets *et al.* 1980, Mazets and Golenetskii 1981*a*). (*a*) GRB 790307, (*b*) GRB 790622, (*c*) and (*d*) GRB 791101 spectra obtained during the first 8 s and the subsequent 24 s, respectively, demonstrate how the cyclotron absorption line evolves with time.

$\sim E^{-2.5}$ fitted to the high energy tail of the burst. Gilman *et al.* (1980) fitted the spectrum of the Apollo 16 event GRB 740427 (Metzger *et al.* 1974) with an optically thin thermal bremsstrahlung spectrum of the type

$$\frac{dN}{dE} = AE^{-1}g(E)\exp(-E/kT) \text{ photons cm}^{-2}\text{ s}^{-1}\text{ keV}^{-1} \tag{3.11}$$

where g is the energy dependent Gaunt factor of the order of unity; T is the temperature of plasma; and k is the Boltzmann constant, with $kT \sim 500$ keV. Using their most comprehensive data base (Mazets *et al.* 1981*b*) from the KONUS experiments, Mazets *et al.* (1981*c*,*d*) adopted thermal bremsstrahlung-like spectra with kT values in the range 10 keV–2 MeV, most of them being 150–400 keV. A few examples of these thermal bremsstrahlung fits are shown in Figure 3.14. The Solar Maximum Mission group (Rieger *et al.* 1982) found a few cases of GRBs in which photons with energies greater than 10 MeV were seen. The spectral fit for one of them, GRB 820320, is shown in Figure 3.15; it is given by a power-law spectrum of the type

$$\frac{dN}{dE} = AE^{-2.5} \text{ photons cm}^{-2}\text{ s}^{-1}\text{ keV}^{-1} \tag{3.12}$$

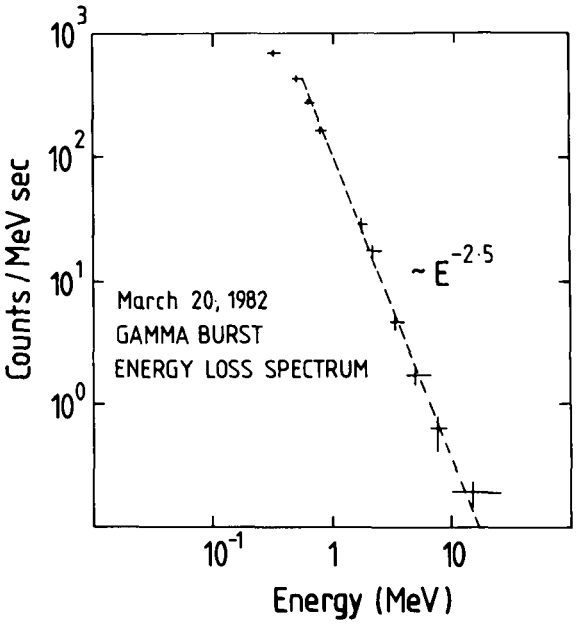

Figure 3.15. Energy spectrum of γ-rays from GRB 820320 as recorded by a CsI crystal in the SMM experiment (Rieger *et al.* 1982). The data can be represented by a power-law spectrum of the type $N(E) \propto E^{-2.5}$.

in the energy range 0.3–15 MeV. Notice that the energy range here does not overlap those in most other experiments.

Liang, Jerigan and Rodrigues (1983) have argued that, in the physical conditions obtained in the emission regions, thermal synchrotron spectra resulting from mildly relativistic electrons in an optically thick plasma (Petrosian 1981) associated with strong magnetic fields are more appropriate. They have shown several examples of excellent fits to the KONUS data based on thermal synchrotron emission. These are of the type

$$\frac{dN}{dE} \propto \exp[-(4.5E/E_c)^{1/3}] \tag{3.13}$$

where $E_c = heB\tilde{T}/m_e c$, $\tilde{T} = kT_e/m_e c^2 \cdot T_e$ is the temperature of the plasma; B is the magnetic field; E is the photon energy; and e and m_e are the charge and mass of the electron, respectively.

Fenimore *et al.* (1982*a*) argue that at temperatures ($kT \sim 300$ keV) implied by bremsstrahlung fits, the free–free cross section is so much smaller than the inverse Compton cross section that the latter might dominate the spectral formation processes. They accordingly view GRB sources as Comptonised X-ray sources, i.e. sources in which an initial X-ray black body spectrum ($kT_{BB} \sim 2.4$ keV) has undergone inverse Compton scattering by a much hotter ($kT_e \sim 150$ keV) plasma. Although the authors offer no explanation as to why the hot plasma should be

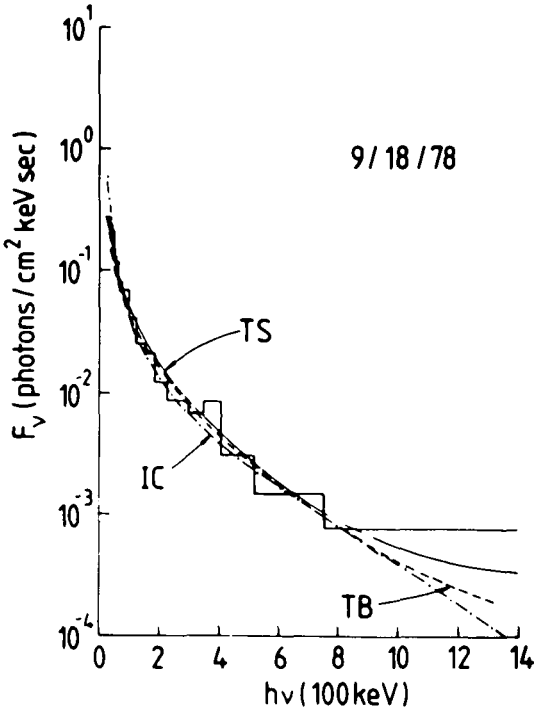

Figure 3.16. Good fits can be obtained by thermal bremsstrahlung (TB), thermal synchrotron (TS) and inverse Compton mechanisms (IC) to the same experimental data on energy spectrum of γ-rays from GRB 780918 (Liang *et al.* 1983).

overlying an X-ray source, their Comptonised X-ray black body fits for the GRB 781104 (Fenimore *et al.* 1982*b*) are as good as or slightly better than the thermal bremsstrahlung fits.

From what has been mentioned above, one might form the impression that different mechanisms operate for different GRBs, leading to a multitude of possible spectral fits. It may well be so; the fits presented, however, do not prove it. This point is illustrated by Figure 3.16 from Liang *et al.* (1983), where equally good fits are obtained for GRB 780918, based on thermal bremsstrahlung, thermal synchrotron and inverse Compton models. Furthermore, Barat *et al.* (1984*a*) have also shown that for two-thirds of their sample of 20 short, single-peaked GRBs, all four spectral types (thermal bremsstrahlung, thermal synchrotron, exponential and power law) give acceptable fits. The point is that, given the freedom in the choice of parameters and poor statistics at the upper end of the spectrum, many laws fit the data which is available only over limited energy spans (in most cases $1\frac{1}{2}$ decades), leading to the impossibility of demonstrating the uniqueness of a fit by a given law.

Attention must also be drawn here to two other aspects. First, as shown in Section 3.4.3, the energy spectra sometimes evolve with time on scales as short as 30 ms. Faced with such fast changing spectra, one questions the validity of using

the event-averaged spectrum as a basis to understand the physical processes operating in and around the burst sources; see, for example, Lamb (1982), Teegarden (1982) and Vedrenne (1984). Secondly, different groups observing the same GRB sometimes disagree over the shapes and absolute values of energy spectra. For example, SIGNE, KONUS and ISEE-3 disagree on the spectrum from GRB 781104 (Vedrenne and Chambon 1983); SMM and ISEE-3 disagree on the spectrum from GRB 800419 (Vedrenne and Chambon 1983); and KONUS and PVO disagree on the spectrum from GRB 790613 (Barat *et al.* 1984*b*).

Murakami (1990) has noted that, based on the observations with the GINGA satellite, the soft X-ray emission by a GRB decays more slowly than the γ-ray emission, lasting for ~ 100 s. The spectrum at very low energies is possibly a black body spectrum with a temperature corresponding to ~ 1–2 keV. By assuming a black body spectrum from a surface with a definite emissivity, Murakami estimates the size of the emission area to be about 1 km in radius for a source distance of 1 kpc. One can turn this argument around to state that, if GRBs originate from neutron stars, then the soft X-ray spectrum constrains the distances of the neutron stars to lie within 1 kpc.

It has been noted by several authors that the power emitted by a GRB in the soft X-ray region is less than a few per cent of the total power; see, for example, Helfand and Vrtilek (1983) and Murakami (1988). If higher energy X-rays and γ-rays are emitted isotropically near a neutron star, then one expects the neutron star to intercept the radiation and re-emit it in the form of soft X-rays as black body radiation. Since this is not what is happening, one has to assume either that the γ-rays are emitted anisotropically away from the surface of the neutron star (Epstein 1986) or that the bulk of the γ-rays are emitted from a region several stellar radii above the surface of the neutron star so that the solid angle subtended by the star is small (Brainerd 1989, Dermer 1989, Ho and Epstein 1989).

Some GRBs show evidence for both an absorption line at $E \approx 20$–40 keV and emission of γ-rays at $E \gtrsim 10$ MeV, e.g. GRB 820320 (Rieger *et al.* 1982; see Figure 3.15), GRB 780325 (Hueter 1987), and GRB 830801b (Boer *et al.* 1992). The absorption lines indicate that the magnetic fields at the emission region are $\sim 10^{12}$ G, which places it close to the neutron star; see Section 3.4.2A. γ-rays with energies $\gtrsim$ a few MeV will undergo absorption in such high fields by pair production; see equation (5.2). It follows therefore that γ-rays with energies $\gtrsim 10$ MeV are produced in a distinctly separate region, farther than a few stellar radii from the neutron star's surface (Mitrofanov *et al.* 1984, Brainerd and Lamb 1987). Similar conclusions were arrived at by Hueter and Lingenfelter (1983) who considered the attenuation of MeV γ-rays by pair production in photon–photon collisions.

It is interesting to know if γ-rays of energies $\gtrsim 1$ GeV are present in GRBs. Bhat *et al.* (1982) carried out a ground-based experiment at Ootacamund, India, that depended on the bunching of GeV γ-rays in microbursts (10–100 μs in duration) for their detection. During a 1.5 y period of its operation, five GRBs that were seen by satellite experiments were in the view of the experiment, but no GeV γ-rays were seen from any of them. From this, the authors have concluded that either

(i) there are no γ-rays at GeV energies in the GRBs in question, (ii) if the GeV γ-rays are indeed present, the micropulsations needed for their detection are absent, or (iii) if the GeV γ-rays and micropulsations do both exist in GRBs, the differential energy spectrum of γ-rays must be steeper than $E_\gamma^{-2.5}$ in the energy range $0.1\ \text{MeV} \leq E_\gamma \leq 5\ \text{GeV}$.

3.4.2 Spectral features

The high resolution Ge detector on ISEE-3 recorded several interesting emission features in GRB 781119 (Teegarden and Cline 1980, 1981). The KONUS data base (Mazets *et al.* 1981*b*–d) revealed the existence of 30 absorption and ten emission features among the 143 GRBs reported. Three of them showed both the absorption and emission features (for example GRB 790622, shown in Figure 3.14(*b*), which could merely be a chance coincidence (Hurley 1984). The number of cases showing features must in reality be higher, for, in weak bursts, poor statistics might be masking the effect; also most detectors do not record spectra with good resolution down to energies of ~ 20 keV, the region that seems to show clear absorption lines (Fenimore *et al.* 1988, Murakami *et al.* 1988). All the absorption features occur at low energies (20–70 keV), and nearly all the emission features are seen at energies greater than 400 keV. Both the absorption and emission features are known to evolve with time; this aspect will be taken up in Section 3.4.3.

3.4.2A Absorption features

Some examples of GRBs showing absorption features in the KONUS data are given in Figure 3.14 (Mazets *et al.* 1980). In a sample of 30 GRBs (from KONUS) showing absorption features, there was only one case, GRB 800419, which was qualitatively confirmed by the HXRBS experiment on SMM (Dennis *et al.* 1982). The reason for non-confirmation of other cases by other experiments might be that none of them had both a good energy resolution and a sufficiently low energy threshold (Hurley 1983*b*). Hueter and Gruber (1982) reported an absorption feature at 55 ± 5 keV in the spectrum of GRB 780325, seen with their HEAO-A4 detectors. Unfortunately there was no confirmation by others (this event occurred prior to the launching of the Venera experiments on GRBs).

Recent observations by the Los Alamos/Tokyo GRB detector aboard the GINGA satellite have revealed three clear examples of GRBs showing absorption lines, each with two lines (Fenimore *et al.* 1988, Murakami *et al.* 1988, Murakami 1990). This was made possible by the fine energy resolution of their detector coupled with a broad coverage of the energy range down to a few keV. One of the examples (GRB 880205) is shown in Figure 3.17. Energies and widths of the absorption lines and ratios of energies of the two lines (Murakami 1990) are shown in Table 3.1.

Most of the absorption features, centred in the region 20–70 keV, account for an absorption of 0.01 to 0.02 of the burst energy (Mazets *et al.* 1981*d*). The line-to-continuum ratio can sometimes be as high as 0.8. The equivalent widths

Table 3.1. *Characteristics of absorption lines seen by GINGA*

Event ID	E_1 (keV)	W_1* (keV)	E_2 (keV)	W_2* (keV)	E_2/E_1
GRB 870303	20.4 ± 0.7	3.5 ± 2.7	40.6 ± 2.6	12.3 ± 6.3	2.0 ± 0.3
GRB 880205	19.3 ± 0.7	4.1 ± 2.2	38.6 ± 1.6	14.4 ± 4.6	2.0 ± 0.15
GRB 890929	26.3 ± 1.5	4.2	46.6 ± 1.7	7.7	1.8 ± 0.2

* W_1 and W_2 are full widths at half maximum

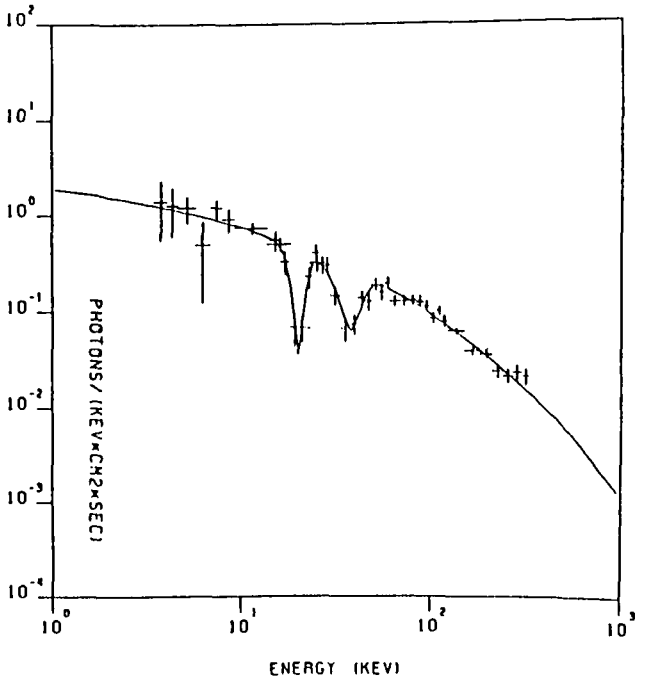

Figure 3.17. Differential photon energy spectrum of GRB 880205 observed in the GINGA experiment (Murakami 1990). Two absorption lines, with a ratio of 2.0 in their energies, are clearly seen.

are in the range 4–30 keV. The authors interpret the absorption features due to resonance cyclotron absorption of photons in the intense magnetic fields surrounding the source regions when their energy matches that of a Landau level. The relation is given by

$$E_\gamma(\text{keV}) = nheB/m_e c = 11.6nB_{12} \tag{3.14}$$

where B_{12} is the magnetic field in units of 10^{12} G, and n is the Landau level number. Accordingly, an absorption feature at 60 keV implies the existence of a magnetic field of $\sim 5 \times 10^{12}$ G in the emission region, if interpreted at the first Landau harmonic. In the light of the latest GINGA observations, the

single absorption lines reported by Mazets *et al.* (1980) around $E_\gamma \sim 45$ keV were probably all due to the second Landau level, in which case the magnetic fields are $\sim 2.5 \times 10^{12}$ G. From a detailed analysis (Wang *et al.* 1989) of the absorption line features seen by the GINGA satellite, it is possible to derive not only the field strength but also the angle between the line of sight and the magnetic field, the temperature of the emitting region, etc. from a careful modelling.

Strictly speaking, the observed absorption features are not narrow lines. They are broad, having equivalent widths 4–30 keV (Mazets *et al.* 1981*d*, Murakami 1990) corresponding to $\Delta E_\gamma/E_\gamma \sim 0.3$. The width may be a result of Doppler broadening or of the variation of magnetic field within the emission region. Doppler broadening of a line of energy E_γ is given by (Trumper 1978)

$$\Delta E_\gamma/E_\gamma = [8 \ln 2(kT/m_e c^2) \cos\theta]^{1/2} \tag{3.15}$$

where θ is the angle between the line of sight to the observer and the magnetic field. For typical values of $\Delta E_\gamma/E_\gamma \sim 0.3$ and $\cos\theta \sim 0.707$, $kT = 16$ keV, a value much lower than the temperatures (hundreds of keV) derived from thermal bremsstrahlung fits. One must postulate, then, that the cyclotron absorption takes place in a relatively cool layer that overlies the hot region which produces the continuum.

There does not appear to be any correlation between the line widths and continuum radiation temperatures (Teegarden 1982), which can be taken as further evidence that two different processes or regions are responsible for the line and continuum behaviour.

Immediately after the publication of absorption features by Mazets *et al.* (1980), there were doubts expressed about the reality of the phenomenon. Interpretations other than that of cyclotron absorption for the low energy features have been put forward by some authors. Lamb (1982) has expressed the view that these features are probably the result of time averaging spectra in which the low energy cut-off varies rapidly. Bussard and Lamb (1982) suggest that the 10–50 keV absorption features are due to photoelectric absorption by heavy atoms in superstrong magnetic fields. Lasota and Belli (1983) show that dips could result from a superposition of two spectra: an optically thin thermal synchrotron spectrum (with a turnover at 55–110 keV) and a softer black body spectrum. Now with a clear confirmation by the GINGA results, the observations and interpretation of the absorption lines by Mazets *et al.* stand vindicated.

3.4.2B Emission features

An example of an emission feature at 460 keV is shown in Figure 3.14(*b*), taken from Mazets *et al.* (1980). According to Mazets *et al.* (1981*d*) the emission features usually occur in the energy range 330–850 keV. Most of them are at 400–460 keV and their energy content is 0.03–0.11 of that of the initial burst. The line to continuum ratios are ~ 0.3. These lines are interpreted as due to e^+e^- annihilations which are gravitationally red-shifted. The energy of the observed lines is given by

$$E_{obs} = m_e c^2 (1 - 2GM/c^2 R)^{1/2} \tag{3.16}$$

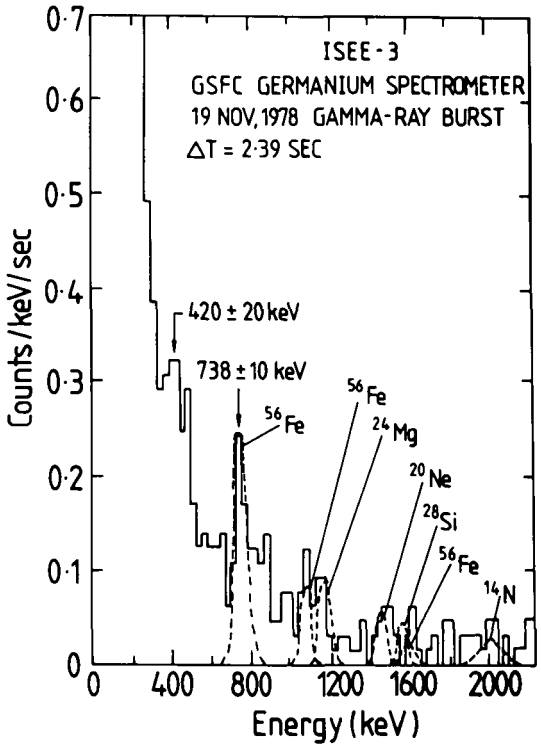

Figure 3.18. Energy spectrum of γ-rays from GRB 781119 obtained by the high resolution germanium spectrometer on ISEE-3 (Teegarden and Cline 1980, 1981). The feature at 420 ± 20 keV can be interpreted as due to a gravitationally red-shifted annihilation line, the one at 738 ± 10 keV due to the red-shifted 847 keV first excited level of Fe, and the others at higher energies due to red-shifted excitation lines from other nuclei.

where M and R are the mass and radius, respectively, of the source object. The observed red-shifts point to gravitational potentials $\sim(0.1\text{–}0.2)c^2$ and are consistent with those expected at the surface of a neutron star. Due to the finite kinetic energies of the e^+e^-, the annihilation line energy may exceed 0.51 MeV (Aharonian, Aloyan and Sunyaev 1980). If such blue-shifts exist, the observed line is a result of both the blue- and red-shifts. Observations indicate that the possible blue-shifts are not very large.

If the emission line widths (~ 250 keV) are entirely due to Doppler broadening, the corresponding electron temperatures, kT, are 15 keV (Teegarden 1982), which are much lower than those of the continuum spectra with $kT \sim$ a few hundred keV; see below for a possible explanation by Ramaty *et al.* (1980) and Ramaty, Lingenfelter and Bussard (1981). Daugherty and Bussard (1980) and Mazets *et al.* (1981*c*) point out that the annihilation lines can also be broadened by the presence of a high magnetic field ($\sim 5 \times 10^{12}$ G).

The high resolution Ge detector on ISEE-3 produced the interesting spectrum from GRB 781119 shown in Figure 3.18 (Teegarden and Cline 1980, 1981).

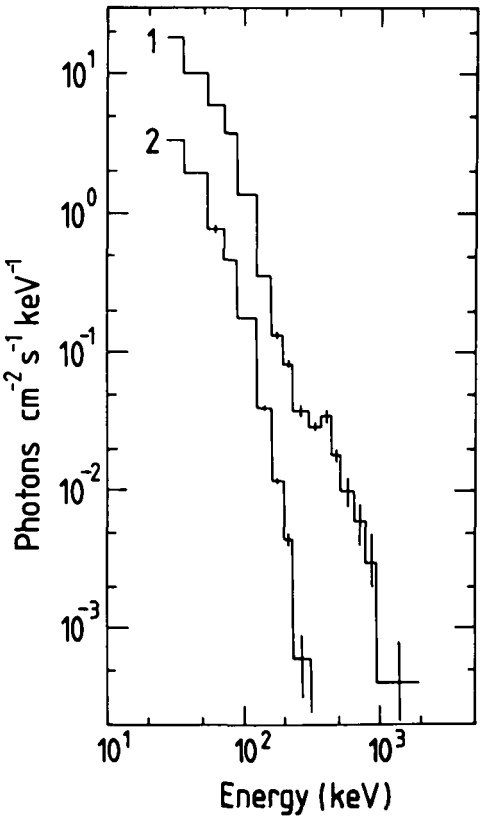

Figure 3.19. Evolution of the energy spectrum of γ-rays from the famous GRB 790305b as detected in the KONUS experiments (Mazets *et al.* 1981*a*). 1: spectrum recorded in the first 4 s interval following the onset, and 2: mean spectrum over the second to eighth 4 s intervals. Notice the disappearance of the feature at ~450 keV in the latter.

Although the feature at 420 $\pm$ 20 keV is termed 'marginal' by the authors, there is confirmatory evidence in the data base of KONUS experiments; see Figure 3.22 (Mazets and Golenetskii 1981*b*). SIGNE, too, confirms its existence over short time scales (Vedrenne and Chambon 1983). Whereas the feature at 420 $\pm$ 20 keV can be interpreted as due to a gravitationally red-shifted annihilation line, that at 738 $\pm$ 10 keV is thought to be due to the first excited level of Fe (847 keV) red-shifted by the same factor as the 511 keV line. The other features in Figure 3.18 at higher energies could be excitation lines from other nuclei, red-shifted by the same factor.

Mazets and Golenetskii (1981*a*) obtained evidence for the existence of an emission feature at 430 keV in the spectrum of the famous GRB 790305b, which is shown in Figure 3.19. The same feature is shown in Figure 3.20 in greater detail. The authors interpret the feature as due to a gravitationally red-shifted annihilation line. Unfortunately the high resolution Ge detector on ISEE-3 was not usable at the time this burst occurred (Cline *et al.* 1981*b*).

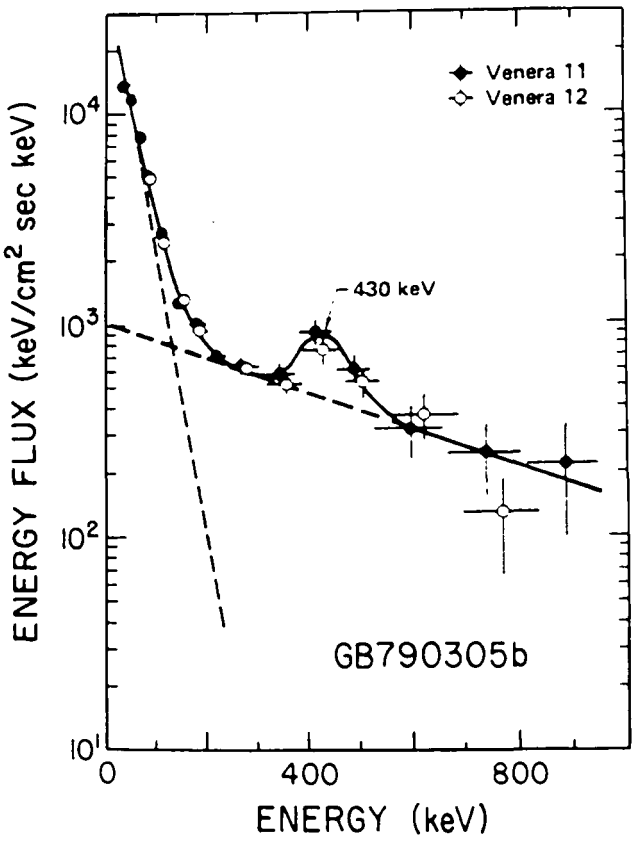

Figure 3.20. Same data as in spectrum 1 of Figure 3.19 (GRB 790305b) is shown here in a semi-log plot. The emission line at 430 keV, together with a continuum comprising two e-folding spectra ($kT = 33$ and 500 keV), fully account for the observed spectrum (Mazets *et al.* 1982*b*).

Ramaty *et al.* (1980, 1981) explain the spectrum from GRB 790305b in terms of radiation originating in a thin ($\sim 10^{-2}$ cm) surface layer that overlies a hot plasma. In a magnetic field $>10^{11}$ G, cooling by synchrotron emission is much faster than annihilation. Synchrotron emission from the rapidly cooling e^+e^- and the subsequent annihilation produce the continuum and the line feature, respectively. This model has been modified further by Liang (1981) by including inverse Compton scattering of the synchrotron photons by the same e^+/e^- ($E \lesssim$ a few MeV) producing the photons. The resulting spectral fits are shown in Figure 3.21. Liang (1981) also shows from first principles that the model can produce intrinsic luminosities as high as 10^{45} erg s^{-1} needed if the burst source was located 55 kpc away in the Large Magellanic Cloud (see Section 3.5).

There have been other interpretations proposed to explain the emission features. Ramaty, McKinley and Jones (1982), studying photon emission, absorption and scattering in a relativistic plasma of e^+e^- and γ-rays, show that an emission line at 430 keV can be produced by the GRASAR (γ-ray amplification through

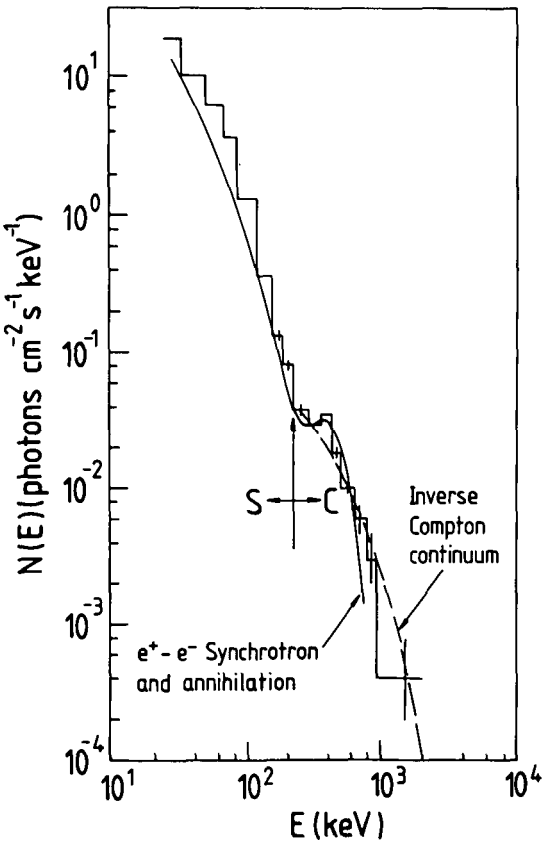

Figure 3.21. Theoretical fits to the energy spectrum of γ-rays from GRB 790305b (obtained by Mazets *et al.* (1979*b*). The continuous line is the fit by Ramaty *et al.* (1980, 1981) on the basis of synchrotron emission by $e^{\pm}$ and the subsequent annihilation of the pairs. The dashed line improves the fit at higher energies (Liang 1981) by considering inverse Compton scattering of lower energy photons on $\sim$MeV $e^{\pm}$.

stimulated annihilation radiation) process, provided the pair chemical potential exceeds ~ 1 MeV. The authors stress that their GRASAR model operates in optically thick regions, thus obviating the necessity to have very large areas for emission regions, such as would be required if the emission were from optically thin regions. I. Katz (as quoted by Teegarden 1982) has put forward an explanation for the 738 keV line seen in the spectrum from GRB 781119. At sufficiently high magnetic fields ($\geq 10^{13}$ G) the cross sections for one-photon annihilation far exceed those for the usual two-photon annihilations; see Figure 2 of Bussard and Lamb (1982). One would then expect to see 1.02 MeV ($=2m_e c^2$) lines. The ratio of energy of the one-photon emission line to that of two-photon emission lines as actually observed in this spectrum is $738/420 = 1.76$ and not 2 as expected. Ramaty *et al.* (1982) point out, however, that the shifts in the annihilation peaks

in their GRASAR model need not be by the same factor for the one- and two-photon peaks.

3.4.3 Variability of energy spectra

Variability of continuum spectrum and spectral features of a GRB is more the rule than the exception. The Franco–Soviet collaboration experiments, SIGNE, have demonstrated this variability of continuum and features on time scales of less than 250 ms (Vedrenne and Chambon 1983) and even on time scales as short as 30 ms in the case of GRB 790305b (Vedrenne 1984).

We show in Figure 3.22 the variability in energy spectra from GRB 781119 over time intervals of 4 s in the KONUS experiments (Mazets and Golenetskii 1981*a*,*b*). Notice how the bump around 400 keV, seen in the first spectrum, disappears in spectra taken a few seconds later and also the general softening of the continuum spectrum with time. One sees essentially similar time evolution in the spectra of GRB 791101 (Figure 3.14*c*,*d*), of GRB 790305b (Figure 3.19) and of several others.

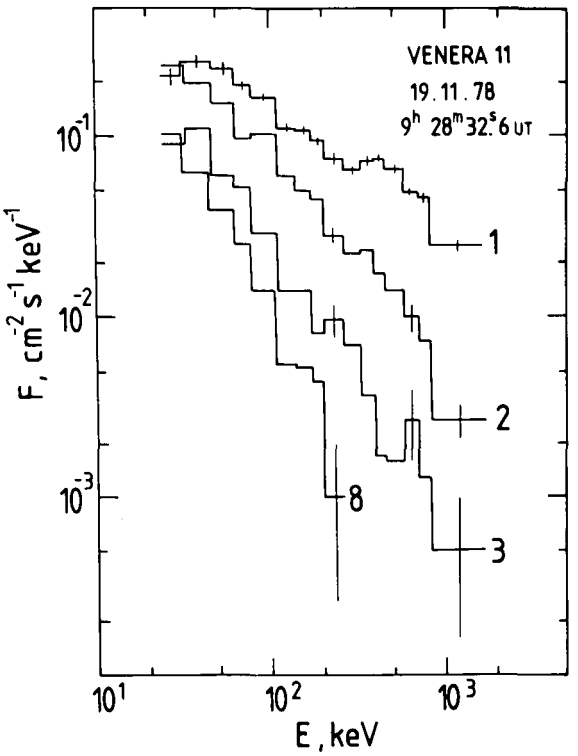

Figure 3.22. Energy spectra from GRB 781119 obtained in the KONUS experiments during the first, second, third and eighth 4 s time intervals from the onset of the burst (Mazets and Golenetskii 1981*a*,*b*). The feature seen by the Ge detector on ISEE-3 in Figure 3.18 at 420 keV can be seen as a broad hump here in the spectrum taken during the first 4 s: it disappears later. Notice also how the spectrum becomes softer with time.

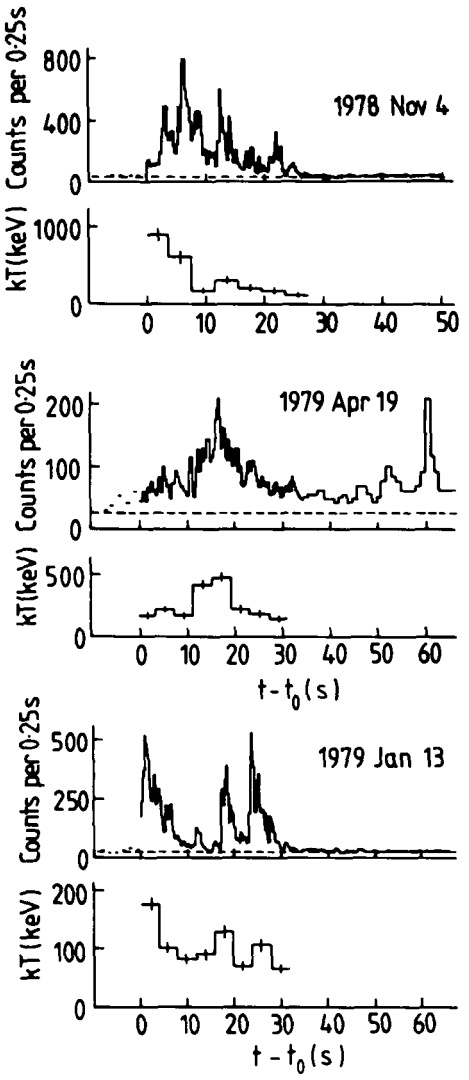

Figure 3.23. Time histories of total counts and spectral variations with time of γ-rays from three separate bursts GRB 781104, 790419 and 790113, as seen by the Leningrad group (Mazets *et al.* 1981*c*, 1982*a*). The figure suggests a positive correlation between the intensity and the characteristic spectral temperature, at least for some peaks.

In particular, the famous GRB 790305b shows both soft ($kT \sim 35$ keV) and hard ($kT \sim 500$ keV) components in its impulsive phase (Figure 3.20), but only the soft component later on during the following oscillations (Mazets and Golenetskii 1981*b*) and also during its subsequent recurrences (Golenetskii *et al.* 1984). Spectral variations, as expressed by the associated changes in the temperatures of the fits for the three bursts GRB 781104, GRB 790419 and GRB 790113, are shown in Figure 3.23, taken from Teegarden (1982). In the first example, the

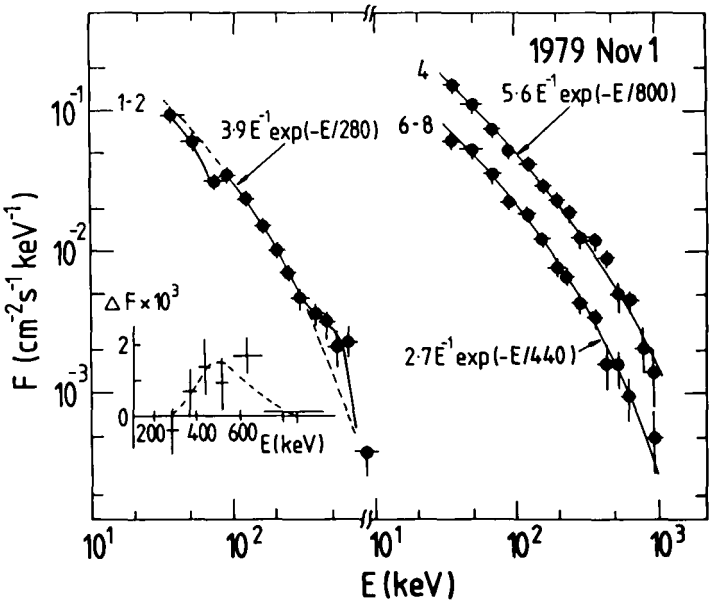

Figure 3.24. Evolution with time of the energy spectra for GRB 791101 from the KONUS experiments (Mazets *et al.* 1981*c*, 1982*a*) is shown. (1–2): the first 8 s of the burst; (4): the fourth 4 s interval; and (6–8): the combined data from the sixth, seventh and eighth 4 s intervals. Notice the disappearance of the absorption and emission features during the later stages of the burst and also the variation of the characteristic temperature with time.

temperature monotonically decreases with time; in the second it peaks well into the burst; and in the third it exhibits ups and downs, suggesting a positive correlation with the peak fluxes. Figure 3.24, also taken from Teegarden (1982), pertains to GRB 791101. It reveals a rich variety of phenomena; for example, at the beginning of the burst, both the emission and absorption features are exhibited and these disappear later. The continuum which was fitted with an optically thin thermal bremsstrahlung form has a temperature $kT = 280$ keV to start with, increasing to 800 keV, before it finally decreases to 440 keV. Time variability of the spectral features has also been seen by Barat *et al.* (1984*c*), who observed short duration line emissions from GRB 781104. The emission features were seen in the energy range 380–450 keV at confidence levels of 87–99 % in four different spectra, each integrated over 250 ms and mostly non-consecutive. The highest line emission flux among the four was 20.1 photons $cm^{-2}\,s^{-1}$.

Mazets *et al.* (1982*a*) have presented the interesting time profile and evolution with time of the continuum spectrum and the absorption feature of GRB 790731; see Figure 3.25. Here $\delta = (S_{tb} - S_{obs})/S_{tb}$, where S_{tb} and S_{obs} are the interpolated thermal bremsstrahlung continuum spectral flux and the observed flux, respectively, at the absorption feature. Likewise the authors also show the time profile

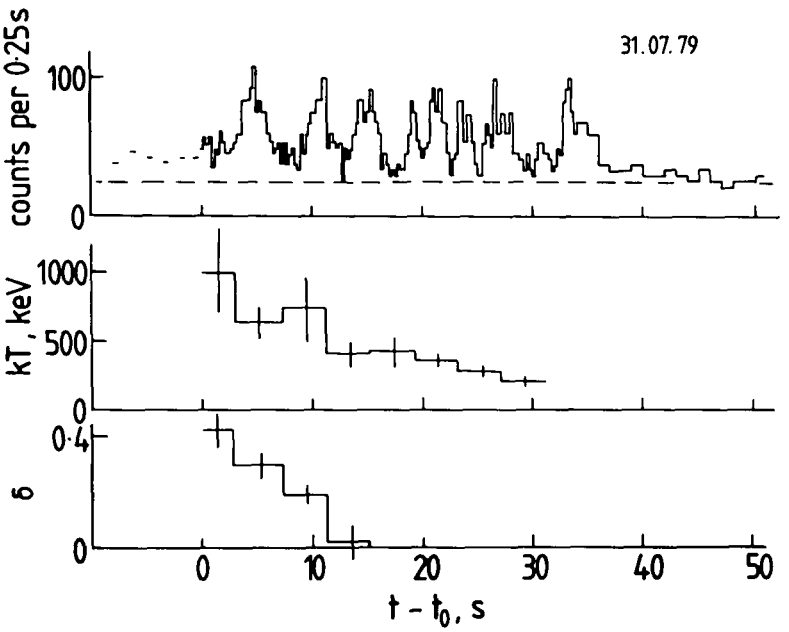

Figure 3.25. Time history of total count rate and variation with time of the temperature, kT, and of the amplitude, δ, of the absorption feature in GRB 790731, as seen in the KONUS experiments (Mazets *et al.* 1982*a*).

and evolution of the continuum spectrum and of the emission feature of GRB 790502; see Figure 3.26.

Spectral features, whenever present, are in most cases strongest during the initial phase and decay away much faster than the continuum. The continuum itself tends to exhibit a cooling down with time, although such behaviour is not universal (see, for example, Figures 3.23 and 3.24). These time variations present both an opportunity and a challenge to any successful modelling of GRB production mechanisms and source objects and a proper understanding of their nature.

3.4.4 Correlations

It has already been mentioned in Section 3.3.2 that the burst fluences (integrals of fluxes over time) show a positive correlation with the corresponding burst duration. It is not clear, however, if most short duration bursts have soft spectra, as claimed by Mazets *et al.* (1982*b*); see the discussion in Section 3.3.1. Golenetskii *et al.* (1983) and Mazets *et al.* (1983) present evidence to show that the fluxes and temperatures of the continuum spectra of GRBs are positively correlated. Due to an unintended drop of voltage across the photomultiplier in one of the six detectors on Venera 14, its energy sensitivity window became displaced to ΔE = 150–700 keV, whereas on Venera 13 it remained at the original ΔE = 40–180 keV. This enabled the authors to compare the count rates in the two energy windows with a 0.25 s resolution and to obtain information on fast

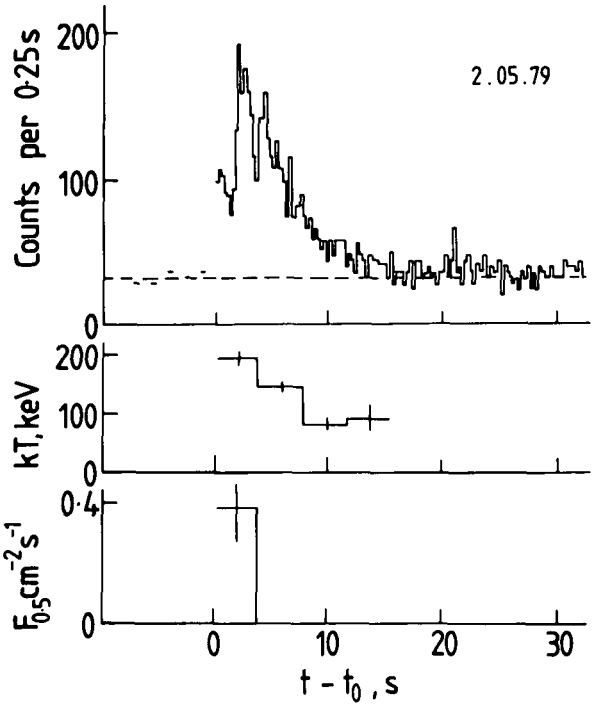

Figure 3.26. Time profile and variation with time of the temperature, kT, and of the annihilation flux, $F_{0.5}$, from GRB 790502, as seen in the KONUS experiments (Mazets *et al.* 1982*a*).

spectral variation. We have shown in Figure 3.27 the count rates (N_{13}, N_{14}) from the GRB 820827c as recorded by detectors on Venera 13 and 14, the ratio N_{14}/N_{13}, and the temperature deduced from this ratio as a function of time. It is qualitatively apparent from the figure that the higher the count rate, the higher is the temperature. Results from a quantitative study of four bursts are shown in Figure 3.28. Fits of the type $L \propto (kT)^{\gamma}$, where L, the luminosity of the source (as reflected by count rate), and T, the temperature (as revealed by the spectral shape), have been tried. The data from GRB 820828 and GRB 820827c are statistically the most significant and yield values for γ of 1.70 ± 0.15 and 1.65 ± 0.10, with correlation coefficients of 0.94 and 0.93, respectively, γ values for all the six plots range from 1.5 to 1.7 for $kT = 100$–1000 keV. γ may vary from burst to burst and within the same burst in its individual peaks. This correlation suggests, then, that the time profile is directly determined by spectral variability of radiation, which, of course, has to have a deeper reason.

Since the luminosity is a function of temperature (kT), volume (V) and electron density (n_e) in the source region, the functional relationship $L \propto T^{\gamma}$ implies that either V and n_e remain constant or that they vary with temperature in a rigidly controlled fashion for the duration of the burst. Different production mechanisms predict different values for γ. For example, optically thin thermal bremsstrahlung models predict $L \propto n_e^2 V T^{1/2}$, which is in disagreement with the observed $\sim T^{1.7}$

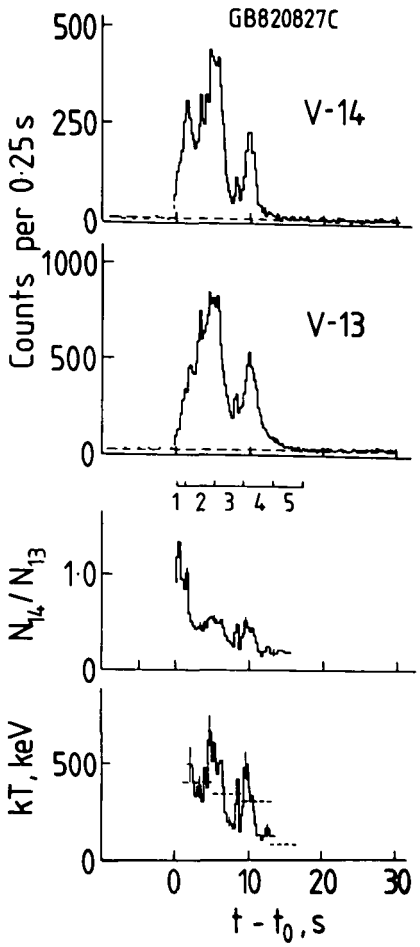

Figure 3.27. Time profiles and variation of hardness ratio, N_{14}/N_{13}, and temperature, kT, of GRB 820827c, as seen in the KONUS experiments (Mazets *et al.* 1983). The dashed lines in the upper two panels are the background counting rates. The temperature values, kT, are determined from the ratios N_{14}/N_{13} of count rates in detectors on Venera 14 and 13. The dashed lines in the bottom-most panel refer to temperatures of time-averaged (4 s) spectra during the intervals 2, 3, 4 and 5 shown in the third panel from the top.

dependence. Similarly, the authors conclude that the $T^{1.7}$ dependence is also in conflict with the thermal synchrotron models of Liang *et al.* (1983).

3.5 Identification of burst sources at other wavelengths

The optical identification of source objects has played a key role in the early development of radio and X-ray astronomies. Likewise the identification of GRB sources at optical and other wavelengths can be expected to be of crucial importance in establishing the nature of the sources responsible for GRBs, in knowing if there is more than one type, and in the successful modelling of GRB

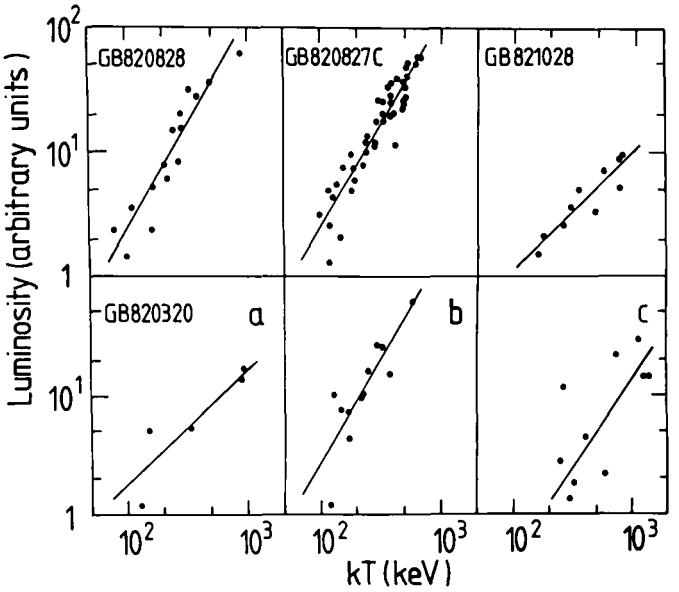

Figure 3.28. Correlation between luminosity and temperature in GRBs inferred by the Leningrad group (Golenetskii *et al.* 1983). Instantaneous luminosity vs kT plots. Top: GRB 820828, 820827c and 821028 events. Bottom: three stages (*a*), (*b*), (*c*) in the same multipeaked burst GRB 820320. (*a*) For the weak initial peak. (*b*) For the decaying stage of the second peak. (*c*) For the initial part of the third peak.

production processes. To do this, a precise localisation of a GRB source is a prerequisite in order to avoid chance associations.

Despite the large number ($\lesssim 500$) of published GRB detections, there are only 10 to 20 source locations which are determined to better than 5 arc min, a value small enough to allow meaningful searches for a counterpart at other wavelengths to be undertaken.

At the outset it must be stated that there is no point object seen in quiescent state with certainty in any of the GRB error boxes in the radio, infra-red, optical or X-ray ranges. The SGR source of the famous GRB 790305b has been associated with the supernova remnant, N49, in the Large Magellanic Cloud; even here there is no point object seen as a counterpart.

3.5.1 *General description of methods*

3.5.1A Catalogue searches

Knowing the GRB source direction, one simply looks up catalogues of interesting astronomical objects to find out if there are any objects in the error boxes. For example, H.F. Helmken and colleagues, at the Centre for Astrophysics, Cambridge, USA, have compiled a catalogue of over 10^5 interesting objects such as pulsars, radio sources, nearby stars, white dwarfs, SNRs, etc. (Hurley 1982).

The association of the well known GRB 790305b with the SNR N49 in the Large Magellanic Cloud was quickly found by this method (Evans *et al.* 1980; see Figure 3.29).

3.5.1B Optical searches

Optical searches may be categorised as follows:

(i) *Standard sky survey plates.* Plates such as those from the Palomar Observatory Sky Survey may be searched for objects in the error boxes. In most cases limiting magnitudes are $m \sim 21$. If found, these objects were probably photographed when they were in their quiescent state.

(ii) *Archival plate searches.* These searches, which assume that the GRBs are repetitive, are made for transient emission of light that was presumably simultaneous with the occurrence of the burst in the past. The signature is a presence of a star-like object in just one plate but not in those taken earlier or later. Schaefer (1981) detected an optical transient, 1928 OT, in the error box of GRB 781119 in this fashion. Schaefer had seen two others, 1901 OT and 1944 OT, in the error boxes of GRB 791105 and GRB 790113, respectively; however, these were seen in only one plate. Sometimes it is possible to find optical transients in two or more plates exposed to the same point in the sky simultaneously. As an example, Moskalenko *et al.* (1989) have seen an optical transient, 1959 OT, in the error box of GRB 791101. Another credible way of claiming an association of optical transients with a GRB source direction is to see them repeatedly at the same point in the sky; for example, Hudec *et al.* (1990) have seen three optical transients (1954 OT, 1946 March OT and 1946 August OT) at the same position near (but not exactly in) the error box of GRB 790325b. Since all photographic plates have defects on them, some of which may be confused with real candidate star images, one has to exercise extreme care in analysing image profiles and shapes. For the intricate details of establishing the reality of optical transients, see Schaefer (1990) and Zytkow (1990). The various claims of seeing optical transients are dealt with in Section 3.5.2.

(iii) *Real time searches.* In these one looks for optical emission in simultaneity with the GRB event. Grindlay, Wright and McCrosky (1974) have argued that a reasonable extrapolation of the observed γ-ray spectrum to optical frequencies would predict optical magnitudes $m_v \sim 0$ for the source object. They have looked for time and spatial coincidences between GRBs and optical flashes present in the records of the Priarie Network of 16 stations intended to monitor meteor trails and, not finding any, have set a lower limit to the magnitude, $m_v \geq 6$, for the optical counterpart of GRB 720514. Deriving a ratio of the energy fluxes in γ-rays and in the optical window of > 100, they conclude that GRBs are not scaled-up versions of solar flares, where one expects this ratio to be ~ 1. Hudec *et al.* (1984), using the Czechoslovak Fireball Network, did not find any optical counterparts for GRB 781124, GRB 790107 and GRB 790325. London and Cominsky (1983)

postulate a model in which γ-rays from a binary source are reprocessed by the companion star, resulting in the emission of optical light. They predict that one can record as many as 100 events in a year, provided that the instrument is sensitive to optical flashes at intensities ~ 200 photons cm^{-2}.

(iv) *Deep sky searches.* These are indicated whenever standard catalogue or survey plate searches do not show up any object (which is mostly the case) and when error boxes are known precisely enough either directly or through the intermediary of optical transients. If the search is deep enough, reaching a limiting magnitude $\gtrsim 25$, some object or other is bound to be seen in the error box, thus allowing one to state that no GRB error box is truly empty. At magnitudes $m_v > 22$, the density of galaxies equals or exceeds that of stars (Tyson and Jarvis 1979). This leads to a dilemma, and the association cannot be relied upon because extragalactic objects, in most cases, are unrelated to GRBs; see, however, Section 3.7 for suggestions by some authors that GRBs might in fact be extragalactic.

3.5.1C X-ray searches

These are of two varieties: (i) real time, and (ii) *post facto.*

(i) Real time searches are carried out by looking at data from an X-ray detector operating contemporaneously (often on the same spacecraft) with a GRB detector. Examples of positive identifications of GRBs at X-ray energies are the Apollo 16 event, GRB 720427 (Metzger *et al.* 1974, Gilman *et al.* 1980); GRB 720514 and GRB 740723 (Terrell *et al.* 1982). One must note that the field of view of an X-ray detector is much smaller than that of a GRB detector, leading to difficulties in establishing associations.

(ii) *Post-facto* searches for associations have been made by collecting new X-ray data from the known GRB directions, by using, for example, the imaging proportional counter (IPC) and the high resolution imager (HRI) on the Einstein Observatory (HEAO-B). Searches were also made using data from EXOSAT (Boer *et al.* 1988, 1990) and GINGA (Murakami *et al.* 1990) satellites. In contrast to case (i), one obtains in these searches information on the quiescent state of the GRB source. Most of the searches ended up in setting upper limits to X-ray fluxes from the GRB sources.

3.5.2 *Results from specific searches*

GRB 790305b. Localisation of the source was achieved on the basis of the International Network first by Evans *et al.* (1980) and later more accurately (~ 0.1 arc min) by Cline *et al.* (1982). The source of this GRB is now designated as GBS 0526−66. As mentioned several times already the source direction error box contains N49, an SNR in the Large Magellanic Cloud (Evans *et al.* 1980); see Figure 3.29. The N49 region was earlier observed to emit at radio wavelengths (Mathewson and Clark 1973). Independent of the occurrence of GRBs, the N49 region was also observed in soft X-rays by the Einstein Observatory eight days before and 38 days after the GRB occurrence, as a part of the X-ray survey of the

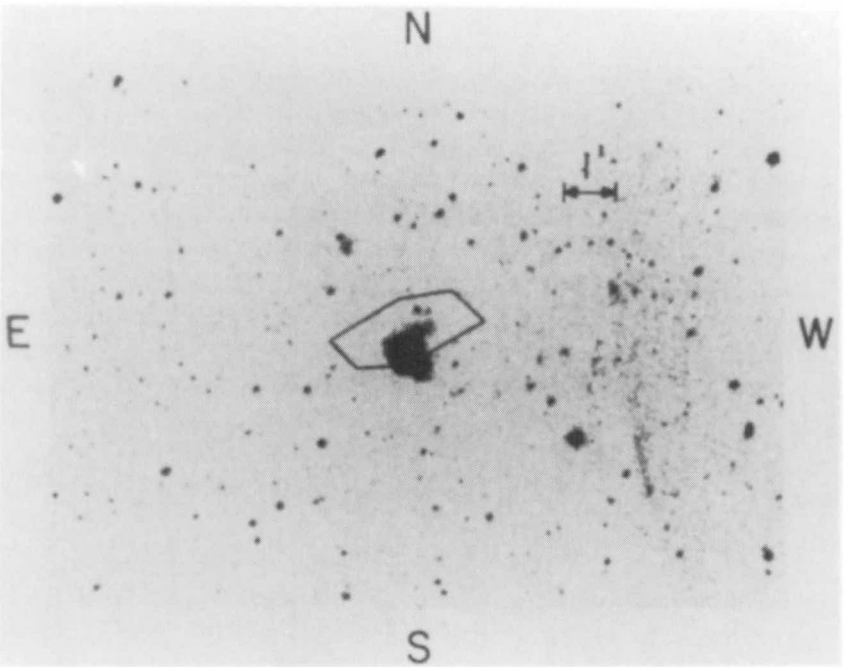

Figure 3.29. Association of the famous GRB 790305b with the SNR N49 in the Large Magellanic Cloud (Evans *et al.* 1980). The hexagon is the GRB localisation error box, and the irregular object near it is N49.

Large Magellanic Cloud. With the moderate resolution of the IPC, the X-ray image of N49 could not be resolved, and the authors conclude that the soft X-ray flux did not change between the two observations by more than 2.2×10^{-12} erg cm^{-2} s^{-1}. The high resolution imager could resolve N49, as shown in Figure 3.30; however, there was no point source seen, leading to an upper limit of 2×10^{-12} erg cm^{-2} s^{-1} in the energy range 0.5–4.5 keV. It is necessary to remark that this is a limit on the quiescent flux and not necessarily on the flux at the time of occurrence of the burst. The refined GRB error box lies within the X-ray diffused image of N49 but displaced by 15 to 55 arc sec.

Recently the N49 region was subjected to a deep optical search by using a CCD camera at the 1.5 m Danish telescope. Several stellar components were seen inside the refined GRB error box (Hurley 1983*a*). Pedersen *et al.* (1984) have also monitored the source position of this burst for ~910 h using a high speed photoelectric photometer with a diaphragm 20 × 80 (arc sec)^2, attached to a 50 cm telescope at ESO/La Silla. During the period October 5, 1983, to February 23, 1984, the authors had seen optical bursts on three occasions lasting for durations of 200 ms (on October 27, 1983), 20 ms (January 30, 1984) and 400 ms (February 8, 1984). The γ-ray detectors on four spacecraft – ICE, PVO, SMM and Prognoz 9 – did not show any GRBs simultaneous with these optical bursts. Neither did these detectors see any of the 16 recurrent bursts reported by the Leningrad group, which may be due to their threshold sensitivities being higher. Even the more

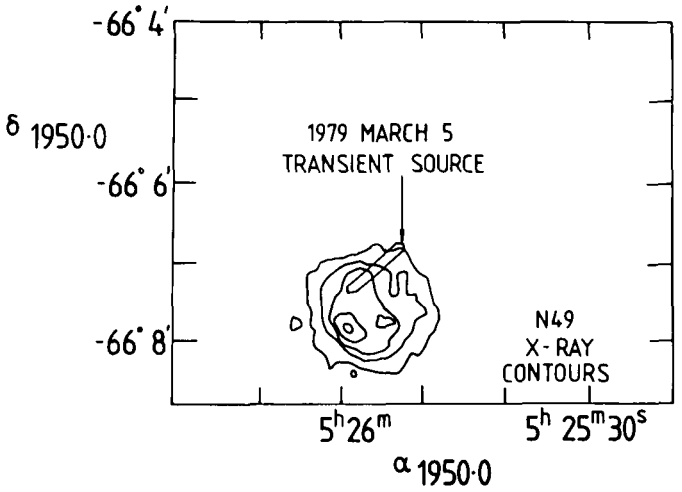

Figure 3.30. More precisely determined localisation error box for GRB 790305b (Cline *et al.* 1982) and the X-ray intensity contours of the SNR N49 obtained by the high resolution imager on the Einstein Observatory. The GRB error box is displaced from the X-ray centre by ~15″–55″.

sensitive KONUS detectors on Venera 13/14 have failed to see any GRBs from GBS 0526−66 on these three occasions, placing an upper limit of $\sim 10^{-6}$ erg cm^{-2} to the fluence of any GRBs that may have been coincidental with the optical transients (K. Hurley, 1991, private communication). If the association of the optical bursts with the source of GRB 790305b is real, the maximum brightnesses during the three optical bursts are $m = 8.4$, 9.9 and 8.7. The inferred values of the ratio of γ-ray to optical energy (L_γ/L_{opt}) during the bursts are less than 6000.

Searches were made for quiescent optical counterparts of GBS 0526−66, but none was found. Present magnitude limits are $m > 17.7$ for a steady quiescent counterpart (Pedersen *et al.* 1986) and $m > 19.4$ for a pulsating ($P = 8$ s) optical counterpart (Boer *et al.* 1989). No counterpart candidate was seen in the infra-red (Schaefer *et al.* 1987).

As mentioned in Section 3.1, association of this GRB with N49 has been questioned by Mazets and Golenetskii (1981*a*) and by Golenetskii *et al.* (1984), mainly on the basis that the Eddington luminosity limit would be violated if the source were located as far away as 55 kpc; the source may therefore be instead a foreground object to N49. Felten (1981) considers the statistics of chance coincidence carefully and arrives at the conclusion that the chance coincidence probability for the association is less than 10^{-3}. Furthermore, Ramaty *et al.* (1980, 1981) and Liang (1981) have shown that there is no difficulty in devising models to provide the requisite luminosity ($\sim 10^{45}$ erg s^{-1}) at the distance 55 kpc without violating the Eddington limit; see Section 3.4.2B. As yet there is no consensus on the reality of association between the GRB 790305b and the SNR N49 in the Large Magellanic Cloud.

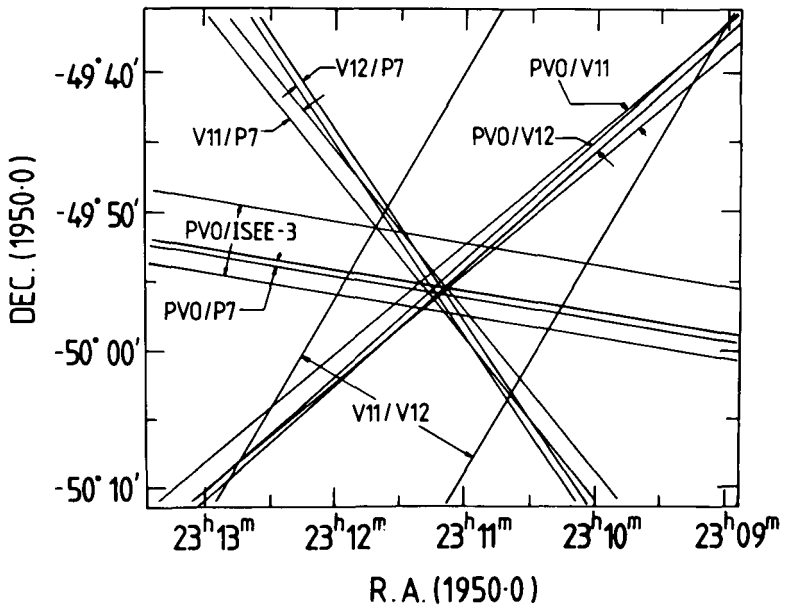

Figure 3.31. The error box determination for the GRB 790406 source direction as shown by Laros *et al.* (1981). The error bands in an approximately 0.5 square degree region centred on their common intersection are shown. The error box is defined by the PVO/V12, PVO/P7 and V12/P7 bands.

GRB 790406. Figure 3.31 shows how this source was localised by combining information from several detectors (Laros *et al.* 1981). The error box is $<1'$ in diameter. Figure 3.32 shows the absence of any optical candidate down to $m_v = 22.5$ in the survey plates taken with the UK Schmidt telescope. The error box is also devoid of known radio, infra-red and X-ray sources. Five objects are seen in the error box in a deep sky search using a CCD camera with the 1.5 m Danish telescope having a limiting magnitude 23.5; see Figure 3.33 (Hurley 1983*a*). It is not clear if these objects are really stars or galaxies.

GRB 790613. The source direction for this burst is localised to within 0.7 arc min^2 (Barat *et al.* 1984*b*). A search of 46 catalogues revealed no object within the error box; nor did the Palomar Observatory sky survey plates show any object down to $m \sim 21$. Radio observations at VLA, too, did not reveal an object (R. Hjellming, 1983, private communication to Barat *et al.* 1984*b*). No optical transients were seen in archival plate searches (600 h exposure at Sonnenberg Observatory and 10 h at Harvard).

GRB 781119. Although the localisation error box for this burst was ~ 10 arc min^2 (Cline *et al.* 1981*b*), the observation of an optical transient by Schaefer (1981, 1990), in an archival search in plates taken in 1928, within the GRB error box, effectively provided the link – one could substitute the much larger GRB error

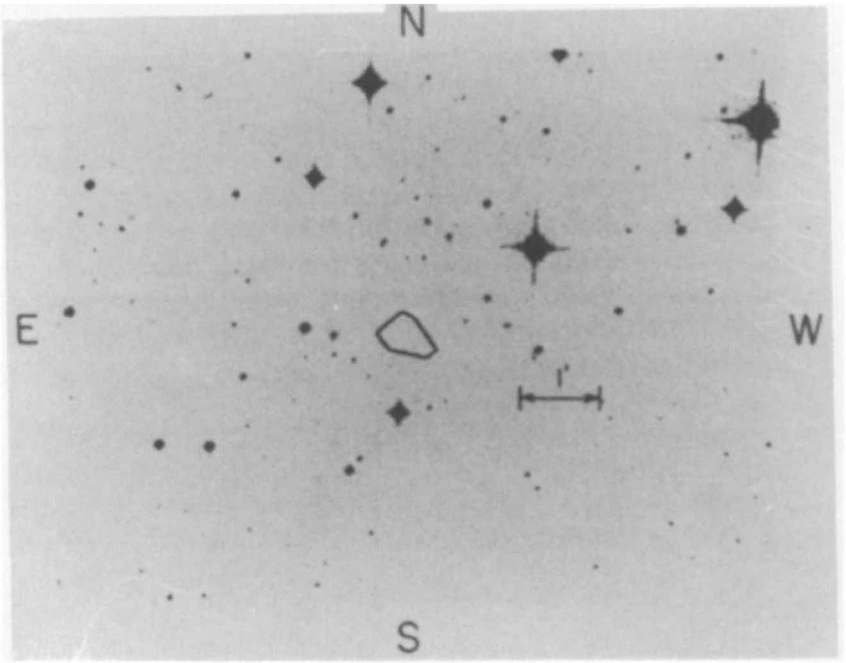

Figure 3.32. The figure shows the absence of any optical objects down to magnitude 22.5 in the error box (determination of which is illustrated in Figure 3.31) for the source direction of GRB 790406 (Laros *et al.* 1981). The photograph is from UK Schmidt plate 3659.

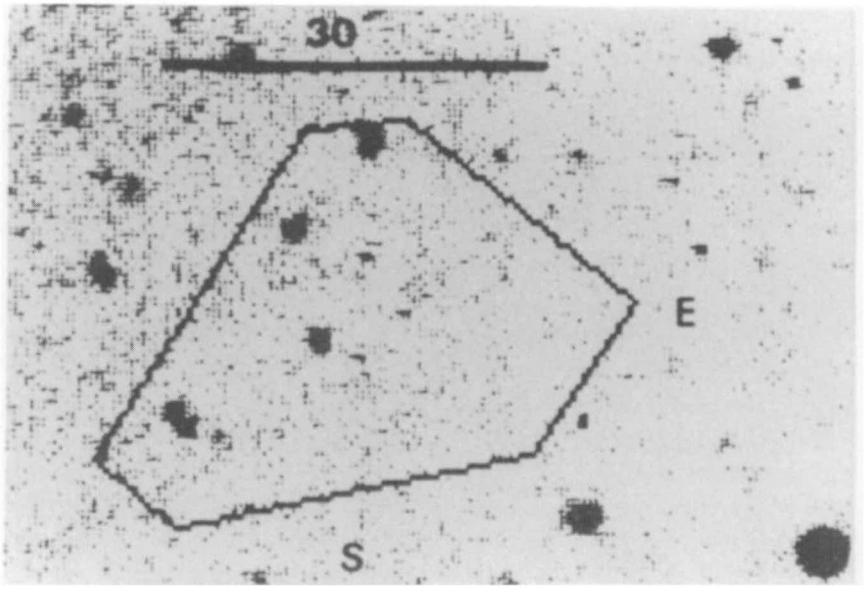

Figure 3.33. A partially processed CCD image of the error box region of GRB 790406 referred to Figures 3.31 and 3.32 (Hurley 1983*a*). The picture is taken at the Cassegrain focus of the 1.5 m Danish telescope at La Silla. Though the five star-like objects (at $m \sim 23.5$) are seen inside the error box, it is not clear if these are stars or galaxies. If they are galaxies, they are probably unrelated to the GRB source.

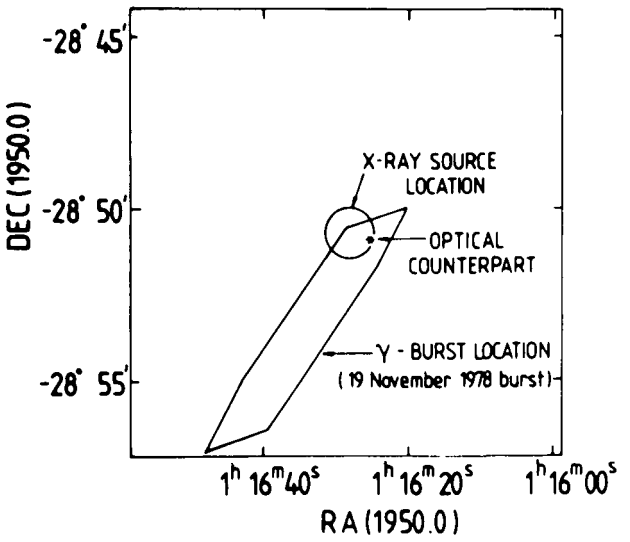

Figure 3.34. Location (90% confidence error circle with 45 arc sec radius centred at RA (1950) = 01 h 16 min 28.58 s, dec (1960) = −28°50′42″) of the quiescent X-ray source which is the probable counterpart for GRB 781119. The GRB source localisation error box (Cline *et al.* 1981*b*), location of the 1928 optical transient position (Schaefer 1981), and the X-ray source error circle determined from the IPC detector on the Einstein Observatory by Grindlay *et al.* (1982) are shown.

box with that of the optical flash which is only of size 8″ × 18″. The optical transient, now known as 1928 OT, was found in the fourth of six identical 45 m exposures taken in succession on November 17, 1928. If a 1 s duration is assumed, the flash has a magnitude $m_B \sim 3$. Assuming that the 1928 and 1978 bursts were similar, Schaefer deduces that $L_\gamma(>30\text{ keV})/L_{opt}$ (B band) is 800. Since the source was seen in 1928 (optical) and again in 1978 (GRB), the recurrence time must be ≤ 50 y. Hjellming and Ewald (1981) found several radio sources in and around the GRB error box with none of them coinciding with the transient error box. Grindlay *et al.* (1982) and Pizzichini *et al.* (1986), based on a 9000 s X-ray guest observation with Einstein Observatory, found an X-ray source with an error circle of 45 arc sec radius centred 42 arc sec north-east of the optical counterpart; see Figure 3.34. The X-ray flux in the 0.5–3 keV band is 1.0×10^{-13} erg cm^{-2} s^{-1}, which is obviously the flux in the quiescent state. Since the quiescent optical flux seems to be variable (see below), the authors could set only a poorly determined limit to the ratio of fluxes $L_X/L_{opt} = 6$–60, which does not constrain the various models. The probable maximum luminosity is only $\sim 10^{31}$ erg s^{-1} and, according to Grindlay *et al.* (1982), supports the hypothesis that either GRBs are produced by accretion instabilities or, if due to thermonuclear flashes, they recur at intervals of at least 50 y. The GRP error box has been searched by Boer *et al.* (1988) in the EXOSAT data. Not finding any point source, the authors state that there is a problem of consistency between the Einstein and EXOSAT data in the framework of dense disk models but that the two are compatible in the slow

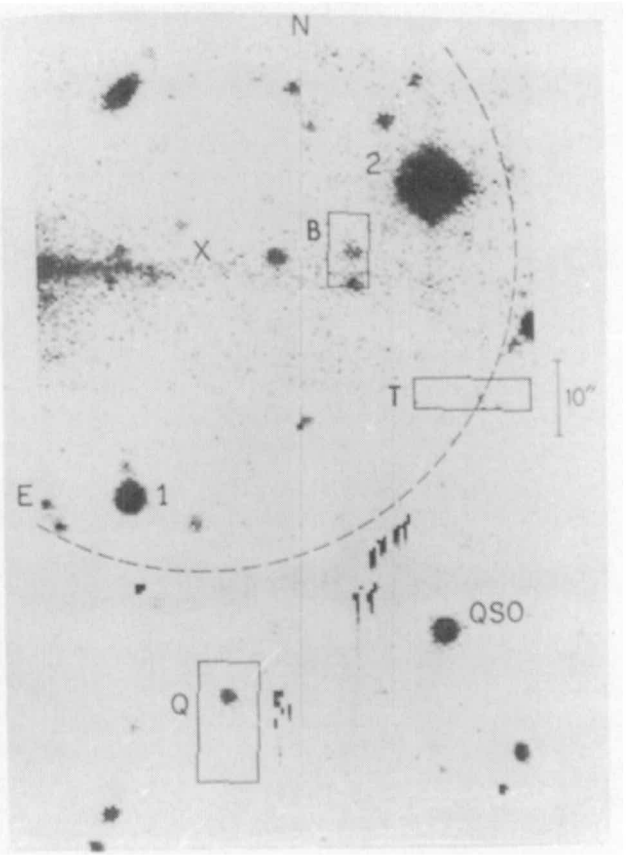

Figure 3.35. The region near the source direction of GRB 781119 is shown (Pedersen *et al.* 1983). The GRB source localisation error box, being much larger than the whole figure, is not shown. T is the 1928 optical transient error box (Schaefer 1981). X and circle: centre and error circle of the X-ray source (Grindlay *et al.* 1982; see Figure 3.34). B, Q: error regions of two radio sources (Hjellming and Ewald 1981). A QSO and two stars (1, 2) are also marked. Two suspected optical counterparts well within T are shown in Figure 3.36.

accretion models if the source distance is greater than 20 kpc. In the thermonuclear models, consistency may be obtained even for source distances as near as 2 kpc. Pedersen *et al.* (1983) conclude that, on the basis of the observed GRB fluence (3×10^{-4} erg cm^{-2}) and X-ray flux (10^{-13} erg cm^{-2} s^{-1}), either the conversion of accretion energy into X-rays is extremely inefficient or the thermonuclear models of GRBs are not correct. In a deep sky search, Pedersen *et al.* (1983) found two objects A and B inside the optical transient error box; see Figures 3.35 and 3.36, at magnitudes $m_R \sim 23.5$. The authors found that object B was definitely variable by more than 1.3 magnitudes, while A was only mildly so. In an almost simultaneous observation, Schaefer, Seitzer and Bradt (1983) identified object A and two others inside the optical flash error box, but not B. These authors found that object A was variable by more than 1 magnitude over periods $\sim$1 d. It is

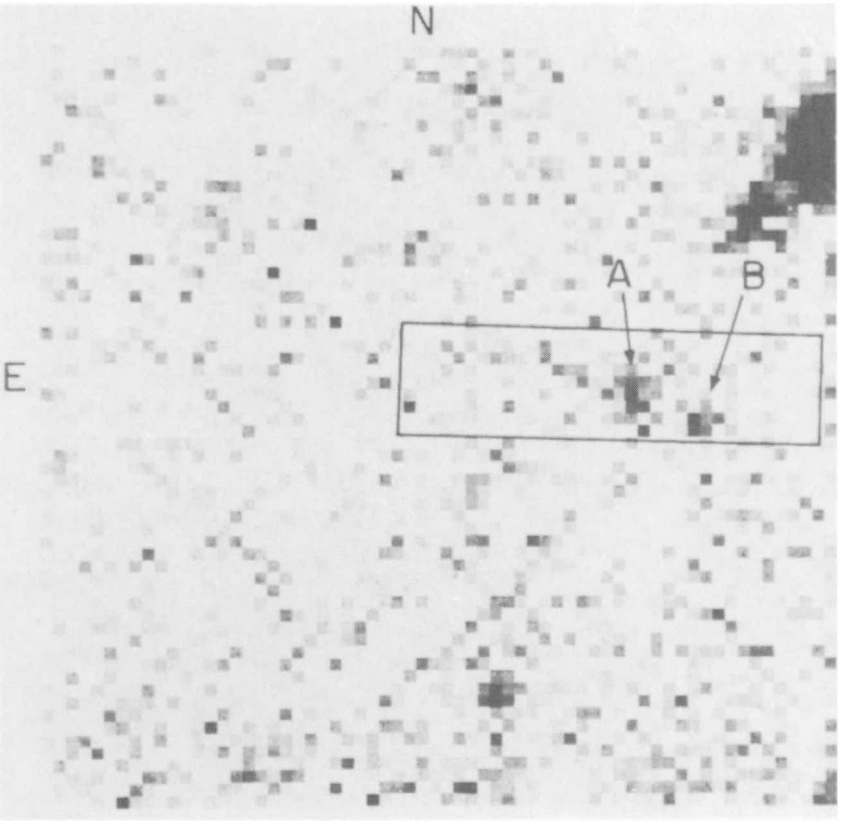

Figure 3.36. A close-up of CCD pictures summed over ~7.75 h exposure of the region near the 4″ × 16″ error box of the 1928 optical transient (Schaefer 1981, Pedersen *et al.* 1983). These workers find the optical object B ($m_R \sim 23.5$) to be variable by more than 1.3 magnitudes, while A is only mildly so. In a comparison paper, Schaefer *et al.* (1983) reported finding object A to be variable and not seeing object B at all.

not clear if either A or B is the GRB source object. If neither is the source, then it is fainter than 25th magnitude. Pedersen *et al.* consider the possibility that the source might have moved out of the transient error box in the 54 years from 1928 to 1982. Assuming a value of 1 km s^{-1} pc^{-1} for the velocity–distance ratio, the object could have moved out by 10 arc sec. They found that there was no star-like image brighter than $m_R \sim 22$ within 25″ of the 1928 error box.

GRB 791105. Schaefer *et al.* (1984) detected in an archival plate search an optical transient in the photographic plates taken on October 4, 1901; see Schaefer (1990) for a critical discussion. If a 1 s duration is assumed for the optical flash (now known as 1901 OT), a magnitude of 6.6 could have been reached. The 1901 optical error box is empty in Palomar sky survey plates. The estimated value of L_γ/L_{opt} is of order 900, provided that the 1901 burst had the same γ-ray intensity as the

one in 1979. The optical transient (1901) and GRB (1979) observations imply that the recurrence time is less than 78 y for this burst.

GRB 790113. The localisation error for this GRB is rather large (~ 78 arc min^2), and several objects are found in the photographic plates taken with the ESO 3.6 m telescope (Barat *et al.* 1984*d*). Schaefer *et al.* (1984) found an optical transient in their archival search in plates taken in 1944. The error box of the optical flash is empty in ESO QB survey plates down to a magnitude ~ 21; however, more recent images taken with the ESO 1.5 m Danish telescope (limiting magnitude ~ 23) show clear evidence of an object in the transient error box. The estimated value for L_γ/L_{opt} is ≈ 800 (Vedrenne 1984). The recurrence time is less than 35 y for this burst, as deduced from the transient (1944) and GRB (1979) observations.

GRB 790325b. Laros *et al.* (1985*b*) have localised the source of this GRB to within an error of ~ 0.3 arc min. Hudec *et al.* (1990) have searched archival plates and found optical transients on three different occasions (April 27, 1954, March 28, 1946, and August 31, 1946) from the same point in the sky, removed by 5 arc min from the localisation by Laros *et al.* (1985*b*). Since the deviation is $\gtrsim 15$ standard deviations, there was some question as to whether there was any error in the localisation. Laros (1988) has re-examined the localisation procedures and asserted that there was no error. The claimed association of the optical transients with GRB 790325b is, therefore, in some doubt.

GRB 791101. Moskalenko *et al.* (1989) have searched the archival plates taken by a seven-camera astrograph in the collection of Odessa University Observatory. They have seen an optical transient in two of the plates exposed simultaneously in two different cameras on October 20, 1959, in the error box of GRB 791101. Based on this 1959 OT, the authors estimate that $L_\gamma/L_{opt} \approx 10^4$. There is no object in the POSS plates at the position of the 1959 OT brighter than 19th magnitude.

Schaefer (1990) has considered all the optical transients considered above and has concluded that, for an assumed $L_\gamma/L_{opt} \lesssim 1000$, the average recurrence time for optical transients from GRB sources is 1.3 y; it lies between 0.41 and 4.8 y at the 99% confidence level.

GRB 720514. An X-ray association with this GRB was reported by Terrell *et al.* (1982) using data from the collimated X-ray detectors (3–12 keV) on the VELA spacecraft. Near coincidence, both in spatial direction and in time (see Figure 3.37), establishes the identity. Since their view was limited (FWHM = 6°), the X-ray detectors on the spacecraft, which are spinning with a period ~ 64 s, may not be viewing the GRB precisely at the time the GRB took place. X-ray peaks from this object were first seen 39 s after the GRB, which was of 3 s duration, and four more times at intervals of a few hundred seconds.

GRB 740723. Terrell *et al.* (1982) have reported X-ray association for this GRB in a similar manner to the burst mentioned above. The first X-ray peak from this

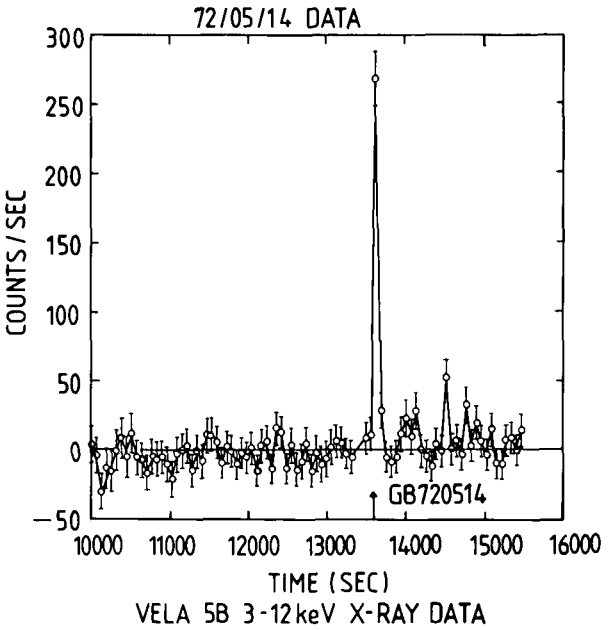

Figure 3.37. Time profile of X-ray counting rate in the 3–12 keV energy band as seen in the collimated X-ray detectors in the direction of GRB 720514 on VELA spacecraft by Terrell *et al.* (1982). The data are 3 s sums at 63.6 s intervals, corrected for the background. Note the recurrence behaviour (smaller peaks to the right of the main peak) on time scales of hundreds of seconds. The GRB event time is shown by an arrow on the x-axis.

GRB was seen 18 s earlier than the trigger for the GRB, which was of 7 s duration. Two more X-ray peaks were seen after intervals of 64 and 699 s. The VELA X-ray detectors also saw some isolated X-ray bursts, which may correspond to GRBs too weak to be detected (Evans, Belian and Conner 1976).

Helfand and Long (1979), searching the Einstein Observatory data base, set the following upper limits for X-ray emission in units of erg cm^{-2} s^{-1} in the 0.5–4 keV energy band: GRB 780305, $<2.1 \times 10^{-12}$; GRB 780329, $<2.1 \times 10^{-12}$; GRB 790406, 2.1×10^{-12}; and GRB 791104, 3×10^{-13}.

There are many other searches reported in the literature, with perhaps less significance than those listed above; see Cline (1983), Hurley (1983*a–c*) and Vedrenne (1984).

3.6 Statistics of gamma-ray bursts

Since GRB sources could not be identified with any known astronomical objects (excepts perhaps in the case of GRB 790305b) an understanding of their origin is rendered difficult. Nevertheless it is possible to make a statistical study of some of the observed properties and hopefully get closer to the solution of origin, at least to know what the source regions are, e.g. Galactic or extragalactic.

3.6.1 *Frequency of occurrence*

In the SIGNE (Franco–Soviet collaboration) experiments, detectors on Prognoz 7, Venera 11 and 12 yielded 40 GRBs in 474 d, i.e. $0.08 \pm 0.01\ d^{-1}$, during the period October, 1978, to April, 1980 (Hurley 1984). The same group later observed 104 GRBs in 399 d, i.e. $0.26 \pm 0.03\ d^{-1}$, in detectors on Venera 13 and 14. This three-fold increase in the detectable rate is attributed to a lower energy threshold and/or a more sensitive trigger algorithm in the latter detectors.

In the KONUS experiments, 143 GRBs were seen in 384 d, i.e. $0.37 \pm 0.03\ d^{-1}$, in detectors aboard Venera 11 and 12. Later, the KONUS group detected 180 GRBs in 400 d, i.e. $0.45 \pm 0.02\ d^{-1}$, in detectors on Venera 13 and 14.

Balloon experiments, though more sensitive in detecting GRBs, are of short duration, and seldom more than one burst is detected in a single flight. Many groups could set only upper limits to the frequency of occurrence of GRBs. The experiments of Bewick *et al.* (1975) and Beurle *et al.* (1981) suggest that the burst frequency is perhaps several thousand per year, i.e. $\sim 25\ d^{-1}$, at fluences $\geq 10^{-8}\ erg\ cm^{-2}$. Meegan *et al.* (1985) made two balloon flights for a total duration of 64 h and detected just one GRB. From this observation the authors set an upper limit of 2300 GRBs y^{-1} at fluences of $\gtrsim 6 \times 10^{-7}\ erg\ cm^{-2}$. Helfand and Vrtilek (1983), using the data base of the Einstein Observatory, have set an upper limit of $10^5\ y^{-1}$, i.e. $274\ d^{-1}$, for GRBs with fluences above $S \sim 10^{-10}\ erg\ cm^{-2}$ at $E_\gamma \sim 1$ keV. The GRO is currently detecting bursts at a rate of about one per day (although the threshold level for fluence is not clear).

If the emission of γ-rays is not isotropic, a certain fraction, depending on the degree of beaming, will go undetected even by the most sensitive detector. In such a situation, therefore, there is no sure method of estimating the true rate of occurrence of GRBs in nature.

3.6.2 *Source distances*

A knowledge of the intrinsic luminosity of GRBs is very important in understanding GRB production mechanisms. The observed quantities are the fluence and the source direction but not the distance, which is essential in calculating the luminosity. The circumstances prevailing at other wavelengths (e.g. red-shifts at optical wavelengths and the dispersion measure at radio frequencies) are simply not there to be utilised with GRBs. Consequently indirect arguments are brought to bear on the subject.

Noting that the spatial density of the GRB sources cannot exceed Oort's upper limit on the local invisible mass density, Schaefer and Ricker (1983) conclude that these sources (with assumed masses of $1.4 M_\odot$) must be further than 3.2 pc from the solar system.

The peak intensity of the weakest confirmed GRB appears to be $2 \times 10^{-7}\ erg\ cm^{-2}\ s^{-1}$ from satellite data (Hurley 1984). If one assumes that the emission is isotropic, and that the source is a neutron star of mass $1.4 M_\odot$, the Eddington luminosity limit allows the source to be placed as far away as 2.5 kpc. However, there are situations where one need not be constrained by the Eddington luminosity limit.

The detected GRB sources are isotropically distributed (see Section 3.6.3), and this implies that either the sources are very near (nearer than a few hundred parsecs), or very far (farther than the edge of the Galaxy). If the sources are far, they have to be beyond about 500 Mpc; at shorter distances the distribution of matter is too inhomogeneous to produce isotropy. For example, the Virgo cluster ($\sim$18 MPc away) would have introduced an unacceptable anisotropy (Jennings and White 1980). Such large distances would imply incredibly high luminosities, and it is usual to fall back on the hypothesis that, by and large, GRBs are Galactic objects.

Schmidt (1978) argues that, due to γ–γ interactions, there is an upper limit to the density of photons in the source regions emitting MeV γ-rays. Combining this with the information on time structure (to gauge the dimensions of source region) and observed intensities, he concludes that GRB sources cannot be further than a few kpc. Cavallo and Rees (1978) arrive at a similar conclusion. Liang (1982) points out that the absence of an observable low energy turnover due to synchrotron self-absorption puts an upper limit on the source luminosity and therefore on its distance at between 10 kpc and 1 Mpc.

As was noted in Section 3.4.1, Murakami (1990) pointed out that soft X-ray emission lasts for a long time ($\sim$100 s) after the main burst in some GRBs. These soft X-rays fit a black body spectrum with a temperature of 1 to 2 keV. If the radius of the emission region is $\sim$1 km (neutron star origin is assumed), then the emissivity and the temperature of the black body spectrum constrain the source distances to values $\sim$1 kpc.

Despite the extraordinarily high intensities needed, there have been suggestions made that GRB sources are extragalactic. Hurley (1989*a*) has listed arguments in favour of distant extragalactic sources. The arguments are centred mainly around the lack of proof that the sources are Galactic objects. Paczynski (1986) has suggested that the recurrences seen from the soft gamma repeater GBS 1900+14 are due to gravitational lensing by a galaxy of mass $\sim 10^{10} M_{\odot}$ of a single burst that originated at cosmological distances with $z = 1$ or 2. The required luminosity in such a case is 10^{51} erg s^{-1}. Paczynski (1987) also suggests that the recurrences from another soft repeater GBS 1806−20 are due to microlensing by a rich cluster of galaxies of a single GRB originating at cosmological distances. Babul *et al.* (1987) suggest that GRBs might originate at the cusps of superconducting cosmic strings at red-shifts as large as 1000 and any microlensing (very probable because of large distance) of such a burst will produce images (observable GRBs) with dissimilar spectra and time profiles.

The question of true distances to GRB sources, therefore, remains wide open; however, we, ourselves, favour a largely Galactic origin.

3.6.3 Angular distributions

A study of angular distributions of the source directions may lead to an understanding of where the GRB sources predominantly lie. Unlike the case of counterpart searches one can utilise here even those localisations with large errors.

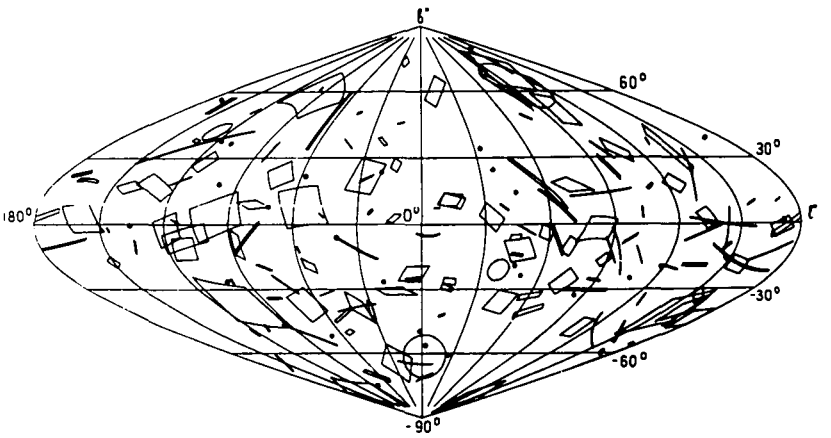

Figure 3.38. Distribution of source directions for 175 GRBs in Galactic coordinates (Golenetskii 1988). Note the different sizes and shapes of the source localisation error boxes.

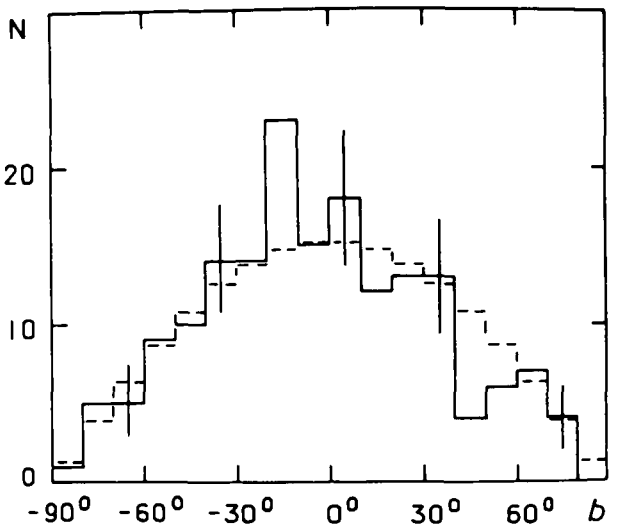

Figure 3.39. Distribution in Galactic latitude, *b*, of the source directions for 175 GRBs is shown by the solid histogram (Golenetskii 1988). The expectation, shown by the dashed histogram, is on the basis of an isotropic distribution.

Source directions for 175 GRBs in Galactic coordinates are shown in Figure 3.38, taken from Golenetskii (1988). The majority of the bursts were localised in the KONUS experiment on the Venera 11–14 spacecraft. As can be seen from the figure, the distribution appears uniform in the sky. Neither the Galactic Plane nor the Galactic Centre show any excess GRB sources. The distribution of the same sample in Galactic latitude is shown in Figure 3.39. The histogram is compatible with isotropic distribution of GRB sources. The distributions in Figures 3.38 and

3.39 do not conclusively tell us if the distances are small (~ 0.3 kpc) on the Galactic scale or large on the cosmological scale. If the GRO observations can extend to sufficiently small fluences, an enhancement in the general direction of the Galactic Plane will be observed if, as we think, the majority of GRBs are Galactic.

Hartmann and Epstein (1989) have analysed the angular distributions in terms of their multipole moments. The method is coordinate free and takes into account the finite sizes of GRB error boxes. The authors find that the dipole and quadrupole moments of the localisations are consistent with isotropic distribution of GRB sources in space. Hartmann and Blumenthal (1989) have tested if the GRBs are associated with objects at great distances by comparing their clustering properties with those of known extragalactic populations. The authors have concluded that, if the spatial correlation of GRB sources resembles that of galaxies or galaxy clusters, the present GRB catalogues must be complete to distances ~ 100 Mpc. Alternatively, if the GRB sources are a Galactic disk population, the same sample depth is less than two disk scale heights.

3.6.4 *log* N–*log* S *distribution*

In these distributions, one plots $N(>S)$, the number of GRBs with fluence, or size, greater than S, versus S. If the sources are uniformly distributed throughout space, one expects to see a relation of the type $N(>S) \propto S^{\delta}$, with $\delta = -3/2$, this form resulting from a cubical dependence of the number of bursts on radial distance (a constant density is assumed) and the inverse square law of burst intensity (monoluminosity is assumed) for isotropic emission. Likewise for sources confined to a thin sheet (approximating to the shape of the Galactic disk), one expects δ to be -1. For sources strung out along an infinite line (approximating the shape of the Galactic arm), on the other hand, $\delta = -0.5$. Since the Galactic volume, disk area or spiral arm length are all finite in extent, one expects the distribution to flatten over at sufficiently small values of S (below which there is no more contribution to the integral), exhibiting a $\delta = 0$ behaviour. One makes additional assumptions on the distribution of intrinsic luminosity of GRB sources, on the radial dependence in the case of halo models, and on the height (above the Galactic Plane) dependence in the case of disk models.

There are many compilations of $\log N$–$\log S$ relations of GRBs published in the literature. We show just one of them in Figure 3.40 (Hurley 1989*a*) together with exceptions for various source locations. The apparent turn-off at low fluences from the $S^{-3/2}$ line was noticed by several in the past. If this turn-off at low fluences is real, then there is an apparent contradiction between the isotropic sky positions of GRBs shown in Figures 3.38 and 3.39 and the size–frequency distribution at low fluences.

Detailed mathematical computations to understand the observed size distributions have been carried out by Yoshimori (1978), Fishman (1979), Jennings and White (1980) and Jennings (1982*a*,*b*). In recent years, however, there has been a growing realisation that the turn-off at low fluences is not real but is caused by instrumental selection biases; see, for example, Higdon and Lingenfelter (1984, 1985), Mazets (1985) and Jennings (1988). According to Golenetskii (1988), the

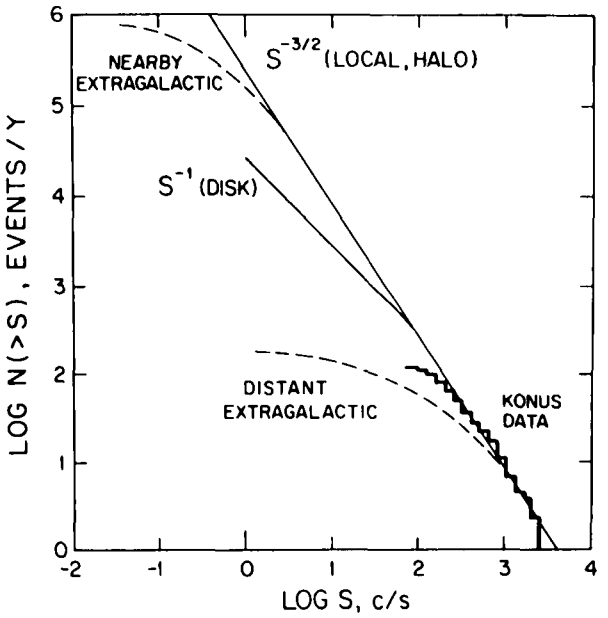

Figure 3.40. Log $N(>S)$ against log S distribution. Observations (histogram) is from KONUS data (Golenetskii 1988) and the distributions expected from (i) local region (distances less than the scale height of Galactic Disk) or Galactic Halo, (ii) Galactic Disk, (iii) nearby extragalactic, and (iv) distant extragalactic sources, as illustrated by Hurley (1989*a*). The turnover for extragalactic sources is due to red-shift effects.

detection threshold for long duration (~ 100 s) bursts is in the region 10^{-5}–10^{-4} erg cm^{-2}, whereas for bursts of 1 s duration, it is as low as 2×10^{-7} erg cm^{-2}. The role played by selection biases is illustrated in Figure 3.41 (Mazets and Golenetskii 1987), where the cumulative burst numbers are plotted on a log–log scale as a function of fluence (erg cm^{-2}), peak power (erg cm^{-2} s^{-1}) and peak counting rate (counts s^{-1}) for the same population of GRBs. The cumulative distribution of peak counting rate appears to suffer the least from selection bias; even here one notices a small deviation at low fluences which Mazets and Golenetskii (1987) attribute to selection biases.

Schmidt *et al.* (1988) and Higdon and Schmidt (1990) have carried out a different test on GRB distributions. This test, called the V/V_{max} test, is insensitive to variations in detection limit and instrumental sensitivity. Consider a GRB originating from a source at a distance r that produces a peak counting rate C_p in the detector. One computes r_{max}, the maximal distance at which the source could lie and still be detected with the same detection algorithm. Assuming space is Euclidean, the observed peak counting rate from a given GRB will depend on its distance as r^{-2}, and $r_{max} = r(C_p/C_{lim})$, where C_{lim} is the limiting (minimal) peak counting rate that triggers detection. The ratio of volumes, V/V_{max}, equals $(C_p/C_{lim})^{-3/2}$. For an isotropic distribution of GBSs in a Euclidean space, one

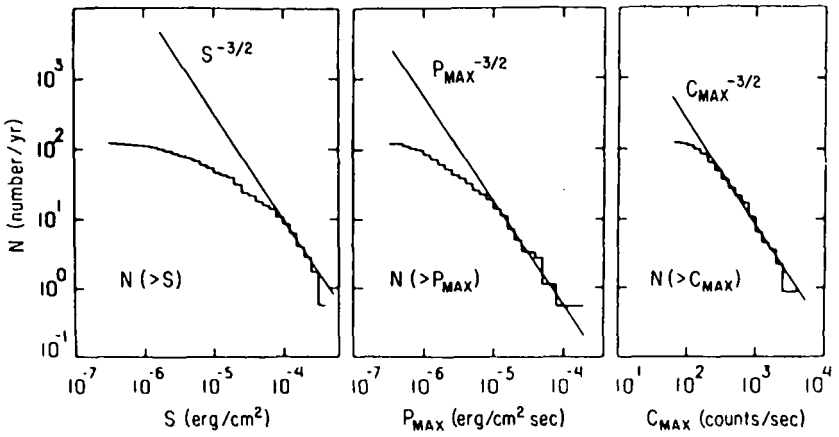

Figure 3.41. Cumulative frequency distributions of KONUS bursts (Mazets and Golenetskii 1987) with duration greater than 1 s, plotted as a function of fluence, peak power and peak count rate in the left, middle and right panels, respectively. The straight lines, $y \propto x^{-3/2}$, are the expectations for isotropic distribution of GRB sources.

expects V/V_{max} to be distributed uniformly between 0 and 1 with a mean of 0.5 and an error of $(12N)^{-1/2}$, where N is the sample size. Schmidt *et al.* (1988) have applied this test to a sample of 13 GRBs from the HEAO A-4 experiment and have found $\langle V/V_{max} \rangle = 0.40 \pm 0.08$. Later, Higdon and Schmidt (1990) applied the same test to a sample of 123 GRBs of duration longer than 1 s recorded by the KONUS experiment and found $\langle V/V_{max} \rangle = 0.45 \pm 0.03$. Both the tests are compatible with an isotropic distribution of GRB sources within a 2σ limit.

Despite these claims of isotropic distribution of GRBs, one cannot but take note of the fact that balloon experiments (Beurle *et al.* 1981, Meegan *et al.* 1985) detect GRBs at a rate much lower than what is suggested by an extrapolation of the $S^{-3/2}$ law to low burst sizes. As an example, Meegan *et al.* (1985) were able to record only one GRB at fluences $\geq 6 \times 10^{-7}$ erg cm^{-2}, when the expectation on the basis of $S^{-3/2}$ extrapolation from observations at higher fluences ($\sim 10^{-4}$ erg cm^{-2}) was 43 bursts. This turn-off at very low fluences suggests that GRBs are perhaps a disk population. A celestial plot of GRBs with extremely low fluences observed by future sensitive detectors will test such a hint, as has already been remarked.

3.7 Source models and mechanisms

> There is something fascinating about science. One gets such wholesome returns of conjecture out of such trifling investment of fact
>
> Mark Twain, *Life on Mississippi* (1874)

During the 24 years that have elapsed since the discovery of GRB (1967) by Klebesadel *et al.* (1973), an impressive body of experimental facts and theoretical insights into the subject has been assembled, and yet the phenomenon remains an enigma. Immediately after the discovery of GRBs, there was a plethora

of models to explain their origin. Candidate objects considered for GRB sources ranged from Fermi-sized primordial black holes and 10 m-sized nuclear goblins to 10 km-sized accreting neutron stars. At the present time (1992), the consensus appears to be that GRBs originate somehow on or near neutron stars with high magnetic fields. We will list these arguments in Section 3.7.1. There is, however, no agreement on the location of GRB sources. The widely differing scenarios of energy release and the actual γ-ray production mechanisms, on which there is also no consensus as yet, are briefly mentioned in Section 3.7.2.

3.7.1 Neutron star origin of gamma-ray bursts

The hypothesis that GRBs originate on neutron stars with intense magnetic fields is supported by the following model-independent considerations:

(i) Fast variations in the time profiles of several GRBs and periodicity observed at least in one case (see Section 3.3) strongly suggest that the source objects are very compact and dense, having densities greater than 10^9 g cm^{-3}.

(ii) Excess counts in the 400–500 keV energy range in the spectra of some of the bursts are interpreted as being due to red-shifted annihilation lines (see Section 3.4.2B). This implies that the gravitational potentials in the emission regions are $\sim(0.1\text{–}0.2)c^2$. Such potentials are obtained near the surface region of a neutron star.

(iii) Deficit counts, in the 20–70 keV energy band, in the spectra of some of the bursts are explained as being due to cyclotron absorption features (see Section 3.4.2A). This points to the existence of magnetic fields of $\sim 2 \times 10^{12}$ G in the source regions. Such intense magnetic fields are believed to exist near neutron stars.

(iv) The maximum surface temperature (and hence the luminosity) that can be achieved by a neutron star in hydrostatic equilibrium occurs when the force of gravity just balances the radiation stress (Colgate and Petschek 1981, Ruderman 1981, Lamb 1982); i.e.

$$\frac{aT_E^4}{4} = \frac{\mu m_H}{\sigma_T}\frac{GM}{R^2} \tag{3.17}$$

Here, a is the Stefan–Boltzmann constant; T_E is the maximum surface temperature; μ is the mean molecular weight per particle; m_H is the atomic mass of hydrogen; σ_T is the Thomson cross section; and M and R are the mass and radius of the star, respectively. Whereas the resulting Eddington luminosities ($\sim 1.3 \times 10^{38}$ erg s^{-1}) can admit the observed GRB intensities up to a reasonable maximum source distance, the limitation imposed on temperature by the above equation, namely

$$T_E = 1.8\mu^{1/4}(M/M_\odot)^{1/4}R_6^{-1/2}\ \text{keV} \tag{3.18}$$

is more restrictive. Here, R_6 is the radius of the object in units of 10^6 cm. Observed energy spectra indicate temperatures ~ 200 keV, whereas equation (3.18) indicates very low temperatures, of the order of a few keV. If, on the other hand, a strong magnetic field is present, and if the plasma is radiation dominated, it can be confined perpendicular to the field provided that the radiation pressure is smaller

than the magnetic pressure, i.e.

$$\tfrac{1}{3}aT^4 \leq B^2/8\pi \tag{3.19}$$

This corresponds to

$$T \leq 170 B_{12}^{1/2} \text{ keV} \tag{3.20}$$

Here, B_{12} is the magnetic field in units of 10^{12} G. So magnetic fields $\sim 10^{12}$ G are indicated in the source regions to account for the observed spectra.

(v) Observed γ-ray fluences and various educated guesses on source distances (see Section 3.6.2) assuming GRBs are Galactic imply that the total energy content of γ-rays is $\sim 10^{38\pm 2}$ erg. Neutron stars with intense magnetic fields are veritable energy reservoirs. For example, Brecher (1982) estimates that magnetic neutron stars have associated with them gravitational binding energies $\sim 10^{53}$ erg, rotational energies (for periods ~ 20 ms) $\sim 10^{49}$ erg, and magnetic field energies $\sim 10^{44}$ erg.

(vi) Association of a GRB with a quiescent optical object has never been seen. It follows that the objects are very faint, with magnitudes greater than 22 (see Section 3.5). Lone neutron stars are poor emitters of light. If they happen to be in binaries, therefore, their companions too have to be poor in emission of light. Ventura *et al.* (1983) outline the possibility of obtaining such low luminosity systems consisting of a neutron star primary and a degenerate star of mass $\sim 0.1 M_\odot$ as the evolutionary end product of a Galactic low mass binary system.

(vii) Periodicity observed in at least one case (see Section 3.3.3), besides supporting the argument given in (i) above, is natural for a neutron star. The well known GRB 790305b showed a periodicity with a period of 8 s, which is rather long considering the youth ($\sim 10\,000$ y) of the neutron star in the SNR N49. Brecher (1982) interprets this high period as that of precession and not of rotation, whereas Ruderman (1981) attributes it to the rotational period of a neutron star with an unusually high magnetic field ($\sim 2 \times 10^{14}$ G) at the pulsar. (Such is the latitude allowed by experimental facts for conjectures!)

It is not known if the neutron star is solitary or has a binary companion. Whether the energy source powering the burst is external to the neutron star or internal to it is also unknown. It is significant that several other astrophysical phenomena invoke neutron stars for their explanation. These are radio pulsars, X-ray pulsars, X-ray bursts, and the lone example of the Jacobson transient. It is not clear if there is any relationship between any of them and GRBs. In particular, X-ray bursts are seemingly very much unlike GRBs in their energy spectra, repetition rate and Galactic distribution (see Vetter 1982, Lewin and Joss 1983). Magnetic fields and accretion rates appear to be key characteristics in some of the models. It is conceivable that variations in these characteristics lead to diverse phenomena; for example, Woosley (1982) thinks that low magnetic fields and high accretion rates onto neutron stars produce X-ray bursts, whereas high fields and low accretion rates result in GRBs. Brecher (1982) is of the view that external

energy sources (accretion) are responsible for X-ray burst production, whereas internal energy sources (e.g. core quakes) produce GRBs.

Any successful model of GRB origin must explain the fast risetimes indicative of rapid transport of energy, burst durations (few tens of milliseconds to several hundreds of seconds), fluences (10^{-8} erg cm^{-2} to several times 10^{-4} erg cm^{-2}), energy spectra, frequency of occurrence and periodicities and recurrences in the few cases that were seen. The models have also to confront the experimental constraints on energy ratios:

$$L_{XQ}/L_{OQ} \sim 6\text{–}60 \tag{3.21}$$

(see Grindlay *et al.* 1982)

$$L_{\gamma T}/L_{\text{opt T}} \sim 800 \tag{3.22}$$

(see Schaefer 1981), and

$$L_{XQ}/L_{\gamma T} < 10^{-9} \tag{3.23}$$

(see Helfand and Long 1979). Here, the subscripts opt, X and Y refer to optical light, X-rays and γ-rays, respectively, and Q and T to the quiescent and transient state of the source object, respectively. Murakami *et al.* (1991) have reported that

$$L_{XT}/L_{\gamma T} \approx 0.05 \tag{3.24}$$

during the peak of GRB 900126. This observation indicates that GRBs are X-ray deficient even during the transient state.

3.7.2 *Source model hypotheses*

A large number of models for GRB production has been published. We will mention briefly only a few of them, referring the reader to the reviews by Prilutskii, Rozental and Usov (1975), Ruderman (1975), Vetter (1982), Katz (1983), Taam (1987), Zdziarski (1987) and Lamb (1988), and to references therein for a more complete coverage.

As a prelude to a description of models, we may first mention the scale of energetics (Ruderman 1981). If the energy powering a GRB is derived from the gravitational potential ($\sim 0.1c^2$) at the neutron star surface, the available energy will be $\sim 10^{20}$ erg g^{-1}. Likewise, the energy available from nuclear fusion ranges from $\sim 10^{18}$ erg g^{-1} (fusion of helium to heavier nuclei) to $\sim 10^{19}$ erg g^{-1} (fusion of hydrogen into helium). Typically, a Galactic GRB source emits a total energy of $\sim 10^{38}$ erg in the form of γ-rays and the mass of material involved in the production of a GRB, then, should therefore be $\sim 10^{19\pm1}$ g ($\sim 10^{-14} M_\odot$).

Van Horn and Hansen (1974) first noted that hydrogen and helium accreted at the surface of a neutron star are subject to thermonuclear runaway for a wide range of accretion rates and surface gravity. This idea has been applied successfully to explain the production mechanism of X-ray bursts; see, for example, Joss (1978, 1979). A neutron star can accrete matter, mostly hydrogen and helium, from the stellar wind blowing out of its companion star or, more likely, from the overflow when the companion expands and fills its Roche lobe. Isolated neutron

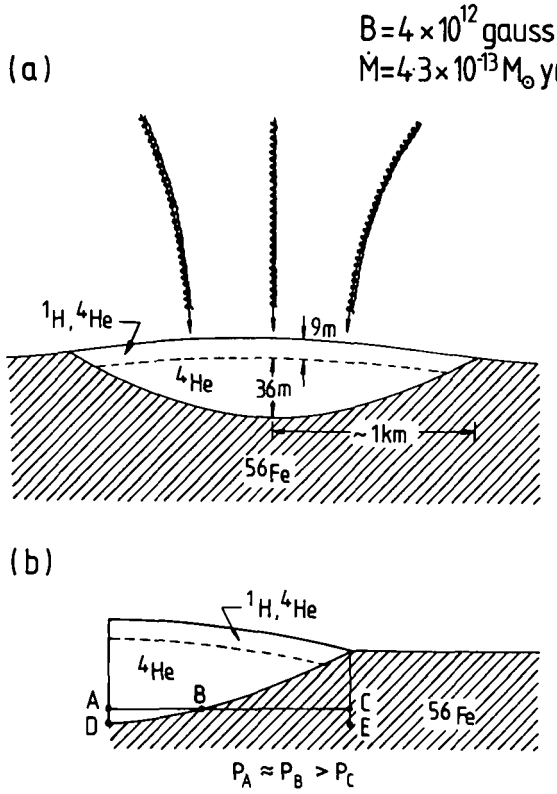

Figure 3.42. (*a*) Magnetically focused accretion onto a neutron star, giving rise to a blister of hydrogen and helium (Woosley 1982). Curvature of blister surface and interface have been exaggerated for purposes of illustration. (*b*) The pressure at an equivalent depth, C, in the iron substrate is less than that at B. The pressure gradient from point B to point C must be balanced by magnetic and crustal shear forces.

stars can accrete matter from the ambient interstellar medium. When the neutron star encounters dense clouds, the accretion rate may increase significantly. The accreted material may first form an accretion disk around the neutron star, conserving its angular momentum, and subsequently spiral down to the neutron star surface. Frictional forces due to differential rotation may heat the material to a high temperature plasma, at which stage soft X-ray emission may take place. In the presence of magnetic fields, the plasma may be channelled to polar cap regions, increasing the local accretion rate by nearly three orders of magnitude compared with what it would have been otherwise for the case of isotropic accretion.

Woosley and Wallace (1982) consider an accretion rate $\sim 10^{-13} M_\odot\ \mathrm{y}^{-1}$ focused by magnetic fields $\sim 10^{12}$ G onto kilometre-sized polar regions of a neutron star; see Figure 3.42. The accreted material is confined to the polar regions above the surface by the magnetic field and a combination of magnetic and crustal stresses below the surface. As the material accumulates, pressure builds up and, at

appropriate pressures and temperatures, hydrogen burns in a steady fashion to form helium. When the helium reaches a critical mass, it explodes either by convective deflagration or detonation, thereby liberating 10^{38}–10^{40} erg km^{-2} of thermonuclear energy. The plasma pressure at temperatures of the order of several billion degrees resulting from the explosion is greater than that of the magnetic pressure. The plasma, then, expands and stresses the magnetic field. Hard γ-ray emission comes from (i) relativistic electrons accelerated by large scale magnetic field recombination, (ii) magnetically confined and rapidly oscillating plasma, and (iii) particles moving with high velocities along the field lines in an optically thin region. The authors predict that soft X-ray emission should follow the GRBs and endure for several minutes to an hour as the surface ashes of the thermonuclear explosion cool down. The model also predicts a direct correlation between burst energy and recurrence period.

Bonazzola *et al.* (1984) also subscribe to the view that GRBs are powered by thermonuclear energy released at a huge optical depth, a few tens of metres below the surface of a neutron star. This extremely short phase is convectively unstable, and, due to the high magnetic field, the convection has an oscillatory character. The thermal energy is then converted into magnetic energy, which propagates very rapidly from the hot regions to the atmosphere of the accreted layer. Electric fields are created by short scale reconnection of the distorted magnetic field lines in the optically thin regions. Electrons are accelerated in these electric fields and produce the γ-rays.

In another scenario, magnetised neutron stars accrete solid objects (instead of tenuous matter) such as comets and asteroids of masses greater than 10^{17} g (Harwit and Salpeter 1973, Newman and Cox 1980, Colgate and Petschek 1981, Colgate 1982, Van Buren 1982). Occasionally a comet or an asteroid is deflected into an orbit with perihelion close to a neutron star. As the object falls in, the magnetic and gravitational fields distort and compress the body to densities $\sim 10^6$ g cm^{-3}. The interaction of matter with the field is initially entirely diamagnetic and the conducting matter parts the lines of force as a diamagnetic fluid. On impact, the object is in the form of a thin sheet of plasma, some 3 mm in longitude and 2.5 km in latitude; see Figure 3.43. After the collisional interaction with the neutron star surface, the matter and field become turbulent to interdiffuse, decreasing the plasma pressure. Temperatures of $\sim 10^8$ K are released in a fireball, and this is responsible for the GRB production.

Van Buren (1982) argues that in the fireball, with energy densities $\sim$10–100 MeV nucleon^{-1}, e^+e^- pair production is ubiquitous. Consequently, spectral information which might have been a clue to the burst mechanism is lost since the fireball looks the same no matter how it was formed. Well before the impact, part of the parent body becomes plasma and falls freely to the neutron star surface, while the asteroid orbit decays over a much longer time. The author suggests, therefore, that one should look for precursor radiation (duration $\sim 10^{-5}$ of the main GRB event and having an optically thick type spectrum) which serves as a diagnostic of the actual mechanism of GRB production. For example, the author suggests, endogenic energy sources cannot produce such a precursor. In this

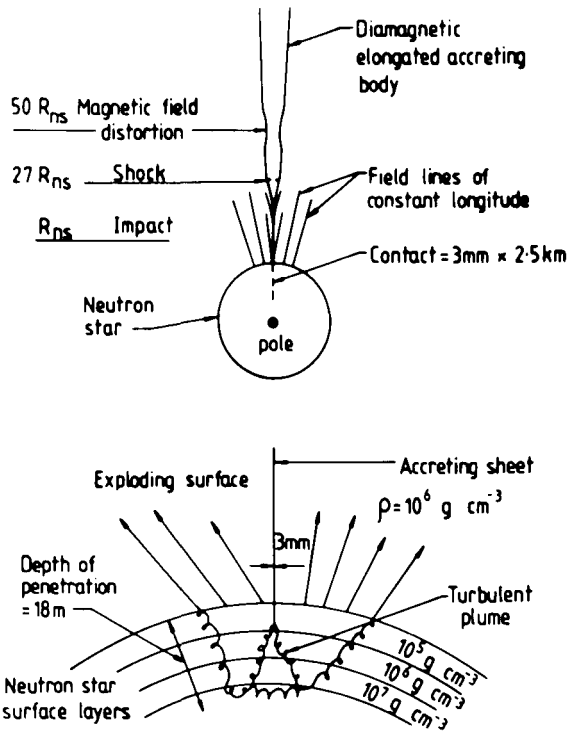

Figure 3.43. Accretion of a solid body onto a neutron star with a magnetic field (Colgate and Petschek 1981). The solid body, compressed and elongated, will be conducting and diamagnetic when it collides with the dipole magnetic field. It enters the dipole field as a diamagnetic compressed sheet of fluid. The body separates the magnetic flux surfaces of constant longitude and expands transversely in latitude. The compression in longitude reduces the thickness to a few mm and adiabatically compresses the matter to 10^6 g cm^{-3} density. It extends in width or latitude to a few km. The impact with the neutron star forms a turbulent mixed plume 20 m below the surface. The energy released by impact explosively ejects the combined surface and accreting matter.

context the observation of soft X-ray emission (Murakami *et al.* 1991) with a black body spectrum ($kT = 1.58 \pm 0.25$ keV) approximately 10 s before the onset of the γ-ray event in GRB 900126 is interesting. On the basis of this observation, the authors rule out accretion of solid bodies (e.g. comets) as the energy source since the risetime of the burst in X-rays (~ 8 s) is longer than the dynamical time scale expected in the case of accretion of solid bodies. The authors have also reported soft X-ray emission up to ~ 30 s after the main burst had ended, thus, once again, setting upper limits to source distances ~ 1 kpc if the source region is of dimensions ~ 1 km.

Many other models have also been suggested. Just to name a few, flare models (Katz 1982), crust quakes in neutron stars (Fabian, Icke and Pringle 1972, Bisnovatyi-Kogan and Chechetkin 1981), and core quakes in neutron stars (Tsygan 1975). Noting that an interesting GRASAR model by Ramaty *et al.* (1982)

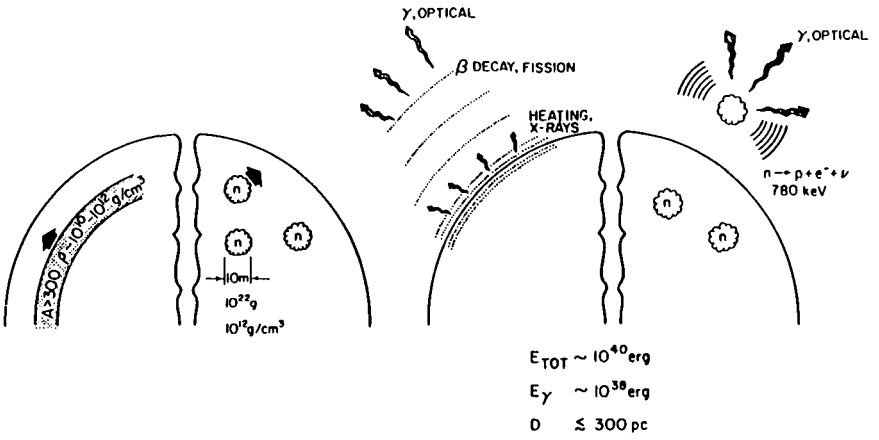

Figure 3.44. Illustration of how GRBs can be due to superdense matter trapped beneath the surface of a neutron star, taken from Hurley (1989*b*). Left-hand panels in each half of the figure refer to non-equilibrium shells (Bisnovatyi-Kogan 1987) and the right-hand panels refer to nuclear goblins (Zwicky 1974).

has been mentioned already in Section 3.4.2B, we will describe below some models in which the source of energy to power a GRB comes within the neutron star, in contrast to the models discussed above.

Zwicky (1974) suggested that nuclear goblins, chunks of superdense, neutron rich nuclear matter, are ejected out of a neutron star. Neutrons in the goblins decay to provide 780 keV electrons, which in turn produce γ-rays by bremsstrahlung. Bisnovatyi-Kogan and Chechetkin (1981) and Bisnovatyi-Kogan (1987) have proposed the existence of non-equilibrium shells of neutron-rich matter which is stable inside the neutron star under great pressures. If there is a disruption in the neutron star, the shell emerges from the star and produces decays, which, in turn, produce γ-rays. These ideas are sketched in Figure 3.44, which has been taken from Hurley (1989*b*).

Arguing that in external energy source models GRB sources emit far too many X-rays in comparison with γ-rays contrary to what was observed, Epstein (1989) has proposed that GRBs are powered by glitches taking place in neutron stars. The author has shown that crust quakes are not capable of producing the giant glitches observed in the Vela pulsar (Downs 1981). He has therefore proposed that differentially rotating neutron superfluid in a neutron star accumulates energy and subsequently transfers it to the crust producing the observed glitches. These glitches excite toroidal oscillations in the neutron star, producing shear motions on the star surface. The motion of the frozen-in magnetic field sets up electric potentials in which electrons and positrons are accelerated. Low energy photons emitted by the warm neutron star (temperature 0.25–1 keV) are upscattered by relativistic e^+/e^- via an inverse Compton process, thus producing GRBs. The author has shown that his model can reproduce the energy spectrum of GRB 811016 observed by Katoh *et al.* (1984). Epstein's model is illustrated in Figure 3.45.

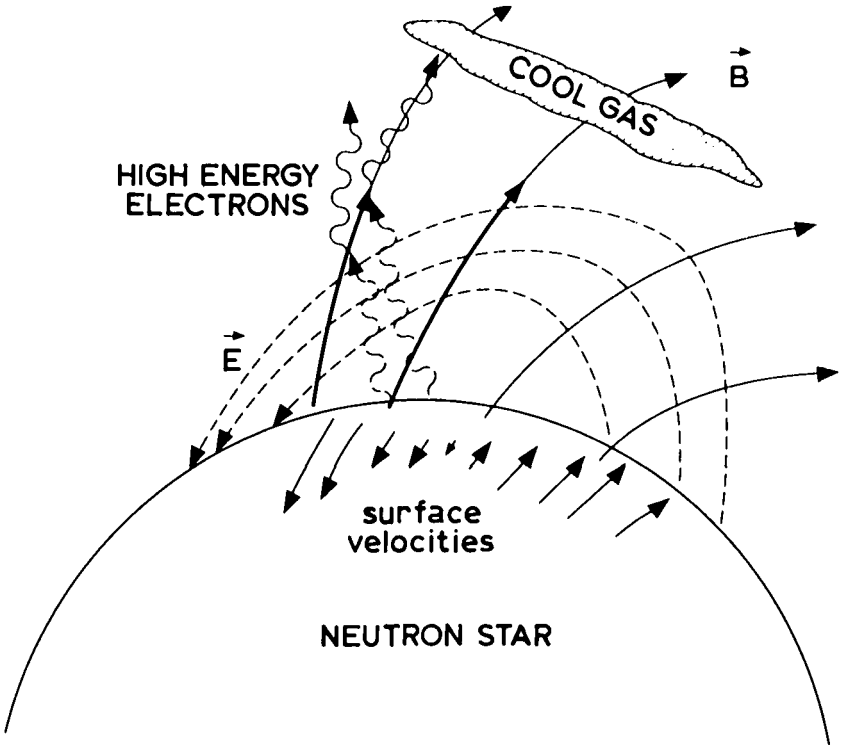

Figure 3.45. A schematic illustration of a glitch-powered GRB, taken from Epstein (1989). Glitches in neutron stars create transverse surface velocities. The motion of the frozen surface magnetic field induces a surface electric potential in which electrons and positrons are accelerated with a finite component along the magnetic field lines. γ-rays (solid wiggly lines) are produced by inverse Compton scattering of X-rays (dashed wiggly lines) by relativistic electrons (thick solid lines). Cyclotron absorption lines are formed in cool electron and/or positron gas near the star's surface.

Lamb (1982) pointed out that the burst durations are much longer than the cooling time of a hot plasma, whether in a strong magnetic field (synchrotron emission dominated) or not (bremsstrahlung dominated). In the accretion models, the burst duration is attributed (Lamb, Lamb and Pines 1973, Colgate and Petschek 1981) to the time interval during which accreting plasma or solid cometary matter rains down on the star. Nuclear burning models (Woosley and Wallace 1982) attribute it to the time necessary for a deflagration wave to propagate across the lake of nuclear fuel or the interval during which nearby fuels successively ignite. In either scenario, there is no difficulty in explaining the short risetimes of GRBs.

Pedersen *et al.* (1983) remarked that the very low values of quiescent X-ray fluxes (a measure of accretion rate) associated with GRBs are hard to understand, unless or course, the conversion efficiency, ε_X, of available energy into X-rays is

very low. According to these authors, the recurrence time, τ_{recur}, of a GRB is given by

$$\tau_{recur} = RS_\gamma \varepsilon_X/(F_X \varepsilon_\gamma)\ \text{s} \tag{3.25}$$

Here, R (~ 100) is the ratio of the gravitational potential energy per nucleon to the thermonuclear energy per nucleon; S_γ (erg cm^{-2}) is the fluence of GRBs; F_X (erg cm^{-2} s^{-1}) is the X-ray flux; and ε_γ (~ 0.2) is the efficiency of conversion of available energy into γ-ray energy. Applying these considerations to GRB 781119, one arrives at $\tau_{recur} \sim 1.5 \times 10^{12} \varepsilon_X$ s; compare this with the value < 50 y (1.5×10^9 s), derived in Section 3.5.2. Likewise, when applied to the consecutively recurrent bursts on March 5, and March 6, 1979, of the burst source of GRB 790305b, the formula predicts $\tau_{recur} \sim 1.5 \times 10^9$ s compared with ~ 14.5 h time interval between the two bursts. These comparisons imply ε_X values of less than 10^{-3}, and such values are hard to accept.

Woosley and Wallace (1982) predict that there should be a direct correlation between burst energy and recurrence period. This is not borne out by the several recurrences of GBS 0526−66 (Golenetskii *et al.* 1984), and of the other two soft repeaters GBS 1806−20 and GBS 1900+14, in which there is no correlation between the burst fluence and mean time between recurrences.

It is not clear if there is any understanding of the shape of energy spectra of photons from GRBs. As detailed in Section 3.4, many of the observed spectra agree with an optically thin thermal bremsstrahlung model. In the presence of intense magnetic fields, and at the temperatures believed to prevail in the source regions, the optical depth for synchrotron losses is greater than that for electron scattering by four orders of magnitude (Lamb 1982). Bremsstrahlung-like fits, though good, may not therefore reflect the actual mechanism of production of the γ-rays. Ruderman (1981) has shown that optically thick hot surface matter in a very strong magnetic field may also give a spectrum for the emitted radiation which departs greatly from a Planck distribution and which resembles the bremsstrahlung emission from an optically thin source. This is the sequel to the reduction of the photon–electron scattering cross section from σ_T in the presence of magnetic fields. See also the additional points made in the discussion presented in Section 3.4.1. The reality of an optically thin thermal bremsstrahlung spectrum is also doubted because of the uncomfortably large aspect ratios (i.e. ratio of $(\text{area})^{1/2}$ to thickness of the source region) that follow in such a case when one considers burst fluences, source distances and temperatures (Lamb 1982).

3.8 Summary

γ-Ray bursts were discovered in 1967 by Klebesadel *et al.* (1973) and, during the past 24 years, the subect of GRBs has received considerable attention, both theoretically and experimentally. To date several hundred GRB events have been fully analysed, and perhaps several hundred more have already been recorded; one awaits their publication. With improvements in detector threshold and trigger algorithms, the rate of collection of GRB events has increased recently and with

one new burst per day from the GRO the number accumulated will grow dramatically.

Most of the detected bursts have risetimes in the range 10–1000 ms, durations in the range of a few tens of milliseconds to several hundreds of seconds and fluences in the range 10^{-8}–10^{-3} erg cm^{-2}. The energy spectra can be fitted in most cases by an optically thin bremsstrahlung-like shape, although other forms of fits can be used. Indeed, in some cases, it is found necessary to use other types of spectral fit. In three cases, the burst sources show evidence for recurrence, and one of them, the most intense burst detected so far, namely GRB 790305b, exhibits a periodicity with a period of 8 s. The distribution of burst sources appears to be isotropic in Galactic coordinates. It is not known, however, if the GRB sources are nearby objects on a Galactic scale with distances $\lesssim 1$ kpc, or far away sources on an extragalactic scale with distances $\gtrsim 100$ Mpc. The source direction of the famous GRB 790305b coincides with that of a supernova remnant, N49, in the Large Magellanic Cloud; however, there is no point source there in the radio, infra-red, optical or X-ray wavelength region. Luminosities of GRBs are $\sim 10^{39\pm1}$ erg s^{-1}, if the source distances are 1 kpc, and could be much higher depending on the distance. A few of the bursts are strongly believed to be associated with objects that also emit optical light, although these associations have not yet been confirmed in real time. Simultaneous emission of soft X-rays has been seen in a few cases, and invariably the power in X-rays is less than a few per cent of the total power of the GRBs.

On the theoretical side, the consensus seems to be that most GRBs come from highly magnetised Galactic neutron stars, though there are a few suggestions that the GRB sources are extragalactic. Models suggested for their origin include non-stationary accretion of material from the interstellar medium, from a binary companion, or in the form of comets and asteroids. In some models, the power source is thermonuclear explosion of accreted matter not far below the neutron star surface, near polar regions. In other models the energy is derived from glitches and vibrations inside neutron stars. There is no consensus on what exactly is the power source. The precise mechanism of charged particle acceleration and subsequent γ-ray production is even less well established.

At the moment, data on GRBs are being gathered by detectors aboard various spacecraft. In the future one wishes to see deployment of large area thin scintillators or xenon counters to increase the counting statistics. Large count rates will help establish the occurrence of precursors, post-burst activity and periodicity if these are of low intensities. The thin nature of counters will minimise errors made in deconvolution of energy-loss count rates in order to obtain true photon energy spectra. Usage of large area Ge detectors will enable one to record the emission and absorption features with high resolution, and this will help to provide an accurate measure of their parameters, such as intensity, width, etc.

It is now widely realised that the burst size spectrum ($\log N(>S)$–$\log S$ curve) saturates at low S due to detector and trigger biases, while the peak count rate (C_p) spectrum ($\log N(>C_p)$–$\log C_p$ curve) is less vulnerable to such biases. Even here, and in the few balloon observations that were made, there is a hint that the

distribution is turning off from that expected for isotropic distribution at low fluences. Simultaneous balloon flights widely separated in distance but having a significant common solid angle of view will go a long way to establish the existence or absence of bursts at low values of S ($\lesssim 10^{-8}$ erg cm^{-2}). It is also important to establish international networks of GRB detectors with well coordinated time-keeping methodology. This will help to localise the burst source directions to $\gtrsim 1$ arc min, which, in turn, will facilitate searches for associations at other wavelengths.

There is a clear need to establish if GRBs are associated with any known class of celestial objects. Real-time searches being planned at several places and continual observation with an optical telescope of the source positions of some of the well known bursts (e.g. GRB 790305b) will be rewarding. With a mean recurrence time ~ 38 d (see Section 3.3.4) for the source of GRB 790305b, the chances of seeing real-time coincidental optical and GRBs are really bright. Even a single observation of a real-time association with an astronomical quality telescope would be extremely valuable. Detectors on the GINGA satellite have already revealed that there are soft X-ray precursors and post-event activity associated with GRBs.

The Burst and Transient Source Experiment (Fishman *et al.* 1985, Fishman 1988) aboard the Gamma Ray Observatory launched in April, 1991, is already collecting data on GRBs at a high rate. Though by itself BATSE can localise sources only coarsely, its high timing accuracy, when combined with data from other experiments, can lead to highly accurate localisations. BATSE can record GRBs with fluxes as low as 5×10^{-8} erg cm^{-2} s^{-1}. Data on source directions of the weak GRBs, even with large errors, can be of great value in knowing if the GRB sources are a Galactic disk population. The Transient Gamma Ray Spectrometer on the WIND spacecraft (Teegarden 1986) expected to be launched in the mid-1990s has a cooled germanium detector to study energy spectra in the range 10 keV–10 MeV. It is expected to yield much information on the absorption and emission features of GRBs. Finally, the High Energy Transient Experiment (HETE), expected to be launched in the early 1990s, has detectors to record ultra-violet, X-ray and γ-ray data simultaneously (Ricker *et al.* 1988). It can localise sources to an accuracy of ~ 10 arc sec and can transmit information to ground-based optical and radio telescopes enabling them to carry out observations on GRB sources in real time. This will go a long way towards the identification of GRB sources.

One can also expect studies of theoretical models to come up with predictions and suggestions on feasible experimental tests that are truly unique to the particular model, besides accommodating the burst features in general terms.

4

Medium energy gamma-rays

4.1 Introduction

For reasons concerned with the availability of contemporary γ-ray data, the lower limit for 'medium energy' quanta can be taken as 35 MeV (this is the lower limit for the important SAS II satellite experiment). The upper limit again comes from satellite data availability and is rather arbitrarily taken as 5000 MeV, the upper limit of the highest COS B satellite energy band; in fact, the photon flux falls off with energy so rapidly that our knowledge about γ-rays above 1000 MeV from satellite experiments is virtually nil. As will be discussed in Chapter 5, however, knowledge blooms again above 10^{11} eV, where Cerenkov radiation produced by γ-ray-induced electrons in the atmosphere allows detections to be made.

Although there are some who still believe that unresolved discrete sources contribute considerably to the diffuse γ-ray flux, the majority view is that the sources are responsible for only 10–20% of the γ-ray flux and that the predominant fraction arises from cosmic ray (CR) interactions with gas and radiation in the interstellar medium (ISM). In fact, some 30 years ago, both Hayakawa (1952) and Hutchinson (1952) had made estimates of the CR–ISM-induced γ-ray flux and had shown it to be within the scope of experimental measurement.

The foregoing is not to say that the discrete sources are unimportant, indeed the reverse is true, and there is considerable interest in ways of explaining the observed γ-ray flux from identified sources (the Crab and Vela pulsars) and the unidentified but definite sources such as Geminga (2CG 195+04 in the COS B source catalogue of Hermsen 1980, 1981).

The explanation of the diffuse component is of considerable interest because of its rather obvious relationship to both cosmic rays and the ISM, namely in regions where we think we know what the cosmic ray flux is, information can be gained about the ISM, and in turn, where the ISM is understood, the cosmic ray flux can be estimated. The need for information about the distribution of cosmic rays in the Galaxy cannot be overstated; despite the elapse of 80 years since the discovery of cosmic rays (Hess 1912), the origin of these particles is still the subject of debate, and knowledge of the manner in which cosmic rays are distributed (local hot spots, large scale intensity gradients, etc.) is likely to give valuable information. The implication that the ISM itself needs further study is not as obvious but it is nevertheless true, particularly for the gas in the inner Galaxy. The situation here

is that, although 21 cm data provide basic information about the gas densities of the atomic hydrogen, our knowledge of the important molecular component is remarkably poor. Molecular hydrogen densities at present are largely inferred from the measurements of the 2.6 mm emission line resulting from the $J = 1 \rightarrow 0$ transition in carbon monoxide (CO) and the factor for converting from the intensity of this line, or more specifically from $\int T \, dV$ (where T is the antenna temperature and V is the velocity), to the column density of H_2, has been the subject of lively debate for some time. The topic of interstellar chemistry, which can significantly affect the value of this conversion factor, is one of considerable complexity and uncertainty, largely due to a lack of precise knowledge of the physical properties of the medium where the chemistry occurs. Thus, γ-ray astronomy holds out the hope of independently 'weighing the Galaxy' in terms of mass of gas.

In what follows, after a brief discussion of the history of the subject, attention will be given to the two major satellite experiments, SAS II and COS B, which have given results in the medium energy region. This section is followed by a detailed examination of the Galactic γ-ray sources, leading to the thorny but interesting question of the pseudo-sources, localised γ-ray excesses due to the irradiation of the lumpy molecular gas by cosmic rays. The relevance of γ-rays to the origin of cosmic rays follows next. The penultimate section deals with the rather sparse contemporary data on extragalactic γ-rays and, finally, new experimental programmes are discussed.

4.2 History

Pride of place for the first detection of γ-rays in this energy bracket appears to be due to Kraushaar *et al.* (1965) using the Explorer II satellite. The detector consisted of a low resolution ($\pm 20°$) scintillation–Cerenkov device and an important result that followed was the determination of the ratio of the Earth's albedo: sky flux of the γ-rays of $\approx 10{:}1$. It was the secondary γ-rays produced by cosmic ray particles in the atmosphere that bedevilled (and still affect) the balloon-borne experiments and led to the first detection of genuine celestial γ-rays being reserved for the satellites.

It was in March, 1967, with the launch of OSO III (Clark, Garmire and Kraushaar 1968, Kraushaar *et al.* 1972), that the subject can really be considered to have started in earnest. The detector recorded 621 photons and for the first time showed a broad peak in intensity towards the Galactic Centre of magnitude of the order of that expected from cosmic ray interactions with Galactic gas (summaries of the OSO III results have been given by Fazio 1970 and Clark 1971). These observations, made with a detector having a resolution of about $\pm 15°$, gave an average integral intensity above 100 MeV of $(1.1 \pm 0.3) \times 10^{-4}\,\mathrm{cm^{-2}\,s^{-1}\,rad^{-1}}$ for $30° > l > 330°$ and $|b| < 15°$. Clearly it was necessary to improve the angular resolution to see, for example, the extent to which the γ-ray intensity mirrored the column density of the gas (only atomic hydrogen, H I, was usually considered at that time) and a number of balloon experiments quickly followed. The peak towards the Galactic Centre necessitated balloon flights in the southern

hemisphere, and those of the Goddard Space Flight Centre group (GSFC) over Australia were successful. The detector adopted comprised a wire spark chamber with a magnetostrictive readout and an angular resolution of about 2° at 100 MeV (Kniffen and Fichtel 1970, Fichtel *et al.* 1972). The instrument is historically important in that it was the prototype of the SAS II satellite experiment, to be described shortly. The result showed that the bulk of the Galactic Centre direction ($335° < l < 20°$) radiation was confined to $|b| \lesssim 7°$ and the 'line intensity' above 100 MeV, $(2.0 \pm 0.6) \times 10^{-4}\,\mathrm{cm^{-2}\,s^{-1}\,rad^{-1}}$, was consistent with the earlier OSO III observation. The GSFC experiment also searched for point sources but was unable to find any at a level of $3 \times 10^{-5}\,\mathrm{cm^{-2}\,s^{-1}}$ above 50 MeV.

In this period a number of other balloon experiments were also carried out, some of which saw a Galactic Centre peak (e.g. Share, Kinzer and Seeman 1973), whereas others did not, the problem being the short exposures available from the balloon flights and the considerable atmospheric background (see Share 1973 for a useful summary).

Although balloon experiments have continued to take place from time to time, and some useful data have accrued on specific 'sources', the bulk of the results have come from the two satellite experiments, SAS II and COS B.

The early results spawned many theoretical analyses and, of course, these are continuing. Before closing this historical section, attention must be drawn to just one of the 'theorists', F.W. Stecker, whose early appreciation of the importance of γ-ray astronomy – and its relationship to other branches of astronomy – provided considerable impetus (see, for example, his published Ph.D. thesis: Stecker 1971).

We turn now to a discussion of the satellite experiments.

4.3 The SAS II satellite

4.3.1 The experimental details

Insofar as considerable attention will be paid later to an analysis of data from this 'small astronomical satellite' (SAS) the experimental arrangement will be described in a little detail. Figure 4.1 shows the spark-chamber telescope carried by the satellite; the various components being labelled. Fuller experimental details have been given by Derdeyn *et al.* (1972), Kniffen *et al.* (1974), and Fichtel *et al.* (1975). The experiment was launched on November 15, 1972, and the orbit was essentially equatorial and roughly circular at a height ranging from 440 to 610 km above sea level. An electronic failure resulted in a premature termination of the experiment after only seven months operation, but nevertheless high quality low background data were accumulated. The 8000 photons observed are still providing useful material for investigation some 20 years after the project was completed. In comparison with the early OSO III experiment, the SAS II sensitivity was about 12 times as great and its angular resolution reduced to a few degrees.

The data were recorded at a 1 kbit $\mathrm{s^{-1}}$ rate on redundant, continuous-loop tape recorders on board the satellite and the records were transmitted (at 20 kbit $\mathrm{s^{-1}}$)

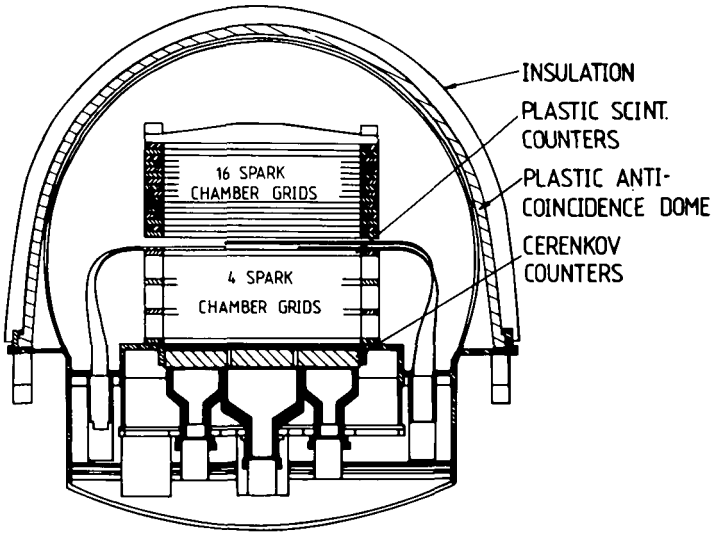

Figure 4.1. Schematic diagram of the SAS II γ-ray experiment (Derdeyn *et al.* 1972).

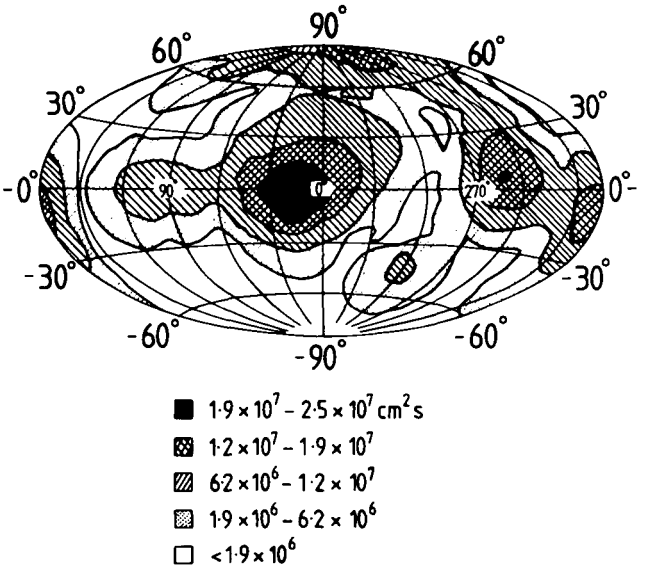

Figure 4.2. Exposure of the SAS II experiment (Fichtel *et al.* 1978*a*,*b*). The horizontal axis is Galactic longitude and the vertical is Galactic latitude. The patchiness is due to the unexpected demise of the apparatus after only seven months in orbit.

once per orbit to a tracking station near Quito. The event epochs were recorded with an accuracy of better than 2 ms in absolute time.

The sky coverage of the experiment, which is an important parameter for analysing the results, is shown in Figure 4.2. It will be noted that, although the

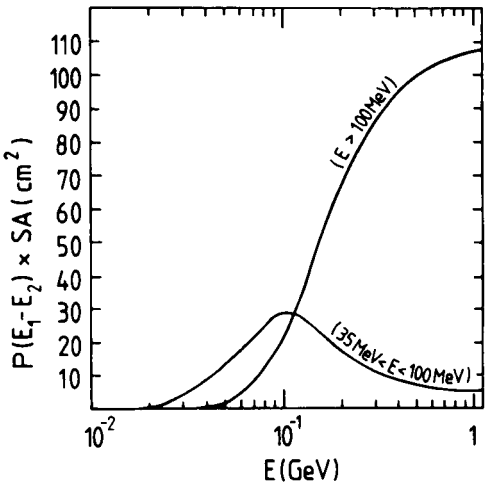

Figure 4.3. Energy response of the SAS II experiment. The ordinate is the product of the probability of finding a photon of energy E in the range E_1–E_2, and the effective detection area. (Lebrun and Paul 1983.)

pointing direction was usually in the general region of the Galactic Plane, a significant exposure occurred for high latitudes as well, particularly in the northern hemisphere.

Energy calibration over the range 30–150 MeV was made prior to the flight using the tagged-photon facility at the 170 MeV electron synchrotron at the National Bureau of Standards (Gaithersburg, Maryland). Later analysis, involving folding in the energy uncertainty with an assumed incident energy spectrum of the form $N(E_\gamma)\,dE_\gamma \propto E_\gamma^{-2}\,dE_\gamma$, gave 'response functions' for the two energy bands 35–100 MeV and greater than 100 MeV, as shown in Figure 4.3.

Of crucial importance in all branches of astronomy is the angular resolution of the telescope, and it is because this is so poor in γ-ray astronomy that there is so much argument about the interpretation of γ-ray data. The angular resolution of the satellite experiments is poor because of the nature of the pair production process and the scattering of the secondary electrons in the spark chamber plates. Figure 4.4 shows the angular resolution as a function of E_γ for SAS II.

4.3.2 A summary of the SAS II results

Figures 4.5 and 4.6 show the longitude and latitude dependences for γ-ray energies above 100 MeV. The main features evident are:

(i) a general concentration of flux in the Galactic Plane ($|b| \lesssim 3°$);
(ii) a general concentration towards the Galactic Centre but extending over $\pm 40°$ in longitude or so, thus confirming the feature observed earlier by OSO III (see Section 4.2);
(iii) intensity peaks corresponding to the positions of two known pulsars, the Crab and Vela (the identification being made positive by the detection of

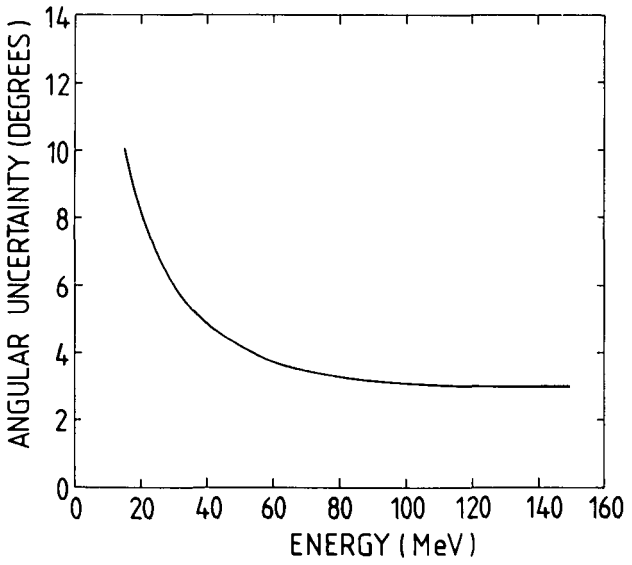

Figure 4.4. Three-dimensional angular uncertainty as a function of energy for SAS II (Kniffen *et al.* 1978).

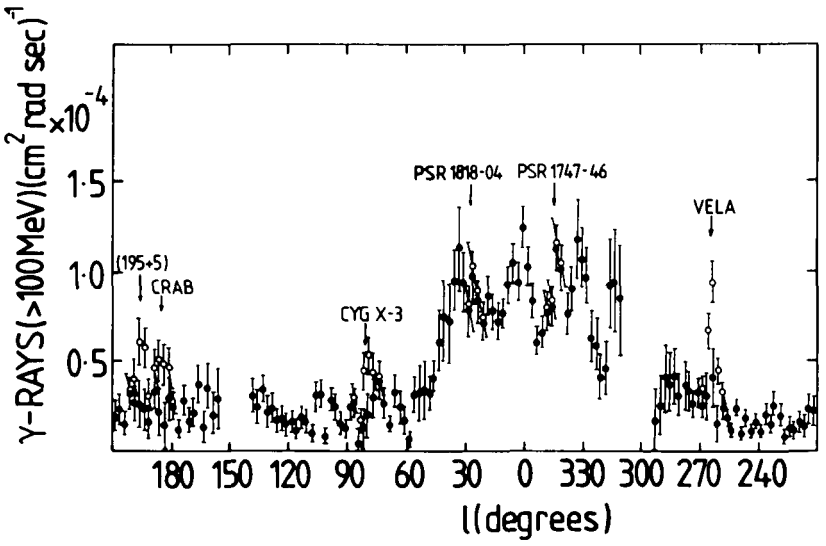

Figure 4.5. Distribution of γ-rays above 100 MeV along the Galactic Plane: SAS II (Thompson *et al.* 1976). The data refer to $-10° < b < 10°$. The diffuse background has been subtracted. Open circles include pulsed components. The two pulsars PSR 1818−04 and 1747−46 are not now thought to be significant γ-ray emitters, but the pulsed components for the other SAS II sources are still accepted.

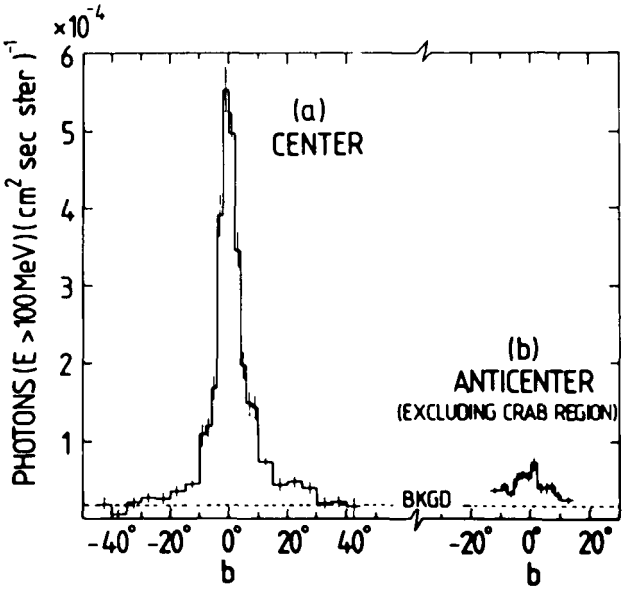

Figure 4.6. Latitude distribution of γ-rays above 100 MeV from the SAS II experiment (Fichtel *et al.* 1975). Dashed line: diffuse background level. (*a*) Data summed from $l = 330°$–$30°$. (*b*) Data summed from $l = 90°$–$170°$ and $220°$–$260°$. Note that the angular resolution is about $\pm 3°$ so that some of the finite width of the narrow peak is instrumental in origin.

pulsed emission at the radio pulsar periods). A strong peak at $l = 195°$, $b = +4°$ (later named 'Geminga') from an object which has no obvious astronomical counterpart (this important source has been variously referred to as 194+04, 195+04 and 195+05, an indication of the uncertainty in position arising from the γ-ray observations alone). The detection of the well known Cygnus X-3 source, identified by its 4.8 h periodicity (Hartman *et al.* 1976);

(iv) the suggestion of the presence of other peaks which may, or may not, be associated with various known Galactic objects;

(v) a small, but finite, diffuse flux at high latitudes, which is probably to be identified with an isotropic extragalactic background. Although not shown in Figures 4.5 and 4.6, the background is relatively stronger in the lower energy bracket (35–100 MeV), indicating that its origin is different in character from that of the corresponding Galactic Plane component.

4.4 The COS B satellite

4.4.1 Experimental details

A European collaboration successfully designed, constructed and launched the COS B satellite carrying a detector rather similar to that on SAS II. The launch occurred on August 9, 1975, and the instrument performed admirably for the

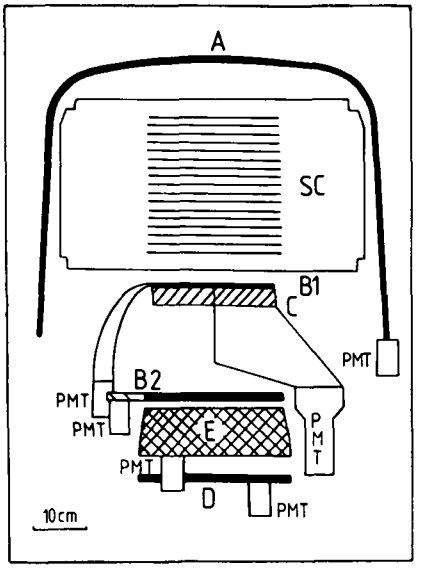

Figure 4.7. Sectional view of the COS B γ-ray detector (Bennett *et al.* 1976). A: anticoincidence counter; SC: spark chamber; B1, B2: scintillation counters; C: directional Cerenkov counter; E: energy calorimeter: caesium iodide scintillator); D: scintillator to provide information on high energy events for which the absorption in the calorimeter is incomplete.

next six and a half years until an already overdue gas shortage caused the mission to be finally terminated. The project was a triumph for international cooperation and marked a stepping stone for an increasing number of multi-nation collaborations.

The COS B detector is shown schematically in Figure 4.7; the similarity to the SAS II apparatus is immediately evident.

Apart from the difference in the lengths of exposure between COS B and SAS II, the most important difference was the character of the satellite orbit: unlike the near circular orbit of SAS II, COS B was placed in a highly eccentric orbit. The philosophy was to increase the useful observation time by having only a small fraction of the sky occulted by the Earth, but the price paid was rather high: the apparatus was smaller than it could have been for a near-Earth orbit and the flux of background cosmic ray particles was an order of magnitude higher. A consequence of the latter was a rather large background of secondary γ-rays produced in the detector, and this has resulted in considerable difficulty in correcting the signal for background – an important feature for latitudes away from the Galactic Plane. An important consequence has been an inability to derive an estimate for the isotropic diffuse flux. Nevertheless, a large number of cosmic γ-rays were recorded ($\approx$200 000), allowing a number of important discoveries to be made.

Prelaunch calibration was performed, as with SAS II, using tagged-photon beams, the energy range involved being 20 MeV–6 GeV. The important sensitivity

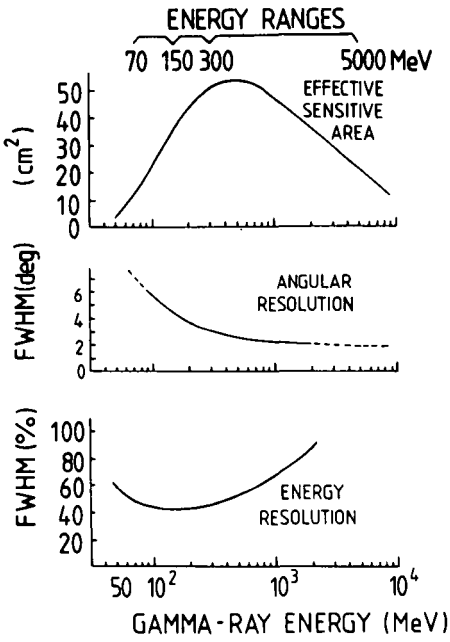

Figure 4.8. Characteristic parameters of the COS B experiment for γ-rays incident along the detector axis (Scarsi *et al.* 1981).

versus γ-ray angle relative to the spark chamber pointing direction was also determined. Selection criteria were devised relating to the pulse height thresholds for the counters of the triggering telescope, the anticoincidence counter and the energy calorimeter. Finally, detailed procedures were devised for the scientists who reduced and analysed the data. The relevant instrumental characteristics, effective sensitive area and angular and energy resolutions are shown in Figure 4.8.

The angular resolution of the detector is of particular importance for later analyses and more description is needed. For a Gaussian distribution of projected angle, θ_x, θ_y, the probability can be written as

$$P(\theta_x, \theta_y) = C' \exp - [(\theta_x^2 + \theta_y^2)/2\sigma^2] \tag{4.1}$$

where C' is a normalisation constant and σ is the half angle of a cone such that 68% of the apparent directions are within the angle of the true direction.

In fact the actual angular distributions are not Gaussian but have extended tails, although these are reduced somewhat in the editing of the records. Following Hermsen (1980) a good approximation is

$$P(\theta_x, \theta_y) = C' \exp - [(\theta_x^2 + \theta_y^2)/\theta_0^2]^c \tag{4.2}$$

Typical values for θ_0 and c are, for the energies indicated: 4.7°, 0.8 (75 MeV); 3.0°, 0.7 (150 MeV); and 1.25°, 0.5 (300 MeV).

4.4.2 A summary of the COS B results

A number of γ-ray maps have been published by the COS B group, and a copy of an important set, which has been extensively used in analyses, is reproduced in Figure 4.9 (Figure 4.10 shows the associated intensity cuts). Inspection of the maps shows the presence of many 'hot spots' of γ-ray emission as well as peaks at the SAS II source positions: the Crab, Vela and '195+5'. It is the detection of these candidate sources (hot spots) which has probably been the most important feature of the COS B results.

The longer exposure time for COS B has provided better statistics and, in turn, has allowed observations to be made to higher energies than was possible with SAS II. For most of the sky the intensities are quoted for the three energy bands already referred to, and for the two pulsars, which were the subject of extended observing, data have been recorded to 1 GeV. The selection of the highest energy band (300–5000 MeV) has turned out to be very important because the generally accepted view is that the bulk of these γ-rays are generated by way of π^0-decay, the pions themselves having been produced by the interactions of the cosmic ray protons and nuclei with the ISM. The search for the origin of cosmic ray protons and nuclei, as distinct from electrons, is bound up with these energetic γ-rays.

4.5 Gamma-ray sources

4.5.1 Introductory remarks

The priority to be attached here to the various satellite results reflects the preference of the authors, but there can be no doubt that the 'γ-ray sources' loom large in any such discussion, and this is the topic with which we will start. Attention will be devoted in turn to the pulsars, other identified sources and finally to the unidentified objects and the thorny question of their nature and the related question of the magnitude of the flux expected to arise from unresolved weak sources.

There have been a number of reviews of 'γ-ray sources' already; Fazio (1973) has covered the early observations and a detailed survey of Galactic sources has been given by Bignami and Hermsen (1983).

4.5.2 Gamma-ray pulsars

As mentioned already, the first definite observation of γ-rays from pulsars came from the SAS II experiment with the detection of the Crab (PSR 0531+21) and Vela (PSR 0833−45) (Thompson *et al.* 1975). Possible detections were also claimed for two old pulsars: PSR 1747−46 and PSR 1818−04 (Ogelman *et al.* 1976). COS B extended the observations of the major sources and found new features but, after some tentative sightings of other pulsars, the view now is that only PSR 0531+21 and PSR 0833−45 have been definitely detected.

Starting with the Crab, observations have been made essentially over the whole of the electromagnetic spectrum, from radio waves to γ-rays. Although results are described here up to 1000 MeV, later we will examine still higher energies – up to 10^{16} eV. Figure 4.11 summarises measurements of the pular 'light curve' at

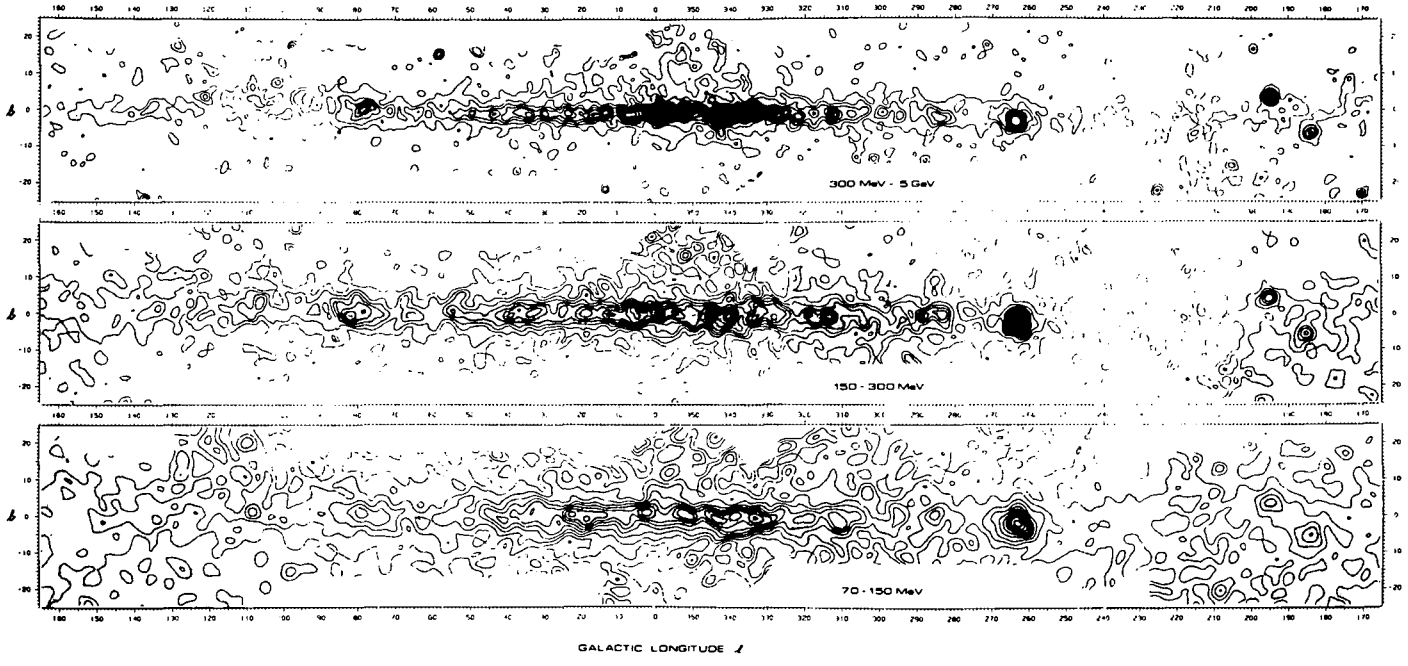

Figure 4.9. Contours of COS B γ-ray intensity from the work of Mayer-Hasselwander *et al.* (1982). The contour levels are indicated as multiples of 5×10^{-5} cm^{-2} s^{-1} sr^{-1} for 70–150 MeV, 3×10^{-5} for 150–300 MeV and 4×10^{-5} for 300–5000 MeV.

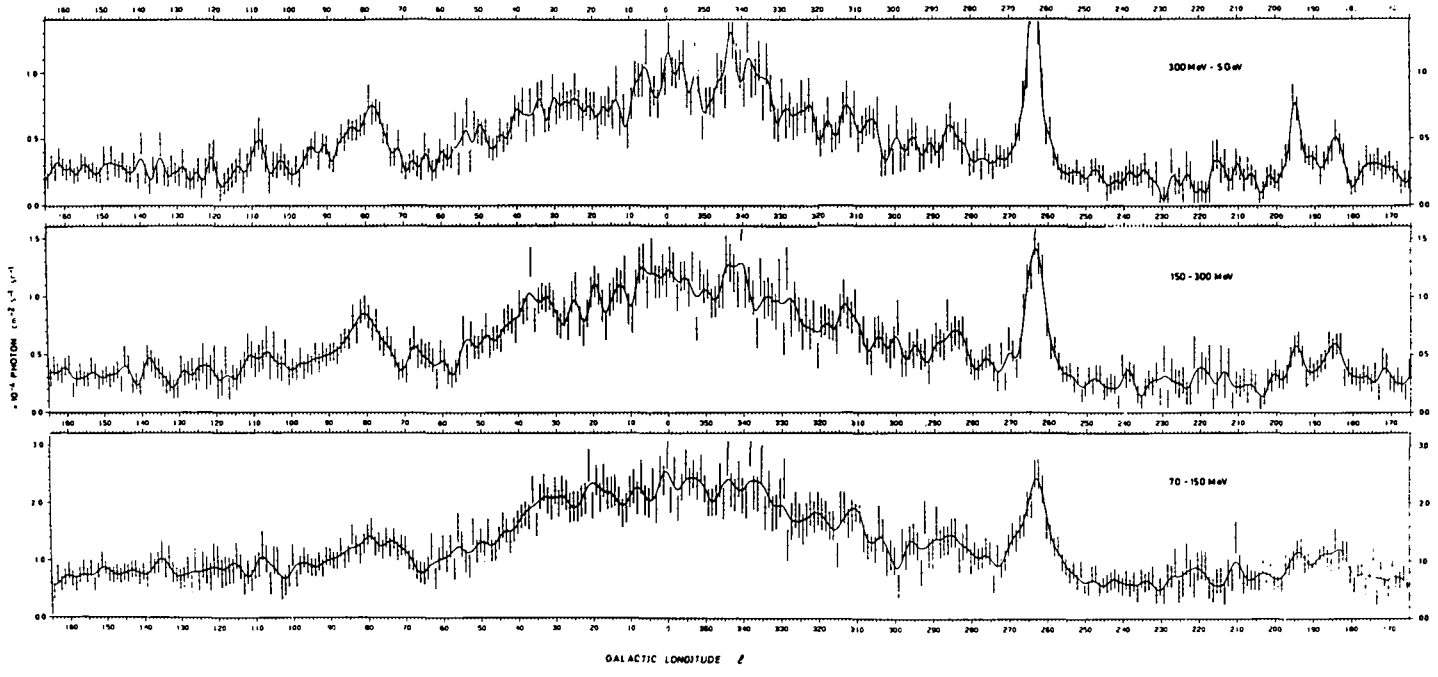

Figure 4.10. Longitude profiles of COS B γ-ray intensity averaged over $\pm 10°$ in latitude. Sold line: surface fitted to the data. (Mayer-Hasselwander *et al.* 1982.)

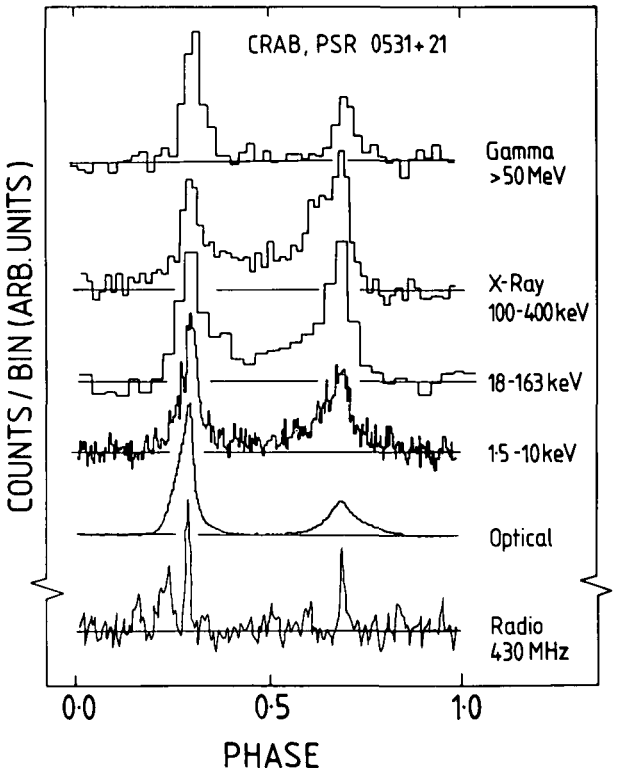

Figure 4.11. Light curves for the Crab pulsar at various wavelengths. The γ-ray data are from a summation of five COS B observation periods (Wills *et al.* 1980).

various wavelengths. It is interesting to note that although the intrinsic widths of the two pulses are similar at all wavelengths (except radio) there are a number of differences:

(i) the ratio of intensity of the interpulse to the main pulse is a function of wavelength (and there is COS B evidence that this ratio is variable above 50 MeV on a time scale of years, Wills 1981);
(ii) the valley between the pulses has a wavelength dependent magnitude.

A notable feature of the energy spectrum at X-ray and γ-ray energies is the increasing fraction of the pulsed component as one proceeds to higher energies; Figure 4.12 shows this feature.

An interesting aspect that follows from the detected spectral shape is that the maximum power of the pulsar is radiated in the γ-ray region, specifically near 10 MeV. Buccheri (1980) has used the known distance of the pulsar, together with the assumption that emission is in two cones, to derive the rate of energy in the γ-ray region: 2×10^{35} erg s^{-1} above 50 MeV. This emission is several orders of magnitude greater than that in the radio region and corresponds to about 0.04% of the energy loss corresponding to its spin down rate.

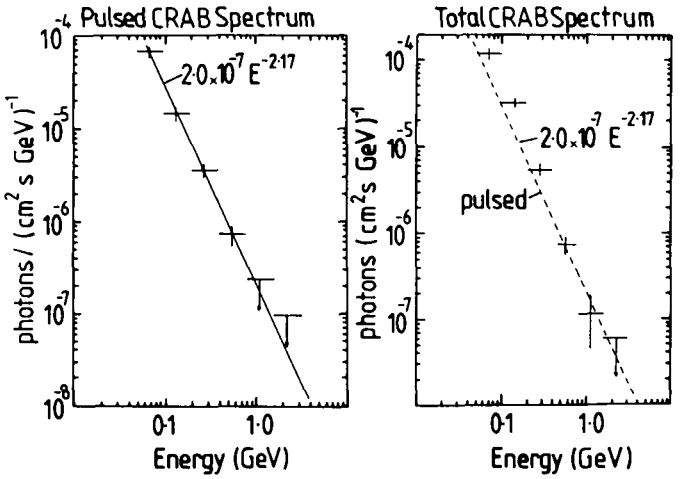

Figure 4.12. Differential photon spectrum for the Crab γ-ray source (2CG 184−05). The line gives the fit to the pulsed component. It is apparent that the pulsed fraction increases with energy (after Hermsen 1981).

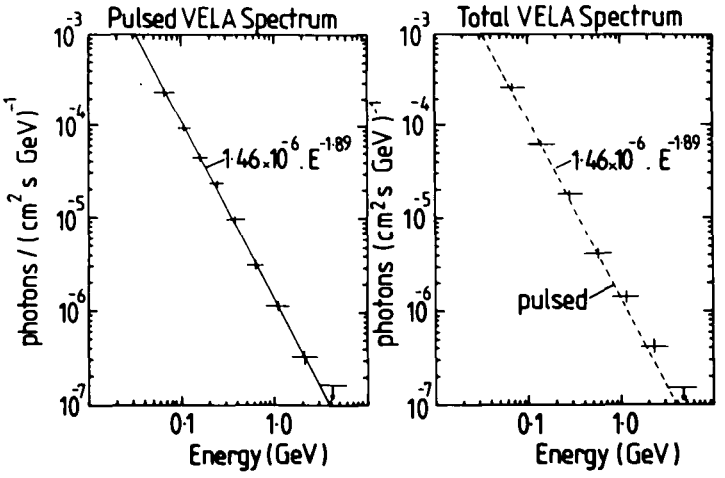

Figure 4.13. Differential photon spectrum for the Vela γ-ray source (2CG 263−02). The line gives the fit to the pulsed component. Most of the emission is seen to be pulsed at all energies (after Hermsen 1981).

Moving to Vela, this is the strongest γ-ray source in the sky at the energies in question (a flux above 100 MeV of 13×10^{-6} cm^{-2} s^{-1}). The energy spectrum (Figure 4.13) is interesting in that the differential exponent ($\gamma = 1.89$) is small and the pulsed fraction is very large indeed; Lichti *et al.* (1980) estimate that at least 90% of the flux is pulsed above 50 MeV. Assuming isotropic emission, the luminosity above 50 MeV is $\approx 4 \times 10^{34}$ erg s^{-1}, corresponding to about 0.3% of the spin down energy loss rate, i.e. a factor of ten higher than that of the Crab.

There are other differences from the Crab, too; for example, the light curves for Vela are very different in the various energy regions: the phase difference between the main pulse and the interpulse differs between γ-rays and the optical region, and for the radio signal there appears to be no interpulse at all. Another remarkable difference is the lack of a detectable X-ray signal from Vela (Knight 1981). More recently, a small (2′) X-ray nebula embedding the Vela pulsar has been detected. However, as yet, no pulsed X-rays have been seen from the Vela pulsar (Harnden *et al.* 1985). As will be described later, there have been detections of Vela at much higher photon energies ($> 5 \times 10^{11}$ eV), but an increased spectral exponent ($\gamma \approx 2.65$) is needed at these energies in order to join the higher and lower energy regions.

A number of models have been proposed to explain the γ-ray emission from the Crab and Vela and for pulsars in general. The inverse Compton mechanism is a strong contender (Apparao and Hoffman 1970, Cavaliere, Morrison and Pacini 1970, and others), the idea here being that energetic electrons from the pulsar generate synchrotron photons, primarily in the X-ray region, and these X-rays are boosted in energy into the γ-ray domain by inverse Compton collisions with the electrons. Schlickeiser (1981) has examined this possibility in detail, paying regard to the accurate formulation of the interaction cross section. He concludes that the energy spectra of γ-rays from the Crab and Vela can best be understood if the Compton interactions occur near the velocity of light cylinder. No doubt the differences in light curves (Figure 4.11) for the various parts of the electromagnetic spectrum are related to the fact that the quanta originate in different regions (e.g. the radio emission probably comes from near the polar caps); there is plenty of scope here for further detailed examination.

4.5.3 The 2CG gamma-ray source catalogue

Before discussing further individual sources it will be useful to consider the overall situation with regard to γ-ray sources. The most comprehensive work along these lines has been carried out by the COS B group, who have produced the '2CG catalogue' (Hermsen 1981) reproduced in Table 4.1. Figure 4.14 shows

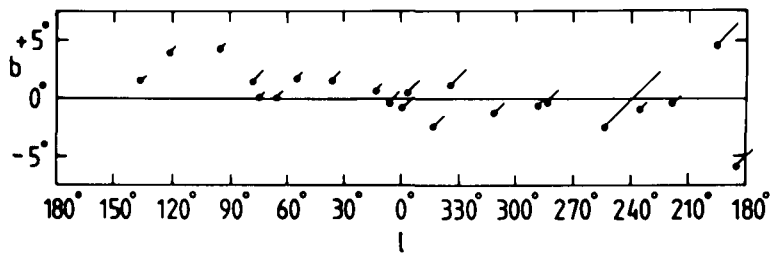

Figure 4.14. 2CG sources from the COS B catalogue of Hermsen (1980, 1981). The dots mark the estimated source positions (typical error radius 1°) and the inclined lines have lengths proportional to the quoted fluxes. The smallest flux shown is 1.0×10^{-6} cm^{-2} s^{-1} for $E_\gamma > 100$ MeV; the largest is for the Vela pulsar: 13.2×10^{-6} cm^{-2} s^{-1}.

the positions and fluxes of these sources (having $|b| < 7°$) on a longitude–latitude (l, b) plot.

The selection criteria used in determining the positions and fluxes are well documented (e.g. Hermsen 1980) and only a brief discussion will be given here.

The so-called 'cross correlation technique' was used to search for statistically significant excesses above the adjacent background values, a technique that involves knowledge of the detector point spread function (PSF). Ideally, one should use only data for which the PSF is narrowest, namely the highest energies, but the small number of γ-rays recorded at high photon energy dictates use of a compromise value; in the COS B case 100 MeV was chosen for most of the analysis. The basic requirement was that the peaks derived by adopting the cross correlation technique should be consistent with 'point' sources and that the excess fluxes should be at a high level of significance, symbolised by a probability of being spurious of $\lesssim 10^{-6}$. It was this latter condition that gave the effective threshold of source flux of $1.0 \times 10^{-6}\,\mathrm{cm}^{-2}\,\mathrm{s}^{-1}$ above 100 MeV apparent in Table 4.1, except for the high latitude source 2CG 289 + 64 (identified with the quasar 3C273) which was the subject of special treatment.

The uncertainty in position is clearly an important limitation in attempts to identify γ-ray sources with objects visible at other wavelengths. An order of magnitude estimate of what this uncertainty should be can be made using the data on angular resolution given earlier in Figure 4.8. There the FWHM is seen to be $\approx 4°$ for a mean energy corresponding to γ-rays above 100 MeV; the corresponding error circle at the 90% level has a radius of $\approx 4.5°$. Now a typical 'source' with flux near $1.0 \times 10^{-6}\,\mathrm{cm}^{-2}\,\mathrm{s}^{-1}$ is due to the detection of about 100 γ-rays, so that we might expect an error circle of radius $\approx 4.5°/100^{1/2} = 0.45°$. In fact, because of the presence of the background against which the source is viewed, the resolution might be expected to be degraded by a factor of, typically, two, i.e. to $\approx 1°$. Inspection of Table 4.1 shows the radii of the positional uncertainty circles are indeed in this region.

From some points of view the 2CG catalogue represents the most important result from the COS B experiment for γ-ray astronomy in this energy bracket, and it has provoked considerable discussion and argument, particularly with regard to the question of whether those sources which have not been identified with 'discrete' objects visible in other wavelengths are genuine or not (see, for example, the useful summary by Hermsen and Bloemen 1982). This topic will be examined in depth later, but some discussion will also be given in this section.

The first question to be considered is whether or not there is support for there being genuine γ-ray peaks at the COS B 'source' positions, whatever the origin of the peaks; in other words, can we discount technical imperfections and statistical fluctuations? The answer is that most (and perhaps all) of the *peaks* seem to be genuine, this conclusion following from SAS II observations, both by way of the identification of some of the obvious sources, e.g. Crab, Vela and Geminga, by the SAS II workers themselves (see Section 4.3.2), and by way of an analysis by Houston and Wolfendale (1983).

Table 4.1. *The 2CG catalogue of gamma-ray sources (Hermsen 1981)*

Source name	Observation periods	Significance (σ_0')	Energy threshold (MeV)	Position l (degrees)	b	Error radius (degrees)
2CG006−00	2, 18, 25	10.2	300	6.7	−0.5	1.0
2CG010−31	30	5.7*	100	10.5	−31.5	1.5
2CG013+00	2, 8, 18, 25	5.3	300	13.7	0.6	1.0
2CG036+01	9, 25, 26	4.9	300	36.5	1.5	1.0
2CG054+01	9, 25, 26	5.3	100	54.2	1.7	1.0
2CG065+00	4, 9, 22, 26	5.5	100	65.7	0.0	0.8
2CG075+00	4, 16, 22, 26, 36	5.8	100	75.0	0.0	1.0
2CG078+01	4, 16, 22, 26, 36	11.9	100	78.0	1.5	1.0
2CG095+04	4, 16, 22	4.9	150	95.5	4.2	1.5
2CG121+04	11, 16, 28	4.9	100	121.0	4.0	1.0
2CG135+01	11, 16, 28	4.9	100	135.0	1.5	1.0
2CG184−05	1, 14, 17, 29	20.6	100	184.5	−5.8	0.4
2CG195+04	1, 14, 29	27.1	100	195.1	4.5	0.4
2CG218−00	14, 18, 21	6.2	100	218.5	−0.5	1.3
2CG235−01	19, 21	5.0	150	235.5	−1.0	1.5
2CG263−02	3, 5, 12, 21	35.7	100	263.6	−2.5	0.3
2CG284−00	5	6.5	100	284.3	−0.5	1.0
2CG288−00	5	4.8	100	288.3	−0.7	1.3
2CG289+64	10, 32	6.5*	100	289.3	64.6	0.8
2CG311−01	5, 7	5.6	150	311.3	−1.3	1.0
2CG333+01	7, 13, 24	5.4	300	333.5	1.0	1.0
2CG342−02	2, 7, 13, 18, 24	8.9	300	342.9	−2.5	1.0
2CG353+16	2, 13, 18, 24	5.1*	100	353.3	16.0	1.5
2CG356+00	13	5.3	300	356.5	0.3	1.0
2CG359−00	2, 18, 24	6.3	300	359.5	−0.7	2.0

* Expressed in units of σ_0.
** Assuming E^{-2} spectra.
*** Intensity ($E > 300$ MeV)/intensity ($E > 100$ MeV), assuming E^{-2} spectra calculating both intensities.
The error radius is at the 90% level.

The argument centres rather on the *cause* or *causes* of the peaks. The alternative view to their explanation as discrete sources, such as previously unidentified pulsars, is that they are due to cosmic ray irradiation of the lumpy interstellar medium. It is well known that there are many dense clouds of molecular gas in the Galaxy, having gas densities of 100 times that in the general ISM, and some of these, on being penetrated by cosmic rays of the same intensity as those locally, might give rise to γ-ray peaks which would pass the COS B selection criteria.

Flux** $E > 100$ MeV (10^{-6} photons cm^{-2} s^{-1})	Spectral*** parameter	Comments		
		CG source	Identification	Other
2.4	0.39 ± 0.08			
1.2				
1.0	0.68 ± 0.14			
1.9	0.27 ± 0.07			
1.3	0.20 ± 0.09			
1.2	0.24 ± 0.09	CG064+00		
1.3		CG075−00		could be an extended feature
2.5		CG078+01		
1.1				
1.0	0.43 ± 0.12	CG121+03		
1.0	0.31 ± 0.10	CG135+01	CTO236+610?	
3.7	0.18 ± 0.04	CG185−05	Crab pulsar	
4.8	0.33 ± 0.04	CG195+04		
1.0	0.20 ± 0.08			
1.0				
13.2	0.36 ± 0.02	CG263−02	Vela pulsar	
2.7				could be an extended feature
1.6				
0.6	0.15 ± 0.07	CG291+65	3C273	
2.1		CG312−01		
3.8		CG333+00		
2.0	0.36 ± 0.09			
1.1	0.24 ± 0.09		Rho Ophiuchus dark cloud?	
2.6	0.46 ± 0.12			may be variable
1.8				

When we include the possibility, perhaps even the 'probability', of cosmic ray particle sources (supernovae, massive, very luminous OB star associations, etc.) being present in these 'giant' molecular clouds, thereby increasing the cosmic ray intensity in the clouds relative to the local value, the potential of irradiated clouds for mimicking γ-ray sources is seen to be rather large. This topic of pseudo-sources is returned to after attention is given to other γ-ray sources which are not the subject of as much dissent.

4.5.4 *Cygnus X-3*

At much higher γ-ray energies (10^{11}–10^{16} eV), the well known X-ray source Cygnus X-3 appears to be a dramatic emitter (see Section 5.3.1D for a discussion), and it is appropriate to examine its γ-ray emission in the present energy bracket in some detail. Its well known characteristic 4.8 h period in the X-ray region (first seen by Parsignault *et al.* 1972) led many γ-ray observers to search for this period in their own energy bands. Balloon observations from 1972 onwards claimed high fluxes, at least until 1977 or so (e.g. Galper *et al.* 1977). SAS II claimed a significant signal (Lamb *et al.* 1977), the pulsed flux above 100 MeV being $(4.4 \pm 1.1) \times 10^{-6}$ cm^{-2} s^{-1} and that above 35 MeV $(10.9 \pm 3.1) \times 10^{-6}$ cm^{-2} s^{-1}. These fluxes, although 'large' compared with those from the 2CG catalogue given in Table 4.1, are appreciably smaller than those of Galper *et al.* (1977), leading to the likelihood that the object is waning. Support for this contention comes from the COS B observations – no pulsed emission was detected in 1975 (Bennett *et al.* 1977) nor in later years (Swannenburg *et al.* 1981, Hermsen *et al.* 1987).

Figure 4.15 presents a summary by Rana *et al.* (1984) of the emission from

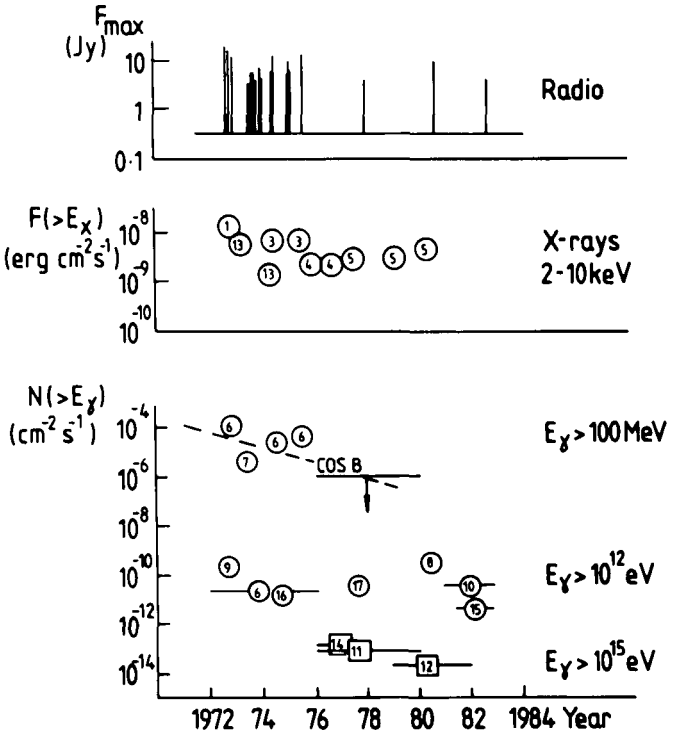

Figure 4.15. Summary of observations for Cygnus X-3 (after Rana *et al.* 1984). The ringed numbers refer to the various experiments. Measurements since 1984 at energies above 10^{12} eV have indicated that Cygnus X-3 has continued to be in a 'low' state. The extent to which it has, in fact, been observed at all since that date is considered later (in Chapter 5).

Cygnus X-3 over the last decade but one. Since that time the output has continued to be low, with claimed outbursts from time to time. Further discussion of this remarkable object, which is almost certainly a binary system involving an energy outflow on occasion of up to 10^{38} erg s^{-1}, is deferred to Section 5.3.1D and 5.4.2.

4.5.5 Geminga

It is a remarkable fact that there is still argument about the explanation for the nature of this, the second strongest γ-ray source at the energies in question. The strength of the source, its lack of significant extension beyond the PSF of the COS B instrument, and the absence of known molecular clouds in that direction, lead to a consensus interpretation as a 'discrete source'. So important has this source been regarded that five observing periods were devoted to it in the COS B project and nearly 1000 γ-rays were detected from it. It is currently an important object on the 'observation' list for the contemporary Gamma Ray Observatory and has recently been detected by that instrument. GRO has confirmed the COS B result (Table 4.1) that Geminga's energy spectrum is much harder than that of the Crab.

Inspection of optical, radio and X-ray records have revealed a number of possible candidates in the (0.4° radius) error box of Geminga, but most had a number of unsatisfactory features (see Schlickeiser 1981 for a useful summary and comments on the likely production mechanism). The best identification came from a detailed search by Bignami and associates (described by Bignami, Caraveo and Paul 1984), and this result will be described in some detail.

With the advent of the Einstein X-ray Observatory, having three orders of magnitude higher sensitivity, Bignami *et al.* (1984) were able to make a careful examination of the Geminga error box. The result was the detection, at a level of $\approx 10^{-12}$ erg cm^{-2} s^{-1}, above a few keV, of a rather peculiar X-ray source (denoted IE 0630+178 in the Einstein Observatory catalogue). The main peculiarity was the absence of a star in the Palomar Observatory sky survey plates. A special optical search was therefore instituted to look for a fainter star than the Palomar limit. The search was successful (Bignami *et al.* 1988) in that a very faint object (G″) with magnitude $m = 25.5$ was detected in the 50 (arc sec)^2 error box occupied by the X-ray source. The spectral shape of the candidate, exemplified by 3×10^{-16} erg cm^{-2} s^{-1} in the visible, 10^{-12} erg cm^{-2} s^{-1} in the X-ray, and 10^{-9} erg cm^{-2} s^{-1} in the γ-ray (above 100 MeV) regions, makes it a strong contender. Figure 4.16 shows the whole energy range.

What seemed to support the identification is the apparent time variability at γ-ray and X-ray wavelengths. The γ-ray situation can be considered first. Thompson *et al.* (1977) gave evidence for a 59 s periodicity in the emission from Geminga, based on the 121 γ-rays detected, and they made a case for a finite rate of change of period over the six-month observing period of $\dot{P} \approx 2 \times 10^{-9}$ s s^{-1}. Clearly the significance was not great, but this was increased after the launch of COS B when Masnou (1977) claimed confirmation of both P and $\dot{P}$ from an analysis of the early COS B results. Remarkably (as it subsequently turned out) in a later publication the COS B collaboration retracted its confirmation, despite three years

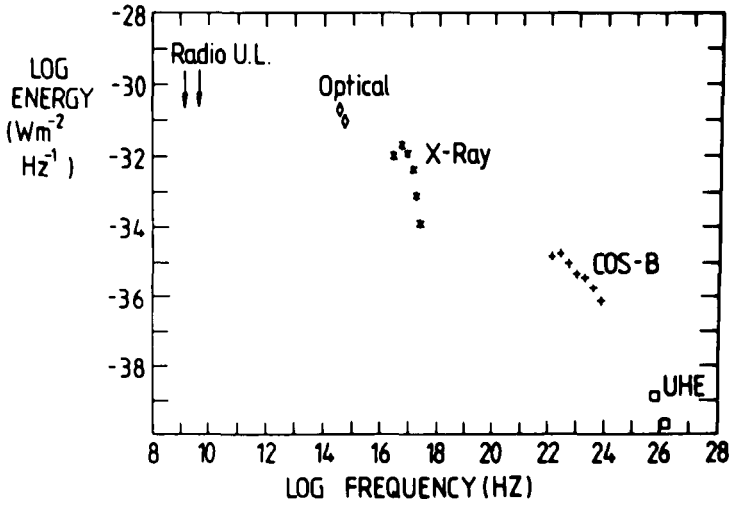

Figure 4.16. Summary of observations on the γ-ray source 'Geminga' (2CG 195+04) from the work of Bignami (1984). At that time an object with magnitude $m = 20.3$ was thought to be responsible (and its optical luminosity is as shown in the figure). However, more recently, another, fainter, object has been favoured – see text.

of satellite operation, on the grounds of a previous underestimate of the statistical uncertainty; see Masnou *et al.* (1981) and Buccheri *et al.* (1985). The GRO observations currently being made have, however, given a much clearer and more accurate picture about the periodicity as detailed below.

We return to X-rays once again for what might turn out to be an elucidation of the situation. Halpern and Holt (1992) have recently discovered soft X-ray pulsations in the energy range 0.07–2.4 keV from ROSAT data on Geminga. The authors have carried out a fast Fourier transform analysis on the event times of data taken during March 14–17, 1991 and found that the object shows X-ray pulsations with a period of 0.273 097 4 s. The X-ray energy spectrum is best fit by a composite of a thermal spectrum with a temperature of (3–4) $\times$ 10^5 K plus a power law spectrum with an energy index of 0.75 to 1.75. Soon after, Bertsch *et al.* (1992) carried out a periodicity search around the X-ray period, in the data from EGRET aboard the GRO and found that the object does indeed show evidence for pulsations in γ-rays at energies above 50 MeV, in the data taken during April–June 1991. The authors have found, in addition, that the period increases at a rate of $(11.4 \pm 1.7) \times 10^{-15}$ s s^{-1}. The GRO results on the period and its variation with time are shown in Figure 4.17. Bignami and Caraveo (1992) have re-analysed the archival COS B data taken during 1975–82 on this object to find that the object was pulsating in γ-rays even then; these findings are in agreement with those of Bertsch *et al.*

The three results just described, when combined with standard theory for rotating neutron stars (Taylor and Manchester, 1981) lead to the conclusion that the object has a characteristic age of 3.2 $\times$ 10^5 y, a magnetic field of 1.6 $\times$ 10^{12} G and a spin down energy loss rate of 3.5 $\times$ 10^{34} erg s^{-1}. The spin down energy loss rate when combined with the observed γ-ray luminosity places an absolute upper limit to the distance of the object of $\sim$380 pc and it could be as near as

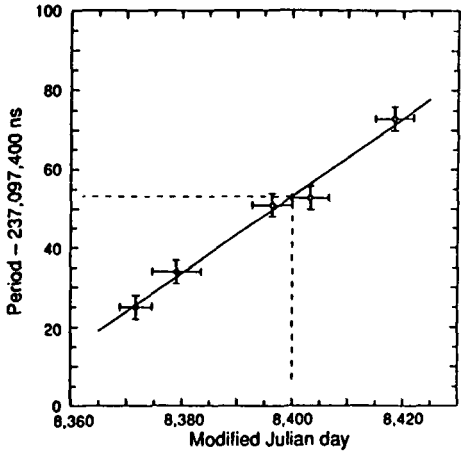

Figure 4.17. Period versus epoch for the Geminga γ-ray source as observed by the EGRET detector aboard the Compton Gamma Ray Observatory (Bertsch *et al.* 1992).

~ 38 pc, depending on the energy conversion efficiency to γ-rays. The predominant emission at γ-ray energies with a much weaker X-ray emission (10^{-3} of $\mathscr{L}_\gamma$), an almost negligible emission ($< 10^{-7}$ of $\mathscr{L}_\gamma$) and the lack of observed radio emission indicate that Geminga is a near unique object. Also it may be the nearest neutron star to our solar system.

Turning now to specific models, a number have been put forward. Several years before the recent discovery of 273 ms periodicity as mentioned above, Fabian and Nulsen (1984) proposed a binary system comprising two magnetised neutron stars; it having been hypothesised by Henrichs and Van der Heuvel (1983) that the rate of formation of such binaries (which might have been thought of as rare) is $\approx 3 \times 10^{-4}\ y^{-1}$, i.e. 1% of the rate of formation of single pulsars.

The difficulty of the rapid slowing down of an isolated pulsar is circumvented, and it is possible to invoke a specific mechanism to give the observed γ-rays. Following Fabian and Nulsen, the idea is that a high potential difference is set up across the small orbital separation ($\approx 10^{10}$ cm), this potential difference being in excess of 10^{12} V, and arising between certain magnetic field lines of the two pulsars. The γ-rays, in turn, come from the 10^{12}–10^{13} eV electrons by way of synchrotron and/or curvature radiation.

In the Fabian–Nulsen model, the observed X-ray and γ-ray period (at a time when both were thought to be around 59–60 s), or rather frequency, is the difference between the spin frequency of the primary neutron star (that with the larger magnetic moment) and the orbital period of the other neutron star. The detailed calculation required Geminga to be at a distance of 11 pc, ignoring any beaming effects. An interesting feature is the prediction that the system is a strong source of gravitational radiation; specifically the loss rate in this mode is $\approx 3 \times 10^{36}$ erg s^{-1}, a value greater than that in electromagnetic radiation. Unfortunately, gravitational wave detectors of adequate sensitivity are not yet available to check this prediction.

With the latest ROSAT and GRO findings, an isolated rotating neutron star model is clearly more favoured for Geminga.

4.5.6 The possibility of pseudo-sources

As has already been remarked, there has been considerable argument as to the nature of the unidentified COS B sources (see the data from the 2CG catalogue in Table 4.1). The poor angular resolution of the detectors, coupled with the uneven γ-ray background, makes it inevitable that doubts arise (no doubt similar considerations will apply – at a lower flux level – to the forthcoming GRO results).

Although the fact that the 2CG catalogue included sources whose statistical significance was shown by straightforward calculation to be very considerable, the crucial role played by the lumpy background (γ-rays from cosmic rays interacting with the interstellar gas, denoted 'CRI', 'cosmic ray irradiation of the ISM') does not appear to have been realised until the work of Li and Wolfendale (1981). These authors used a statistical analysis based on the likely numbers of giant molecular clouds in the inner Galaxy ('direct' information by way of detailed CO maps were not then available) to claim that between 40 and 60% of the 2CG sources could be explained solely on the basis of CRI. In fact, a later analysis of the masses of molecular clouds (to be described), which reduces them somewhat, means that the Li and Wolfendale estimate should be revised downwards a little (to 30–50%).

The situation is epitomised by the 2CG source associated with Rho Ophiucus. Initially, this was considered to be a discrete source, but the accumulation of more γ-ray data by COS B led to the appreciation that it can be explained by CRI. Figure 4.18 shows the situation. It should be remarked that the object has not ceased to be of interest; in fact, it may be very important because of the information it gives about the magnitude of the cosmic ray intensity in that region. Although this topic is taken up again later, it can be remarked here that the cosmic ray intensity may be significantly higher there than locally (Issa and Wolfendale 1981*a*, Morfill *et al.* 1981). Some other 2CG 'sources' may also be associated with molecular clouds which contain higher than average cosmic ray intensities (see Section 4.6.4.).

Perhaps the strongest evidence against accepting the totality of the 2CG sources as genuine comes from the work of Houston and Wolfendale (1984). These workers have drawn attention to the fact that, whatever the fraction of genuine sources in the data, some genuine sources will be lost because of the confusion caused by the lumpy background, and the confusion will be greatest in the inner Galaxy. Houston and Wolfendale argue that the hypothesis that the source catalogue is correct in its entirety can be checked by evaluating the loss, correcting for it, and then deriving the total flux from all sources, resolved and unresolved.

A detailed study was made of the efficiency of detection of a source as a function of source strength, longitude and latitude. As expected, the efficiencies are often quite low. For example, even a comparatively strong source, of strength 1.3 f.u. (1 f.u. $= 1 \times 10^{-6}\,\mathrm{cm^{-2}\,s^{-1}}$ with $E > 100$ MeV) has only a 20% probability of being detected at a longitude $l = 30°$. A source of strength 1 f.u. – the most common source strength in the 2CG catalogue – has a detection probability of less than 10% at $l = 30°$ and still only $\approx 50\%$ at $l = 120°$.

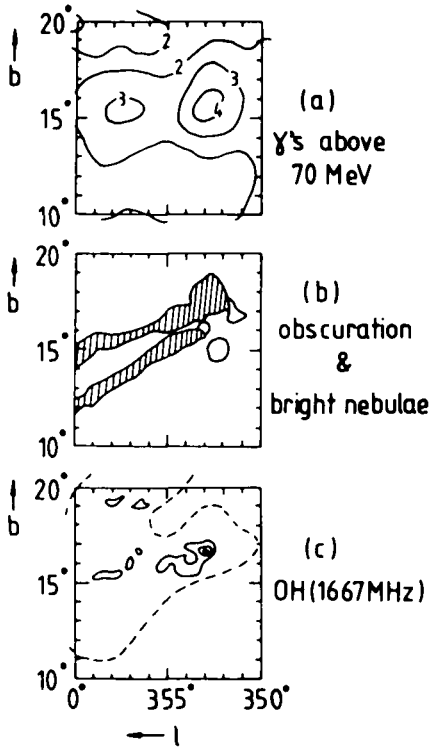

Figure 4.18. The Rho Ophiucus region. (*a*) γ-rays above 70 MeV from COS B (Mayer-Hasselwander *et al.* 1982). (*b*) An indication of cloud geometry from the *Atlas of Galactic Dark Nebulae* due to Khavtassi (1960). The shaded area relates to the heaviest obscuration recorded; 'bright nebulae' (unshaded) will also be targets for cosmic ray interaction. (*c*) Contours of CO emission from the 1667 MHz maps of Wouterloot (1981); the contour intervals are 0.06, 0.10, 0.14 K, ... It is apparent that the γ-ray-emission roughly mirrors that of the gas.

The net result is that if all the 2CG sources are assumed genuine, then the corrected source spectrum can be derived. Figure 4.19 illustrates the situation. Considering the inner Galaxy, the log N–log F_γ plot is seen to be very steep indeed, so steep in fact that, for any reasonable choice of the radial (Galactocentric radius) distribution of sources (and their form must satisfy the corrected log N–log F_γ plot), the total integrated γ-ray flux, from both resolved and unresolved sources, is impossibly high. Quoting Houston and Wolfendale, with a radial source distribution of a form similar to that of SNR raised to the power p, i.e.

$$\rho(R) \propto \{\rho_{\mathrm{SNR}}(R)/\rho_{\mathrm{SNR}}(R = 10)\}^p \tag{4.3}$$

where R is in kpc, $p = 3$ is needed, and the total integrated flux above 100 MeV is 430 f.u. Now, the total observed flux is only 230 f.u., so this is an impossible situation.

Moving to the question, again, of what fraction of the γ-ray sources are genuine and what fraction of the total flux is due to genuine sources, recourse has to be

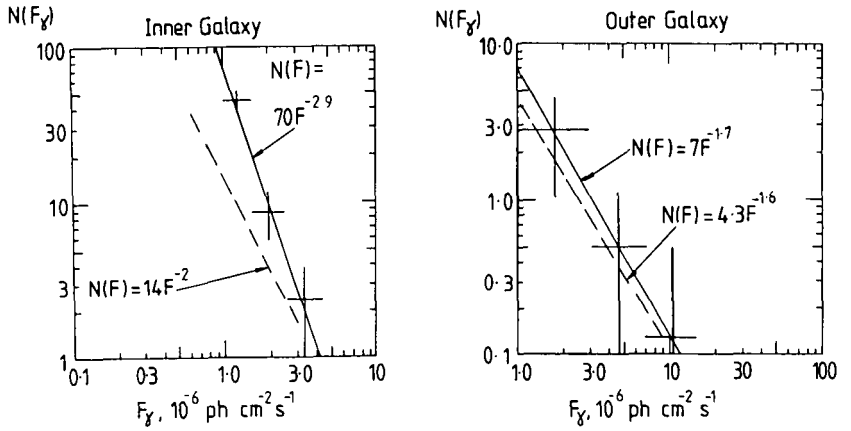

Figure 4.19. Differential distribution of source fluxes for COS B as corrected by Houston and Wolfendale (1984) to allow for loss by confusion (full lines). Their attempt at rejecting likely pseudo-sources due to cosmic-ray-irradiated gas gives the 'genuine source' distributions shown by the dotted line.

made to models for their distribution in the Galaxy. An SNR-type distribution (equation 4.3) with $p = 1$ and individual γ-ray luminosities of the order of those observed for the few identified sources, give a model which appears to be consistent with all the observations, including the statistical estimate of pseudo-sources made earlier. The corresponding fractions of pseudo-sources are 60% for the inner Galaxy and ~30% for the outer Galaxy. The $\log N$–$\log F_\gamma$ plots for genuine sources are also shown in Figure 4.19. The corresponding fraction of the Galactic flux due to unresolved sources is ~20% for the inner Galaxy and ~15% for the outer Galaxy. (This topic is considered in more detail later.) These ideas concerning the fraction of pseudo-sources received a measure of confirmation with the work of Pollock *et al.* (1984, reported by Bignami *et al.* 1984). 2CG sources in the range $l = 0°$–$90°$ have been reinterpreted in the light of the CRI problem referred to above, and using the recent CO data, with the result shown in Table 4.2. Insofar as the energy threshold differs from that in the 2CG catalogue (300 MeV compared to 100 MeV), a proper comparison with previous predictions of the number of pseudo-sources cannot be made – in fact, the numbers involved are so small that a precise comparison is not possible in any case. Nevertheless, the situation is heartening. Out of seven sources, three have moved into the category of being satisfactorily explained in terms of CRI, a number not inconsistent with the 30–50% referred to above.

Surprisingly, perhaps, one of the 2CG sources (054+01) is now categorised as 'variable', as is a new one at 083+03 (Pollock *et al.* 1981).

More recently still, Grenier, Hermsen and Pollock (1991) have produced another catalogue, under stricter selection conditions than hitherto, which includes yet more 'variable sources'. These are listed in Table 4.3.

It is necessary at this stage to point out that this catalogue is not unique; other

Table 4.2. *Reanalysis of 2CG sources in the first quadrant (Bignami* et al. *1984)*

Out of seven sources, three now appear consistent with cosmic-ray-irradiated gas and there is a new one too.

Name	l (degrees)	b (degrees)	Flux ($\times 10^{-7}$ cm^{-2} s^{-1})	No. of obs.	Confidence parameter
(*a*) Objects detected above 300 MeV in addition to the gas					
2CG078+01	78.1	2.3	4.8	7	52.8
2CG075+00	76.1	0.5	3.8	7	
2CG054+01	55.0	2.2	5.9	1	9.2 variable
083+03	83.0	3.2	5.3	1	8.6 variable
2CG013+00	13.9	0.2	4.9	4	7.3
(*b*) Objects above 300 MeV satisfactorily explained by the gas, with limits on the extra flux					
2CG036+01			3.7	5	0.6
2CG065+00			2.1	4	0.0
2CG095+04			2.4	4	1.2

Table 4.3. *The latest COS B source catalogue for γ-rays above 300 MeV (Grenier* et al. *1991). The number of spurious sources in the list is expected to be less than one.*

l (degrees)	b (degrees)	Flux ($\times 10^{-7}$ cm^{-2} s^{-1})	Comment
76.0	0.4	3.7	constant
78.2	2.0	4.5	constant
82.8	3.2	1.2	variable
135.0	1.4	2.5	constant
139.2	−0.8	1.0	constant
184.6	−5.8	7.3	constant
195.1	4.2	14.2	constant
263.5	−2.5	41.7	constant
322.2	−1.7	3.0	variable
343.1	−2.9	3.9	variable
347.1	−1.9	0.5	variable
357.6	−1.2	4.3	variable

COS B 'groups' have also given catalogues which, in the event, do not agree completely with Table 4.3. In view of the fact that the GRO source catalogue will surely be superior, it is not profitable to make a more detailed analysis of the COS B sources at this stage.

4.6 The diffuse Galactic emission

4.6.1 General remarks

Even as early as the first satellite experiments, notwithstanding their crude angular resolution, attempts were made to interpret what appeared to be a diffuse Galactic γ-ray component in terms of cosmic ray interactions (see, for example, the work of Clark *et al.* 1968, Stecker 1969, Fichtel *et al.* 1972, Strong, Wdowczyk and Wolfendale 1973). These attempts have continued, with increasing sophistication, and also, it is hoped, with increasing accuracy in the end product.

Implicit in most of the analyses is the assumption that the contribution to the observed γ-ray flux from unresolved discrete sources in the Galaxy is small. In addition to the arguments presented already, mention should also be made of a number of indirect estimates of the contribution; without exception, they give values in the region of 25% of the observed flux (e.g. Protheroe, Strong and Wolfendale 1979, Ma and Wolfendale 1989). A particularly strong suggestion that the contribution is not large is the fact that, along the Galactic Plane, the γ-ray intensity correlates well with the synchrotron radio emission (Haslam *et al.* 1981). The latter is accepted to be almost entirely of a diffuse nature and due to the spiralling of GeV electrons in the tangled magnetic field. Particularly safe from unresolved sources is the Galactic Anti-Centre direction ($l = 90$–$270°$) and all longitudes for $|b| > 10°$, where most discrete sources are expected to be readily recognisable.

When examining the correlation of the diffuse γ-ray intensity with the column densities of gas in the ISM, to deduce the corresponding cosmic ray intensity, it is usually important to distinguish between the two major cosmic ray components: electrons and 'nuclei' (the latter are primarily protons – in fact, the nuclear component will often be referred to just as 'protons', although in practice all the nuclear components are included in the calculations). Figure 4.20 (from Fichtel 1983) gives an estimate of the constituent γ-ray spectra for the general Galactic Centre direction and demarcates the regions where the proton (π^0) and electron (bremsstrahlung + Compton) components are likely to be important. An alternative manner of presentation, and one which indicates some of the disparity amongst the various predictions, has been given by Bhat, Mayer and Wolfendale (1984*a*) and is shown in Figure 4.21. The fractions of the important proton component for the various energy ranges adopted in the SAS II and COS B experiments are indicated in this figure.

It is important to point out that there is still considerable uncertainty in the inverse Compton contribution (and this accounts for some of the spread in Figure 4.21). A good summary has been given by Bloemen (1985). The problems are two-fold: uncertainty in the scale height of the electrons, and, remarkably, some uncertainty in the distribution of starlight away from the solar system. The uncertain scale height relates to the standard problem of the nature of the 'Galactic halo' – a topic of many years' standing. Inspection of other (edge-on) galaxies shows that some have such a radio halo and others have not. Our view is that there is probably a modest halo around our Galaxy of scale height $z_{1/2} \simeq 1$ kpc

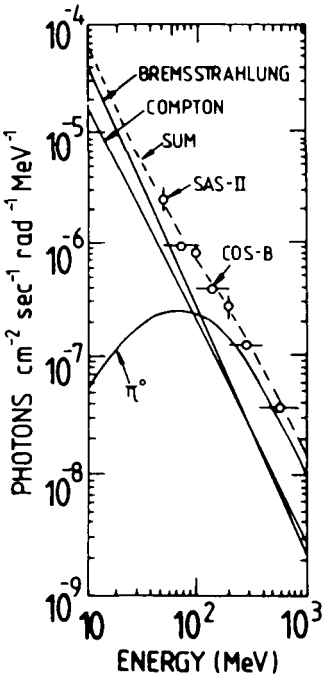

Figure 4.20. Energy spectrum of γ-rays from the general direction of the Galactic Centre. The calculated spectra are from Fichtel (1983) and must be regarded as only approximate; the actual division between the various components is difficult to determine and is subject to argument. The experimental intensities are from Mayer-Hasselwander *et al.* (1982) for COS B and Fichtel (1983) for SAS II.

for the radio emissivity, but that this is due to the fall-off of magnetic field with height above the Plane, the fall of cosmic ray flux being less rapid. It is unlikely that there will be a satisfactory answer to this problem for some time to come.

The starlight distribution is more tractable, and in Figure 4.22 we present the results of recent calculations by Chi and Wolfendale (1991); this should be of value when more precise γ-ray data are available.

4.6.2 Gas in the Galaxy

Hydrogen is the dominant gas component in the Galaxy, with helium present to the extent of about 36% by mass, and heavier nuclei contributing a further 2%. Interstellar grains are probably responsible for about 1% by mass of the ISM. Although the distribution of atomic hydrogen (HI) is reasonably well known, from studies of the 21 cm radiation, that of the molecular component (H_2) is the subject of much debate, for the reasons mentioned in Section 4.1.

As an estimate of the large scale distribution of gas, assuming azimuthal symmetry, we can consider the surface densities of HI and H_2 given by Gordon

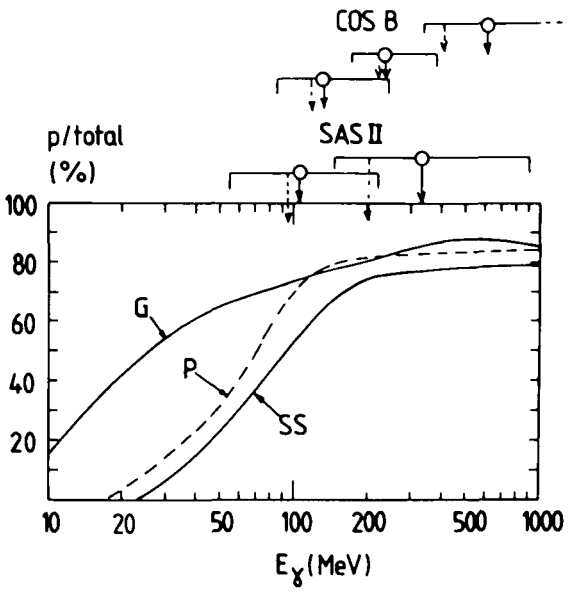

Figure 4.21. The fraction of the γ-ray flux due to protons as a function of γ-ray energy (Bhat *et al.* 1984*a*). The median energies for the energy bands for the SAS II and COS B measurements are indicated, as are the limits such that 67% of the signal lies within. Dotted vertical lines: energies at which one should consult the graphs in order to find the appropriate proton fraction. G, P, SS: different authors' predictions (G: Goned 1981; P: Poon 1983, both for the 'local spectrum'; SS: Sacher and Schonfelder 1984, the 'Anti-Centre spectrum', 116°–136°). It will be noted that protons are dominant for the higher band for SAS II and the two upper bands for COS B.

and Burton (1976) and shown in Figure 4.23. By surface density, $\sigma(R)$, we mean $\int_{-\infty}^{\infty} \rho(z)\,dz$ at a fixed Galactocentric radius, R. By way of example, a mean density of $\rho = 1$ atom cm^{-3} over a scale height $z = 150$ pc on either side of the Galactic Plane would be given as $300 \times 3 \times 10^{18} \approx 10^{21}$ atom cm^{-2}, i.e. $10^{21} \times 1.7 \times 10^{-24} \times (3 \times 10^{18})^2/2 \times 10^{33} \approx 1$ solar mass pc^{-2} ($= 1 M_\odot$ pc^{-2}). This plot has been extensively used in γ-rays analyses.

The first realisation of the importance of the then newly discovered H_2 component came from the work of Dodds *et al.* (1974) and Solomon and Stecker (1974). At that time, singularly high surface densities of H_2 had been claimed by Scoville and Solomon (1973) from the carbon monoxide (CO) observations, and the early conclusions are thus of little value now. In what follows, more recent estimates of H_2 will be used, but it needs to be stressed that these are still in doubt.

As remarked already, the column density of molecular hydrogen is inferred from data on CO. However, although there has now been a comprehensive survey of the Galaxy in CO, the conversion factor from $\int T\,dV$ for the ^{12}CO line to the column density of molecular hydrogen, $N(H_2)$ is still in doubt. Attention focuses on the conversion quantity $X = N(H_2)/\int T\,dV$ and estimates for the important

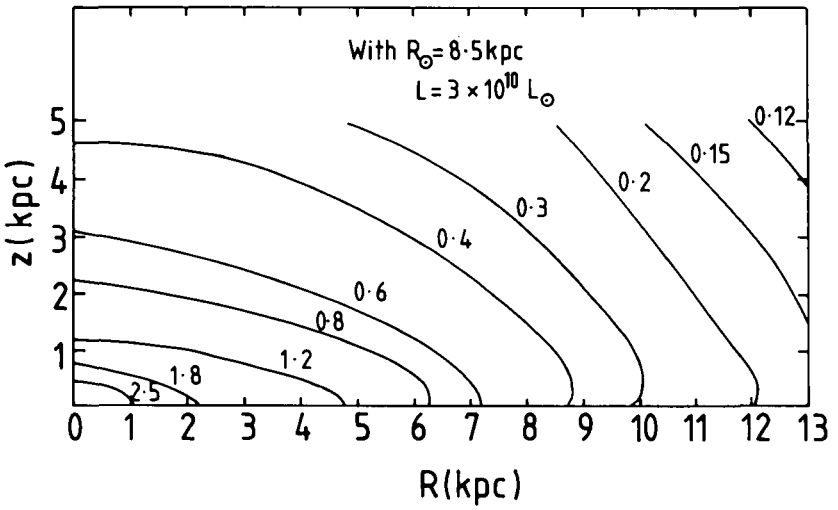

Figure 4.22. The distribution of starlight energy density (in eV cm^{-3}) in the Galaxy from the work of Chi and Wolfendale (1991). A Sun to Galactic Centre distance of 8.5 kpc has been adopted, and an input starlight energy of $3 \times 10^{10} L_{\odot}$ is assumed. The energy density is proportional to input energy, in first approximation, but absorption and scattering effects associated with the conversion from optical energy to infra-red energy cause implications when more accurate results are required. The values given in the figure are considered accurate to about 30%.

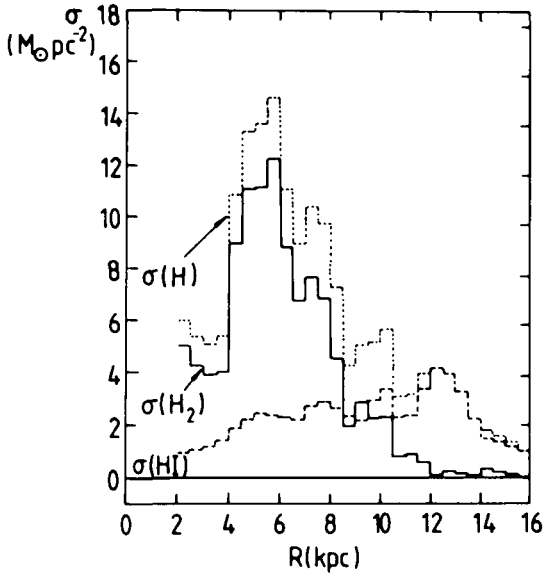

Figure 4.23. Distribution with Galactocentric distance R of the surface densities of atomic and molecular hydrogen, from the early 'standard' work of Gordon and Burton (1976). The Sun is at $R = 10$ kpc. The surface density of molecular hydrogen is necessarily imprecise because of problems with the conversion from the measured CO intensity to molecular hydrogen column density and possible radial dependence of the conversion factor. H: HI + H_2. The problem is discussed in the text.

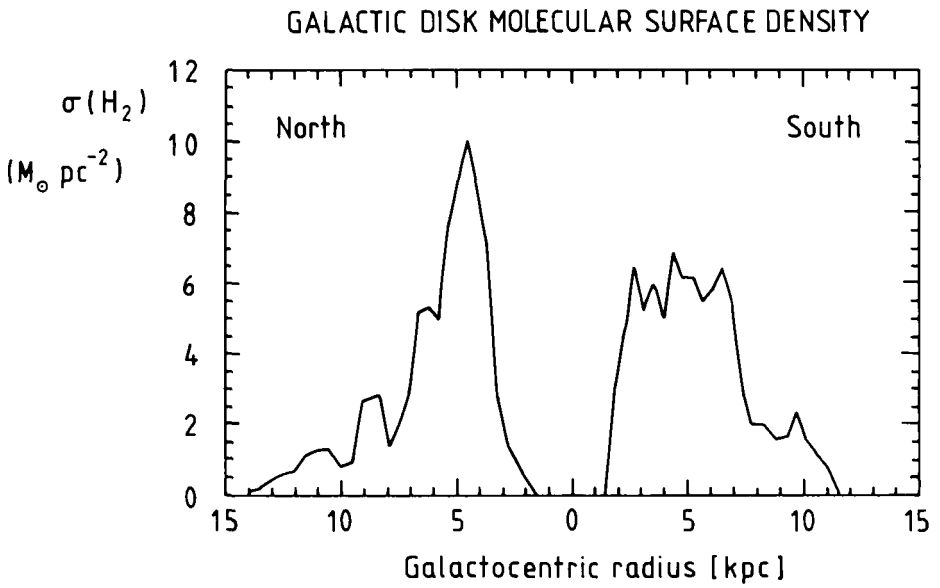

Figure 4.24. Surface density of molecular hydrogen (in $M_\odot$ pc^{-2}) as a function of Galactocentric radius for the two Galactic hemispheres separately, from the work of L. Bronfman (1991, private communication). Radial symmetry is assumed for each hemisphere. The Sun to Galactic Centre distance is taken as 8.5 kpc. A value of the conversion factor $X = 2.3$ was adopted; this may be rather too large (see Section 4.6.5).

region of the molecular ring at Galactocentric distance $R \sim 6$ kpc vary from about 3 to 1. Although we feel that the value of X chosen by the Columbia group (Bronfman *et al.* 1988) is somewhat too high, we present the surface density of H_2 in the Galaxy given by these authors; this is shown in Figure 4.24 for the two hemispheres separately. The topic will be taken up again in Section 4.6.5.

4.6.3 *Correlation of gamma-ray intensity with gas column density*

Correlations in the outer Galaxy. Many studies have been made of this correlation, both for HI alone and HI + estimated H_2, the studies being made for several different latitude and longitude ranges. The objective is usually to determine the manner in which the intensity of the initiating cosmic rays varies with position in the Galaxy, and thereby to throw light on the cosmic ray origin problem. Specifically, a firm distinction has still to be made between the majority of cosmic ray protons being of Galactic or of extragalactic origin. The extent to which such a distinction is possible will become clear shortly.

It has long been known that there is only a little molecular gas in the outer Galaxy (second and third quadrants) and, in consequence, this region has been studied rather well. Inspection of Figure 4.6 shows a problem, however, namely the γ-ray flux is small and the statistical errors are relatively large.

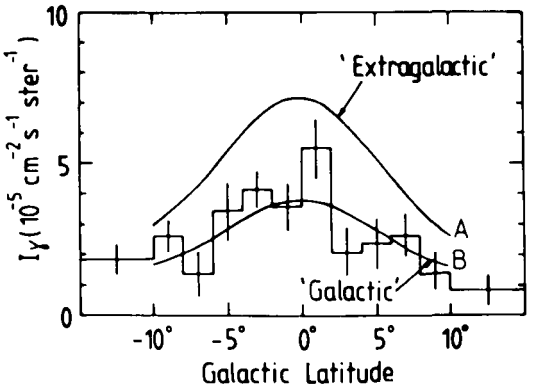

Figure 4.25. Comparison of the latitude distribution of γ-rays above 100 MeV in the Galactic Anti-Centre (SAS II: Fichtel *et al.* 1975) with the predictions for a Galactic origin of the particles (B) and an extragalactic origin (A). The analysis is from the work of Dodds *et al.* (1975). The data are averages over 90°–100°, 160°–170° and 200°–260°; the Crab direction has been omitted. It is interesting that both the observations and the predictions have changed somewhat with time, in the sense that there was a recalibration of the intensities, and later estimates of gas densities gave rise to different predictions, but the conclusions appear to be still valid.

A number of analyses have been made of the SAS II data, and Figure 4.25 shows the result of an early one.

As in correlation studies, we write the γ-ray intensity as

$$I_\gamma = \frac{q}{4\pi} N(\mathrm{H}) + I_b \tag{4.4}$$

where $N(\mathrm{H})$ is the column density of gas in atoms cm^{-2}, q is the emissivity for the energy range in question in γ-rays atom^{-1} s^{-1}, and I_b is the background flux, a quantity which comprises both instrumental and extragalactic components.

The important quantity of relevance to cosmic ray studies is q, the γ-ray emissivity. Clearly, this quantity is proportional to 'the cosmic ray intensity', or, more accurately, the appropriate combination of the intensities of its electron and proton components. Under the assumption that the ratio of protons to electrons is independent of position in the Galaxy, an assumption which is only approximately valid, we can revert to using the term 'cosmic ray intensity', and this approximation is followed here. We are, of course, mindful of the fact that the relative contributions of protons and electrons as parents of the detected γ-rays depend on γ-ray energy (see Figures 4.20 and 4.21).

The earliest work relating to q, and the magnitude of the cosmic ray intensity in the outer Galaxy, is that of Dodds, Strong and Wolfendale (1975). Figure 4.25 shows the results of their study using the SAS II data. In the figure, comparison is made of the latitude distribution expected on the basis of a constant cosmic ray intensity at all R (extragalactic origin) and one that follows the approximately known radial distribution of SNR (Galactic origin). It is apparent that a Galactic

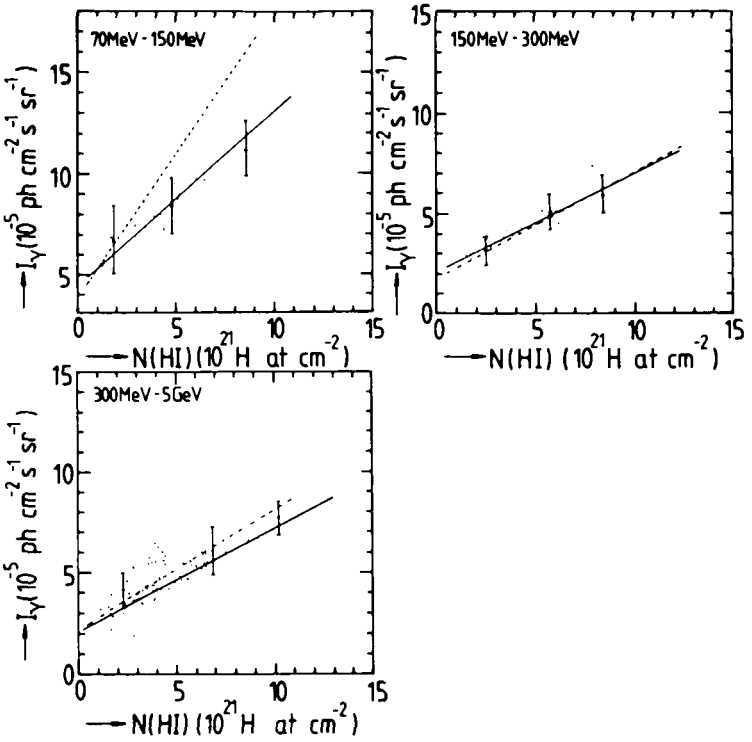

Figure 4.26. Comparison of COS B γ-ray intensities and HI column densities (4° × 4° bins) in the second and third Galactic quadrants. The regions containing point-like sources have been excluded. Typical statistical errors are indicated. Solid lines: least squares fit to the data points; dashed lines: for the local Galactic region as given by Strong *et al.* (1982) using 'high' latitude data ($|b| = 11°–19°$). The near equality of the full and dashed lines for the two upper energy brackets is taken by the authors of this work (Bloemen *et al.* 1984*a*) to indicate that the average cosmic ray gradient in the outer Galaxy is small here. See also Figure 4.27.

origin is favoured. There is an immediate problem, however, when it is realised (Figure 4.21) that some 30–50% of the γ-rays in question ($E_\gamma > 100$ MeV) come from electrons. Electrons, certainly being of Galactic origin (see Section 4.6.6), will probably have a steep gradient, and it is not inconceivable that the important proton component has little or none. Thus, it is imperative to examine the situation for γ-rays of higher energy, where the cosmic rays responsible are almost entirely protons (and associated heavier nuclei). This will be done shortly.

Returning first to the straightforward correlations of I_γ with N(HI) in the outer Galaxy, an important set of results which came from the analysis of COS B observations by Bloemen *et al.* (1984*a*), are shown in Figure 4.26. There is seen to be a reassuringly good correlation.

Bloemen *et al.* have gone on to examine the detailed (l, b) dependence of the correlation of I_γ with N(HI) for the situation where N(HI) is divided into radial

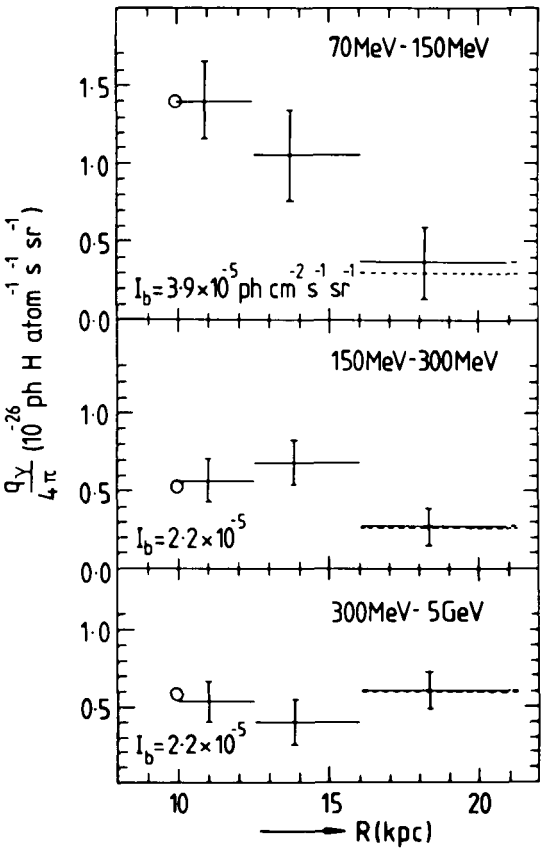

Figure 4.27. Radial distribution of q_γ (i.e. a constant times the cosmic ray intensity) in the outer Galaxy for the three COS B energy ranges, from the work of Bloemen *et al.* (1984*a*). The local emissivity values of Strong *et al.* (1982) are shown for $R = 10$ kpc as circles. Dashed lines: $R > 16$ kpc, showing the q_γ values after correction for π^0 decay input spectrum.

distance bands (10–12.5 kpc, 12.5–16 kpc and beyond 16 kpc). Regions where there are possible sources (see 2CG catalogue, Table 4.1) are excluded. The resulting values are shown in Figure 4.27. A rather dramatic result is seen in this figure. Although there is a strong gradient for the lowest energy band (for which the primary particles are almost entirely electrons), that for the second band is smaller, and a gradient in the highest energy band ($\approx 80\%$ protons) is essentially absent. If true, this would be a most important result, suggesting that the protons could well be extragalactic. In view of its importance, Bhat, Mayer and Wolfendale (1986) have reanalysed the COS B data for $E_\gamma > 300$ MeV with the results shown in Figure 4.28; it will be seen that there might now be a small gradient. This topic is taken up again in Section 4.6.6 in greater detail, where it will be concluded that there *is*, indeed, a gradient.

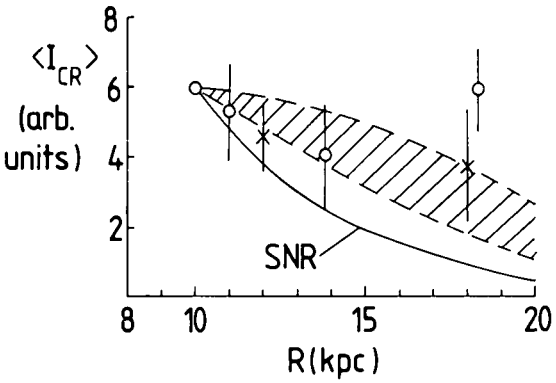

Figure 4.28. Gradient of cosmic ray intensity in the outer Galaxy for COS B data with $E_\gamma > 300$ MeV, namely the regions where protons dominate as the initiating particles. ○: from the analysis of Bloemen *et al.* (1984*a*) (and as shown in Figure 4.27); ×: from an alternative analysis by Bhat *et al.* (1986). The shaded area represents expectation for the situation where the source distribution follows that marked SNR but the flaring of the trapping region causes the particle lifetime to be longer in the outer Galaxy. The limits correspond to extreme assumptions about the diffusion coefficient. Later work (Bloemen *et al.* 1986) – see Section 4.6.6 – has confirmed the gradient.

Correlations at high latitudes The rather uncertain molecular hydrogen component is confined mainly to the inner Galaxy (Figure 4.23) and, although it is not negligible locally, the uncertainties are not too great. This means that correlation studies of I_γ with gas column densities can be carried out with some confidence. The correlation of I_γ with HI alone has some value, and such early analyses of SAS II data were carried out by Fichtel and colleagues (e.g. Fichtel *et al.* 1978*a,b*). Figure 4.29 shows the results. It is from these plots, and the corresponding ones for the lower energy bracket, that the extragalactic component of the γ-ray flux has been determined. The correlation is seen to be good.

As remarked already, molecular gas is not completely negligible, and a proper allowance for its presence is necessary, particularly in view of the fact that there is some correlation between $N(\mathrm{HI})$ and $N(\mathrm{H_2})$, and this is longitude dependent, i.e. neglect of $N(\mathrm{H_2})$ can lead to incorrect estimates of local cosmic ray intensities.

Correlations at intermediate latitudes. In earlier work, before extensive CO data were available, the galaxy count technique was used to estimate the total column density of gas ($N(\mathrm{H_t})$) as a function of l and b, i.e. $N(\mathrm{H_t}) = N(\mathrm{HI}) + 2N(\mathrm{H_2})$. The principle of the method is to make the reasonable assumption that the 'density of galaxies' brighter than some limiting magnitude (in number of galaxies per square degree) is constant outside the confines of our own Galaxy. The number per square degree seen at the Earth will, however, be dependent on the column density of dust along the line of sight to the edge of the Galaxy. In turn, if the dust-to-gas ratio is constant, the total column density of gas can be derived. Lebrun and Paul (1983) have used this technique with the SAS II results (as have Issa, Strong and

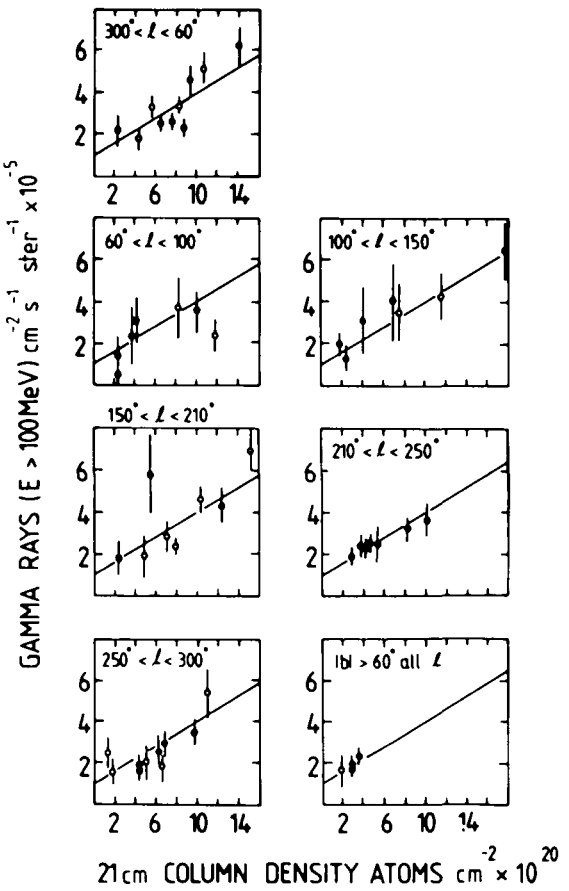

Figure 4.29. SAS II γ-ray intensity versus column density for HI for latitudes $|b|$ greater than 12.8° for the indicated longitude intervals (Fichtel *et al.* 1978*a*,*b*). Solid lines: best fit to all the data points. The intercepts give the extragalactic intensity.

Wolfendale 1981*a*) and Strong *et al.* (1982) have done the same thing with the COS B observations.

Referring to the range $|b| = 10$–$20°$, we can examine the work of Issa *et al.* Here, the relation between galaxy counts, N_g (=number of galaxies per square degree in the Lick galaxy catalogue) and the column density of gas as a whole in atoms cm^{-2}, $N(H_t)$ was taken from Strong and Lebrun (1982):

$$N(H_t) = 2 \times 10^{21} \log\left(\frac{N_g^0}{N_g}\right) \text{atom cm}^{-2} \tag{4.5}$$

where $N_g^0 = 50$ is the estimated galaxy count extrapolated to the situation of no Galactic absorption.

The result for the smoothed radial distribution is given in Figure 4.30, the apparent gradient for $R > 10$ kpc is in accord with the results shown in

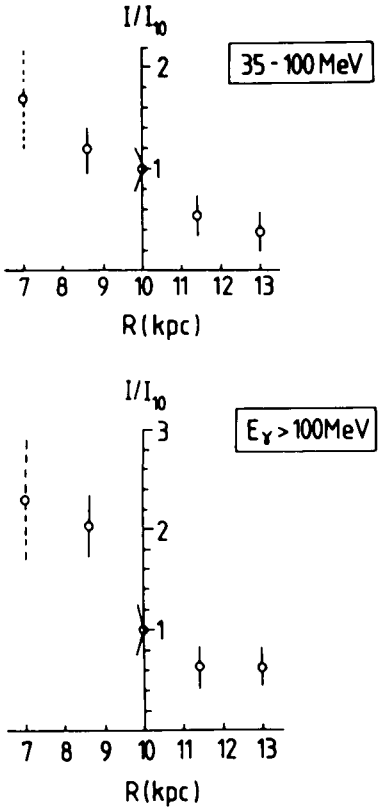

Figure 4.30. Local cosmic ray gradient from the analysis of SAS II data by Issa *et al.* (1981*a*,*b*). Electrons predominate for the lower energy band. In the higher band protons probably contribute 50–70% of the initiating particles. I_{10} is the local cosmic ray intensity. (In this work, as in all early work, the Sun was assumed to be at a Galactocentric distance of 10 kpc.)

Figure 4.25. The rather steep rise in the inner Galaxy is considered later, in Section 4.6.6.

More extensive analysis of the COS B data, undertaken by Strong *et al.*, gives the important results shown in Figure 4.31. There are many interesting features in these plots. There is good general agreement with observation and expectation on the basis of a constant cosmic ray intensity over the region in question, but the gradient claimed in Figure 4.30 shows through as an excess of observation over expectation in the inner Galaxy and a deficit in the outer. The nearby molecular clouds in Orion and Taurus (l: 160°/220°, b: $-19°/-11°$) are clearly visible. There is an interesting reduction in the predicted γ-ray intensity in the direction of the Perseus cluster of galaxies (this cluster is at $l \sim 150°$, $b \sim -14°$); this is quite definitely due to the fact that the value of N_g in this direction is excessive (because of the cluster) and the result is an underestimate of $N(H_t)$. Inevitably this sensitivity to galaxy clustering is a shortcoming of the galaxy-count method.

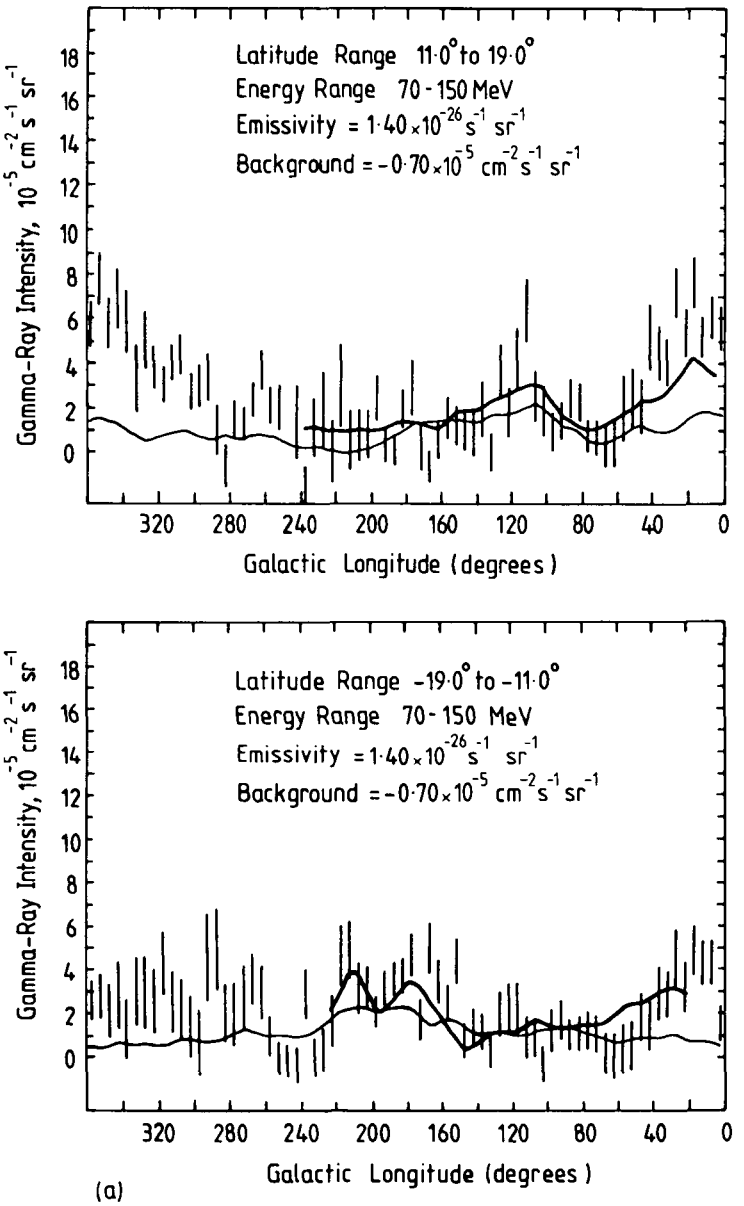

Figure 4.31. Comparison of measured and predicted γ-ray intensities for COS B (Strong *et al.* 1982). The lower line corresponds to the contribution from interactions with atomic hydrogen alone. The upper line relates to all gas, the column densities being derived from the galaxy-count method.

Continuing in a critical vein, the method is also sensitive to the undoubted variations from place to place of the dust-to-gas ratio (it is the dust which absorbs the light and thus reduces the number of galaxies seen along a particular line of sight). Strong *et al.* (1982) use the differences in observed and expected γ-ray flux

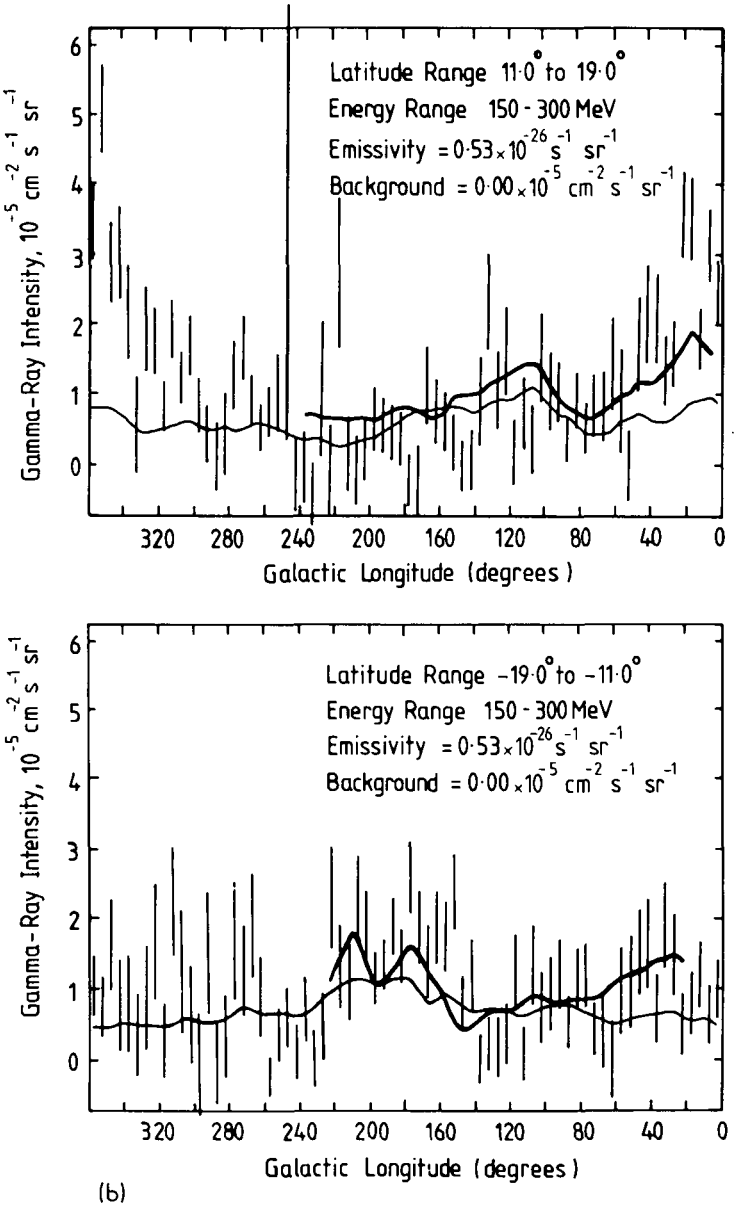

Figure 4.31. (*Continued.*)

for those regions where galaxy counts are not available, $220° < l < 10°$, to estimate the column densities of molecular gas, but this seems to be a rather risky procedure.

Correlation with gas in the inner Galaxy. This is the region where the biggest uncertainty arises because of the problems already mentioned concerning the difficulty of converting such information as is available (from CO) into the column

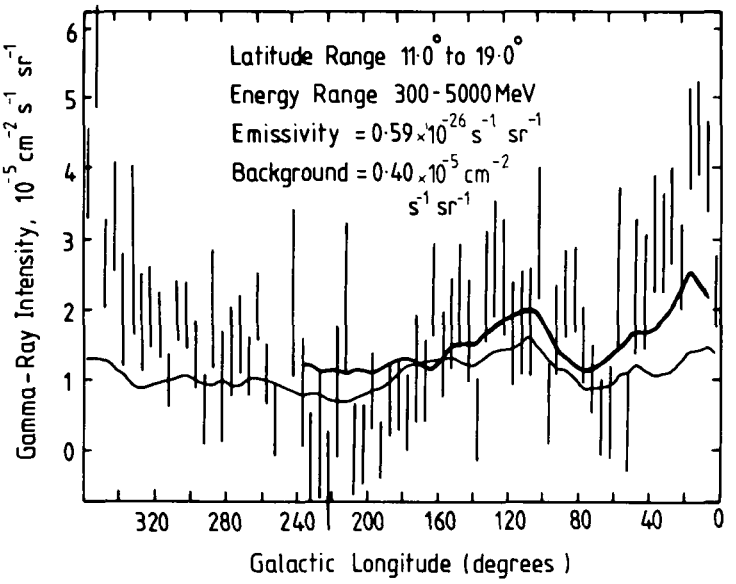

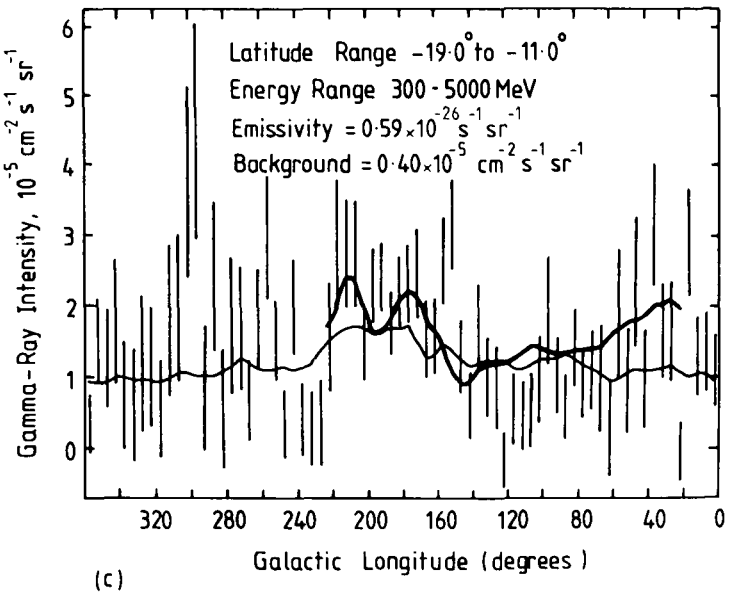

(c)

Figure 4.31. (*Continued.*)

densities of molecular hydrogen. However, several studies have been made. The results of a detailed analysis by the COS B group (Bloemen *et al.* 1986) are given in Figure 4.32. In this figure, radial symmetry is assumed (i.e. the intensity is a function of radius only) and the cosmic ray intensity is inferred as a function of Galactocentric distance. It will be seen that there is a 'cosmic ray gradient' for all the energy bands. Bloemen *et al.* divided up the γ-rays between proton- and

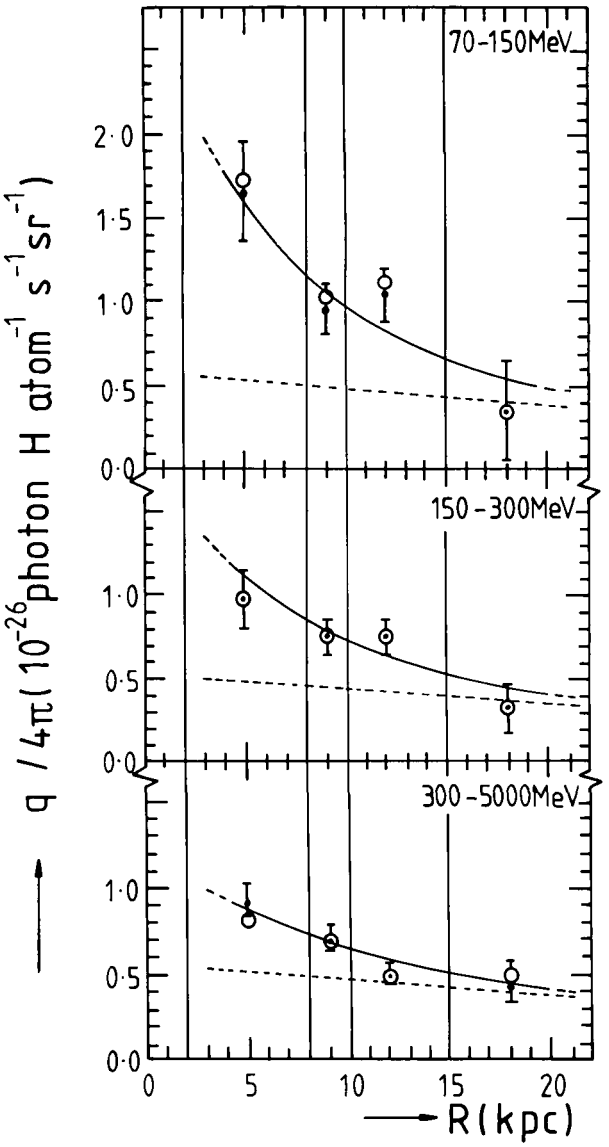

Figure 4.32. Radial distribution of cosmic ray emissivity in the Galaxy as a whole from the COS B group (Bloemen *et al.* 1986). The dashed line relates to the nuclear (mainly proton) component. The different symbols refer to differing estimates of the values.

electron-parents, and it will be noted that the proton gradient itself is very small. However, Bhat *et al.* (1986) have used essentially the same γ-ray data but a different CO $\rightarrow$ H_2 conversion to demonstrate greater gradients, as shown in Figure 4.33. Later work on the CO $\rightarrow$ H_2 conversion factor tend to confirm that Figure 4.33 is probably nearer the truth.

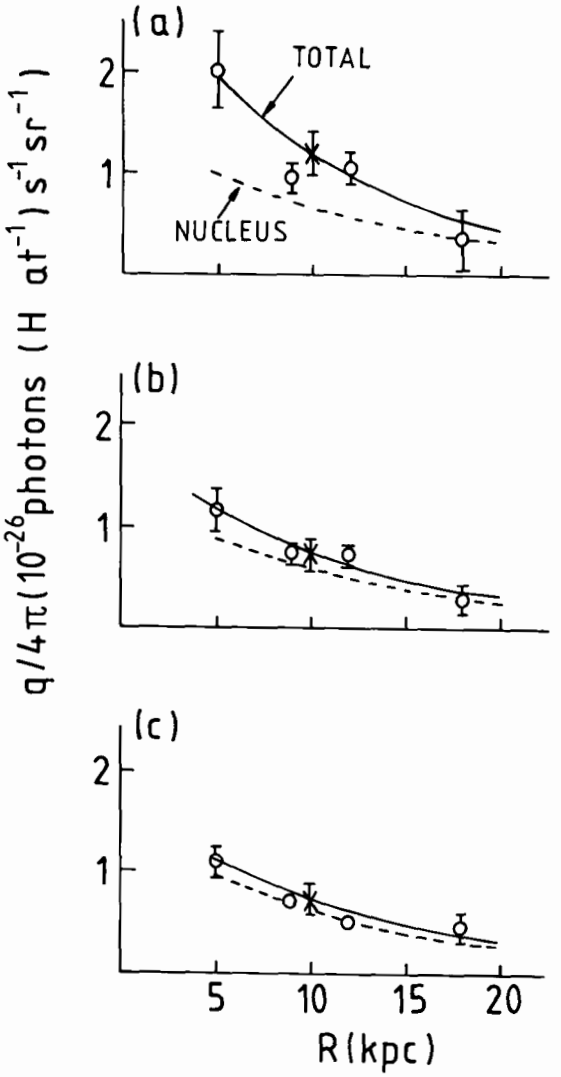

Figure 4.33. Radial distribution of cosmic ray emissivity in the Galaxy as a whole from the Durham group (Bhat *et al.* 1986). The data used are the COS B γ-ray intensities and the group's own estimate of the distribution of molecular hydrogen in the Galaxy.

4.6.4 Gamma-rays from specific molecular clouds

Eventually, when γ-ray data of great precision become available, the study of γ-ray intensity profiles from known molecular clouds will be of great value in examining in detail the interiors of those clouds which are 'inert' (i.e. without embedded sources), as well as in studying cosmic ray production in the clouds which have sources within them. Although such information is not yet available, at least a start has been made.

This topic has already been touched on in Section 4.5.3 in connection with the

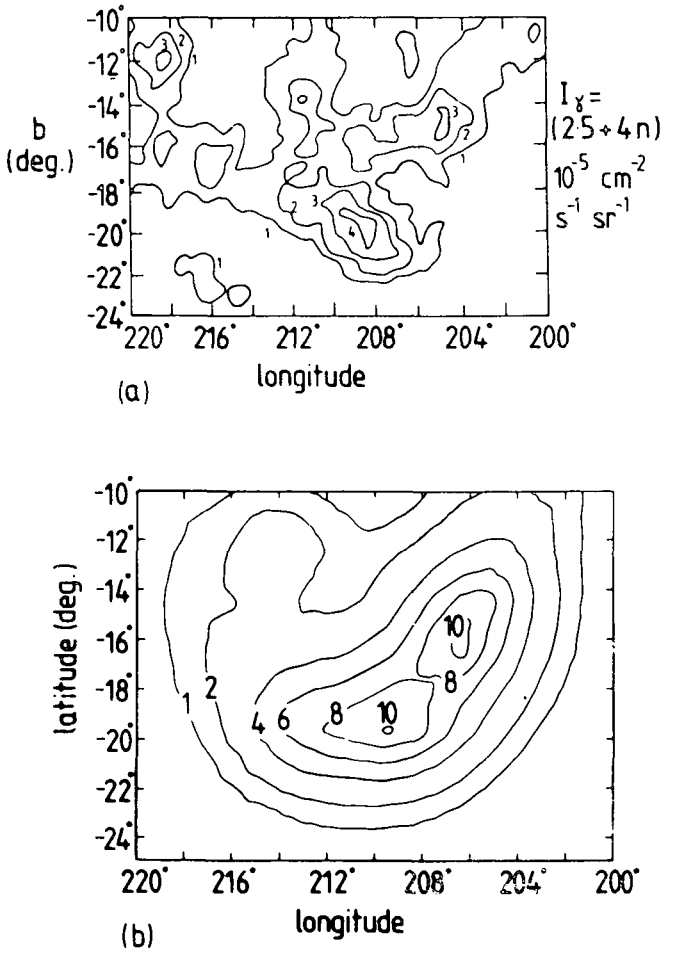

Figure 4.34. The Orion molecular cloud region. (*a*) γ-rays above 100 MeV from the COS B collaboration (private communication, 1984). (*b*) CO contours smoothed to the resolution of the COS B data; the basic CO data are from Kutner *et al.* (1977) and have been smoothed by Houston and Wolfendale (1985). *n* is the contour number.

possibility of distant cosmic-ray-irradiated clouds simulating the so-called γ-ray sources. Here, we deal with the subject in more detail, and we start with the nearby clouds in the Orion region, clouds which are so close that their structure is revealed even with the poor angular resolution of the contemporary γ-ray detectors.

The SAS II data for the Orion region were analysed by Wolfendale (1980), and it was shown that the γ-ray flux could be understood in terms of cosmic ray irradiation of these clouds. The later COS B data, with its improved statistical precision (Caraveo *et al.* 1980, 1984, Caraveo 1981), has allowed the correlation of γ-ray intensity with gas density to be examined in greater detail.

Figure 4.34 shows the contours of γ-ray intensity, from COS B for the Orion

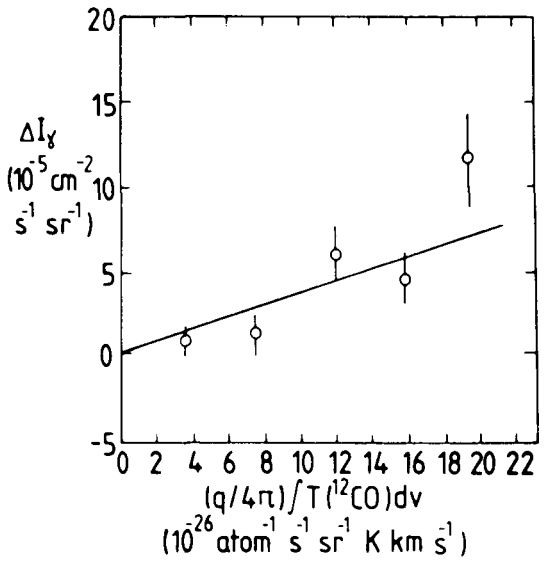

Figure 4.35. Correlation of ΔI_γ ($= I_\gamma$ observed) $- (q/4\pi)N(\mathrm{HI}) - I_\gamma$ (background), with $(q/4\pi) \times (\int T(^{12}\mathrm{CO})\,\mathrm{d}V)$ for the Orion molecular clouds (see Figure 4.34). $(q/4\pi)$ is the emissivity per hydrogen atom and $N(\mathrm{HI})$ is the column density of atomic hydrogen. The reasonable correlation indicates that cosmic ray particles are not excluded from regions of the clouds where a significant fraction of the mass resides. (From Houston and Wolfendale 1985.)

region, together with the corresponding smoothed ^{12}CO velocity-integrated antenna temperature ($\int T(^{12}\mathrm{CO})\,\mathrm{d}V$), i.e. the quantity proportional to the column density of molecular hydrogen. Figure 4.35 shows the correlation of the component of γ-ray intensity attributable to cosmic ray interactions with H_2 gas (i.e. total minus background and minus the product of HI interactions) as a function of $\int T(^{12}\mathrm{CO})\,\mathrm{d}V$. The near linearity is an important feature in that it shows that the initiating cosmic rays penetrate the bulk of the gas in the clouds and indicates that γ-rays can be used as a probe of gas in various regions of the Galaxy.

Bloemen *et al.* (1984*b*) and Houston and Wolfendale (1985) have examined the correlation for Orion and used it to derive the relationship between the H_2 column density and $\int T(^{12}\mathrm{CO})\,\mathrm{d}V$, making the reasonable assumption that the cosmic ray intensity is the same in the Orion clouds (about 500 pc away) as that locally. Clearly, if the cosmic ray intensity is uniform across the clouds (as the Houston and Wolfendale analysis suggests) this is a meaningful approach. Due to different assumptions, mainly about the γ-ray emissivity, the two groups derive somewhat different results for the conversion factor, X. Writing $X = 2N(\mathrm{H_2})/\int T(^{12}\mathrm{CO})\,\mathrm{d}V$ in units of 10^{20} mol cm^{-2} K^{-1} km^{-1} s, the values are: $X = 1.9 \pm 0.4$, Houston and Wolfendale (1985); $X = 2.6 \pm 1.2$ Bloemen *et al.* (1984*b*).

Other clouds have also been examined by the γ-ray technique. As mentioned earlier (Section 4.5.6), the cloud complex in Rho Ophiucus has been extensively studied. Knowledge about molecular clouds from the other branches of astronomy

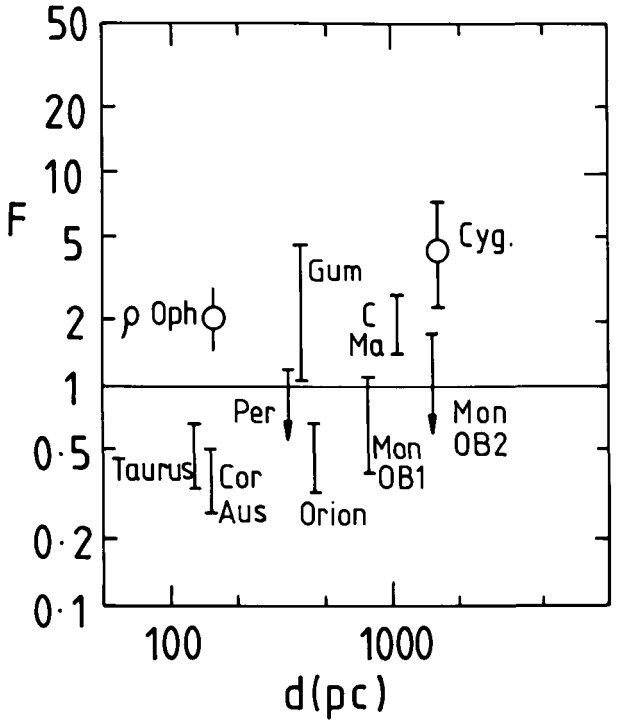

Figure 4.36. Enhancement of cosmic rays in comparison with the local value (F values) for a number of molecular clouds. The plot is an update of work by Issa and Wolfendale (1981*a*,*b*). ○: clouds which have been (tentatively) identified with γ-ray sources in the COS B 2CG catalogue of Hermsen (1981). (Despite the update, there are still problems with the cloud masses, and some of the F values are probably still uncertain by a factor ~ 2.) d is the distance from the Sun.

is still rudimentary (although probably better than the γ-ray information, at least in terms of statistical precision), but an analysis was attempted by Issa and Wolfendale (1981*b*) for a number of clouds. A variety of ^{12}CO data were used (much of it from Blitz 1980) together with the SAS II catalogue of Fichtel *et al.* (1978*a*) and initial COS B results. An attempt has also been made now (Figure 4.36) to update the analysis by adopting the more recent COS B observations.

A prominent feature of the results is the presence of a number of clouds for which the observed γ-ray fluxes appear to need a considerable enhancement of cosmic ray intensity in these clouds. This feature has been noted by a number of workers (particularly for Eta Carinae, e.g. Montmerle 1979, 1982), although it is necessary to sound a note of caution that the identification of the γ-ray peaks with distant giant molecular clouds is fraught with difficulty. These 'coincidences' are approximate spatially, and, unlike in the case of Orion, the distant clouds appear 'point-like' within the poor angular resolution of the present instruments. Furthermore, it is not inconceivable that there are discrete sources of γ-rays

(pulsars?) embedded within the clouds, as distinct from sources of cosmic ray particles.

The importance of the high cosmic ray enhancement factors (F values), seen in Figure 4.36, to the question of the origin of cosmic rays is taken up in Section 4.6.6.

4.6.5 Relevance of cosmic gamma-rays to the mass of gas in the Galaxy

The interrelation of cosmic rays, gas and γ-rays has been stressed already, and recent work has enabled interesting conclusions to be drawn about the mass of gas in the Galaxy.

It might be thought that the embryonic subject of γ-ray astronomy, with its statistically small sample of γ-rays ($\approx 10^5$ only), of poor energy and angular resolution, would not be able to compete with the older subject of radio astronomy and the data of high precision obtainable there. There is a problem, however, with radio estimates of the mass of gas in molecular clouds, and this is associated with the difficulty already referred to in relating the observations of CO to densities of H_2. Interstellar chemistry is not only a difficult subject, with vast numbers of possible reactions to contend with, but the physical conditions inside the clouds (temperature, degree of ionisation, etc.) are poorly known. In consequence, in the authors' view, the γ-ray results on the gas content of the Galaxy is probably as good as, and possibly better than, that available from radio.

Bhat *et al.* (1984*b*) examined the problem in detail, and their method will be described here. It is true that there has been continuing work on this topic, and indeed there is still no concensus; however, the general arguments of Bhat *et al.* are being increasingly accepted. The argument is in two parts. Examination of the local giant molecular clouds, particularly those in Orion, yields a value of X which is a factor of about two smaller than that used by some radio astronomy groups – e.g. Sanders, Solomon and Scoville (1984), who will be referred to as 'SSS'. Arguments are then put forward for a continuation towards the inner Galaxy, of the low energy cosmic ray gradient determined in the outer Galaxy (see Figure 4.33 and Section 4.6.3), and this requires an even lower value of X in the inner Galaxy. Arguments based on interstellar chemistry, such as it is understood, suggest that $X(R) \propto (M(R))^{-1}$, where M is the 'metallicity', namely the ratio of density of atoms such as oxygen to that of hydrogen. It is well known (e.g. Pagel and Edmunds 1981) that there is a metallicity gradient in the Galaxy with $M(6\,\text{kpc})$ about twice that locally. The same argument, but with less detail, was advanced earlier by Blitz and Shu (1980).

Figure 4.37 shows the situation at $R = 6$ kpc. It is found that adopting $X(R) \propto (M(R))^{-1}$ yields a γ-ray emissivity there roughly as observed. A measure of confirmation comes from an analysis of γ-rays from the Galactic Centre, a topic of interest to the present work in its own right. The metallicity here is $M(R = 0) \approx 3$–5 times the local value, and the ensuing inferred gas mass appears to give a much more reasonable result for the cosmic ray intensity in this region. Figure 4.38 summarises the situation.

The result of applying the 'correction' to X can be seen in Figure 4.39, where the 'Durham' estimate of the surface density of H_2, found using the technique of

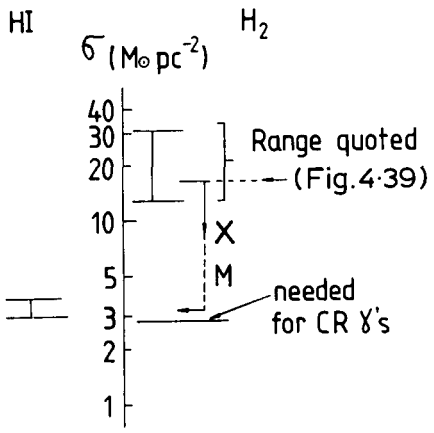

Figure 4.37. Surface densities of HI and H_2 at 6 kpc from the Galactic Centre (after Bhat *et al.* 1984*b*). A range of surface densities for H_2 have been quoted; the effect of the new X value and metallicity correction ($M'(6) = 2$) on $\sigma_{H_2}(6)$ from Figure 4.39 is indicated. A consistent picture is seen to result. (M' is the metallicity divided by the local value.)

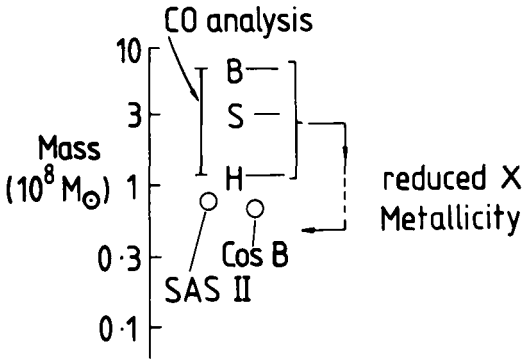

Figure 4.38. Mass of gas within 400 pc of the Galactic Centre, after Bhat *et al.* (1984*b*, 1985*a*). B, S and H are estimates by Bania (1977), Scoville *et al.* (1974) and Heiligman (1982), respectively, using different X values. ○: what would be expected from the γ-ray observations if the cosmic ray intensity were the same at the Galactic Centre as locally. The B, S, H masses would require unreasonably low cosmic ray intensities at the Galactic Centre. Adoption of the reduced X value and $M'(0) = 3$ results in a mass ($\sim 5 \times 10^7 M_\odot$), which would correspond to a cosmic ray intensity at the Galactic Centre a factor ~ 2 times that locally – a much more reasonable result. Notwithstanding our preference, there is still considerable argument about the mass of molecular gas in this region.

Bhat *et al.* and its later refinement, is shown, along with other estimates. Details are given in the caption. Although the SSS estimate of the surface density of H_2 is clearly too high, it is apparent that there is still some doubt about the correct form to take. It is interesting to note that previous estimates of $\sigma_{H_2}(R)$ in the outer Galaxy were too *low*, because the metallicity is lower there, as is the temperature.

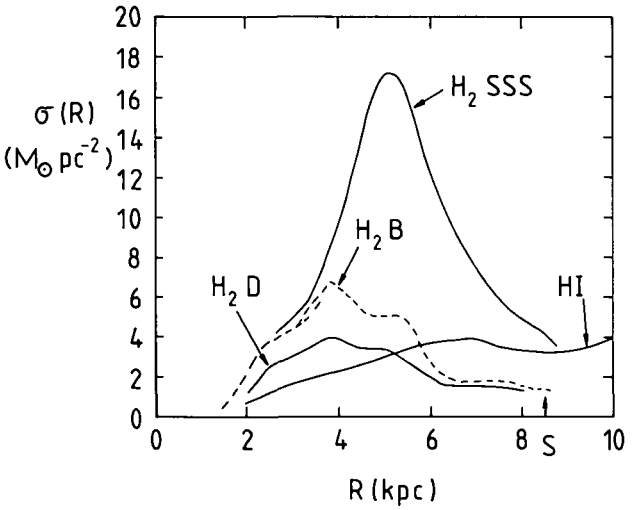

Figure 4.39. Dependence of the surface density of atomic and molecular hydrogen on Galactocentric distance for Sun to Galactic Centre distance of 8.5 kpc. HI: mean of estimates of atomic hydrogen by Gordon and Burton (1976) and Li, Riley and Wolfendale (1983). H_2SSS: estimate by Sanders *et al.* (1984) for the Northern hemisphere. H_2B: average for N and S hemispheres (from Figure 4.24) from L. Bronfman (1991, private communication) with X reduced from the value of 2.3 adopted there to the latest Columbia value (Dame 1991, private communication) of 2.0. H_2D: the 'Durham' distribution, which has $X = 1.3$ in the inner Galaxy and 1.8 locally (the X values relating to application to the Columbia CO measurements). The best estimate of $\sigma(R)$ for H_2 is probably between H_2B and H_2D.

With more precise GRO data expected soon, further studies of the molecular hydrogen in the outer Galaxy will be needed.

The implications of the lower estimates of the mass of molecular gas in the Galaxy – for subjects as diverse as star formation processes and the stability of the Oort cloud of comets – are the subject of contemporary work.

4.6.6 Relevance of cosmic gamma-rays to the origin of the cosmic radiation

Unlike cosmic ray particles, cosmic γ-rays travel in straight lines and, insofar as much of the γ-ray flux is caused by cosmic ray particles interacting with gas in the ISM, one would hope for strong clues to be given with regard to the question of cosmic ray origin, at least for particles below about 10 GeV.

These studies are relevant in two main ways: (i) the information provided by large scale intensity gradients, and (ii) the cosmic ray enhancement factors (F values) for particular objects and localised regions.

The large scale intensity gradients were discussed in Section 4.6.3, and it was pointed out that there is agreement about a strong gradient for cosmic ray electrons. As for the important proton component, it appears that there is now agreement that there is a gradient, although there is argument about its magnitude.

By reference to Figures 4.32 and 4.33 it can be seen that, in going from the solar position to a point halfway to the Galactic Centre, Bloemen *et al.* give an increase in proton flux by a factor 1.1, whereas Bhat *et al.* give an appreciably bigger factor of 1.4.

It is not surprising that the proton gradient is small because the undoubted rapid diffusion of the particles throughout the Galaxy away from their points of origin has a profound smoothing effect. In the absence of knowledge of the magnitude of the diffusion coefficient $D(R, z, E)$ and its dependence on radial distance, R, scale height, z, and energy E, and the nature of the Galactic 'container', however, accurate calculations cannot be made of the relationship between the distribution of sources and the ensuing distribution of the cosmic ray intensity. However, Bhat *et al.* (1986) have made an order of magnitude estimate by assuming simple diffusion in the z-direction to a boundary whose height is proportional to the scale height of HI in the outer Galaxy. Limiting forms are taken for $D(R)$, and the result is shown by the hatched area in Figure 4.28.

Comparison with Figures 4.32 and 4.33 shows no inconsistency, but because of the disparity in gradients 'found' by the two groups it is not yet possible to pick out the 'best' diffusion coefficients nor the 'best' source distribution.

Mention should also be made of the analysis by Kniffen, Fichtel and Hartman (1983). These authors made the assumption that the cosmic ray intensity, I_{CR}, is proportional to the density of total gas, and they chose a value X (CO $\rightarrow$ H_2 conversion) to give consistency for the total intensity. Understandably, a gradient of cosmic ray intensity resulted, since the initial assumption of $I_{CR} \propto \rho_{gas}$ implies a Galactic origin, but the assumption of X being R-independent is *ad hoc.* In a similar way, the earlier analysis of Issa *et al.* (1981*a*) in which, for comparatively local regions, correlation of I_γ with N(HI) was studied (the neglect of H_2 is not catastrophic because the correlation of H_2 with HI is not strong) gave results which are useful but not compelling.

So far we have dealt with the large cosmic ray gradient. Gradients on smaller scales should also exist because of the patchiness of all the properties of the ISM. Bhat *et al.* (1984*a*) have claimed a considerable local gradient which may be due to an enhanced cosmic ray intensity in the Loop I local SNRs. This idea has been followed up in some detail, as will now be described.

It is likely that the North Galactic Spur (a Loop I radio feature) should be identified with the remnant of a supernova which is centred on a point some 130 pc away from the Sun and has at present a radius of 115 pc (Berkhuijsen, Haslam and Salter 1971). Although it was originally thought that the initial energy of the SNR needed to be much greater than the value of 10^{51} erg typical of conventional supernovae, more recent supernova models (e.g. by Blandford and Cowie 1982) can explain many features with only a typical initial explosion. Blandford and Cowie predict a γ-ray intensity from the SNR surface of order $7 \times 10^{-6}\,\mathrm{cm^{-2}\,s^{-1}\,sr^{-1}}$, and, remarkably, this is close to the estimate made for the Loop I remnant by Bhat *et al.* (1985*b*) from their analysis of the SAS II and COS B data. Figure 4.40 summarises the situation using the SAS II results.

The COS B data have been examined in a similar fashion, with the result shown

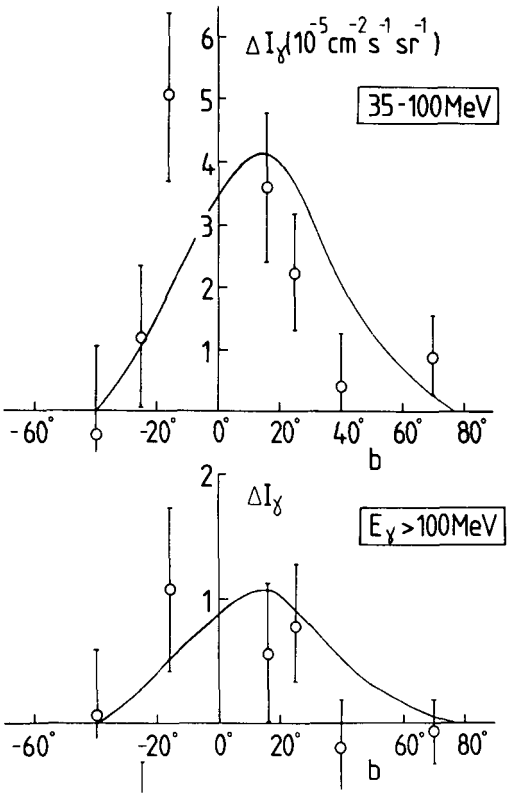

Figure 4.40. Excess γ-ray intensity associated with the Loop I SNR, from Bhat *et al.* (1985*b*). SAS II data on γ-ray intensities were used. Cuts are taken across the remnant and ΔI_γ is the difference between the excess of observation over expectation for a cosmic ray intensity within the remnant to that outside the remnant (this technique minimises the effect of systematic errors on the expected values). Full line: approximate expectation for the case where the cosmic ray intensity is uniform within the remnant (in fact it clearly is not, but the effect on the shape is small). Electrons predominate as parents in the 35–100 MeV region and protons for $E > 100$ MeV.

in Figure 4.41 (from van der Walt and Wolfendale 1988). Attention there is restricted to γ-ray energies above 300 MeV, where there is reasonable confidence that the primaries are mainly protons. Unfortunately, although the statistical precision of the intensities is higher than for SAS II, the orbit problems referred to already mean that data can only be used in the latitude range b: 10–20°. Nevertheless, the results support the earlier contention that there *is* an excess of proton flux within the Loop.

Rogers and Wolfendale (1987) have gone further and have claimed evidence for excesses of cosmic ray flux in Loop III and the Vela region. If these results are accepted, we can produce a graph of cosmic ray energy (in protons) versus SNR 'radius', as shown in Figure 4.42.

The theoretical line shown in Figure 4.42 comes from the work of Blandford

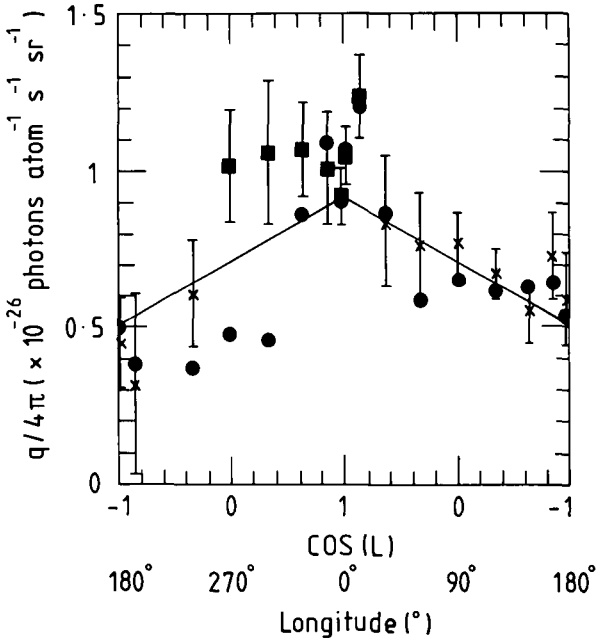

Figure 4.41. γ-ray emissivity for $E_\gamma > 300$ MeV as a function of longitude for $10° < b < 20°$. The total gas column densities used to derive the emissivities include HI, H_2, and an estimate of the column density of HII using the model of Lyne, Manchester and Taylor (1985). ×: positions outside the boundaries of Loop I. ■: positions inside Loop I. ●: corresponding 408 MHz brightness temperatures normalized to the γ-ray emissivity at $L = 170°$. Solid line: least-squares fit of the emissivity as a function of cos L of the points outside the Loop and represents the local cosmic ray gradient. It is seen that the emissivities within the boundaries of Loop I do not follow the local gradient and are consistently higher than expected from the gradient. Since protons predominate as initiating particles for $E_\gamma > 300$ MeV, this result supports the contention that there is an excess of all γ-ray energies.

and Cowie (1982), in which the SNR shocks accelerate cosmic rays as they pass through the ISM. Although there can be no question of either the observations or the theory being accurate, it is interesting to note that SNRs could well have an 'efficiency' for accelerating cosmic ray protons of about 10%, in which case the majority of cosmic rays in the Galaxy of energy below about 10 GeV could be due to SNRs.

4.6.7 *Variations of the gamma-ray spectral index across the Galaxy*

The subject has reached the stage where searched for spectral index variations have some validity and some interesting results have been forthcoming. Large scale variations, associated with a dependence of the e/p ratio on Galactocentric distance, were reported by Issa *et al.* (1981*a*,*b*), Mayer-Hasselwander (1983) and Bloemen *et al.* (1984*b*, 1986).

Bloemen (1987) also drew attention to the interesting result shown in Figure 4.43.

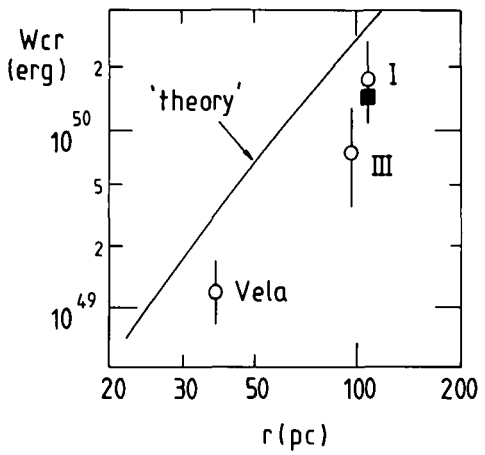

Figure 4.42. Total cosmic ray energy as estimated from γ-ray observations for Loop I, Loop III, and the Vela SNR. ○: estimates from Bhat *et al.* (1985*a*) for Loop I and from Rogers and Wolfendale (1987) for Loop III and the Vela SNR. ■: our new estimate for Loop I following a procedure somewhat different from that of Bhat *et al.* Solid line: prediction by Blandford and Cowie (1982).

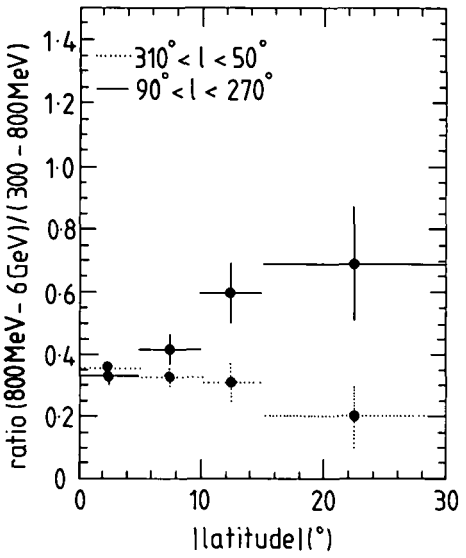

Figure 4.43. Latitude dependence of the ratio of the γ-ray intensity between 800 MeV and 6 GeV and the intensity between 300 and 800 MeV as found by Bloemen (1987). At the highest latitudes the spectrum towards the outer Galaxy is significantly flatter than that towards the inner Galaxy. The observed flattening with latitude for the outer Galaxy is explained by Bloemen *et al.* as being due to a Galactic wind. Towards the inner Galaxy the spectrum shows a slight steepening with latitude which cannot be easily explained by the Galactic wind model.

This indicates that there is a Galactic latitude dependence of the spectral shape. Bloemen (1987) invokes a Galactic wind as being responsible, but Rogers *et al.* (1988) propose that there is a difference in spectral shape of the γ-rays (and the initiating particles) between the Galactic arm regions and the interarm regions. The latter suggestion is in the spirit of cosmic ray acceleration by SNR shocks, which occur preferentially in spiral arms, but it is premature to decide between the contrasting views.

4.7 Extragalactic gamma-rays

4.7.1 General remarks

The poor statistical precision of γ-ray results from SAS II and the background problems with COS B mean that, although the subject of extragalactic γ-rays is of considerable interest, the uncertainties are very great.

As with the Galactic γ-rays, two components can be discerned: 'discrete' sources, and a general diffuse background; the subject will be dealt with in that order.

By analogy with the results at other wavelengths, the potential extragalactic sources comprise individual galaxies of various types, from 'normal' galaxies to quasars. Galaxy clusters should also be included and, as will be demonstrated, examples have been found in each class.

Again, by analogy, the diffuse background might be expected to be the subject of great debate as concerns the fraction of the flux to be identified with unresolved discrete sources as distinct from a *bona fide* diffuse component; it is.

The GRO has already reported seeing more than a dozen extragalactic sources.

4.7.2 Discrete sources of extragalactic gamma-rays

At the energies in question, the number of identified extragalactic objects is small at present.

Most important is the observation of the 'nearby' quasar 3C273. Figure 4.44 summarises the measurements above 1 keV. Inspection of the 2CG catalogue (Table 4.1) shows that this object appears therein and this is the only source of extragalactic origin definitely detected in the COS B analysis. Upper limits for many other potential sources have been given by Pollock *et al.* (1981); the conclusion that is drawn about the form of the spectrum of extragalactic sources (active galaxies) is that it must steepen significantly between the X-ray and high energy γ-ray regions (Bignami *et al.* 1979).

Returning to 3C273, inspection of the smooth curve, which gives a reasonable fit to the experimental intensities in Figure 4.44, shows that the peak luminosity (in terms of energy content per decade of photon energy) is in the MeV region. This is a remarkable result and is an indication of the initial energy production process being efficient at rather high energies. The attendant increase in spectral slope above about 2 MeV is interesting, and its possible significance will be discussed later.

Taking the COS B energy range alone, i.e. the last three points on the energy spectrum in Figure 4.44, a slightly different spectral shape has been given:

$$N(E_\gamma) = (3.7 \pm 1.4) \times 10^{-6}(E_\gamma/150)^{-2.5}\ \mathrm{cm}^{-2}\ \mathrm{s}^{-1}\ \mathrm{GeV}^{-1} \qquad (4.6)$$

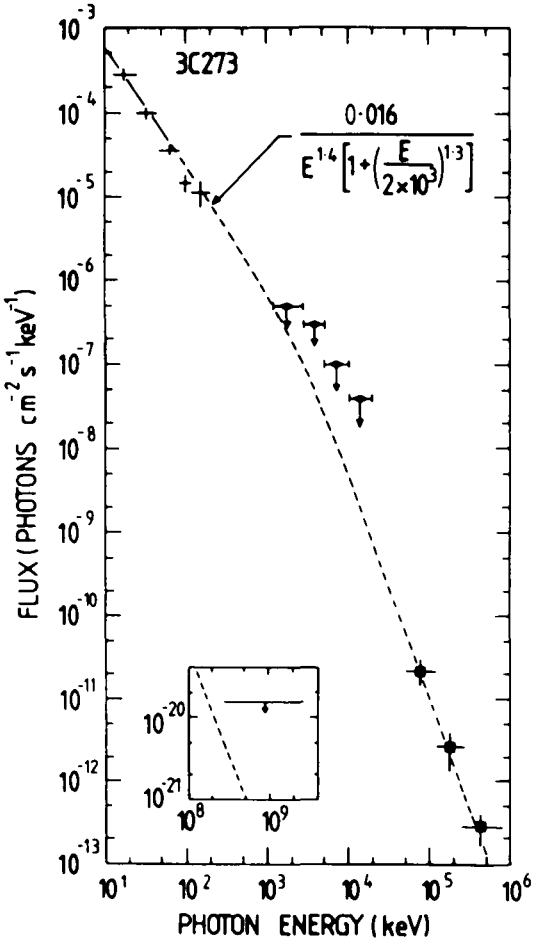

Figure 4.44. Summary of hard X-ray and γ-ray measurements for the quasar 3C273 (after Trombka and Fichtel 1982). The data points are from various sources.

where E_γ is the energy in MeV (Bignami *et al.* 1981); but the difference from the form given in Figure 4.44 is not significant.

At X-ray energies there is the well known variability of output, but none has been detected so far in the γ-ray energy region, possibly because the γ-ray data are so sparse.

The nearest quasar is QSO0241+622, and this is tantalisingly close to the COS B source 2CG135+01. However, there is also a Galactic source nearby (GT0236+61), and identification is not clear cut (Dean and Ramsden 1981).

Preliminary results from the GRO can also be mentioned here. The EGRET detector (see Section 4.8.3) has detected the quasar 3C279 – an unexpected result since this quasar was not seen by SAS II or COS B and would have been had its flux at the earlier times been the same as measured now. The flux is of order

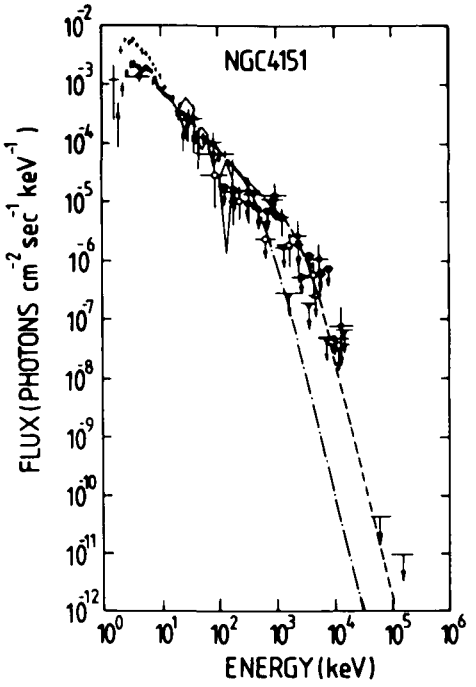

Figure 4.45. Summary of hard X-ray and γ-ray measurements for the Seyfert galaxy NGC 4151 (after Trombka and Fichtel 1982).

$10^{-6}\,\mathrm{cm}^{-2}\,\mathrm{s}^{-1}$ above 100 MeV, which is variable by a factor of 6; reports are arriving of detections from other quasars, too.

Coming down a little in energy scale, we reach the Seyfert galaxies. These galaxies are prominent emitters at X-ray and longer wavelengths, and might be expected to show up in γ-rays too. Emission has been found from the prominent Seyfert NGC 4151 up to about 10 MeV (see Dean and Ramsden 1981 for a useful summary), and the results are shown in Figure 4.45. No finite flux was claimed by the SAS II or COS B workers, but Houston and Wolfendale (1982) think that there might be a weak signal in the SAS II results ($E > 35$ MeV). Whether this is true or not, the spectrum from this object, too, shows a steepening above 1 MeV or so. A similar situation exists for the Seyfert galaxy MCG 8−11−11 in that the galaxy has been detected up to a few MeV (Baker *et al.* 1981).

GRO measurements of NGC 4151 below 1 MeV show that for the first observing period at least (mid-1991) this galaxy is currently in a low state.

Radio galaxies would also be expected to be γ-ray emitters in that the electrons which generate the observed synchrotron radiation can also interact with gas to provide bremsstrahlung γ-rays. The prominent radio galaxies Cygnus A and Centaurus A are strong candidates, and γ-rays have indeed been detected from the latter, but only up to about 10 MeV (Figure 4.46) (although there is some evidence for its detection above 10^{11} eV; this is considered later). Including an

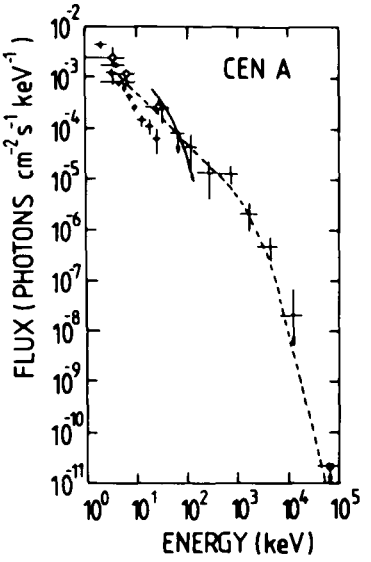

Figure 4.46. Summary of hard X-ray and γ-ray measurements for the radio galaxy Centaurus A (NGC 5128), after the summary by Fichtel (1982). The steepening in the spectrum above a few MeV is very marked in the case of all the extragalactic 'sources' of Figures 4.40, 4.44 and 4.45.

upper limit in the SAS II/COS B energy region, there is again a spectral steepening above 1 MeV.

The final group of extragalactic objects comprises 'normal' galaxies. Following Houston and Wolfendale (1982), the simplest model which can be used to make predictions is where γ-ray emission is proportional to galactic mass (for galaxies not grossly dissimilar in type to our own). In such a case, adopting a rate of emission of γ-rays from our Galaxy of $1.3 \times 10^{42}\,\mathrm{s}^{-1}$ above 100 MeV (Worrall 1977), we have

$$F_\gamma = \frac{0.14}{4\pi}\frac{M}{M_G}\frac{1}{d_k^2}\,\mathrm{cm}^{-2}\,\mathrm{s}^{-1} \tag{4.7}$$

where M/M_G is the mass of the galaxy in terms of the mass of our Galaxy, and d_k is the distance in kpc.

Inspection of astronomical data shows that there are only three 'normal' galaxies which have a chance of being detected: the Large Magellanic Cloud (LMC), the Small Magellanic Cloud (SMC) and Andromeda (M31); for these the expected fluxes are 3.7, 0.5 and $0.7 \times 10^{-7}\,\mathrm{cm}^{-2}\,\mathrm{s}^{-1}$, respectively. None has been detected with certainty at the satellite energies, but P.A. Riley (1982, private communication) has presented evidence for a flux of order $7 \times 10^{-7}\,\mathrm{cm}^{-2}\,\mathrm{s}^{-1}$ for the LMC, to be compared with a more sophisticated model predicting $9 \times 10^{-7}\,\mathrm{cm}^{-2}\,\mathrm{s}^{-1}$ for this galaxy (see also Houston, Riley and Wolfendale 1983). At least there is no gross discrepancy, but clearly this aspect of the subject is still in its infancy.

M31 has not yet been observed at the energies of interest here, but, as will be demonstrated in Chapter 5, there may be evidence for its detection at TeV energies.

The question of the likely flux of γ-rays from the LMC and SMC has been examined recently by Fichtel *et al.* (1991) and Sreekumar and Fichtel (1992). These authors assume dynamic balance in the galaxy and use synchrotron studies, allied with assumptions about the electron–proton ratio, to predict a flux above 100 MeV of approximately 2.3×10^{-7} cm^{-2} s^{-1} from the LMC. This value is not far from our own prediction (3.7×10^{-7} cm^{-2} s^{-1}).

For the SMC, Sreekumar and Fichtel (1992) conclude, again from studies of synchrotron radiation and using other information, that the cosmic ray intensity in this galaxy is a factor three–five times lower than if dynamical equilibrium were present. The predicted γ-ray flux is only $\sim 10^{-8}$ cm^{-2} s^{-1} above 100 MeV (a factor of five smaller than 'our' prediction, given above).

4.7.3 The diffuse extragalactic flux

The evidence for a diffuse extragalactic flux is based on the SAS II results (Figures 4.6 and 4.29), which indicate high latitude fluxes over and above the expected contribution from Galactic cosmic ray interactions in the ISM. The paucity of the data does not allow a positive identification, however; for example, inverse Compton interactions of electrons with the 2.7 K radiation in an extended Galactic halo could mimic an extragalactic component, and the present lack of statistics means that we cannot detect the expected non-isotropic distribution from Compton emission. However, we proceed and assume that the quanta *are* extragalactic.

At lower energies (X-rays), there is no doubt that there is an extragalactic flux, and indeed its magnitude is considerable. The γ-ray spectrum fits well to the X-ray results, and this feature tends to confirm the extragalactic origin of the γ-rays. Figure 4.47 shows the situation.

The most interesting feature seen in Figure 4.47 is the apparent presence of a 'bump' in the region of a few MeV, and this has led to many speculations. The bump has had a chequered history; it originated in the Apollo satellite observations and was initially of considerably greater magnitude than shown, but much was shown later to be due to induced radioactivity in the detector. The spectrum shown in Figure 4.47 is, hopefully, the asymptotic limit.

A number of rather exotic suggestions have been put forward to explain the bump. Ginzburg (1968) and Stecker (1969) have independently pointed out that the enhancement could arise from π^0 decays in the Universe at early epochs when both the cosmic ray intensity and the gas density might have been bigger, the resulting γ-rays being red-shifted. Stecker (1969) has gone further and postulated that the interactions responsible were not pp (i.e. $p + p \rightarrow \pi^0 + \cdots$) but $p\bar{p}$, the antiprotons being primordial. The question of whether or not the Universe is baryon-symmetric, and extragalactic antiprotons thereby being common, is still not resolved. The original model of Omnes (1969) based on a baryon-symmetric cosmology has had considerable opposition, the problem being the rather obvious one of how protons and antiprotons are separated in their respective families

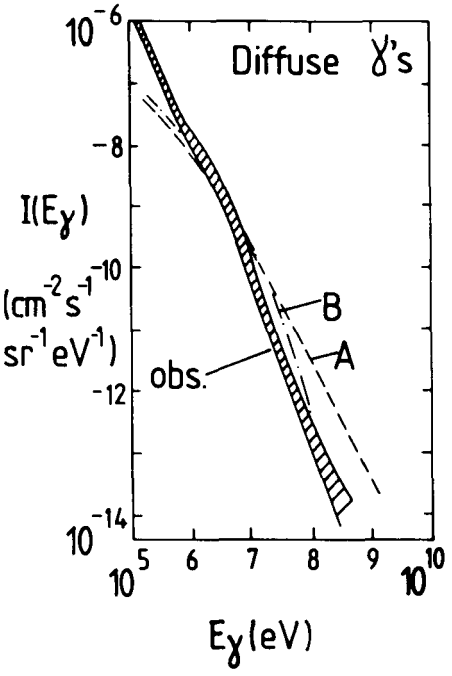

Figure 4.47. The energy spectrum of diffuse X- and γ-rays derived from the work of Trombka *et al.* (1977) and Fichtel *et al.* (1978*a,b*). The 'bump' at a few MeV is apparent. There are many possible explanations; variants of a model due to Strong *et al.* (1974), and referred to in the text, are indicated.

before annihilation occurs. Some form of domain structure is called for, and Brown and Stecker (1979) (and later papers by Stecker and associates) still consider that symmetry cannot be ruled out, and, in turn, that the γ-ray bump *could* be an indicator of the annihilation products. A key observation for the next generation of satellites will be to search for γ-rays from the interface between clusters of galaxies and antigalaxies (Fichtel 1981, 1983), these units being essentially the results of the domains in the early Universe.

Another explanation, due to Strong, Wdowczyk and Wolfendale (1974) and indicated in Figure 4.47, is in terms of an extragalactic origin of cosmic rays and their interaction, at early epochs, with the 2.7 K microwave background. Interestingly, the energetics are reasonable (see the figure), but the predicted shape is not too good.

There are other more mundane explanations for the extragalactic spectrum. Although normal galaxies are insufficient by about a factor of 20 to explain the observed flux (e.g. Strong, Wolfendale and Worral 1976), the integrated emission from more energetic galaxies can almost certainly do so. Here, the prominent feature of a turn-down at a few MeV for 3C273 and NGC 4151 referred to in the previous section adds weight to this suggestion. The energetics of the situation are also acceptable, although it will be appreciated that the paucity of detected sources causes considerable uncertainty.

More recently, yet another possible explanation for at least a part of the diffuse extragalactic flux has been put forward. Strong and Bignami (1983) have claimed the detection of γ-rays from the direction of NGC 1275 in the Perseus cluster (the signal can be seen rather clearly in Figure 4.31). This cluster is at a distance of 116 Mpc (using a Hubble constant $H_0 = 50\ \text{km s}^{-1}\ \text{Mpc}^{-1}$), and the flux claimed is $8 \times 10^{-7}\ \text{cm}^{-2}\ \text{s}^{-1}$ above 70 MeV. The manner in which the γ-rays are produced is not clear (one or more very energetic galaxies in the cluster or cosmic rays interacting with the intercluster gas, or both?), but they do seem to be present. Houston, Wolfendale and Young (1984) have followed this up by examining the SAS II data base in detail in a search for an excess flux from the directions of specific clusters. Although the statistical precision is understandably poor, there does seem to be an excess, and when integrated over all clusters, suitably weighted according to γ-ray 'strength', the predicted contribution to the extragalactic diffuse flux is $(6.0 \pm 2.4) \times 10^{-4}\ \text{cm}^{-2}\ \text{s}^{-1}$ above 35 MeV, to be compared with the observed value of $\approx 7.4 \times 10^{-4}\ \text{cm}^{-2}\ \text{s}^{-1}$. Here, then, is another contender.

A final brief comment can be made about the role of the extragalactic γ-ray flux in constraining models of cosmic ray origin. If cosmic rays were of extragalactic origin and had the same intensity everywhere in the Universe, or were concentrated in galaxy clusters, then their interactions with extragalactic gas would generate a higher γ-ray flux than is seen (Said *et al.* 1982). In fact, the excess of prediction over observation is not large for the constant cosmic ray intensity case, but this situation is unlikely; more likely is the model in which cosmic rays are generated in active galaxies in clusters, and here the excess of prediction over observation is large. The argument against extragalactic cosmic rays is quite a strong one.

4.8 New experimental programmes

4.8.1 General remarks

Although balloon flights are still continuing from time to time, these are devoted mainly to rather low γ-ray energies (< 10 MeV), and their necessarily short durations yield rather poor quality data. It is from new satellite experiments that we expect major new advances to occur, and here there are two projects in hand: GAMMA I and the GRO.

4.8.2 GAMMA I

After many delays, this observatory was launched in 1990, using a Soviet satellite.

The detector is similar to those on SAS II and COS B, namely a multilayer spark chamber with anticoincidence protection against charged cosmic ray events. Improvements over the earlier satellite detectors include a more accurate energy calorimeter, and a sensitive area higher by nearly a factor three (although the product of area times solid angle is about the same).

As with COS B, the project is international in character, the contributors being the then USSR (Moscow Space Research Institute, Moscow Physical Engineer

Training Institute, Lebedev Physics Institute of Moscow, and A.I. Ioffe Physical Technical Institute of Leningrad); France (Section d'Astrophysique du CEA/ Saclay, and Centre d'Etude Spatiale des Rayonnements); and Italy (Istituto di Fisica Cosmica of Milano, Istituto di Astroficia Spaziale at Frascati, and Istituto TESRE at Bologna).

Unfortunately, it is necessary to report that the high voltage system for the spark chamber failed before observations could be made, and this means that the only data available are with the 'triggering' telescope, which has an FWHM of more than 10°.

Nevertheless, some useful results are being obtained on variable γ-ray emitters, particularly the Vela pulsar.

4.8.3 Gamma Ray Observatory

Launched on April 5, 1991, after a considerable delay due to the Space Shuttle disaster, NASA's Gamma Ray Observatory is already providing important data (some preliminary results have been referred to already). There are four instruments, covering between them the energy range 30 keV–30 GeV.

Following the description given by Fichtel (1982), their capabilities can be listed as follows:

(i) A survey of high energy γ-ray sources and diffuse emission with a point source sensitivity of better than 5×10^{-8} cm^{-2} s^{-1}, angular resolution of $\sim 0.1°$ for strong sources, and an energy resolution of 15% at energies above 100 MeV.

(ii) A survey of sources and diffuse emission with sensitivities 10^{-5} cm^{-2} s^{-1} and energy resolution around 10% between 0.1 and 30 MeV.

(iii) Detection and identification of nuclear γ-lines with an energy resolution of 4% and sensitivity 4×10^{-5} cm^{-2} s^{-1}.

(iv) Observations of γ-ray bursts, including studies of their spectral and temporal behaviour.

The orbit is near circular at 450 km altitude and an inclination of 28°. Pointing directions are known to an accuracy of about 2′ and absolute times are accurate to about 100 μs. The characteristics of the four instruments are summarised in Table 4.4.

Other aspects of the detectors can also be considered; in turn:

Oriented scintillation spectrometer experiment (*OSSE*). Energy range 0.1–10 MeV. Detectors: four large actively shielded and passively collimated NaI scintillators. Contributing laboratories: Naval Research Laboratory; North-Western University; Royal Naval College, London; Rice University.

Compton telescope (*COMPTEL*). Energy range 1–30 MeV. Detectors: upper liquid scintillator, lower NaI (Tl) crystal – the γ-ray interacts to produce Compton electrons in both detectors. The instrument can determine the polarisation of the radiation. Contributing laboratories: Max Planck Institut für Extraterrestrische

Table 4.4. *Summary of GRO detector characteristics*

					BATSE	
		OSSE	COMPTEL	EGRET	Large area	Spectroscopy
Energy range (MeV)		0.1–10	1–30	20–3 × 10^4	0.03–1.9	0.015–110
Energy resolution (FWHM) (%)		12.5 at 0.2 MeV 6.8 at 1.0 MeV 4.0 at 5.0 MeV	8.8 at 1.27 MeV 6.5 at 2.75 MeV 6.3 at 4.43 MeV	~20 at 100–2000 MeV	32 at 0.06 MeV 27 at 0.09 MeV 20 at 0.66 MeV	8.2 at 0.09 MeV 7.2 at 0.66 MeV 5.8 at 1.17 MeV
Effective area (cm^2)		2013 at 0.2 MeV 1480 at 1.0 MeV 569 at 5.0 MeV	25.8 at 1.27 MeV 29.3 at 2.75 MeV 29.4 at 4.43 MeV	1200 at 100 MeV 1600 at 500 MeV 1400 at 3000 MeV	1000 each at 0.03 MeV 1800 each at 0.1 MeV 550 each at 0.66 MeV	100 each at 0.3 MeV 127 each at 0.2 MeV 52 each at 3 MeV
Position localisation (strong source)		10 (arc min)^2 error box (special mode; 0.1 × Crab spectrum)	8.5 arc min (90% confidence at 2.75 MeV – 20σ source)	5–10 arc min (1σ radius; 0.2 × Crab spectrum)	1° (strong burst)	–
Field of view		3.8 × 11.4°	~64°	~0.6 sr	4π sr	4π sr
Maximum effective geometric factor (cm^2 sr)		13	30	1050 (~500 MeV)	15000	5000
Estimated source sensitivity (10^6 s; off Galactic Plane)	line	(2–5) × 10^{-5} cm^{-2} s^{-1}	3 × 10^{-5} to 3 × 10^{-6} cm^{-2} s^{-1}			0.4% equivalent width (5 s integration)
	continuum	2 × 10^{-7} cm^{-2} s^{-1} keV^{-1} (at 1 MeV)	5 × 10^{-5} cm^{-2} s^{-1}	5 × 10^{-8} cm^{-2} s^{-1} (>100 MeV) 1.5 × 10^{-8} cm^{-2} s^{-1} (>1000 MeV)	6 × 10^{-8} erg cm^{-2} (10 s burst)	

Physik; University of Leiden; University of New Hampshire; European Space Agency, ESTEC.

Energetic gamma-ray experiment telescope (*EGRET*). Energy range 20 MeV–30 GeV. Detectors: multilevel thin plate spark chamber system (similar to SAS II and COS B), NaI (Tl) total energy calorimeter beneath the spark chamber and plastic scintillator anticoincidence dome. Precision: for sources of moderate strength, the position should be determined to about 10 arc min; diffuse emission spatial variations in the energy spectrum should be measurable on a scale of a few degrees. Contributing laboratories: Goddard Space Flight Center; Stanford University; Max Planck Institut für Extraterrestrische Physik; Grumman Aerospace Corporation.

Burst and transient source experiment (*BATSE*). Energy range: 50–600 keV. Detectors: eight wide field modules; four have the same viewing path as the other telescopes on the GRO and four view the opposite hemisphere. Time resolution 100 μs, burst location accuracy $\approx 1°$, sensitivity 6×10^{-8} erg cm^{-2} for a 10 s burst. Laboratory involved: Marshall Space Flight Center.

5

Ultra high energy gamma-rays

5.1 Introduction

Studies of ultra high energy gamma-rays (UHEGR)* i.e. γ-rays at energies greater than 100 GeV, provide us with information on the conditions existing in remote celestial regions, such as magnetic and electric fields, matter and radiation densities, and on the acceleration mechanisms of charged particles. Additionally such studies have an important bearing on the problem of the origin of the cosmic radiation. There is, as yet, no universally accepted identification of either the sources or the mechanisms of production of cosmic rays, though, as was pointed out in Chapter 4, there are strong arguments made in favour of some. The problem is confounded by the fact that cosmic rays, almost all of which are charged particles, undergo frequent deflections in the interstellar magnetic fields, making it impossible to know the source directions. Thus, even a primary cosmic ray proton of energy as high as 10^{15} eV has a Larmour radius in the ISM of only ~ 0.3 pc and has its initial direction almost isotropised. Electrically neutral radiation is free from this problem. The more commonly occurring neutral particles are neutrons, neutrinos and γ-rays. Neutrons are unstable; they would not survive in most cases from source to Earth even after allowing for relativistic time dilatation, with a decay mean free path of only 9.2 $(E/10^{15}$ eV) pc. Neutrinos, being weakly interacting, are not easy to detect. γ-rays, on the other hand, are ideal as their production and interaction cross sections are rather high and they are stable.

There are strong hints that ultra high energy charged particles (specifically electrons) exist in regions far removed from the solar system. Shklovskii (1953) suggested that the optical continuum from the Crab nebula must be due to synchrotron emission by high energy electrons and positrons in the nebular magnetic fields, and subsequent observations of the polarisation of photons at radio, optical and X-ray wavelengths confirmed this suggestion. This shows that relativistic electrons of energy up to at least 10^{14} eV exist in the Crab nebula, a fact which has made the prospect of detecting UHEGR from this and other similar celestial sources very attractive. If a finite flux of UHEGR is detected, the source

* γ-rays in the range 100–10 000 GeV are sometimes referred to as 'very high energy gamma rays', whereas those above 10^{14} eV are termed 'ultra high energy gamma rays'. Here, for the sake of brevity, we UHEGR for both.

direction is known immediately, being part of the discovery process itself. Further studies of energy spectra and time variations in intensity are likely to throw light on both the physical conditions and the charged particle acceleration mechanisms operating in the environs of the source object.

Production mechanisms of UHEGR have been reviewed in the past by several authors; see, for example, Felten and Morrison (1966), Fazio (1967) and Stecker (1971). As mentioned in Chapter 1, UHEGR are produced in the interactions of high energy protons with matter ($p + p \rightarrow \pi^0 \rightarrow 2\gamma$) and of high energy electrons with matter (bremsstrahlung), with magnetic fields (synchrotron and curvature radiation mechanisms), and with ambient light (inverse Compton process).

Once produced, UHEGR travel from the source to the observer undeflected, although some attenuation by γ–γ collisions may occur en route. The absorption mechanism was considered in Chapter 1. It was shown there that the threshold for γ–γ collisions is given by

$$E_\gamma > m_e^2 c^4/\varepsilon \tag{5.1}$$

where m_e is the rest mass of the electron and ε is the energy of the ambient photon. The consequence is that extragalactic space, in which ε relates to the 2.7 K radiation, is transparent out to about 100 Mpc for $E_\gamma < 10^{14}$ eV and ~ 10 kpc for $E_\gamma \sim 1.10^{15}$ eV.

Another mechanism for absorption, but in a very different environment, is pair production by interaction with intense magnetic fields in the magnetospheres of pulsars. The threshold photon energy for this process (Sturrock 1971, Manchester and Taylor 1977) is given by

$$E_\gamma(\text{eV}) > 4 \times 10^{18}/B_\perp(\text{G}) \tag{5.2}$$

where $B_\perp$ is the magnetic field transverse to the direction of the γ-ray.

Unfortunately, observations on UHEGR from celestial bodies are beset with the difficulty of having to detect very low fluxes in the presence of considerable backgrounds from charged cosmic rays. The rarity of UHEGR can be gauged from the fact that the total number of UHEGR claimed to have been detected during the past 30 years in approximately as many experiments is less than a few thousand. To date there has been one claim (Vacanti *et al.* 1991) of detection of TeV γ-rays from the Crab nebula/pulsar at the 20σ level and about 20 other claims for having detected UHEGR from celestial sources at the 4–5σ level over the energy range 100 GeV $< E_\gamma < 10^6$ TeV, and much more work needs to be carried out before this branch of γ-ray astronomy becomes as well established as the others.

If the energy spectrum observed at medium energies (e.g. from the Crab pulsar) is extrapolated to $E_\gamma = 1000$ GeV, it is found that the expected number of γ-rays incident over 1 m^2 area is only 16 y^{-1}. This number is so low as to make it almost impossible here to use balloon- or satellite-borne detectors. Fortunately, however, observations on UHEGR can be carried out by ground-based experiments by exploiting the transducing role of the terrestrial atmosphere itself: an incoming UHEGR interacts with the atmosphere, producing a very broad distribution of

secondaries, tertiaries etc., and it is these that a ground-based detector can record. The γ-ray shower axis can be as far away as 100 to 200 m from the detector, and yet the detector would be able to detect the progeny. This feature allows one to use detectors of modest physical size (a few to few tens of square metres) and be able to record the incidence of celestial γ-rays over tens of thousands of square metres. The gain in the effective collection area by more than three orders of magnitude is what makes it possible for both the atmospheric Cerenkov and extensive air shower techniques to detect the very small flux of cosmic UHEGR.

Extensive air showers initiated by charged primary cosmic rays constitute a large irreducible background to the detection of UHEGR. Further, since cosmic rays arrive uniformly in time (albeit with statistical fluctuations) and almost isotropically in space, present experiments cannot isolate the diffuse component of UHEGR. The aim, therefore, is to detect UHEGR from point sources which stand out as spikes in an otherwise uniform spatial distribution. If, in addition, the UHEGR intensity varies with time in a well defined fashion (as happens for pulsars) it provides an additional handle for the observer.

Basically, two techniques are employed in the detection of UHEGR. These are: (i) the atmospheric Cerenkov technique in the energy range 100 GeV $< E_\gamma <$ 100 TeV, and (ii) the extensive air shower technique at $E_\gamma > 100$ TeV. The two techniques are described in the next section. The various observations and results are described in Section 5.3, and the implications of the results and various theoretical models are discussed in Section 5.4. A few of the inconsistencies and puzzles posed by some observations are presented in Section 5.5, and finally a summary is given in Section 5.6.

5.2 Observational and analytical techniques

In this section we will briefly outline the salient features of the atmospheric Cerenkov technique and the air shower technique, and we describe the periodicity analysis in situations where the UHEGR emission is believed to be periodic in nature.

5.2.1 The atmospheric Cerenkov technique

Blackett (1948) first suggested that Cerenkov light produced by charged cosmic rays in the terrestrial atmosphere should contribute about 10^{-4} of the night sky background. Galbraith and Jelley (1953, 1955) demonstrated that cosmic ray showers do indeed produce Cerenkov light pulses in the atmosphere. Chudakov *et al.* (1962) were the first to apply this technique to detect celestial γ-rays. See Jelley and Porter (1963) and Jelley (1967) for earlier reviews, and Porter and Weekes (1978), Ramana Murthy (1980) and Weekes (1988) for the more recent. See also the *Proceedings of the International Workshop on Very High Energy Gamma Ray Astronomy* (Ramana Murthy and Weekes 1982).

A high energy γ-ray, on entering the Earth's atmosphere, initiates an electromagnetic cascade shower. Electrons and positrons in the shower with velocities above the local light velocity (c/μ) produce Cerenkov light, μ being the refractive index in air where the light is produced. The dependence of energy threshold,

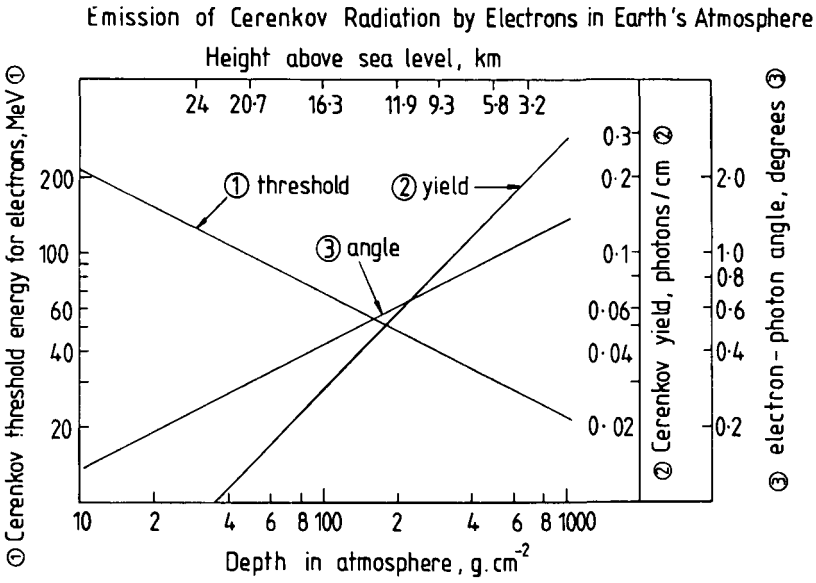

Figure 5.1. Variation with depth in the terrestrial atmosphere of: (1) threshold energy for electrons to emit Cerenkov radiation; (2) intensity of emission; and (3) angle of emission of Cerenkov radiation. For electromagnetic cascades the depth region 100–400 g cm^{-2} in the atmosphere is the most relevant.

emission angle and the rate of production of Cerenkov radiation on the depth in the atmosphere is shown in Figure 5.1. Although the electrons and photons in the cascade are absorbed in the atmosphere, the optical Cerenkov light penetrates the atmosphere, reaching the detectors at mountain altitudes or at sea-level. The Cerenkov light flash ($\Delta T \approx 10$ ns) created by a 300 GeV γ-ray, for example, may contain a few million photons spread over distances of the order of several hundred metres from the axis. If the field of view of a detector is restricted to a cone of 1° in diameter, the Cerenkov photon density is $\sim 7/m^2$ near the core of the shower, dropping off drastically beyond about 100 m from the axis. To a good approximation, Cerenkov photon density is proportional to the γ-ray energy. Several authors calculated the lateral distribution of Cerenkov photons; see Browning and Turver (1977), for example. The calculations (see Figure 5.2) reveal that the photon density depends on the half-angle of the cone of view and is affected by the geomagnetic field. The authors have also shown from their calculations that, for the same γ-ray energy, the magnitude and the shape of the lateral distribution of Cerenkov photon density vary from shower to shower due to fluctuations in shower development. Since the magnitude of Cerenkov light is very small, observations can be carried out only during clear moonless nights, and this makes the duty factor very small, typically 5–10%.

A celestial source may appear to be a point as seen from Earth, but Coulomb scattering of the electrons in the cascade and the finite emission angle of Cerenkov light spoil the resolution to make the source look like a diffuse object of 1–2° in

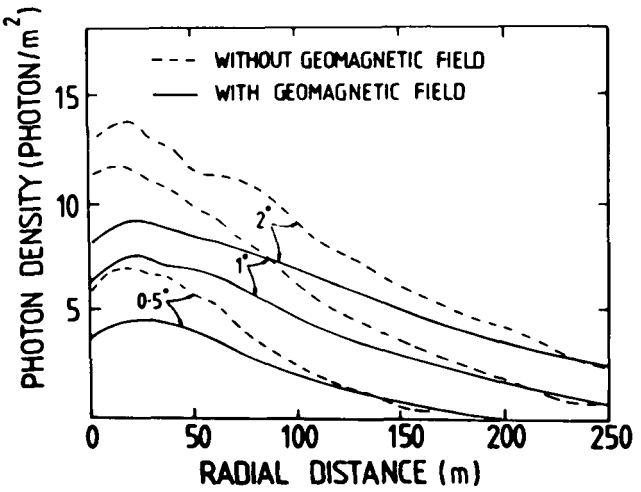

Figure 5.2. Lateral distributions found by Browning and Turver (1977) of Cerenkov photons produced by $e^{\pm}$ in the atmosphere with and without geomagnetic field for an incident γ-ray energy of 100 GeV. Calculations apply for an altitude of 2300 m above sea-level. Numbers attached to the curves represent the half-angle of the field of view in degrees. The figure is taken from Porter and Weekes (1978).

diameter. In practice, the low intensity Cerenkov light is collected and focused by a large parabolic mirror on to the cathode of a fast photomultiplier, in front of which is a mask to limit the view to a cone of 1–3° in diameter. It is routinely demonstrated in each experiment (see, for example, S.K. Gupta, 1983, unpublished Ph.D. thesis, University of Bombay) that most of the Cerenkov photons arrive in a flash of less than 10 ns in width and with mutual angular separations of $< 1.5°$.

The night sky background (NSB) is $\approx 7 \times 10^7$ photons $cm^{-2}\ s^{-1}\ sr^{-1}$ when the view does not include a bright star with magnitude < 5 (P.V. Ramana Murthy and S.C. Tonwar, 'Optical night sky background at Ootacamund, Tamilnadu, India', 1976, unpublished). The NSB and the atmospheric Cerenkov radiation produced by extensive air showers (EAS) initiated by charged primary cosmic rays constitute the background to the γ-ray signal. The NSB is almost completely eliminated by taking fast ($\tau \sim 10$ ns) coincidences between several photomultipliers looking at different mirrors. The NSB can also be eliminated by demanding a majority logic among the several photomultipliers or by adding pulses from all the photomultipliers and then biasing off at a suitable discrimination level; see Figure 5.3. With the NSB almost eliminated, cosmic-ray initiated EAS remain the only background to UHEGR signals, but these are not easy to remove. As it is, the cosmic ray background primaries are less efficient in producing a trigger than UHEGR signals for two reasons: (i) even at energies $> 10^{12}$ eV much of the energy is 'wasted' in producing nuclear excitations and in the subsequent decays of pions and muons into neutrinos. This energy is thus lost to the electromagnetic component responsible for producing the Cerenkov emission; and (ii) at energies

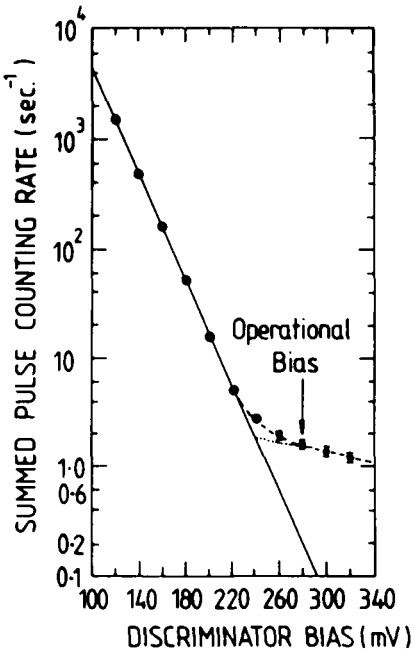

Figure 5.3. Signals from all the 18 photomultipliers, each viewing a parabolic mirror in the Ooty group's set up, are summed and discriminated. The figure shows the counting rate as a function of discriminator bias. The steep portion represents contributions from photomultiplier noise and NSB; the flatter portion is due to air showers and γ-ray showers. If the discriminator is operated at 280 mV bias, there will be a negligible number of chance coincidences among the triggers for showers (S.K. Gupta, 1983, unpublished Ph.D. thesis, Bombay University).

below 10^{12} eV, the nucleus-induced EAS become not only even more inefficient for the reason just stated, but the secondary pions are emitted at larger angles and thus spread out the generated Cerenkov light to larger radial distances. The progressively increasing advantage γ-rays enjoy over cosmic rays with decreasing energy is clearly demonstrated in Figure 5.4, taken from Turver and Weekes (1978).

Grindlay (1971) made use of Cerenkov light produced by muons in EAS (the 'second maximum') as a veto to reduce the EAS background, but this technique is efficient only at $E \gtrsim 10^{13}$ eV because at lower energies there are too few muons in showers.

The Mount Hopkins collaboration (Vacanti *et al.* 1991) successfully employed the imaging technique in which one makes a detailed study of the Cerenkov image produced by each shower to reject nearly 97% of cosmic-ray-induced shower background. The authors noted that, although the images of Cerenkov light pool of γ-ray-induced and cosmic-ray-induced showers appear largely similar, there are small but important differences between the two. It is these differences that the authors exploited by measuring the image shape at the focal plane of their reflector (see below for a description of their reflector) with a high resolution camera, and then, by making suitable cuts on the image parameters, they rejected the cosmic

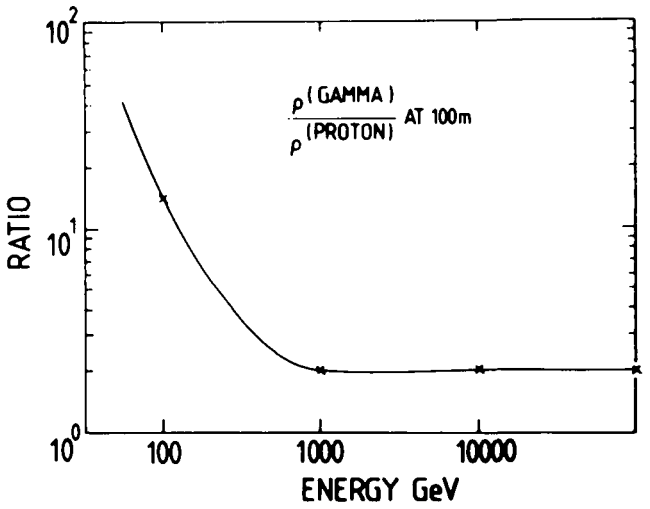

Figure 5.4. The ratio of Cerenkov photon densities ρ(GAMMA)/ρ(PROTON), at 100 m from axis (for γ- and proton initiated cascades), is shown as a function of energy of the initiating particle; taken from Turver and Weekes (1978).

ray showers. The spectacular success of this technique in establishing a γ-ray signal is described in Section 5.3.1A.

Although troublesome as a background, the cosmic-ray-produced Cerenkov radiation has some value for calibration, the charged primary cosmic ray energy spectrum being well studied in this energy range.

The cosmic ray background rate is proportional to the product of collection area, A, and to the solid angle of view, $\pi\theta^2$ (θ small), whereas the γ-ray (signal) rate is proportional to A. If the experiment operates for a time T, then the standard deviation in the background counts is proportional to $(AT\theta^2)^{1/2}$, whereas the excess counts due to signal are proportional to AT. The signal-to-noise ratio, then, is proportional to $AT/(AT\theta^2)^{1/2} = A^{1/2}T^{1/2}\theta^{-1}$. To sharpen the γ-ray signal one has to maximise the observation time T and decrease θ, the half-angle of the cone of view. There is a limit, however, of $\theta \sim 0.5°$, below which one cannot decrease the angle; the fraction of Cerenkov light collected and consequently the detection efficiency falls very rapidly below this value. To maximise the collection area, A, for a given γ-ray energy, one decreases the Cerenkov photon density threshold by using larger mirror area. This also results in the more important advantage of lowering the γ-ray energy threshold.

If the source is pulsating, the sensitivity of a given detector system is improved by a factor of five to ten compared to that for a steady source. However, searches for pulsed γ-rays can be significant only if one has an accurate knowledge of the period, P; in the case of a pulsar, where P is varying with time, one needs also the period derivative, $\dot{P}$, of the object, this being determined from measurements carried out at other frequencies at an epoch as close to that of the experiment as possible.

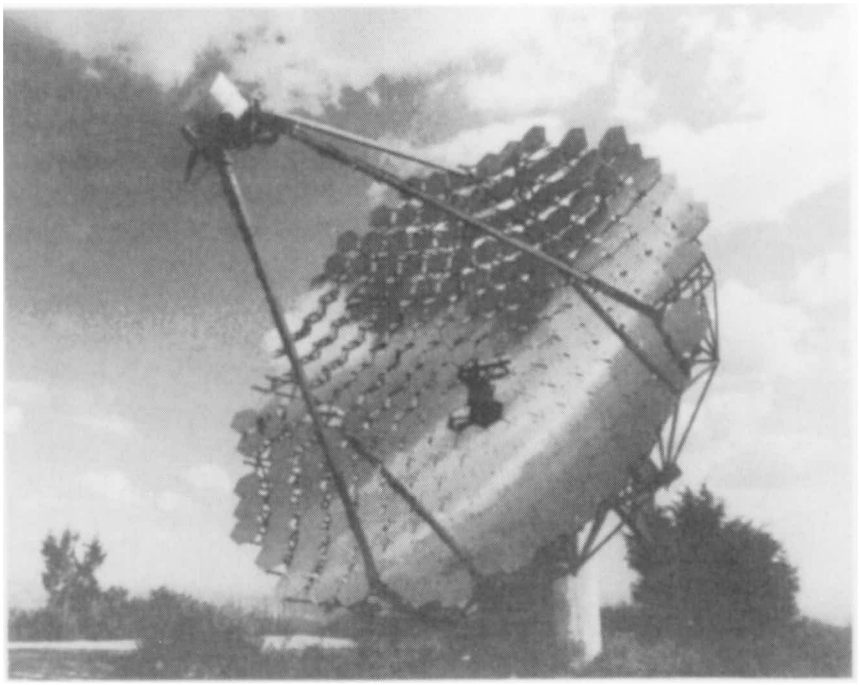

Figure 5.5. A picture of the 10 m reflecting night sky Cerenkov telescope of the Fred Lawrence Whipple Observatory at Mount Hopkins, USA. (Smithsonian Institution – courtesy of Prof. T.C. Weekes.)

In the past, groups from the USSR, UK, Ireland, the USA, Australia, India, South Africa, France and Japan have carried out several experiments to detect UHEGR using the Cerenkov technique; see the reviews by Porter and Weekes (1978) and Weekes (1988) for details of some of these experiments. We will mention here only a few of them to illustrate the detector systems generally used.

The 10 m diameter dish of the Smithsonian Astrophysical Observatory at Mount Hopkins, Arizona, USA, is shown in Figure 5.5. It consists of 248 individual mirror elements and has a computer-controlled alt-azimuth mounting (Cawley *et al.* 1990). The dish has a focal length of 7.3 m and an angular resolution of 0.35°. In its latest mode of operation, the dish is equipped with 109 photomultipliers at its focal plane to be used as an imaging device of the Cerenkov light flash. These photomultipliers provide 91 pixels of size 0.25° and 18 of 0.5° giving a full field of 3.75°. Figure 5.6 shows the 20-mirror array of the Tata Institute of Fundamental Research. The array, consisting of eight parabolic mirrors of 1.5 m diameter and 12 of 0.9 m diameter (P.N. Bhat *et al.* 1980), is currently operated at Pachmarhi, India. Each mirror is equatorially mounted and viewed by a photomultiplier placed at its focus. During most runs the mirrors are grouped into four banks, photomultiplier pulses are summed in each bank and discriminated, and a majority logic (any three out of four banks) is used to eliminate NSB and to trigger on UHEGR and cosmic ray EAS.

Figure 5.6. The 20 parabolic mirror array to detect Cerenkov light produced by showers. The array was operated by the Tata Institute of Fundamental Research group at Ootacamund (Ooty), until 1985, and now at Pachmarhi, India. Two small mirrors were not used in the experiment. (Photograph by A.R. Apte.)

The University of Durham, UK, operated a spaced array of four γ-ray telescopes at Dugway, Utah. Each telescope consisted of three paraxial parabolic mirrors of 1.5 m diameter mounted on a computer-steered alt-azimuth platform (Gibson *et al.* 1982*a*). The telescopes were deployed at the centre and one at each of the apices of an equilateral triangle of side 100 m. Each telescope acts independently and generates its own trigger by a three-fold coincidence between the photomultipliers viewing the three mirrors. Improved versions of Cerenkov telescopes of similar design are being currently operated by the same group at La Palma in the Canary Islands, and at Narrabri, Australia; see Brazier *et al.* (1989).

The objective is usually to determine if a celestial object steadily emits UHEGR, and to do this a common practice is to aim the mirrors at a point in the sky in the path of the object and hold them fixed there. The event rate is expected to change as the object moves in and out of the detector field of view (drift scan mode). A variant of this technique is to track the object for some time between two spatial angles θ_1 and θ_2, followed by tracking the now-empty field for the same time between the same angles and then comparing the resulting 'on-source' and 'off-source' rates (on–off mode).

For pulsed emission studies, on the other hand, the mirrors are locked on the object under investigation and made to track it for as long as possible (typically 1–6 h); event times and pulse heights are recorded. Later the event times are examined for the expected periodicity.

5.2.2 *The air shower technique*

At energies above 10^{14} eV, the electromagnetic cascade showers initiated in the terrestrial atmosphere by celestial γ-rays can penetrate down to sea-level, though it is ~ 28 radiation lengths deep. At $E_\gamma \sim 10^{14}$ eV densities of $e^\pm$ in the shower at sea-level are small (10–0.1) m^{-2} at distances 1–100 m from the core of the shower. It is, therefore, more convenient to work with γ-rays at $E_\gamma \lesssim 10^{15}$ eV, which result in higher densities of $e^\pm$. One samples at sea-level or mountain altitudes particle densities at several points on a horizontal plane by using detectors (usually of dimensions ~ 1 m^2) spread out to distances of several hundred metres. The technique was primarily developed for studying the charged component of primary cosmic rays at energies $E_0 > 10^{14}$ eV. We denote these latter showers by EAS (extensive air showers), and refer to the former as γ-ray showers. In EAS one has, besides $e^\pm$, muons ($\sim 5\%$ of $e^\pm$), pions, nucleons and other hadrons ($\sim 1\%$ of $e^\pm$). In EAS experiments one also employs detectors to study the identity, energy, number and lateral distribution of $\mu^\pm$ and hadrons in order to gain an insight into high energy interaction characteristics and primary composition. This technique, which is four decades old, was described in the past by several authors; see, for example, Galbraith (1958) and Greisen (1960). Unlike the experiments based on the atmospheric Cerenkov technique, these experiments with particle detector arrays can be carried out day and night and in any weather, making the duty factor much higher.

To illustrate the kind of air shower detector arrays one employs to detect UHEGR, we show two arrays. The first one is the array at Kolar Gold Fields, India (P.N. Bhat *et al.* 1985), shown in Figure 5.7. It consists of 127 charged particle density sampling scintillators, each of 1 m^2, among which 61 are instrumented for fast (~ 1 ns) timing measurements of the arrival of the air shower front and seven muon detectors each of 28.8 m^2 in area. The detectors are spread over a hexagonal area of dimensions 240 × 208 m. The second one, shown in Figure 5.8, is the array of Dugway, Utah (Rosenberg 1991) operated by the Utah–Michigan–Chicago collaboration. It consists of 1089 scintillators instrumented for both the density and time measurements and 16 patches of muon counters (buried underground), each of area 160 m^2. The latter array is the largest in operation, spread over an area of 480 m × 480 m, aimed at detection of UHEGR.

To estimate the shower size, N, one fits to the sampled particle densities a lateral distribution function of the following type (see Nishimura and Kamata 1952):

$$\rho(r) = \frac{N}{2\pi r_1^2} f(s) \left(\frac{r}{r_1}\right)^{b-2} \left(1 + \frac{r}{r_1}\right)^{b-4.5} \tag{5.3}$$

Here $\rho(r)$ is the density of particles per metre squared at a distance r from the shower core; s is the age parameter of the shower; $f(s)$ is a function of s; and r_1 is the Moliere scattering unit (~ 80 m at sea-level). From such a fit the core location is determined, together with the age parameter and shower size, which is

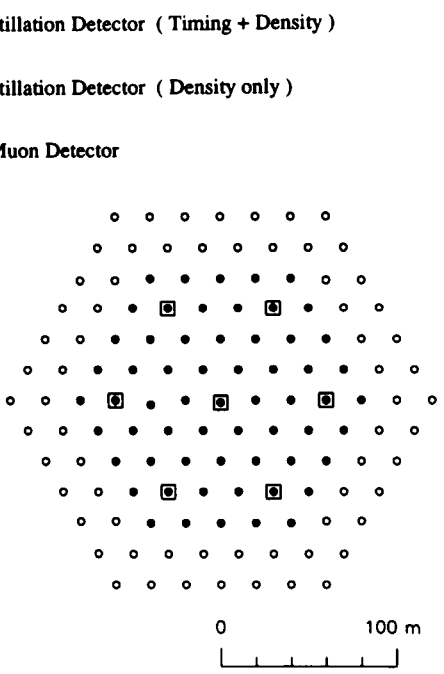

Figure 5.7. The Kolar Gold Fields array (P.N. Bhat *et al.* 1985) to detect PeV γ-rays.

given by

$$N = \int_0^\infty 2\pi r \rho(r)\, dr \tag{5.4}$$

The energy, E, of the primary charged cosmic ray or the γ-ray is found from N by using an E–N relationship computed from the known (or extrapolated where necessary) cross sections for various strong and electromagnetic interaction processes.

The arrival direction of the primary cosmic ray or γ-ray is obtained from fast timing information obtained by suitably designed detectors. If, for example, one employs two timing detectors separated by a distance d on a horizontal plane, the projected zenith angle, θ_p, in a vertical plane containing the two detectors is given by

$$\theta_p = \sin^{-1}(tc/d) \tag{5.5}$$

Here c is the velocity of light and t is the difference in arrival times of the shower front at the two detectors. For typical values of $\theta_p \sim 30°$, $d \sim 50$ m and the error in timing measurements, $\Delta t \sim 3$ ns, one can measure θ_p to an accuracy of around 1°. Using several non-collinear timing detectors for redundancy and improving accuracy, it is possible to determine the spatial zenith angle and azimuthal angle of the arrival direction of the shower. This information, together with that on

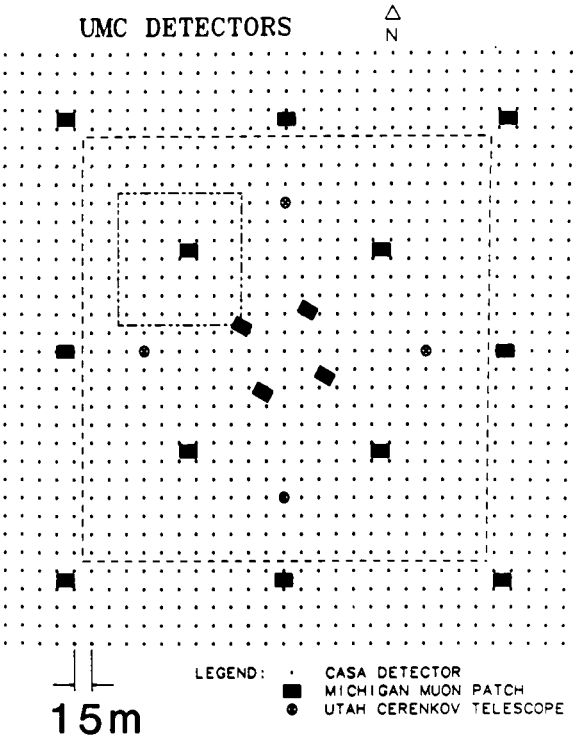

Figure 5.8. The array of the Utah–Michigan–Chicago collaboration (Rosenberg 1991) to detect PeV γ-rays.

event time, enables the shower direction in celestial coordinates to be found. If there is enough redundancy built into the timing system, one can also solve for the finite radius of curvature ($R \sim 3$–5 km) of the shower front instead of assuming it to be flat; see Yodh (1989) for more details.

The EAS (which are the background to the UHEGR signal) are overwhelmingly large in number compared to γ-ray showers, and it is imperative to first reduce the EAS background and then to look for spikes either in the spatial or temporal distributions of the recorded events. Such spikes can, then, be attributed to γ-rays.

To reduce the EAS background, use is made of two entities: (i) the age parameter, s, of the shower, and (ii) the muon content. The energy in an electromagnetic cascade, as it penetrates the terrestrial atmosphere, is attenuated much faster than that in a nuclear–electromagnetic cascade in which the energy is carried forward through relatively stable hadrons and the follow-through nucleons. As a result, γ-ray showers look much older ($s > 1$), i.e. the lateral distribution of $e^{\pm}$ in the shower is much flatter than in the EAS ($s \sim 1$). Thus a cut is made on s, e.g. $s > 1.1$, to enrich the data sample in UHEGR. However, Hillas (1987) carried out Monte-Carlo calculations to show that in the 10^{15} eV energy range the γ-ray showers should not have greater age values than the cosmic ray showers. Also, Chung and MacKeown (1988) have shown that there is a considerable overlap in the age parameters of the γ-ray and cosmic ray showers

at energies $\gtrsim 10^{15}$ eV. The usefulness of the age parameter to select preferentially UHEGR showers thus becomes questionable.

Next to $e^{\pm}$, the most abundant charged particles in EAS are $\mu^{\pm}$. In γ-ray showers there are far fewer muons than in EAS. The production cross section for a muon pair in the Coulomb field of nuclei by a γ-ray is much lower than that of an $e^{\pm}$ pair, being given by

$$\sigma(\mu^{\pm})/\sigma(e^{\pm}) = (m_e/m_\mu)^2 = 2.3 \times 10^{-5} \tag{5.6}$$

More relevant for muon production in γ-ray showers is the photo-production of charged pions which subsequently decay into $\mu^{\pm}$. Even here, in collisions with 'air' nuclei, the ratio

$$\sigma(\gamma + N \rightarrow \pi^{\pm} + \cdots)/\sigma(p + N \rightarrow \pi^{\pm} + \cdots) \approx 10^{-2} \tag{5.7}$$

is very small, and one expects, therefore, far fewer $\mu^{\pm}$ in a γ-ray shower than in an EAS. Braun and Sitte (1965), Wdowczyk (1965), Stanev and Vankov (1985) and Stanev, Gaisser and Halzen (1985) have made detailed calculations and have shown that the ratio of the number of muons in a γ-ray shower to that in a conventional EAS is ~ 0.1. One, then, looks for anomalously low muon densities as an additional signature of a γ-ray shower. One must, however, exercise caution in using this criterion; claims have been made by various authors for detection of UHEGR signals from Cygnus X-3, Hercules X-1 and Crab, but with a muon content no different from that in the background cosmic ray showers. See Section 5.3 for details.

5.2.3 *Periodicity analysis*

UHEGR emission can be either steady or periodic in nature, the latter being more attractive from the observational and analysis points of view. With the discovery of pulsars (Hewish *et al.* 1968), a new class of potential sources of UHEGR opened up for observations.

Pulsars are high on the list of potential objects for a number of reasons: (i) independent evidence exists that high energy processes are occurring in their vicinity, (ii) the precisely pulsed nature of emission relieves the observer from devoting as much (or even more) time to study cosmic ray background and systematic errors, and (iii) if the data are divided into N bins in the phase plot, the cosmic ray background reduces by a factor N, as a result of which the sensitivity of an experiment goes up by $N^{1/2}$, a factor which is usually five to ten.

The higher the spinning down energy-loss rate ($\propto \dot{p}p^{-3}$), and the smaller the distance of a pulsar, the higher is the chance of detecting it. The figure of merit (FM) is given by

$$FM \propto \dot{P}/D^2P^3 \quad [\text{i.e. } \propto (\tau_{ch}D^2P^2)^{-1}] \tag{5.8}$$

Here D is the distance to the pulsar, P is the period of the pulsar, and τ_{ch} is the characteristic age of the pulsar. One therefore concentrates on the nearest, youngest and fastest pulsars. The recently discovered millisecond pulsars are an exception. Having been recycled and spun-up by accretion (V. Radhakrishnan and

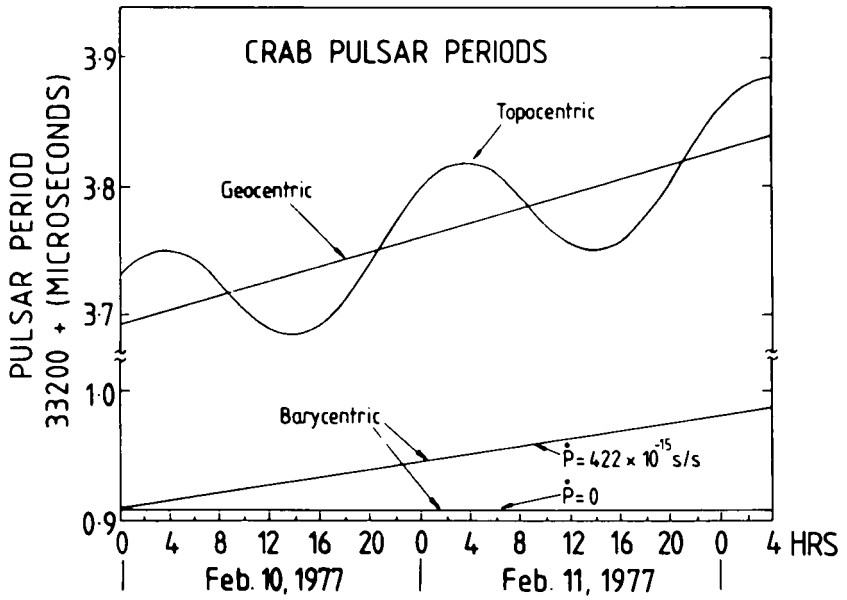

Figure 5.9. Variation of Crab pulsar period with time. Periods at the solar system barycentre for $dP/dt = 0$ (hypothetical) and for $dP/dt = 422 \times 10^{-15}$ s s^{-1} (observed) are shown by the two lines at the bottom. Uppermost line: result of Doppler shift due to the Earth's orbital motion. Sinusoidal line: result of Doppler shift due to the Earth's rotation. Note that the ordinate scale is vastly expanded.

G. Srinivasan 1981, unpublished), they are probably not as active as the first-born pulsars. Since the UHEGR signal is very weak, one cannot determine the pulsar elements (P, $\dot{P}$, epoch) from the data themselves; it is necessary to obtain the elements from observations made at other frequencies. Pulsars are known to undergo sudden speed-ups (glitches), and it is desirable, therefore, to obtain the elements from as recent an observation as possible.

Because the UHEGR signal is weak, it is necessary to accumulate data over long stretches of time ($T \sim 100$ d), at the same time keeping the phase information. If the pulsar of period P is observed for a time T, then the number of pulsar cycles elapsed, N, is given by $N = T/P$. In order to avoid wash-out of signal due to smearing, ΔN has to be kept small ($\lesssim 0.01$). This, then, calls for accuracies $\sim 10^{-10}$ in time keeping ($\Delta T/T$) and in the period ($\Delta P/P$), in the case of the Crab pulsar. For time keeping, one uses an atomic clock directly or, more generally, a laboratory temperature controlled quartz clock regularly calibrated with the time signals derived from an atomic standard some distance away. Currently there are two satellite systems in operation from which time signals can be received, enabling one to calibrate laboratory clocks to maintain absolute universal coordinated time (UTC); these systems are the US Navy Navigational Satellite System (accuracy ~ 30 μs) and the Global Positioning Satellite System (accuracy ~ 100 ns).

The Doppler shifts, $\Delta P/P$, introduced in P by the Earth's orbital and rotational motion can be quite large, $\sim 10^{-4}$ and 10^{-6}, respectively; see Figure 5.9. To keep

clear of these effects, one reduces the event arrival times to the solar system barycentre, which is the nearest available inertial frame. Doppler shifts in the period can also arise if the source happens to be a component of a binary system, e.g. Hercules X-1. To eliminate them, one reduces event times to the centre of mass at the binary system, which can be regarded as an inertial frame. Any velocity component between an isolated pulsar (or the centre of mass of the binary) and the solar system barycentre produces a constant Doppler shift between the emitted and observed periodicities. This is only of academic interest since the observed periodicity absorbs the constant factor and one never knows (or bothers to know) the exact periodicity of the signal at emission.

The recorded event times, after correction to the solar system barycentre and the centre of mass of the binary (where necessary), are then subjected to periodicity analysis. Generally one employs one of three methods for this: (i) epoch folding, (ii) the Rayleigh test, and (iii) the Protheroe test. In the epoch folding method, one folds the event times modulo the pulsar period, and a histogram is made of the resulting event phases. The cosmic ray background events are distributed over all the phase bins more or less uniformly, whereas the UHEGR signal events populate only one or a few of the phase bins. Any statistically significant excess in one or more bins is attributed to a pulsed UHEGR signal. In the Rayleigh test, one computes the Rayleigh power defined by

$$Q = \left\{ \left(\sum_{i=1}^{N} \cos \phi_i \right)^2 + \left(\sum_{i=1}^{N} \sin \phi_i \right)^2 \right\} \Big/ N \tag{5.9}$$

Here ϕ_i is the phase of the ith event and N is the total number of events. The UHEGR signal, if present, will result in large values of Q; see Mardia (1972) and Protheroe (1985*a*) for details. For a discussion on the relative merits of the epoch folding and Rayleigh tests, see Leahy, Elsner and Weisskopf (1983). The Protheroe test is designed specifically for cases where a narrow peak is expected to ride over a uniform background in phase distribution. Since this test is somewhat *ad hoc* in its formulation, one has to carry out a large number of Monte-Carlo calculations to gauge the significance of the Protheroe statistic; see Protheroe (1985*b*) for details.

Whenever one finds evidence for a periodic UHEGR signal, the expectation is that the signal rides over a uniform cosmic ray background, thus producing a DC excess over the rates for neighbouring intervals in time or in space. Sometimes one finds evidence only for a pulsed signal without any DC excess. A critical discussion on how to assess the statistical significance in such situations can be found in Lewis (1989).

5.3 Results on UHEGR emission

Porter and Weekes (1978) have summarised UHEGR flux values and upper limits in the energy range $10^{11} < E_\gamma < 10^{14}$ eV from nearly 100 celestial objects looked at by various experiments. The objects included pulsars (both steady and pulsed emissions), novae, supernovae, supernova remnants, magnetic

variables, flare stars, X-ray sources, BL Lac type objects, galaxies, galactic clusters and quasars. More recent summaries can be found in Grindlay (1982), Nagle, Gaisser and Protheroe (1988) and Weeks (1988); see also the proceedings of workshops on UHEGR held at Ooty (Ramana Murthy and Weekes 1982), Durham (Turver 1987), Little Rock (Yodh, Wold and Kropp 1990) and Ann Arbor (Matthews 1991) and the Rapporteur papers at the recent international cosmic ray conferences (Protheroe 1987, Fegan 1990, and Samorski 1992).

5.3.1 Galactic objects

5.3.1A A Crab pulsar/nebula

The Crab nebula, the best known SNR in the Galaxy, is located 2 kpc away from the solar system. The supernova explosion took place in the year 1054 AD, and is well documented in ancient Chinese records. Its angular size is a few arc min across as seen from the Earth. A 33 ms pulsar was discovered in the remnant by Staelin and Reifenstein (1968) and Comella *et al.* (1969). The pulsar is known to emit at other frequencies besides radio: optical (Cocke, Disney and Taylor 1969), X-ray (Fritz *et al.* 1969), and γ-ray (Hillier *et al.* 1970). With such ample evidence for the existence of high energy particles and the associated processes, it was natural that the Crab nebula and pulsar should be favourite objects to look at in almost all the previous observations on the UHEGR. Since, as already explained, the angular resolution of a source is seldom better than 1° in the observations at these energies, one cannot distinguish steady emissions from the pulsar and the nebula.

Chudakov *et al.* (1962, 1965) carried out the first extended observations on the Crab and set an upper limit of 5×10^{-11} photons $cm^{-2}\,s^{-1}$ at $E_\gamma > 5 \times 10^{12}$ eV. An interesting account of the early history of UHEGR observations can be found in Chudakov (1989). Fruin *et al.* (1964) and Long *et al.* (1965) set upper limits of 1.3×10^{-11} photons $cm^{-2}\,s^{-1}$ at $E_\gamma > 2.7 \times 10^{13}$ eV. Fazio *et al.* (1972), from a three-year observation of the Crab nebula with the 10 m dish at Mount Hopkins, found a positive effect at the 3.1σ level. The flux averaged over all the observation time was given as $(4.4 \pm 1.4) \times 10^{-11}$ photons $cm^{-2}\,s^{-1}$ at $E_\gamma > 2.5 \times 10^{11}$ eV. The authors noted, however, that much of the effect was contributed by runs during three separate periods, each between 60 and 120 days after an observed spin-up (glitch) of the pulsar; see Figure 5.10. If averaged only over these periods, the flux went up to $(1.21 \pm 0.24) \times 10^{-10}$ photons $cm^{-2}\,s^{-1}$ which was a 5σ effect.

The Whipple collaboration (Vacanti *et al.* 1991) have reported a spectacular success in the detection of γ-rays from the Crab in the TeV energy range by employing the imaging technique already described in Section 5.2.1. The authors tracked the Crab several times and also a blank background region (on–off method). The raw data showed a 5σ excess in the event rate in the direction of the Crab over the background. When the authors made a cut based on azwidth (angular width of the Cerenkov light image at the weighted centre perpendicular to the line joining the optic axis and the centre of the image), accepting only showers with azwidth $\leq 0.2°$, nearly 97% of the cosmic ray background was

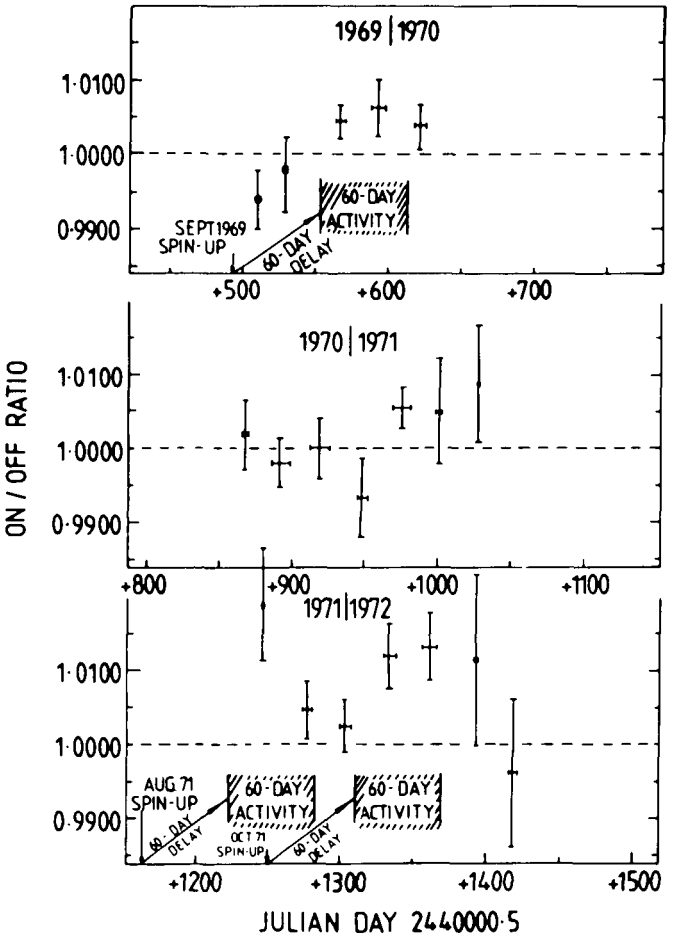

Figure 5.10. Ratio of the counts recorded from the Crab nebula/pulsar to those from an arbitrary reference direction (Fazio *et al.* 1972). The authors operated the Mount Hopkins 10 m reflector for three consecutive years. Notice the relationship in time between the pulsar spin-up epoch and on/off ratios greater than unity, signifying UHEGR emission by the Crab nebula/pulsar.

rejected, while 70% of the UHEGR signal was retained. This increased the statistical significance of detection to the 20σ level; the result is shown in Figure 5.11. The prescription for the cut was based on a Monte-Carlo calculation, made prior to the observations, by Hillas (1985) on the Cerenkov light image shapes produced by γ-ray and cosmic ray showers. The authors have deduced a DC (unpulsed) flux of 7×10^{-11} photons $\text{cm}^{-2}\,\text{s}^{-1}$ at $E_\gamma > 0.4$ TeV from the Crab with an integral spectrum of the type $E_\gamma^{-(1.4\pm0.3)}$ in the energy range $0.4\ \text{TeV} < E_\gamma < 4\ \text{TeV}$. The Whipple collaboration further finds that the steady emission is constant on a monthly basis, thus making the Crab a steady candle. The signal does not show the periodicity of the Crab pulsar seen at other

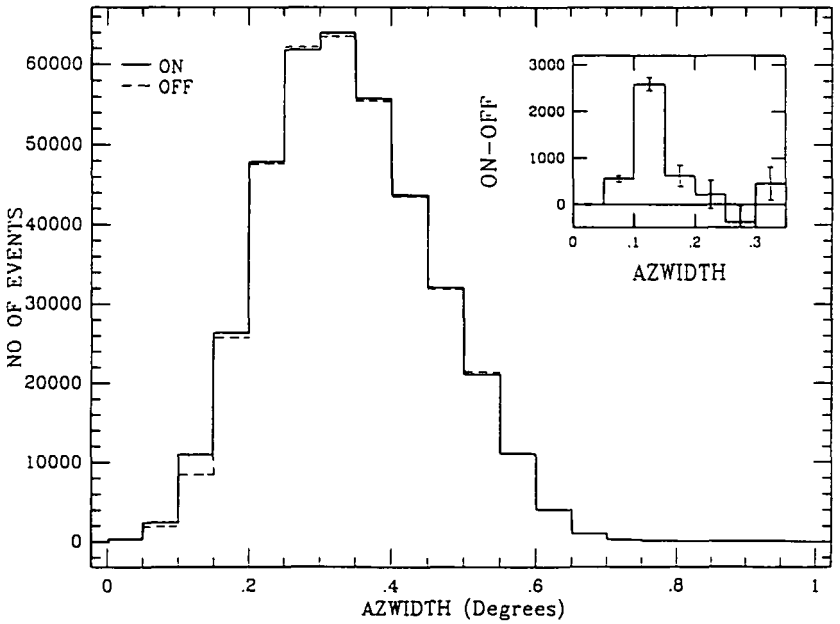

Figure 5.11. The azwidth distribution of the Cerenkov images in the data of the Whipple group (Vacanti *et al.* 1991) both in the on-source (the Crab) direction and in the off-source direction. Differences in the ON and OFF event numbers are shown in the inset as a function of azwidth. The γ-ray signal stands out clearly in the bins with azwidth less than 0.25°.

wavelengths. The result on the steady emission implies that the luminosity of the Crab at $E_\gamma > 0.4$ TeV is 8×10^{34} erg s^{-1}.

Light curves of emission of electromagnetic radiation by the Crab pulsar at various wavelengths were shown in Figure 4.11. The curves exhibit two peaks, the main and the interpulses being separated by 0.42 in phase. Emission of UHEGR from this object was studied in several experiments. The latest Whipple result sets an upper limit (99% confidence level) of 7×10^{-12} photons cm^{-2} s^{-1} at $E_\gamma > 0.4$ TeV. This result, along with some other earlier representative results, are shown in Table 5.1. The Ooty group (Gupta *et al.* 1978) observed two peaks in the phase plot of UHEGR with a mutual separation of 0.42 in phase, as was seen at lower energies. The UHEGR pulsed emission was not constant in time. The Mount Hopkins and the Ooty groups who observed the pulsar for several years detected signals during some observations but not during the others.

The Durham group (Gibson *et al.* 1982*b*) and the Ooty group (Vishwanath 1982) find that the emission of UHEGR is variable over days, tens of minutes, minutes or even tens of milliseconds. In particular, the Durham group (Gibson *et al.* 1982*b*) and the Ooty group (P.N. Bhat *et al.* 1986) have reported seeing bursts of pulsed UHEGR emission lasting for ~ 15 min at TeV energies, with the same periodicity as at the radio frequencies. The Ooty group has found some corroborative evidence from another atmospheric Cerenkov array which they

Table 5.1. *Results on pulsed emission of UHEGR from the Crab pulsar*

Time-averaged fluxes

Group	Epoch	Effect (σ)	Threshold energy (TeV)	Flux ($\times 10^{-11}$ cm^{-2} s^{-1})	Reference
Ooty	Feb., 1977	3.6, 2.2*	4.5	0.4**	Gupta *et al.* (1978)
				0.29	S.K. Gupta (1983, unpublished Ph.D. thesis)
	1978	–	2.5	<0.2	S.K. Gupta (1983, unpublished Ph.D. thesis)
	1979	–	1.9	<0.2	S.K. Gupta (1983, unpublished Ph.D. thesis)
	1980	–	1.5	<0.27	S.K. Gupta (1983, unpublished Ph.D. thesis)
	1985	5.1, 1.5*	1.2	25**	P.N. Bhat *et al.* (1986)
Durham	Oct., 1981	6.8	3	20**	Gibson *et al.* (1982*b*)
				0.15	
	1982	4.5	1.0	0.79	Dowthwaite *et al.* (1984*b*)
Edwards	1982	3.5	0.2	2.5	Tumer *et al.* (1985)
Whipple	1986–8	–	0.7	<0.45	Weekes *et al.* (1989)
	1988–9	–	0.4	<0.7	Vacanti *et al.* (1991)
Sandia	1987–8	–	0.2	<1.3	Akerlof *et al.* (1989)
Pachmarhi	1987–8	–	1.1	<0.6	P.N. Bhat *et al.* (1990*a*)
	1988–9	–	1.8	<0.2	
Ooty (PeV)	1984–7	–, 3.9	200	0.041	Gupta *et al.* (1991*b*)

* Two significant peaks are reported in the phasogram by the authors.
** When averaged over periods during which the effect was seen

operated simultaneously at a site 11 km away from the first. The γ-ray flux values, when averaged over the burst durations, are nearly two orders of magnitude higher than the steadily pulsating fluxes of UHEGR. We have shown in Figure 5.12 the time-averaged intensities or upper limits of the pulsed UHEGR flux at various energies presented in Table 5.1. Also shown in the figure is the extrapolation of the energy spectrum observed at medium high energies by the COS B satellite (Lichti *et al.* 1980). From the figure two points can be seen to emerge. (i) The intensities seem to show a scatter much larger than the uncertainties (a factor of around two) in thresholds and collection areas. If this scatter is due to variability of the source, it is not clear if one can obtain and draw any inference from the energy spectrum. (ii) If one assumes that the true long term time-averaged intensities lie along the points 4 and 5 in the figure, they are clearly one order of magnitude lower than the extrapolated line. It appears that the spectral index in the integral power law spectrum steepens from -1.17 at $E_\gamma \sim 1$ GeV to ~ -1.5 at $E_\gamma \lesssim 1$ TeV. Time-averaged luminosity of this object at $E_\gamma > 1$ TeV is $\sim 10^{34}$ erg s^{-1}, if one assumes that the emission is isotropic.

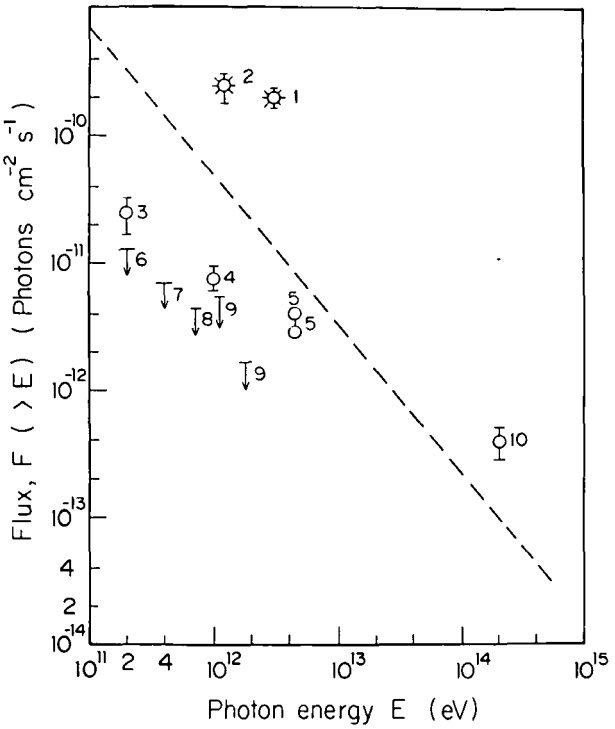

Figure 5.12. Time-averaged pulsed fluxes from the Crab pulsar as a function of energy. Data points 1 and 2 refer to burst emission, averaged over the duration of the burst. Dashed line: extrapolation from COS B data (Lichti *et al.* 1980). (1) Gibson *et al.* (1982*b*); (2) P.N. Bhat *et al.* (1986); (3) Tumer *et al.* (1985); (4) Dowthwaite (1984*c*); (5) Gupta *et al.* (1978); (6) Akerlof *et al.* (1989); (7) Vacanti *et al.* (1991); (8) Weekes *et al.* (1989); P.N. Bhat *et al.* (1990*a*); (10) Gupta *et al.* (1991*b*).

We next consider emission of UHEGR by the Crab at $E_\gamma \gtrsim 10^{15}$ eV. Dzikowski *et al.* (1983) observed this object during 1968–71 and again during 1975–82 using an air shower array. There was no fast timing information and, hence, the shower arrival directions could not be known. Since the air shower intensity drops with increasing zenith angle, the event time itself defines a broad probable right ascension region from which a shower arrived. When the authors sorted out their data into bins, 3 h and 2.5 h RA, they found an excess of 58.8 ± 14.6 showers riding a background of 115.2 events in the right ascension bin centred on the Crab nebula/pulsar region (5 h 30 m RA). This excess amounted to a flux of 2×10^{-13} cm^{-2} s^{-1} at $E_\gamma > 2 \times 10^{16}$ eV. Since the phase analysis of the event times was not given, one does not know if the excess showers are due to a pulsed component from the pulsar or due to steady emission from the nebula/pulsar. It may be pointed out that, since the source direction is known only crudely, $\Delta\theta \sim 30°$ in this observation, one cannot be sure that the UHEGR are coming from the Crab. When this flux is combined with the fluxes around 10^{12} eV from atmospheric Cerenkov work, the spectral index of the differential energy spectrum has a value

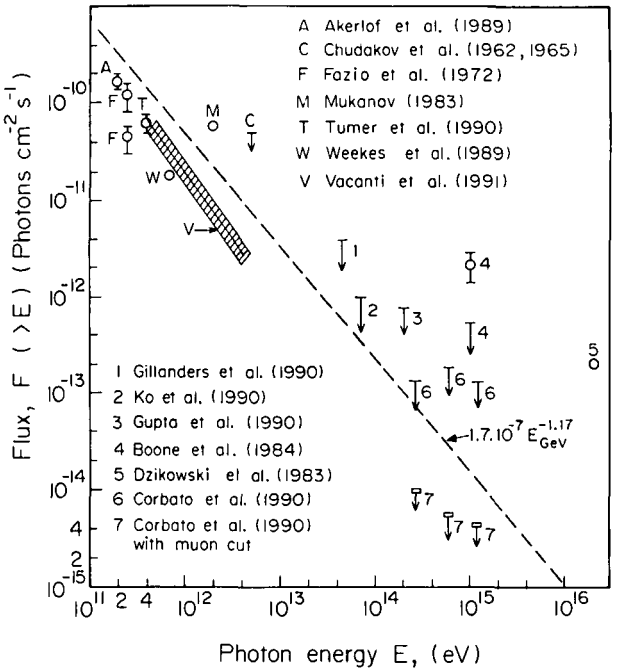

Figure 5.13. Unpulsed fluxes from the Crab nebula/pulsar as a function of energy. Dashed line: extrapolation from COS B data (Lichti *et al.* 1980).

-1.4, i.e. the spectrum is very flat. Dzikowski *et al.* found that muon densities in the showers from this bin are 0.6 of those from the other bins, a high value for primary γ-rays, as in the other claims (as detailed later on) on the Crab, Cygnus X-3 and Hercules X-1. The luminosity of the source at $E_\gamma > 2 \times 10^{16}$ eV is estimated to be $\sim 3 \times 10^{36}$ erg s^{-1}. The authors add that, although the γ-ray origin of the showers is preferred, it is just possible that the primaries are instead protons coming from the early stage of the supernova explosion; however, a remarkably low Galactic magnetic field is required for such a hypothesis.

Boone *et al.* (1984) observed the Crab nebula/pulsar region on December 9, 1980, and again on three nights in February, 1981, using their 'Fly's Eye' device to detect Cerenkov flashes initiated by cosmic ray/γ-ray primaries. The data were binned in 1 h wide right ascension bins based on event times (individual shower directions could not be determined). From the data taken on December 9, 1980, the authors found 34 ± 11 excess showers (a 3.1σ effect) in the right ascension bin centred on Crab nebula/pulsar. This yielded a flux of $(2.1 \pm 0.7) \times 10^{-12}$ cm^{-2} s^{-1} at $E_\gamma > 10^{15}$ eV. No signal was found in the 1981 data, corresponding to an upper limit of 5.3×10^{-13} cm^{-2} s^{-1} on the flux at $E_\gamma > 10^{15}$ eV, i.e. a factor of four lower than the flux value seen in the same experiment two months earlier. There is clearly the suspicion again that UHEGR emission from the Crab nebula/pulsar is variable. We have shown in Figure 5.13 and in Table 5.2 the unpulsed γ-ray fluxes from the Crab as reported by the various authors.

Table 5.2. *Results on unpulsed emission of UHEGR from the Crab*

Time-averaged fluxes

Group	Epoch	Effect (σ)	Threshold energy (TeV)	Flux ($\times 10^{-11}$ cm^{-2} s^{-1})	Reference
Sandia	1987–8	5.0	0.2	17	Akerlof *et al.* (1989)
Moscow	1960–2	–	5	<5	Chudakov *et al.* (1965)
Mount Hopkins	1969–72	3.1	0.25	4.4	Fazio *et al.* (1972)
Tienshan	1981–2	–	2	5.8	Mukanov (1983)
Sandia	1987	4.3	0.4	6.3	Tumer *et al.* (1990)
Whipple	1986–8	8.9	0.7	1.8	Weekes *et al.* (1989)
	1988–9	20	0.4	7.0	Vacanti *et al.* (1991)
Lodz	1968–82	4	2×10^4	0.02	Dzikowski *et al.* (1983)
Fly's Eye	1980	3	1000	0.21*	Boone *et al.* (1984)
	1989	–	70	<0.099	Ko *et al.* (1990)
Whipple (EAS)	1989	–	45	<0.39	Gillanders *et al.* (1990)
Ooty	1984–7	–	200	<0.077	Gupta *et al.* (1991*b*)
Utah–Michigan	1988–9	–	270	<0.023 <0.001**	Corbato *et al.* (1990)
KGF	Feb. 23, 1989	4	100	1.3*	Acharya *et al.* (1990*a*)

* When average over the burst duration.
** When μ-poor showers are selected.

Gupta *et al.* (1991*b*), on the basis of marginal evidence for pulsed emission coincidental with the interpulse (but not at the main pulse), have reported a time-averaged flux of $(4.1 \pm 1.2) \times 10^{-13}$ cm^{-2} s^{-1} at $E_\gamma > 2 \times 10^{14}$ eV.

A transient emission of UHEGR at PeV energies on February 23, 1989, has been reported by three different groups recently. Attention was first drawn to this episode by the Baksan group (Alexeenko *et al.* 1989). Soon, the other two groups (Acharya *et al.* 1990*a* and Aglietta *et al.* 1991) searched their data and found evidence for the burst. This was the first time that a burst of UHEGR at energies $\sim 10^{15}$ eV was reported by three different groups working at contiguous longitudinal belts. The observations are shown in Figure 5.14. It appears that, from these three reports and the null results reported by the Akeno and HEGRA arrays, that the burst lasted from four to eight hours. The time-averaged (over the burst duration) flux from this burst is $(1.3 \pm 0.4) \times 10^{-11}$ photons cm^{-2} s^{-1} at $E_\gamma > 10^{14}$ eV. The implied luminosity over the burst duration is 5×10^{36} erg s^{-1}, averaged over the duration of the burst. Two important features reported by the KGF group (Acharya *et al.* 1990*a*) are: (i) the muon density in the UHEGR signal is 0.93 ± 0.34 of that in the background cosmic ray showers (this aspect will be further discussed in Section 5.5); and (ii) the light curve, as is evident from Figure 5.15, shows that most of the UHEGR signal populates the pulsar phase region

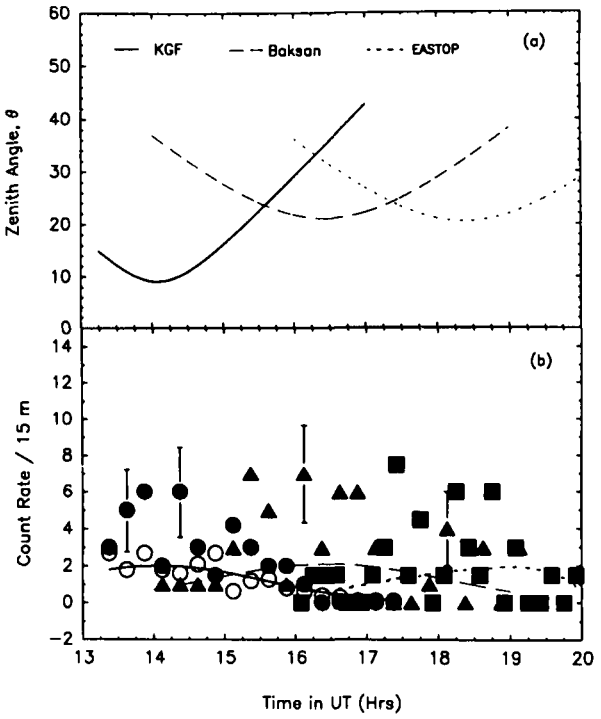

Figure 5.14. Data on the burst from the Crab seen by the Baksan, the Kolar Gold Fields (KGF) and the EAS–TOP groups on February 23, 1989. (*a*) Variation of the zenith angle of the source as a function of time in the three arrays. (*b*) Observed count rates/15 m for KGF (●), Baksan (▲) and EAS–TOP (■) arrays, and the expected backgrounds for KGF (○, ——), Baksan (– – –) and EAS–TOP (· · ·) arrays.

0.0–0.5; this suggests that the signal is coming from the Crab pulsar rather than from the nebula.

The implications of the various results described above will be briefly mentioned in Sections 5.4 and 5.5.

5.3.1B Vela pulsar

The Vela pulsar ($P = 89$ ms) is located 500 kpc away from the solar system. Being located in the southern skies, it is accessible for observation only from sites near the equator or in southern latitudes, and it has been observed so far only by three groups at TeV energies. Grindlay *et al.* (1975*b*) and Grindlay (1982) reported a time-averaged flux of $(1.0 \pm 0.3) \times 10^{-11}$ photons cm^{-2} s^{-1} at $E_\gamma > 3 \times 10^{11}$ eV, from their observations at Narrabi, Australia, during 1973–4. Based on the data taken at Ooty, India, during 1979–80, 1982–3 and 1984–5, P.N. Bhat *et al.* (1987*a*) claimed to have detected pulsed UHEGR from the Vela pulsar; the reported flux is $(9 \pm 3) \times 10^{-13}$ photons cm^{-2} s^{-1} at $E_\gamma > 5.4 \times 10^{12}$ eV. The most recently published result is from Brazier *et al.* (1990*a*), who carried out

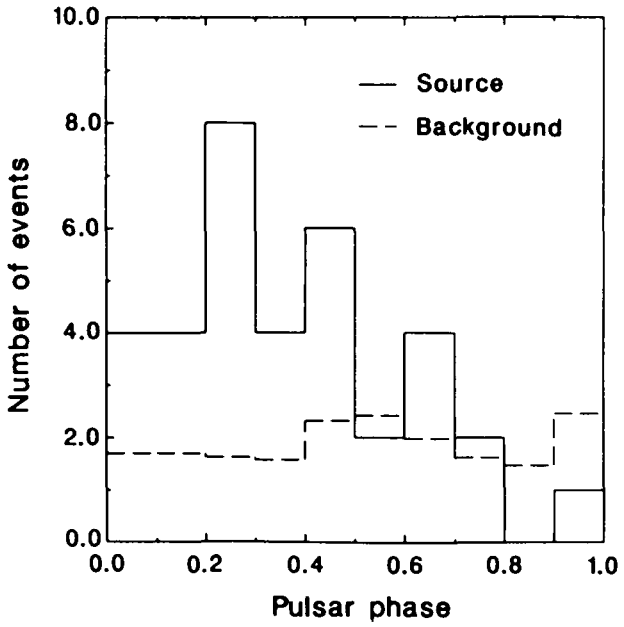

Figure 5.15. Phase (for Crab pulsar period) distribution of the events during the burst in the KGF data. Histogram with dashed lines is the same for background events.

measurements at Narrabri during 1987; these authors reported a 3σ upper limit of 7.5×10^{-11} photons $cm^{-2}\,s^{-1}$ at $E_\gamma > 3 \times 10^{11}$ eV, for the pulsed flux.

Results from all the above observations are presented in Figure 5.16. While it is clear from the figure that the observed fluxes and the upper limit are one to two orders of magnitude lower than the extrapolated values based on the COS B observations (Kanbach *et al.* 1980), more observations are needed to firmly establish that the Vela pulsar emits pulsed TeV γ-rays.

5.3.1C PSR0355+54

Located at a distance of ~ 1.5 kpc from the solar system, PSR0355+54 is an isolated short period (~ 156 ms) pulsar characterised by extremely low timing noise and occasional large glitches (Lyne 1987). P.N. Bhat *et al.* (1987*b*) observed this pulsar in December, 1987, at Pachmarhi, India. When the data were analysed for periodicity using a contemporaneous ephemeris, the authors found evidence (a 4.3σ peak) for steadily pulsating emission from the object, at a flux level of $(7.9 \pm 2.0) \times 10^{-12}$ photons $cm^{-2}\,s^{-1}$ at $E_\gamma > 1.3$ TeV. The result is shown in Figure 5.17. The same group observed this object again during October, 1989, to January, 1990, with a slightly modified reflector array, but found no evidence for any UHEGR emission (Acharya *et al.* 1991); the authors placed a 95% confidence level upper limit of 5.4×10^{-13} photons $cm^{-2}\,s^{-1}$ at $E_\gamma > 3.4$ TeV. The Whipple collaboration (Lamb *et al.* 1991) also observed this object during September–December, 1990, and did not find any evidence for pulsed emission with or without

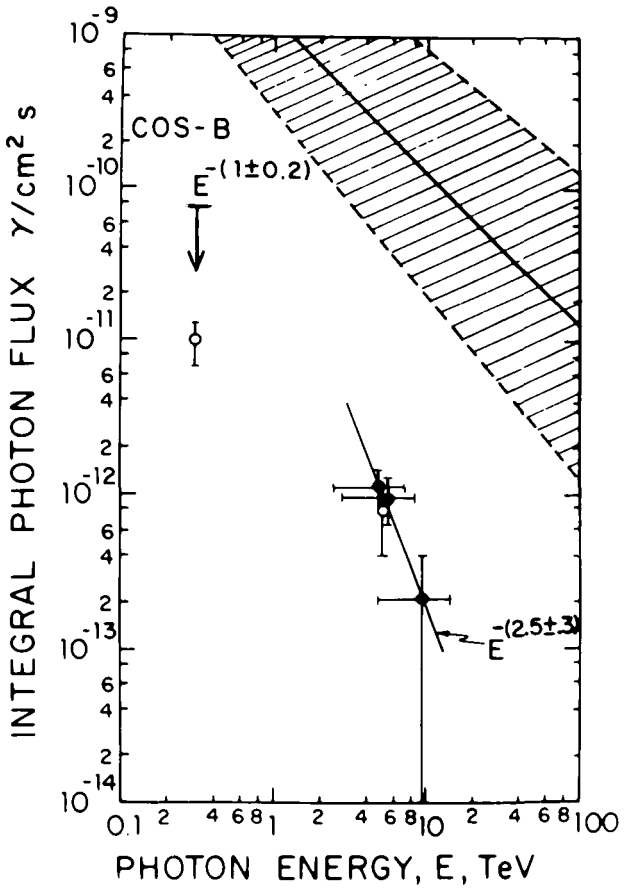

Figure 5.16. Integral energy spectrum of γ-rays from the Vela pulsar. O, ●: from Grindlay (1982), Grindlay *et al.* (1975*b*) and P.N. Bhat *et al.* (1987*a*). Upper limit is from Brazier *et al.* (1990*a*). The shaded region is the extrapolation from COS B data (Kanbach *et al.* 1980).

the azwidth cut; an upper limit of 2.2×10^{-12} photons $cm^{-2} s^{-1}$ was placed at $E_\gamma > 0.4$ TeV for pulsed emission.

5.3.1D Cygnus X-3

Cygnus X-3, located at ~ 11.4 kpc from the solar system, is an X-ray binary system, discovered by Giacconi *et al.* (1967). It has been seen in medium energy γ-rays by two groups (Galper *et al.* 1977 and Lamb *et al.* 1977), but not by COS B (Swanenburg *et al.* 1981 and Hermsen *et al.* 1987). Results on UHEGR emission at TeV energies by this object are summarised in Table 5.3. The Crimean Astrophysical Observatory group (Vladimirsky, Stepanian and Fomin 1973, Neshpor *et al.* 1979, Stepanian *et al.* 1982) carried out extensive observations on this object. Figure 5.18 (Vladimirsky *et al.* 1973) shows a drift scan in which it can be seen clearly that the object emits UHEGR. Later the authors showed that

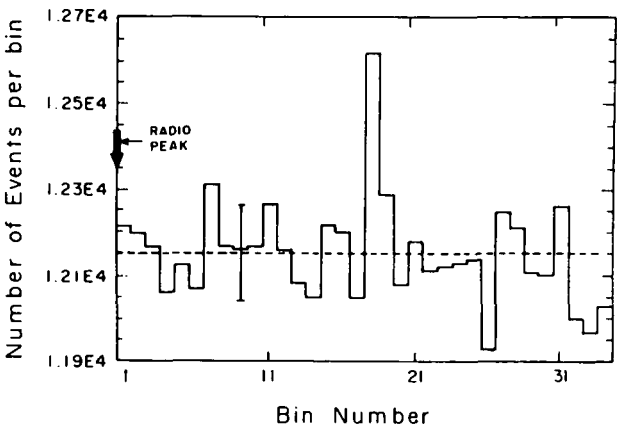

Figure 5.17. Phasogram of the events seen in the direction of PSR0355+54 by the Pachmarhi group (P.N. Bhat *et al.* 1990*b*). The 4.3σ peak occurs in the bin centred on phase 0.51 with respect to the radio main pulse.

Table 5.3. *Results on pulsed emission of TeV gamma-rays from Cygnus X-3*

Time-averaged fluxes

Group	Epoch	Effect (σ)	Phase	Threshold energy (TeV)	Flux ($\times 10^{-11}$ cm^{-2} s^{-1})	Reference
Crimea	1972–7	5.4, 3.0	0.15–0.20	2	18	Neshpor *et al.* (1979)
			0.78–0.83	2	9	
Mount Hopkins	1976	–	–	0.3	<6.5	Weekes and Helmken (1977)
Dublin/Mount Hopkins	1980	3.5	0.6–0.8	2	15	Danaher *et al.* (1981)
Iowa/JPL/UC	1981	4.4	0.5–0.7	0.5	8	Lamb *et al.* (1982)
Durham	1981, 1982	4.1	0.625–0.655	1.3	20*	Dowthwaite *et al.* (1983)
					0.3	

* Peak flux over 10 min interval.

the object pulsates with a period of 0.199683 d (~4.8 h) and also that the intensity is modulated with a 34.1 d period, also seen in X-rays. The 4.8 h period is interpreted as that of the binary orbital period, whereas the 34.1 d period is thought to be due to precession. A phasogram of UHEGR from this object is shown in Figure 5.19 (Danaher *et al.* 1981). After 1982, there were no convincing reports of 4.8 h periodicity at UHEGR; see Fegan (1990) and Ramana Murthy (1990). An examination of Table 5.3 reveals that (i) the intensity is variable in time, and (ii) whereas the Crimean group sees emission in two peaks at phases ~0.18 and 0.80 (X-ray minimum is taken as zero phase), the other groups see it in only one

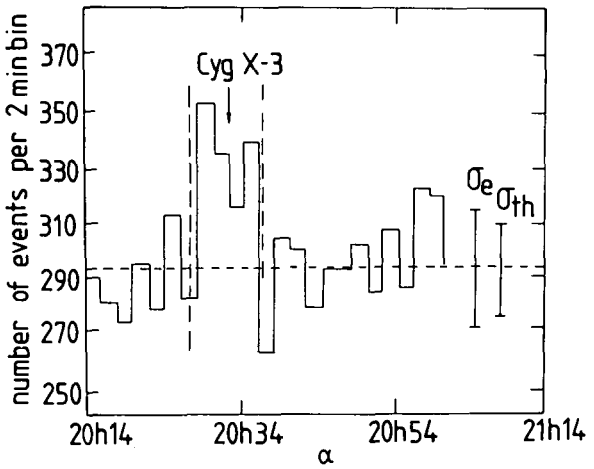

Figure 5.18. The first detection by the Crimean Astrophysical Observatory Group of UHEGR from Cygnus X-3; counts vs right ascension (Vladimirsky *et al.* 1973). σ_e: experimental standard deviation; σ_{th}: theoretical statistical error.

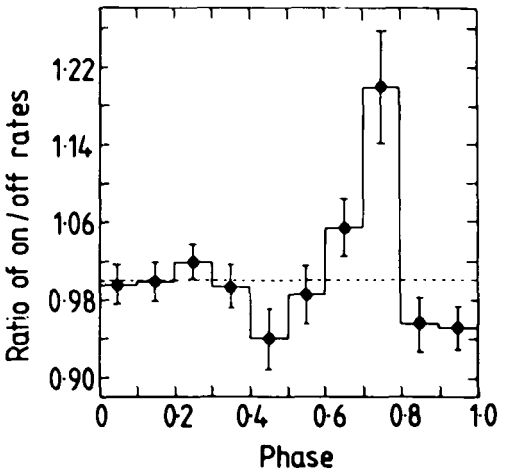

Figure 5.19. Phase histogram of UHEGR emission for Cygnus X-3 from the work of Danaher *et al.* (1981).

peak at ~0.5–0.8. Even among the latter, there are finer differences in the phase which perhaps arise from using differing X-ray ephemerides (Porter 1983). Neshpor *et al.* (1979) deduce that the luminosity of the source is 1.2×10^{37} erg s^{-1} during the first peak ($\phi \sim 0.18$) and 6×10^{36} erg s^{-1} during the second ($\phi \sim 0.80$), assuming isotropic emission. The object is seen to have high luminosity ($\sim 10^{37}$ erg s^{-1}) at PeV energies too; see below.

It was conjectured that the power house needed for such a high luminosity must be a pulsar with a period in the region of several to several hundred milliseconds.

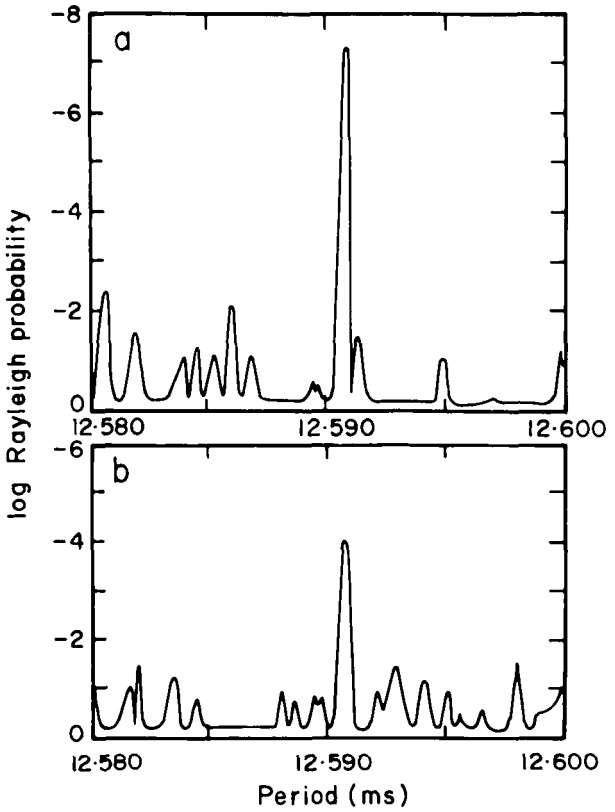

Figure 5.20. Chance probability for periodicity in the TeV showers recorded by Chadwick *et al.* (1985*a*) in the direction of Cygnus X-3 as a function of trial period. The upper panel shows the burst seen on September 12, 1983, and the lower panel shows that seen on October 2, 1983.

The object is unfavourably located for the pulsar to be detected in optical light. The radio size of the system is much too large (ten times the orbital separation) to let one detect a radio pulsar. An intense emission of TeV γ-rays over a 7 min duration on September 12, 1983, enabled Chadwick *et al.* (1985*a*) to carry out a periodicity search in TeV γ-ray emission. The authors claimed that they detected a TeV γ-ray pulsar with a period of 12.5908 ms; see Figure 5.20. Subsequently, the same group (Brazier *et al.* 1990*b*) reconfirmed their own discovery, having observed the 12.6 ms periodicity on several occasions. The total data set enabled Brazier *et al.* (1990*b*) to derive the first time derivative of the period to be $(1.9 \pm 0.3) \times 10^{-14}$ s s^{-1}; see Figure 5.21. This claim, however, was not confirmed by the Haleakala (Resvanis *et al.* 1987*a*), Whipple (Fegan *et al.* 1989) and Pachmarhi (P.N. Bhat *et al.* 1988) groups, who searched their data on Cygnus X-3 for the 12.6 ms periodicity. Even when the Haleakala and the Pachmarhi groups restricted the search to the very narrow windows in period and in 4.8 h phase, as specified by the Durham group, there was no evidence for the 12.6 ms

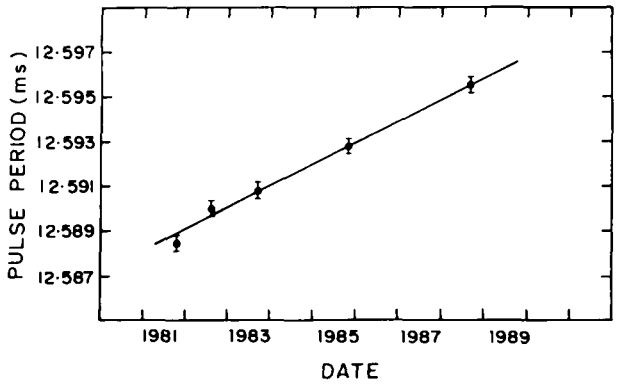

Figure 5.21. Variation in the 12.6 ms period of the pulsar in Cygnus X-3 from TeV γ-ray observations of the Durham group (Brazier *et al.* 1990*b*) between 1981 and 1988. The slope is given by $(1.9 \pm 0.3) \times 10^{-14}$ s s^{-1}.

periodicity. Gregory *et al.* (1990), observing Cygnus X-3 with their atmospheric Cerenkov detector at large zenith angles (72–80°) reported detecting pulsed UHEGR at energies above 10^{14} eV with a period 12.5953 ± 0.0002 ms and at the 4.8 h phase of 0.55–0.58, whereas the predictions based on Brazier *et al.* (1990*b*) prescriptions were 12.5962 ms and 0.62, respectively. It is not clear if the claim of Gregory *et al.* can be taken as confirmation of the Durham group's claim in view of the differences between the predictions and observations.

Barring the Durham group, no group ever found a Rayleigh power exceeding 12.6 (compare with 16.8 found in the discovery by Chadwick *et al.* 1985). Also, occurrences of Rayleigh powers in the range 10–12.5 at 4.8 h phases far removed from 0.625, the value recommended by the Durham group, are not uncommon. It must be pointed out that the 12.6 ms pulsations are not seen even by the Durham group every time they look at Cygnus X-3 around the 4.8 h phase of 0.625. It is just possible that the 12.6 ms pulsations even at the 4.8 h phase of 0.625 are quite rare, and it so happened that the pulsations did occur during the Durham group's observations but not during the others. In view of all this, there is a clear need for the 12.6 ms periodicity to be confirmed by an independent group before accepting its reality.

Turning to PeV energies, the Kiel group (Samorski and Stamm 1983*a*,*b*, Stamm and Samorski 1983) published impressive evidence for having detected pulsed UHEGR at $E_\gamma > 10^{15}$ eV from Cygnus X-3. These authors operated a 28 scintillator (each 1 m^2 in area) array at Kiel for four years (1976–9). They also recorded fast (nanosecond) timing information from 22 detectors, which enabled them to determine the shower direction to an accuracy of around 1°. The authors could determine for each shower the size N (to an accuracy of $\pm 30\%$), core location (± 1 m), and age parameter s (± 0.1).

The authors plotted the shower directions in bins of $\sim 4° \times 3°$ in right ascension–declination grid. Although they did not find any excess in the Cygnus X-3 direction compared to the background among the showers with $s < 1.1$, they

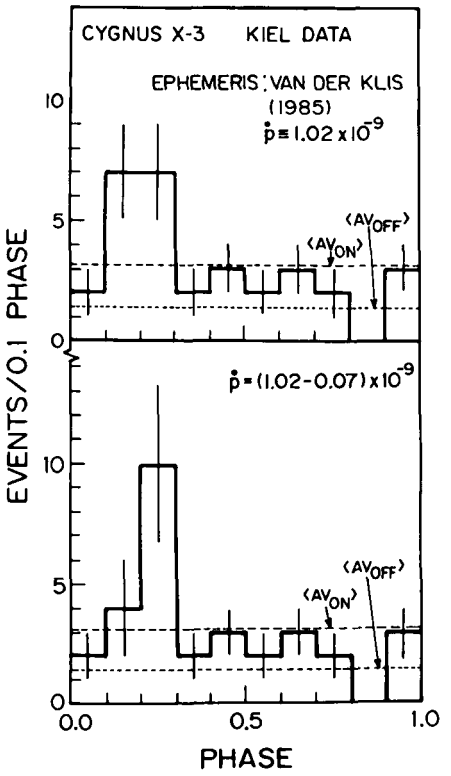

Figure 5.22. Phasograms ($P = 4.8$ h) of the Kiel group's data on Cygnus X-3 using barycentre event times and van der Klis ephemeris (Samorski and Stamm 1985). Phasograms in the upper and lower panels are computed with $\dot{P} = 1.02 \times 10^{-9}$ and 0.95×10^{-9} s s^{-1}, respectively. Background showers simulate both the DC excess and the periodicity only at a probability level of 7×10^{-7}.

found a 4.4σ excess for showers with $s > 1.1$; they found 31 showers when the average for the bin was 14.4. The probability that the average fluctuated to 31 or more is $\sim 10^{-4}$. Regarding the periodicity of the signal, Stamm and Samorski used in their discovery papers of 1983 an X-ray ephemeris given by Parsignault *et al.* (1976) and heliocentric event times to derive the phasogram. Later the same authors (Samorski and Stamm 1985) used the more accurate ephemeris given by van der Klis (published later by van der Klis and Bonnet-Bidaud 1989), corrected the event times to the solar system barycentre, and made the phase analysis; the result is shown in Figure 5.22. The authors state that, based on both the DC excess of events in the direction of Cygnus X-3 and periodicity test, the null hypothesis (that the effect is produced by chance fluctuations in the background) is ruled out; i.e. it is probable only at a level of $\sim 7 \times 10^{-7}$. The authors give a time-averaged flux of $(7.4 \pm 3.2) \times 10^{-14}$ photons cm^{-2} s^{-1} at $E_\gamma > 2 \times 10^{15}$ eV.

Turning to the question of luminosity, Cawley and Weekes (1984), assuming a distance to the source of 11.4 kpc, correct the above flux for absorption due to interaction of UHEGR with the 2.7 K black body radiation (a correction factor

of 3.3) and estimate the luminosity at $E_\gamma > 2 \times 10^{15}$ eV to be 2×10^{37} erg s^{-1}. This may be compared with luminosities of this object at X-rays and at all energies in excess of 10^5 eV of 10^{37} and 2×10^{38} erg s^{-1}, respectively. Samorski and Stamm (1983*a*) deduced the energy spectrum of γ-rays from this object to be

$$N(>E_\gamma) = (2.5 \pm 0.9) \times 10^{-7} E_\gamma(\text{GeV})^{-1.128 \pm 0.013} \text{ cm}^{-2} \text{ s}^{-1} \qquad (5.10)$$

by combining all the data in the range 10^8 eV $< E_\gamma < 10^{16}$ eV. The authors should have seen several events above $E_\gamma > 2 \times 10^{16}$ eV on the basis of extrapolation of the above spectrum but saw none; thus, there is probably a cut-off or steepening of spectrum above about $E_\gamma > 2 \times 10^{16}$ eV.

Samorski and Stamm (1983*c*) have also observed muons in the showers; the ratio of average muon densities at 10 m distance from the shower core being given as

$$\langle \rho_\mu(10 \text{ m})_{\text{on}} \rangle / \langle \rho_\mu(10 \text{ m})_{\text{off}} \rangle = 0.77 \pm 0.09 \qquad (5.11)$$

Here the subscript 'on' refers to showers in the source direction (γ-rays with negligible EAS background) and 'off' to those in other directions (all are EAS). This ratio is much larger than the value expected for γ-ray initiated showers – a fact that is hard to understand; see Section 5.5 for a discussion.

Lloyd-Evans *et al.* (1983*a*,*b*) observed Cygnus X-3 for four years during 1979–82 with the Haverah Park, UK, air shower set-up. These authors also found an excess of showers (1.7σ) in the direction of Cygnus X-3. When they analysed the event times of showers in the Cygnus X-3 direction for periodicity using the ephemeris of van der Klis and Bonnet-Bidaud (1981), they found that the phasogram shows a peak in the phase interval 0.225–0.250. They saw 73 events in this phase bin, whereas the average is 39. The statistical chance of observing such a peak in any one of the 40 bins is 2.8×10^{-5}, and anywhere in the entire plot, $40 \times 2.8 \times 10^{-5} \sim 10^{-3}$. The authors give an integral flux of $(1.5 \pm 0.3) \times 10^{-14}$ cm^{-2} s^{-1} at $E_\gamma > 3 \times 10^{15}$ eV, which is a factor of around three lower than the Stamm and Samorski flux values. Lloyd-Evans *et al.* found, in agreement with the Kiel group, that the spectrum steepens at $E_\gamma > 2 \times 10^{16}$ eV. Lloyd-Evans *et al.* did not present any data on muon densities.

C.L. Bhat, Sapru and Razdan (1986) have analysed data taken during 1976–7 in an experiment that detected atmospheric Cerenkov light produced by EAS and UHEGR at energies greater than 5×10^{14} eV. The experiment was carried out at Gulmarg, India, at an altitude of 2743 m above sea-level. It consisted of recording coincidences between two photomultipliers facing upwards to the sky during clear moonless nights. The field of view was large, with a cone of half-angle 70°. The authors analysed the event times to see if they exhibited the 4.8 h periodicity appropriate to Cygnus X.3. The 'on-source' events, i.e. events in the approximate right ascension range, 1600–0000 h, exhibited a 4.5 peak in the phase interval $\phi = 0.55$–0.60, whereas the 'off-source' events (in the right ascension range 0000–1600 h) did now show a peak. From this the authors deduced a flux of $(1.6 \pm 0.4) \times 10^{-12}$ cm^{-2} s^{-1} for UHEGR at $E_\gamma > 5 \times 10^{13}$ eV. This flux is higher, by a factor of 4.7, than that given by the Stamm–Samorski spectrum, and

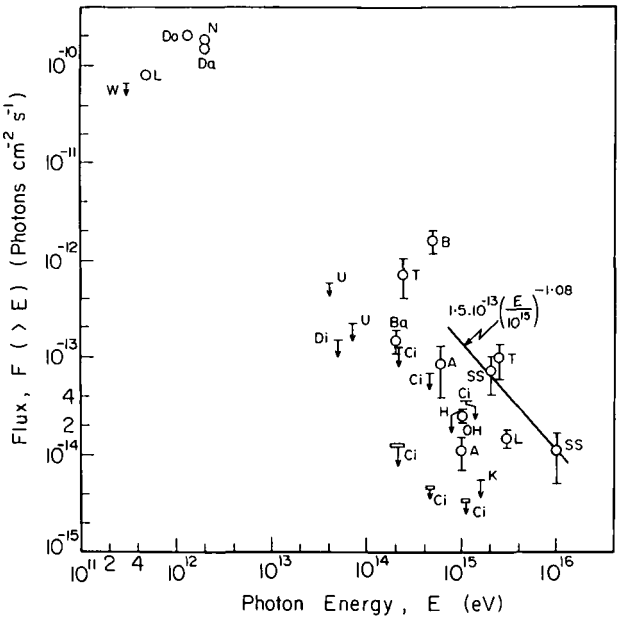

Figure 5.23. Integral energy spectrum of γ-rays from Cygnus X-3. Data are from Neshpor *et al.* (1979) (N); Weekes and Helmeken (1977) (W); Danaher *et al.* (1981) (Da); Lamb *et al.* (1982) (L); Dowthwaite *et al.* (1983) (Do); Cassiday *et al.* (1990*a*) (U); Dingus *et al.* (1988*a*) (Di); Protheroe (1987) (Ba); Ciampa *et al.* (1990) (Ci); C.L. Bhat *et al.* (1986) (B); Kifune *et al.* (1986) (A); Muraki *et al.* (1991) (OH); M.V.S. Rao (1986, private communication) (K); Lloyd-Evans *et al.* (1983*a*,*b*) (L); Samorski and Stamm (1983*a*,*b*) (SS); and Tonwar *et al.* (1988) (T). The Utah–Michigan collaboration (Ci) has given upper limits with muon cuts (lower set of points) and without the cuts (upper set of points). The straight line is the fit given by Samorski and Stamm (1983*a*).

may point to a decreasing intensity of emission with time as conjectured by Rana *et al.* (1984).

The discovery by Stamm and Samorski that Cygnus X-3 emits UHEGR at energies above 10^{15} eV triggered a large number of experiments all over the world to confirm and improve upon the original discovery. There have been many reports from these observations on Cygnus X-3. For the most part, the fluxes are lower by one to two orders of magnitude compared to the Stamm–Samorski fluxes. Moreover, the situation is quite confusing, with some groups seeing the signal with muon-poor selection, others without it; some with a cut on the age parameter, others without it; and some seeing both a DC excess and 4.8 h periodicity, others seeing only one of these attributes. Several groups observed peaks in the 4.8 h phase plots at phases different from 0.2, the value seen in the discovery. For details on all these aspects, see the Rapporteur papers by Protheroe (1987), Fegan (1990) and Samorski (1992) at the international cosmic ray conferences held at Moscow, Adelaide and Dublin respectively. We show a sample of results on fluxes of UHEGR from Cygnus X-3 in Figure 5.23.

There have been reports from three groups on the UHEGR emission at energies $E_\gamma \gtrsim 10^{18}$ eV. The Fly's Eye group (Cassiday *et al.* 1989, 1990*b*) reported a flux of 4×10^{-18} cm^{-2} s^{-1} above 2×10^{18} eV, which implies a luminosity of 1.9×10^{35} erg s^{-1} at these energies. A 4.8 h periodicity test shows that the events are concentrated in the phase region $0.05 < \phi_{4.8h} < 0.35$. The Haverah Park group (Lawrence *et al.* 1989, 1990), however, do not confirm this result; the authors have stated that at the 95% confidence level, the UHEGR flux is less than 4×10^{-18} cm^{-2} s^{-1} at $E_\gamma > 0.5 \times 10^{18}$ eV (a factor of four lower than the Fly's Eye result, assuming an E_γ^{-1} spectrum), if the signal is due to neutral hadrons, and a factor of two higher if the signal is due to photons. The Akeno group (Teshima *et al.* 1990) have reported a flux of $(18 \pm 7) \times 10^{-18}$ cm^{-2} s^{-1} at $E_\gamma > 0.5 \times 10^{18}$ eV; these authors found that the signal does not show any 4.8 h periodicity. Faced with the discrepancy between the Haverah Park result and the other two, and the differences between the detailed feaures of the showers in the observations of the Fly's Eye and the Akeno groups, it is not clear if one can accept the emission of UHEGR at $E_\gamma > 10^{18}$ eV as real. Jones (1990) has pointed out that at energies $\lesssim 10^{18}$ eV, neutrons can live long enough to survive the journey from the source to Earth and, indeed, under certain conditions, may even dominate photons in the 'UHEGR' signal.

The Soudan group (Marshak *et al.* 1985) reported detecting muons deep underground (depth: 1900 hg cm^{-2}; atmospheric muon energy threshold: 0.6 TeV) in the direction of Cygnus X-3, exhibiting a 4.8 h periodicity, and resulting in a flux of 7.3×10^{-11} muons cm^{-2} s^{-1}. Soon after, the Mont Blanc group (Battistoni *et al.* 1985) analysed the muon data from their nucleon decay detector (depth: 5000 hg cm^{-2}; atmospheric muon energy threshold: 3 TeV) and found excess muons in the approximate direction of Cygnus X-3 showing a 4.8 h periodicity at a flux level of 5×10^{-12} muons cm^{-2} s^{-1}. One cannot understand these results in terms of conventional physics, and a large number of papers were published incorporating new ideas and new physics. However, the Kamiokande group (Oyama *et al.* 1986) did not confirm the above findings. Upper limits to excess muon fluxes in the direction of Cygnus X-3 given by this group were 3.7×10^{-12} and 1.7×10^{-12} cm^{-2} s^{-1} for depths of 2400 and 5000 hg cm^{-2}, respectively. A detailed review of both the observations and the implications (if the effect is real) can be found in Weekes (1988).

To sum up, the evidence of UHEGR signals presented by the Kiel and Haverah Park groups is quite convincing, though one does not understand at this stage why muon densities in such γ-ray initiated showers in the Kiel data are so large and why one does not see the UHEGR signal in many of the observations undertaken after 1983. With planned large exposures by the Utah–Michigan–Chicago air shower array (Rosenberg 1991), one can expect a definitive answer on the fluxes of UHEGR from Cygnus X-3 at PeV energies quite soon.

5.3.1E Hercules X-1

This object, discovered by Tannanbaum *et al.* (1972), is a pulsating and eclipsing X-ray binary located at a distance of 5 kpc from the solar system. In

optical light, and in X-rays, the source shows modulations on the time scales of 1.24 s (period of the neutron star), 1.7 d (binary orbital period), and 35 d (precession of the accretion disk?). Hercules X-1 is not a radio source; nor has it been seen in medium energy (~ 1 GeV) γ-rays. The X-ray period of the neutron star varies with time, somewhat irregularly but confined to a range 0–10 μs/y; see Sunyaev *et al.* (1990). Trumper *et al.* (1978) detected two spectral features at 58 and 110 keV, which were interpreted as being due to quantised electron (Landau) levels, indicating a surface magnetic field strength of 3.5×10^{12} G.

The Durham group, Dowthwaite *et al.* (1984*c*), observed this source on April 17, and during July 3–13, and October 7–11, 1983. During one of the four scans on April 17, the authors saw a count rate in excess of 3σ for three minutes periodic at a $>3\sigma$ level at the X-ray period. The peak γ-ray flux at $E_\gamma > 1000$ GeV during the burst activity was 1.2×10^{-9} cm^{-2} s^{-1}. The outburst occurred at a phase of 0.76 in the 1.7 d period and 35 d before a detected turn-on in X-rays. The July data, however, showed an overall periodicity only at the 2σ level. The best period determined by the authors from their own data, $P = 1.237787$ s, agrees well with that derived from the contemporary X-ray measurements. The time-averaged flux is given by the authors as $(3 \pm 1.5) \times 10^{-11}$ cm^{-2} s^{-1} at $E_\gamma > 1$ TeV. The time-averaged luminosity at $E_\gamma > 1$ TeV from Hercules X-1 is computed by the authors to be 2×10^{35} erg s^{-1}, a value which is 0.5% of the X-ray luminosity, including soft X-rays.

The Whipple group carried out extensive observations on Hercules X-1 (see Weekes 1988 for a summary) at TeV energies. They detected several episodes of pulsed γ-ray emission lasting for a few to several tens of minutes. In most of the observations, the period at TeV γ-rays differed from that at X-rays, the differences being in the range -1.0 to $+0.8$ ms; these differences are much larger than the variations in the X-ray periods. It is important to note that the differences are not due to Doppler shifts introduced by the orbital motion of the neutron star; event times were corrected to the centre of mass of the binary before carrying out the periodicity tests. Two of the episodes are remarkable. The UHEGR emission in the episode on June 16, 1985, continued for at least 70 min, even after the neutron star had gone into eclipse by its companion; Gorham and Learned (1986) have suggested that the high energy proton beam produced by the pulsar is steered in the magnetic field of the companion star before hitting the target producing UHEGR. In the other episode, the one that occurred on June 11, 1986 (Lamb *et al.* 1988), the UHEGR signal showed a periodicity of 1.2358 s, 2.1 ms (-0.16%) lower than the X-ray period. Likewise, the episode observed at TeV energies by the Haleakala collaboration (Resvanis *et al.* 1988) on May 13, 1986, as well as the two episodes observed at PeV energies by the Los Alamos collaboration (Dingus *et al.* 1988*b*) on July 24, 1986, showed the same anomalous period as in the case of Whipple. Figure 5.24, taken from Goodman (1990), shows the evidence for an anomalous period in the data of the three observations. The Ooty group (Gupta *et al.* 1990) claimed to have seen four separate episodes over a span of few months during the same year. Each of these episodes was, however, statistically not so strong as those in the three references cited above. Gupta *et al.*

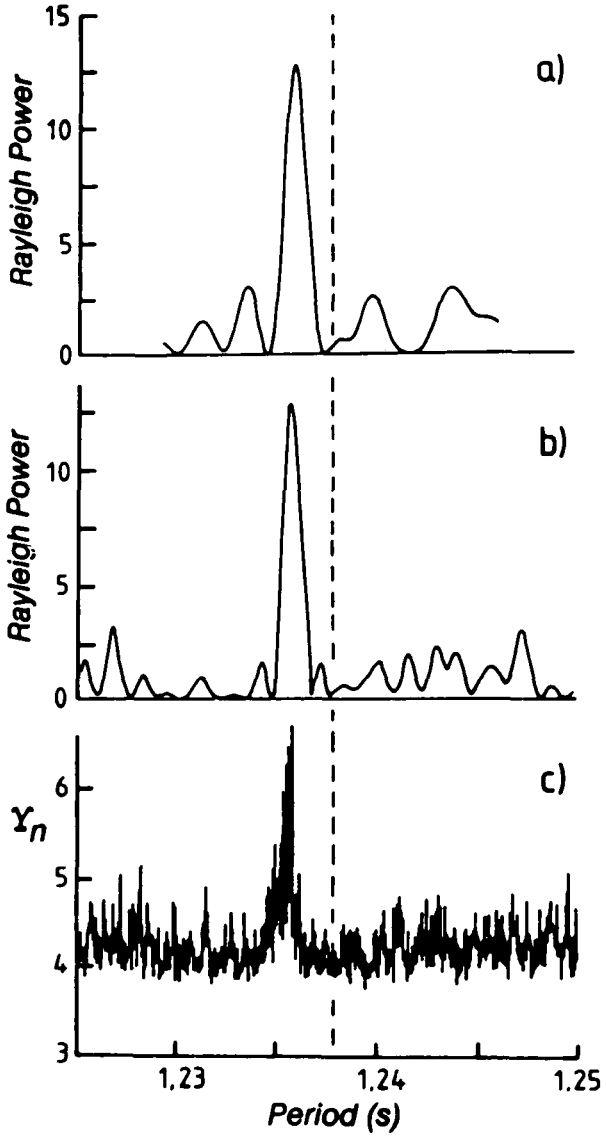

Figure 5.24. Results of periodicity search in the episodes from Hercules X-1 by (*a*) the Haleakala group; (*b*) the Whipple group; and (*c*) the Los Alamos group, as presented by Goodman (1990). Peaks indicate that fluctuations in the background cannot mimic the periodicity signature of the data. The three peaks align well at a period $P = 1.2358$ s, which is distinctly lower than the X-ray period, 1.2379 s, shown by the dashed line.

combined data from all their episodes to show that the period was the same as in the case of the other three. Lewis, Lamb and Biller (1991), however, have criticised the procedure of obtaining a precise period by combining data segments with large gaps when each segment does not show by itself strong evidence for

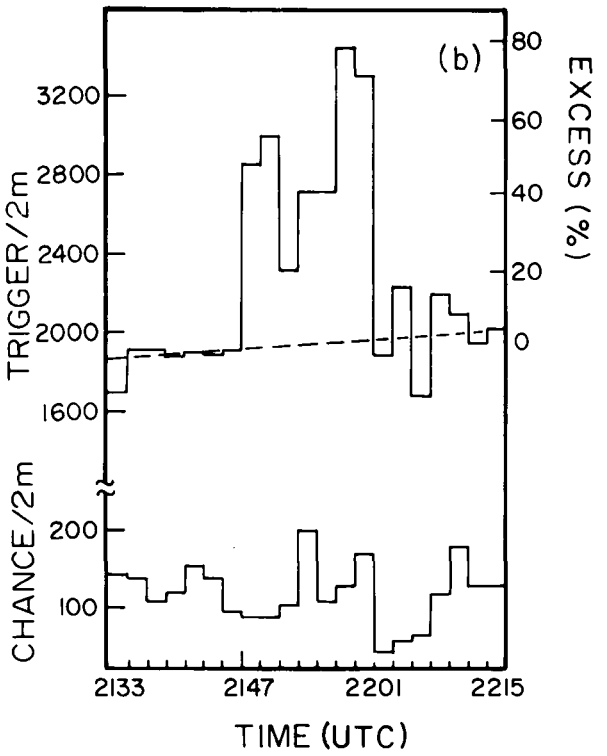

Figure 5.25. Trigger and chance coincidence rates as a function of time during the burst of TeV γ-rays seen by the Pachmarhi group (Vishwanath *et al.* 1989) in the direction of Hercules X-1 on April 11, 1986.

periodicity. There have been more results published by other groups, some seeing UHEGR pulsations at the same anomalous period (-0.16% w.r.t. the X-ray period), a greater anomalous (-0.34%) period and no anomaly (i.e. same period as at X-rays); see Fegan (1990) for a review of all these results. Possible explanations for the emission of UHEGR with periods different from the X-ray periods were offered by K.S. Cheng and Ruderman (1989) and Slane and Fry (1989); these will be elaborated in Section 5.4.

The Pachmarhi group (Vishwanath *et al.* 1989) observed one 14 min episode of TeV γ-ray emission by Hercules X-1. The authors noted an enormous increase in the trigger rate in the on-line monitor, whereas there was none in the chance coincidence rate. Results from the off-line analysis are shown in Figure 5.25. After presenting arguments against spurious causes, the authors interpreted the excess triggers over the interpolated background base line, as being due to γ-rays. The time-averaged (over the burst duration) flux is given as $(1.80 \pm 0.04) \times 10^{-8}$ photons $cm^{-2}\,s^{-1}$ at $E_\gamma > 0.4$ TeV. If one assumes a differential energy spectrum of the type E_γ^{-3}, the luminosity of the source during the burst comes out to be 1.8×10^{37} erg s^{-1}. The 1.7 d and 35 d phases at the time of the burst are 0.19 and 0.31, respectively. A malfunctioning of the event time recording system prevented

the authors carrying out a reliable periodicity test. The same group saw no further bursts in their 1987 (16.7 h), 1988 (7.3 h), 1989 (31.9 h) and 1990 (42.2 h) data.

The Fly's Eye group (Baltrusaitis *et al.* (1985) observed Hercules X-1 at PeV energies during five consecutive nights, July 10–14, 1983. The authors performed the periodicity test on the data of each night and found evidence for pulsations with the X-ray period only during 40 min (the first half of the night of July 11) of observation but not during the other nights. The observed signal corresponds to a flux of $(3.3 \pm 1.1) \times 10^{-12}$ photons $cm^{-2}\,s^{-1}$ at $E_\gamma > 5 \times 10^{14}$ eV, leading to an estimated luminosity of 10^{37} erg s^{-1} in PeV γ-rays during the episode. A large number of reports on Hercules X-1 at PeV energies were presented at the recent international cosmic ray conferences held at Adelaide and Dublin. Almost all the observations yielded no positive results. For a summary of the results, see the Rapporteur papers of Fegan (1990) and Samorski (1992).

As in the case of the Crab and Cygnus X-3, some observations on Hercules X-1 do seem to suggest that the 'UHEGR' signal is non-photonic in nature. Dingus *et al.* (1988*b*) found that, in the two episodes on July 24, 1986, the muon density in the signal is the same as (or even greater than) in the background cosmic ray showers. The Whipple group (Lewis *et al.* 1988) have reported that the TeV 'UHEGR' signal, seen so clearly in the episode on June 11, 1986, in the full data set, vanishes when the azwidth cut is applied; recall that the azwidth cut was designed to reject cosmic ray showers and retain the γ-ray signal. We will return to this topic in Section 5.5.

5.3.1F Vela X-1

Vela X-1 is an X-ray binary in the southern skies located 1.4 kpc away from Earth in the direction R.A. = 09 h 00 m and decl. = $-40°21'$. At X-ray energies the system exhibits two periodicities: one at $\sim$283 s, attributed to the rotation of the neutron star, and another at 8.96 d, attributed to the orbital motion. Protheroe, Clay and Gerhardy (1984) were the first to claim that the object emits UHEGR at PeV energies with a periodicity of 8.96 d. These authors saw eight showers in the phase bin centred on $\phi_{8.96d} = 0.65$ when the background was 1.5 events. The time-averaged flux is given by the authors as $(9.3 \pm 3.4) \times 10^{-15}$ photons $cm^{-2}\,s^{-1}$ at $E_\gamma > 3 \times 10^{15}$ eV; this corresponds to a luminosity of $\sim 2.3 \times 10^{34}$ erg s^{-1}. Subsequently the Potchefstroom group (North *et al.* 1987, Raubenheimer *et al.* 1989) detected repeatedly pulsed ($P = 283$ s) Tev γ-rays from this object. There were more observations by other groups, both at TeV and PeV energies; see Protheroe (1987) and Fegan (1990) for details. The energy spectrum of UHEGR from this object is shown in Figure 5.26.

5.3.1G Galactic Plane

At medium high energies ($\sim$1 GeV), a prominent feature of the γ-ray sky is the emission of γ-rays by the entire Galactic Plane, reaching a peak in the direction of the Galactic Centre; see Figures 4.5 (from SAS II) and 4.9 (from COS B). One can expect similar features at UHEGR. Berezinsky and Kudryavtsev (1990) predicted a γ-ray flux of 6.6×10^{-13} $cm^{-2}\,sr^{-1}\,s^{-1}$ at $E_\gamma > 10^{14}$ eV from

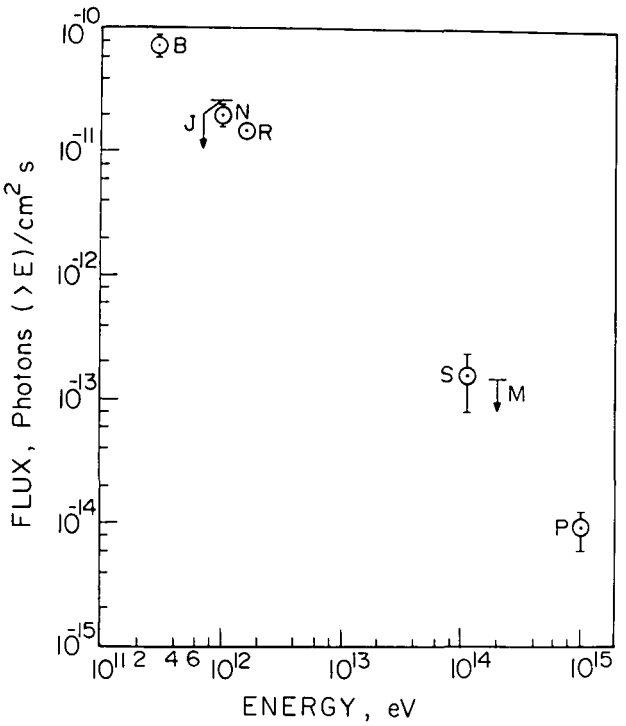

Figure 5.26. Integral energy spectrum of γ-rays from Vela X-1. Data are from Carraminana *et al.* (1989) (B); Bond *et al.* (1990) (J); North *et al.* (1987) (N); Raubenheimer *et al.* (1989) (R); Suga *et al.* (1987) (S); Matano *et al.* (1990) (M); and Protheroe *et al.* (1984) (P).

the Galactic Centre. The authors expect the angular spread to be in the ranges $320° < l < 40°$ and $-1° < b < +1°$, as in the case of medium high energy γ-rays. One must, however, recognise here that it is not easy to establish emission of UHEGR from the Galactic Plane or the Galactic Centre; the cosmic ray background is far greater in the ground-based observations at UHEGR than in the satellite-borne observations at medium high energy γ-rays.

The Crimean Astrophysical Observatory group (Fomin, Vladimirsky and Stepanian 1977, Stepanian *et al.* 1982) found that there is a deficit of $-(0.7 \pm 0.2)\%$ of high energy events from the Galactic Plane over a wide range of latitudes, $320° < l < 170°$ and $|b| < 1.5°$. The result is shown in Figure 5.27. Although it is only a 3.5σ effect, it is significant that a similar deficit was seen in several other experiments: Chudakov *et al.* (1964), Weekes *et al.* (1972, 1979), Grindlay *et al.* (1975*b*) and Dowthwaite *et al.* (1985). Fomin *et al.* (1977) explained this decrease by postulating that the Galactic Plane actually produces UHEGR by inverse Compton scattering of starlight on very high energy electrons, and that the dip seen in the UHEGR emission is due to the light radiation density at $|b| < 1.5°$ being lower because of absorption by dust in the Galactic Plane. There are some

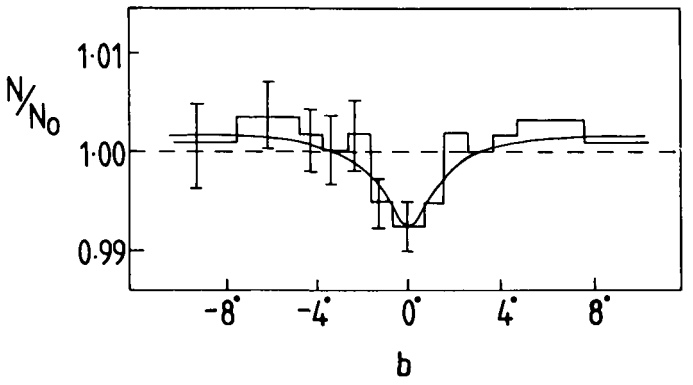

Figure 5.27. Relative counting rate of the EAS $N/\langle N\rangle$ where $\langle N\rangle$ is the average counting rate, as a function of Galactic latitude, b, after Stepanian *et al.* (1982). The data are averaged over a wide range of Galactic longitude, $320° < l < 170°$. The dip at $b = 0°$ is of magnitude $-(0.7 \pm 0.2)\%$.

inconsistencies in the observations, however. Dowthwaite *et al.* (1985) reported that the dip in the Galactic Plane (at $l = 80°$, Cygnus X-3 region) was $(8 \pm 3)\%$ of the cosmic ray background, whereas the Crimean group found a deficit of less than 1 % at $320° < l < 170°$. A later observation by the Whipple group (Reynolds *et al.* 1987) of the Cygnus X-3 region showed no evidence for either a deficit at the Galactic Equator or an excess at $b = (0 \pm 5°)$ from it. An upper limit of 1.5 % was found for the deviation from the background, in contrast with the results of Dowthwaite *et al.* (1985). Recently, the Whipple group (Reynolds *et al.* 1990) scanned six different Galactic longitude regions around the Galactic Plane and found neither an excess nor a deficit with respect to the background; the authors have placed an upper limit of $\sim 2\%$ for any production or absorption in the Galactic Plane of γ-rays at TeV energies. At PeV energies, the Utah–Michigan collaboration (Matthews *et al.* 1992) placed an upper limit of 8×10^{-5} (90% confidence level) on the ratio of diffuse γ-ray flux from the Galactic Plane to the cosmic ray background in the region $30° < l < 220°$ and $|b| < 10°$.

On the whole, the situation regarding observations of the Galactic Plane is far from satisfactory; see Weekes (1988, 1992). So far there has been no convincing demonstration that there is UHEGR emission from either the Galactic Plane or the Galactic Centre. In the absence of such a ridge (excess over background), any report of a dip at the Galactic Equator is of doubtful significance. Clearly more observations are desirable.

5.3.1H Primordial black holes

According to Page and Hawking (1976), it is conceivable that the hot and highly compressed regions believed to exist shortly after the 'Big Bang' might have collapsed into black holes. These objects are called primordial black holes (PBH) as distinct from stellar black holes. PBH in the mass range 10^{14}–10^{15} g would

have survived until the present epoch. Their temperatures are as high as 10^{12} K, and the event horizon radius is as small as 1 fermi or even less. With such small confines, quantum mechanical effects come into play and lead to particle emission by PBH through spontaneous creation of pairs of particles near the event horizon. As the particle emission progresses, the mass of the PBH decreases, raising its temperature and leading to even more copious production of particles. The system is thus clearly in a runaway state; for details, see Carr (1976) and Page and Hawking (1976). The PBH with masses $\sim 5 \times 10^{14}$ G, should they exist, must be evaporating at this epoch so fast as to effectively explode. According to the elementary particle mode of evaporation, $\sim 10^{30}$ γ-rays at $E_\gamma > 10^{12}$ eV are emitted over a period of 0.1 s.

Porter and Weekes (1979) looked for seven or more Cerenkov flashes occurring in less than 0.1 s. Not finding any, the authors set an upper limit (99% confidence level) of 3×10^4 pc^{-3} y^{-1} to PBH explosions. In observations at mountain altitudes, P.N. Bhat *et al.* (1982) looked for bursts of low energy photon showers ($\geq$ three showers within a time span of a few tens to a few hundreds of milliseconds) produced by 5 TeV γ-rays, but did not find any. The authors set a 99% confidence level upper limit to PBH explosions of 1.6×10^3 pc^{-3} y^{-1}.

5.3.1I Other sources

In the literature one finds many claims of detection of emission of UHEGR from the various celestial objects. In most cases, the emission was not seen by more than one group; in some there are discrepancies and in others the statistical significance is not very strong. Many X-ray binaries, in addition to those already mentioned above, are believed to emit UHEGR; see the review by Chadwick, McComb and Turver (1990). Rather than describing the observations on each source, we have shown in Table 5.4 results from observations on the various sources.

5.3.2 Extragalactic objects

It has been seen that the luminosities of most of the Galactic objects in the UHEGR range lie in the range 10^{34}–10^{36} erg s^{-1} and most of the detections were only at a flux level which was an order of magnitude (or less) greater than the detection threshold. It follows, then, that, in order to be detectable by Earth-based detectors, the luminosity of an extragalactic object must be 10^2 to 10^{10} times higher than in the case of a Galactic object.

5.3.2A SN 1987a

SN 1987a is the most intensively studied supernova with the panoply of all modern instrumentation, not only in all the windows of the electromagnetic spectrum, but in neutrinos as well. It occurred on February 23, 1987, in the Large Magellanic Cloud, located approximately at a distance of 55 kpc from Earth in the direction of R.A. = 05 h 36 m and decl. = $-69°12'$. Observations on this object helped open the observational neutrino astronomy window besides providing

Table 5.4. *Results of UHEGR emission from various sources*

Source	Threshold energy (eV)	Flux ($cm^{-2} s^{-1}$)	Reference
4U0115+64	10^{12}	$(7 \pm 1.4) \times 10^{-11}$	Chadwick *et al.* (1985)
	2×10^{11}	$(2.0 \pm 0.4) \times 10^{-9}$	Resvanis *et al.* (1987*b*)
	4×10^{11}	4.4×10^{-10}	Brazier *et al.* (1990*c*)
	4×10^{11}	$<3.0 \times 10^{-11}$	Macomb *et al.* (1991)
	1.5×10^{12}	$(2.7 \pm 1.0) \times 10^{-11}$	P.N. Bhat *et al.* (1987*b*)
	4.8×10^{12}	$<3.8 \times 10^{-11}$	P.N. Bhat *et al.* private communication
IE2259+586	4×10^{11}	$(2 \pm 0.8) \times 10^{-10}$	Brazier *et al.* (1990*c*)
	6×10^{11}	$<2.4 \times 10^{-11}$	Cawley *et al.* (1991)
PSR1957+20	4.3×10^{12}	$<1.4 \times 10^{-11}$ * $<1.8 \times 10^{-10}$**	Acharya *et al.* (1990*b*)
	2.7×10^{12}	1.6×10^{-10}†	Brink *et al.* (1990)
	5×10^{14}	$(3.5 \pm 0.8) \times 10^{-13}$††	Sinha *et al.* (1990)
	1×10^{14}	8×10^{-11}†	Gupta *et al.* (1991*a*)
Sco X-1	3×10^{11}	$(1.2 \pm 0.4) \times 10^{-10}$	Brazier *et al.* (1990*d*)
	2×10^{14}	$<1.5 \times 10^{-13}$	Matano *et al.* (1990)
	1.8×10^{14}	$<1.3 \times 10^{-13}$	Kakimoto *et al.* (1990)
	2.5×10^{14}	$(2.4 \pm 0.3) \times 10^{-13}$	Tonwar *et al.* (1990)
Centaurus X-3	1.9×10^{12}	$(1.3 \pm 0.9) \times 10^{-10}$	North *et al.* (1990)
	2.5×10^{11}	6×10^{-10}	Brazier *et al.* (1990*d*)
Geminga	1×10^{12}	$(5 \pm 3) \times 10^{-11}$	Zyskin and Mukanov (1983)
	2×10^{11}	$<1.6 \times 10^{-10}$	Helmken and Weekes (1979)
	1×10^{12}	$<6 \times 10^{-11}$	
	1.7×10^{12}	$<2 \times 10^{-11}$	P.N. Bhat *et al.* (1987*c*)
	6×10^{12}	$<2.4 \times 10^{-12}$	Kaul *et al.* (1989)
AM-Hercules	2×10^{12}	$(5.6 \pm 2.1) \times 10^{-11}$	C.L. Bhat *et al.* (1991)

* Time-averaged pulsed flux.
** At the Lagrange points L4 and L5.
† At the Lagrange point L4.
†† During the eclipse, 0.2 to 0.3 in orbital phase.

valuable information relating to astronomy, particle physics, the general theory of relativity, etc.

It has long been conjectured that supernovae contribute to the production and acceleration of cosmic rays. If this is so, it is possible that the cosmic rays produced in supernovae interact with the matter within the shell itself producing neutral pions, which in turn decay into γ-rays. There is very little known about the various parameters obtained in a supernova shell like the one around SN 1987a, to predict the TeV and PeV γ-ray fluxes with any degree of confidence. Despite these

Table 5.5. *Results on UHEGR emission from SN 1987a*

Epoch (days)	Threshold energy (TeV)	Upper limit flux ($cm^{-2}\,s^{-1}$)	Upper limit luminosity ($erg\,s^{-1}$)	Reference
270–276	1	2.3×10^{-11}	1.7×10^{38}	Raubenheimer *et al.* (1988)
290–310	3	6.1×10^{-12}	8.4×10^{37}	Bond *et al.* (1988)
1–400	0.4	1.5×10^{-10}	4.0×10^{38}	Chadwick *et al.* (1988)
680–830	0.4	2.8×10^{-10}	1.6×10^{38}	Brazier *et al.* (1990*e*)
430–520	75	5.7×10^{-14}	1.0×10^{37}	Bond *et al.* (1989)
314–356	100	0.9×10^{-12}	3.0×10^{39}**	Gaisser *et al.* (1989*b*)
1–180	100	1.9×10^{-11}	9.4×10^{40}**	Ciampa *et al.* (1988)
180–460	100	4.0×10^{-11}	1.7×10^{39}	Castagnoli *et al.* (1990)
335–725	100	3.6×10^{-13}	3.0×10^{37}	Kaneko *et al.* (1990)

* Epoch is in days from the explosion (February 23, 1987).
** Upper limit to proton luminosity.

difficulties, Gaisser *et al.* (1987, 1989*a*) and Yamada *et al.* (1988) made some predictions on UHEGR fluxes from this object.

There were several observations made on this object to detect UHEGR, all of which ended in placing upper limits to the fluxes, except for a transient which we describe later on. The results are summarised in Table 5.5.

Although Bond *et al.* (1988) did not see any steady emission of γ-rays above 3 TeV from SN 1987a, they reported an excess of counts over the background baseline during the nights of January 14 and 15, 1988; see Figure 5.28(*a*). It is significant that these counts are in the direction of SN 1987a, as shown in Figure 5.28(*b*). The epoch of this episode, it was pointed out by the authors, coincided with the central time of the X-ray flux increase detected by the Ginga Satellite (Tanaka 1989). The time-averaged γ-ray flux during these two nights was $(1.9 \pm 0.5) \times 10^{-11}\,cm^{-2}\,s^{-1}$ at energies greater than 3 TeV.

5.3.2B LMC X-4

This object in the southern skies is at a distance of 55 kpc from the solar system. It exhibits three periodicities in X-rays: 13.5 s (rotation of neutron star), 1.4 d (orbital motion) and 30.5 d (precession of neutron star). Protheroe and Clay (1985) carried out a periodicity analysis ($P = 1.4$ d) on the event times of air showers arriving from the direction of LMC X-4. The authors have seen 12 events in the phase region $0.90 < \varphi_{1.4d} < 0.95$ when 2.65 events were expected. The probability of random fluctuations in the background producing such an effect was estimated by the authors as 0.01. The observation yields a flux of $(4.6 \pm 1.7) \times 10^{-15}$ photons $cm^{-2}\,s^{-1}$ at $E_\gamma > 8 \times 10^{15}$ eV, leading to a time-averaged luminosity of $10^{38}\,erg\,s^{-1}$. The JANZOS group (Tanimori 1990) have

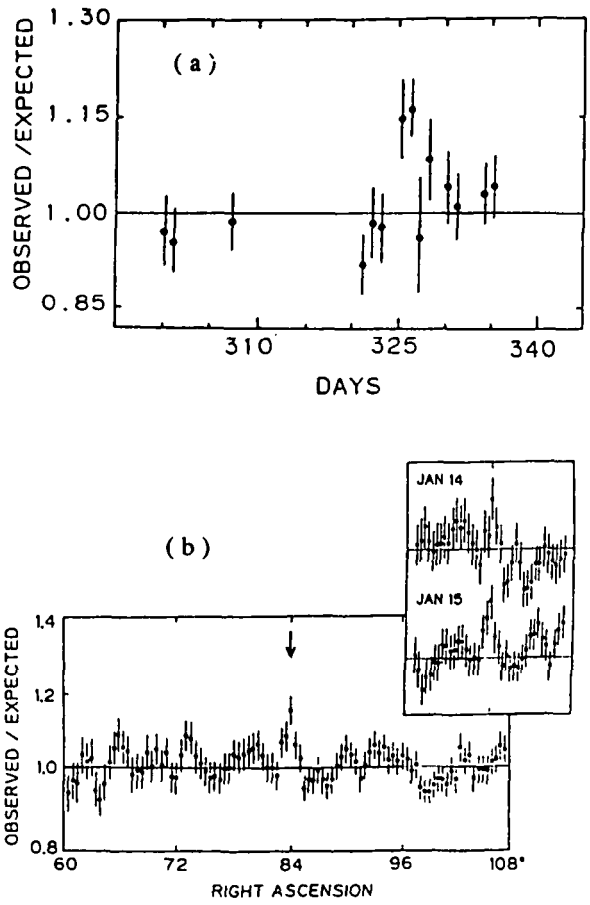

Figure 5.28. (*a*) Deviation of counts from the baseline in the observations of Bond *et al.* (1988) is plotted as a function of number of days after the explosion of the supernova. (*b*) The same quantity during January 14 and 15, 1988, is plotted as a function of right ascension. Notice the excess at 84°, the direction of SN 1987a.

reported an upper limits of 2.3×10^{-13} photons $cm^{-2}\ s^{-1}$ for the flux of γ-rays from the object at $E_\gamma > 10^{14}$ eV.

5.3.2C M31

M31, the Andromeda nebula, belongs to the local group of galaxies, and is located at a distance of 670 kpc from the solar system. Although Weekes *et al.* (1972) had previously set an upper limit of 3.8×10^{-10} photons $cm^{-2}\ s^{-1}$ at $E_\gamma > 1.4 \times 10^{11}$ eV from this object, Dowthwaite *et al.* (1984*a*) found a positive signal of 3σ at a flux level of 2.2×10^{-10} photons $cm^{-2}\ s^{-1}$ at $E_\gamma > 10^{12}$ eV. The result is based on drift scans made during 1983 at Dugway, Utah. There were 240 ± 79 excess counts in the source direction. The null (no signal) hypothesis fits the data only at a level of 1% likelihood. According to the authors, the luminosity

of M31 at $E_\gamma > 1000$ GeV is 4×10^{40} erg s^{-1} assuming isotropic emission and a power-law differential spectrum with a spectral index of -3. However, a subsequent observation by the Whipple group (Cawley *et al.* 1985) contradicts this claim; the authors report an upper limit of 1.6×10^{-10} photons cm^{-2} s^{-1} at a lower energy of $E_\gamma > 4 \times 10^{11}$ eV. More observations are needed before one can consider this object as a source of UHEGR.

5.3.2D Centaurus A

Centaurus A (NGC 5128), a 'nearby' active galaxy (distance ~ 6 Mpc) is known to exhibit violent activity at radio frequencies. It is also visible in the X-ray region (Bowyer *et al.* 1970). Grindlay *et al.* (1975*a*) looked for possible UHEGR emission from this object during 1972–4 using the pair of 7 m dishes of Hanbury Brown–Twiss interferometer at Narrabri, Australia. The authors compared the rates from the source direction with those from neighbouring 'off-source' directions. The frequency of excess counts in the source direction versus the magnitude of excess counts in units of standard deviations during the data cycles for three years is shown in Figure 5.29. Whereas the lower panel shows all the events, the upper panel shows events which are mainly due to UHEGR. This selection is made possible by rejecting showers showing a secondary Cerenkov pulse in a beam slightly offset from the main one and attributable to muons in a cosmic-ray-initiated EAS. In each of the three years, the authors detected a positive signal (3.9, 1.0 and 2.5σ). The combined signal, amounting to a 4.6σ excess over the background, corresponded to a flux of $(4.4 \pm 1.0) \times 10^{-11}$ photons cm^{-2} s^{-1} at $E_\gamma > 300$ GeV. The authors give a probability of $< 2 \times 10^{-5}$ that the excess counts are not due to a γ-ray source. The beam width being only 0.45° (FWHM), the extended ($\sim 5°$) radio lobes associated with this object cannot be the source of the detected UHEGR. When combined with X-ray measurements, the observations are consistent with an energy spectrum having a differential spectral index of -1.7. The experiment of Grindlay *et al.* suggests that the source may be variable in the emission of UHEGR in a similar manner to the situation at microwave frequencies. If isotropic emission is assumed, the luminosity is $\sim 2 \times 10^{41}$ erg s^{-1} at 300 GeV $< E_\gamma <$ 3000 GeV. In a recent observation, the Durham group (Brazier *et al.* 1990*f*) failed to confirm the findings of Grindlay *et al.* The Durham group places an upper limit of 7.8×10^{-11} photons cm^{-2} s^{-1} at $E_\gamma > 2.5 \times 10^{11}$ eV.

At PeV energies, Clay *et al.* (1984*b*) placed an upper limit of 10^{-14} photons cm^{-2} s^{-1} at $E_\gamma > 10^{15}$ eV, and the Mount Chacaltaya group (Kakimoto *et al.* 1990) have placed an upper limit of 7.5×10^{-14} photons cm^{-2} s^{-1} at $E_\gamma > 1.8 \times 10^{14}$ eV. One must note here that the PeV observations of both Clay *et al.* and Kakimoto *et al.* suffer the disadvantage of enormous attenuation ($\sim 10^4$) of γ-rays in transit from the source to Earth due to pair production in their interaction with the 2.7 K microwave background radiation. As in the case of M31, one has to conclude that this object is not an established γ-ray emitter at TeV and PeV energies.

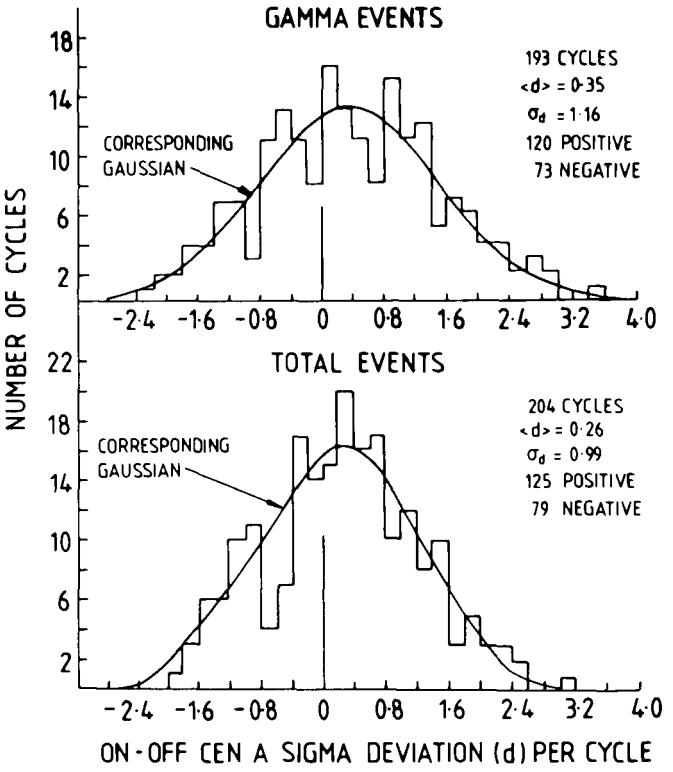

Figure 5.29. Distributions of observed deviations, in standard deviations, from the background in the direction of Centaurus A in the experiment of Grindlay *et al.* (1975*a*). All data (1972–4) are included. The mean number of standard deviations, $\langle d \rangle$, per cycle and the standard deviations of the histograms (σ_d) are shown. Lower panel: distribution for all showers; upper panel: showers enriched in γ-rays by rejecting some which showed signals from muons. In both panels there are more positive than negative deviations, signifying UHEGR emission by Centaurus A.

5.3.2E 3C273

This object is a quasar with a redshift of $z = 0.158$, which, if interpreted as cosmological, implies a distance of $\sim$900 Mpc from the solar system. It was clearly identified by the COS B experiment as a source of medium high energy γ-rays. Several observations at TeV as well as PeV energies failed to record any emission from the object. Upper limits to UHEGR fluxes from some of the observations are listed below:

$< 9 \times 10^{-12}$ cm^{-2} s^{-1} at $E_\gamma > 5$ TeV by Long *et al.* (1965),
$< 4 \times 10^{-11}$ cm^{-2} s^{-1} at $E_\gamma > 0.3$ TeV by Weekes *et al.* (1972).
$< 2 \times 10^{-10}$ cm^{-2} s^{-1} at $E_\gamma > 0.3$ TeV by Grindlay *et al.* (1975*b*),
$< 4 \times 10^{-10}$ cm^{-2} s^{-1} at $E_\gamma > 0.15$ TeV by Cawley *et al.* (1985),
$< 9 \times 10^{-11}$ cm^{-2} s^{-1} at $E_\gamma > 0.6$ TeV by Vacanti *et al.* (1990),
$< 1 \times 10^{-13}$ cm^{-2} s^{-1} at $E_\gamma > 300$ TeV by Tanimori (1990).

5.3.2F Cosmic strings

Grand unified theories (GUTs) predict that cosmic strings may exist in the Universe as relics of the ultra dense state of matter and ultra high temperature phase transitions which prevailed within 10^{-35} s of the big bang; see Kibble (1976). The detection of such strings would be of great importance to the GUT description of the early Universe. These strings are extremely long, very thin, high density objects and, in some theories, may be superconducting (Witten 1985). Ostriker, Thompson and Witten (1986) have suggested that oscillations of the strings could radiate electric and magnetic fields. Villenkin (1988) pointed out that the theory of Ostriker *et al.* leads to detectable fluxes of high energy cosmic rays and γ-rays up to energies $\sim 10^{15}$ eV.

Byrne *et al.* (1990) searched for 40 TeV γ-rays that might owe their origin to such cosmic strings. The signature adopted in the search was either an impulse burst of events over periods of ~ 1 d from a point source or an extended object with a long time scale activity. The authors divided the sky in the region $16.7° < \delta < 46.7°$ and $0° <$ R.A. $< 360°$ into 300 cells of dimensions $6° \times 6°$. None of the cells showed statistically significant evidence for repetitive impulsive activity. The 3σ deviation flux limit over a single day's observation has been set at 3.3×10^{-11} photons cm^{-2} s^{-1} at $E_\gamma > 40$ TeV.

5.4 Source models and implications

UHEGR are invariably produced by electrons (and positrons) and nuclei in their interactions with matter, radiation and magnetic field by the various processes listed in Chapter 1. The result is a flux of UHEGR with an intensity several orders of magnitude lower than that of the primary cosmic rays. As was mentioned in Section 5.1, it has not yet been possible to measure such a low intensity of diffuse UHEGR (though some upper limits were set) in the presence of the very considerable cosmic ray background. At this stage, therefore, we can consider only point sources of UHEGR.

The point sources are considered in Sections 5.4.1 and 5.4.2, and the discernible implications in the areas of cosmic radiation and X-ray astronomy are touched upon in Section 5.4.3.

5.4.1 Production of UHEGR in supernova remnants

As was mentioned in Section 5.1, there exists indirect evidence from studies of the optical continuum from the Crab nebula that high energy $e^{\pm}$ are present in the envelope of this SNR. Their expected interactions can be considered following the analysis of Ginzburg and Syrovatskii (1964). The characteristic synchrotron photon energy, E_γ, emitted by an electron of energy E_e in a transverse magnetic field $H_\perp$ is given by

$$E_\gamma(\text{eV}) = 5 \times 10^{-9} H_\perp(\text{G})(E_e/m_e c^2)^2 \tag{5.12}$$

Thus, an electron of 10^{14} eV moving in a transverse magnetic field of 3×10^{-4} G would produce 60 keV X-rays. The lifetime of electrons against synchrotron

emission, given by

$$t_{1/2}(\mathrm{s}) = 5 \times 10^8 (m_e c^2/E_e) H_\perp^{-2} \tag{5.13}$$

is quite small, however, and in the example cited above $t_{1/2}$ is only about one year. It is clear, therefore, that high energy electrons in the Crab nebula cannot have survived since the time of the initial explosion, an event which occurred 940 years ago. Instead, the electrons must be accelerated on a continual basis even at the present time. If the electrons in the SNR are secondary to protons, in the sense that they are produced through the decay chain $\pi^\pm \rightarrow \mu^\pm \rightarrow e^\pm$, then there should be a significant flux of UHEGR resulting from the decays of π^0 mesons which are produced along with charged pions (Cocconi 1959, Gould and Burbidge 1965). The predicted fluxes are, in fact, a few orders of magnitude higher than the values/upper limits observed experimentally, and it must be concluded, therefore, that the high energy electrons in the remnant are accelerated as such. The actual mechanism of acceleration of electrons is as yet uncertain, but various suggestions have been made: Fermi acceleration in the magnetic irregularities in the remnant and production and injection by the pulsar associated within the SNR being favoured.

Although the existence of ultra high energy electrons in the remnant is inferred by invoking synchrotron emission to explain X-ray emission from the nebula, it is the inverse Compton scattering of high energy electrons against the ambient light which most effectively leads to the production of UHEGR. Several authors have calculated the expected UHEGR fluxes produced by this process; see Rieke and Weekes (1969) and references quoted therein. The predictions of UHEGR fluxes are uncertain by an order of magnitude because of the lack of precision of the inferred electron fluxes in the SNR, which, in turn, result from the uncertainty in the magnetic field. As an example of the predictions we can take the calculations of Rieke and Weekes (1969) who derived expected fluxes in the range 10^{-11}–10^{-10} $\mathrm{cm}^{-2}\,\mathrm{s}^{-1}$ at $E_\gamma > 1$ TeV. Observed fluxes at TeV energies (as shown in Figure 5.13) are generally consistent with the predictions of this model. K.S. Cheng *et al.* (1990) have proposed an interesting alternative model. The authors have postulated that, though the column density in the Crab nebula is too small to be an effective target for proton beams inside the remnant to produce neutral pions, the proton beam could be accumulated within the remnant by trapping the relativistic protons in the nebular magnetic field; this will increase the collision probability for a given proton. The predictions are in agreement with observations at TeV energies. Neither of the two models addresses the question of how the electron/proton beam is accelerated in the first place. Even if the charged particle beams are produced by the 33 ms pulsar in a pulsed fashion, the periodicity signature is lost as the encounters responsible for the γ-ray production are well spread out randomly in time. The lack of periodicity in the TeV γ-ray signal in the observations of the Whipple group (Vacanti *et al.* 1991) is consistent with this.

Turning to γ-ray emission by SN 1987a, Gaisser *et al.* (1987, 1989*a*,*b*) have proposed that protons can be accelerated by a first order Fermi mechanism in the pulsar wind shock within the supernova shell. The authors discuss in great detail

how predictions of γ-ray fluxes at the Earth depend on a number of factors: (i) the mixing of the accelerated particles with the gas in the expanding envelope, (ii) the spectral exponent of the particle spectrum, and (iii) the absorption of γ-rays within the 5000 K black body radiation sphere (thermal photons). The present upper limits from observations, summarised in Table 5.5, imply that the luminosity of the accelerated proton beam in the shell is less than 10^{38} erg s^{-1}.

5.4.2 *Production of UHEGR in pulsar and X-ray binary environs*

Pulsars are believed to be rapidly rotating neutron stars possessing enormous magnetic fields ($\sim 10^{12}$ G); see Manchester and Taylor (1977) and Smith (1977). It is attractive to postulate that such rapidly rotating oblique magnetic dipoles generate intense electric fields in which charged particles are accelerated to very high energies. Despite intense theoretical efforts, a self-consistent understanding of the pulsar magnetospheres and the processes going on there has proved to be a very difficult proposition; see Michel (1982). This is so even in the case of radio emission by pulsars, where there is already considerable observational information. The situation with respect to UHEGR emission, about which there exists only a limited body of observational data at present, is even less clear.

Gunn and Ostriker (1969) outlined a possible scenario in which electrons and protons are accelerated to very high energies near the velocity-of-light cylinder around a pulsar in which the magnetic dipole moment makes an angle with its rotation axis; see also Ostriker (1972). According to these authors, the rotating magnetic dipole moment emits low frequency electromagnetic waves with the same frequency, Ω, as that of the pulsar. Since the gyrofrequency, $\omega_0 = eB/mc$, is very much larger than the wave frequency, Ω, particles injected in the wave zone find themselves in strong, nearly static crossed electric and magnetic fields. In a time very short compared to the period of the wave, the particles move relativistically in nearly the same direction as the wave's propagation vector. Thereafter they ride the wave at essentially a constant phase. The energy of the particle turns out to be independent of where it is injected provided it is far into the wave zone to begin with. According to the authors, the particle attains an energy E given by

$$E = 3.6 \times 10^{13} A(Z/A)^{2/3} \Omega_2^{4/3} (B_{s,12})^{2/3} R_6^2 \text{ eV} \tag{5.14}$$

Here, Z and A are the atomic number and atomic mass of the particles; Ω_2 is the neutron star angular velocity in units of 10^2 rad s^{-1}; $B_{s,12}$ is the surface field in units of 10^{12} G; and R_6 is the neutron star radius in units of 10^6 cm. For the Crab pulsar, the above equation predicts energies of 2×10^{13} and 2×10^{14} eV for electrons and protons, respectively. The authors invoke Goldreich–Julian theory (Goldreich and Julian 1969) and find that the rate of injection of particles is quite high. UHEGR could then be produced either by inverse Compton scattering of the electrons or through the decays of π^0 mesons produced in the nuclear interactions of protons with matter.

Goldreich and Julian (1969) have considered a pulsar model in which the dipole magnetic moment is aligned with the rotation axis. In this case, the open field lines extend beyond the light cylinder and close in a boundary zone near the

supernova shell. Charged particles escape along these lines and are electrostatically accelerated up to energies of

$$E_{\max} = 3 \times 10^{12} Z R_6^3 B_{12} P^{-2} \text{ eV} \tag{5.15}$$

where Z is the charge of the particle, P is the pulsar period in seconds, and the other symbols are as defined above. It can be seen that, in the case of the Crab pulsar, particles can be accelerated up to $\sim 3 \times 10^{15}$ eV.

Both models just considered deal with the acceleration of charged particles at or beyond the light cylinder. On the other hand, Sturrock (1971), Ruderman and Sutherland (1975) and Massaro and Salvati (1979), among others, have considered models in which charged particles ($e^{\pm}$) are accelerated in the gaps near polar caps across which electric potentials of $> 10^{12}$ eV have been calculated to exist. These models were developed largely to explain the various features observed in radio emission and low energy γ-rays, but high energy γ-rays could also result from curvature radiation emitted by these high energy electrons or through inverse Compton scattering. There is one difficulty, however, in getting UHEGR away from the pulsars in these models. In the regions where the γ-rays are produced, the magnetic fields are quite intense, approaching 10^{12} G. In such intense fields, γ-rays undergo pair production even at energies as low as several MeV. Massaro and Salvati (1979) have shown that γ-rays of 100 GeV energy become attenuated by three to four orders of magnitude in the pulsar magnetospheres. In this context, the view expressed by Shabad and Usov (1982) is relevant. In the usual picture the curvature radiation photons are emitted tangentially to the line of force of magnetic fields and propagate in straight-line paths. As they do so, the pitch angle between the photon wave vector and the magnetic field increases until a certain value when the photon gets absorbed through pair production. Shabad and Usov (1982) point out that, if the resonant behaviour characteristic of vacuum polarisation in a magnetic field is considered, the above picture changes considerably. The trajectories of γ-quanta are strongly bent towards the direction of the magnetic field (instead of being straight), provided the latter is sufficiently intense. Consequently the absorption of γ-rays by pair production on the magnetic field is suppressed.

A. Cheng, Ruderman and Sutherland (1976) have considered particle acceleration in the outer gaps of the pulsar magnetospheres at distances ~ 0.6 times the light cylinder radius. At such distances, UHEGR absorption is considerably less because of the r^{-3}-dependence of the magnetic field strength. For example, the Sturrock condition (equation 5.2) tells us that, in the case of the Crab pulsar, attenuation is severe only at $E_\gamma > 10^{12}$ eV. The authors propose that γ-rays up to 10^{11} eV can be produced by electrons accelerated in the outer gap.

K.S. Cheng, Ho and Ruderman (1986*a*,*b*) have further considered the outer gap models in greater detail, and have shown that the production of γ-rays in the energy range 10^{12}–10^{13} eV is entirely feasible in these models. In the outer gaps, charged particle production and acceleration can be maintained by the large $\boldsymbol{E} \cdot \boldsymbol{B}$ deep within the gap. The total potential drop deep in the gap along $\boldsymbol{B}$ is of the order of 10^{15} V. The primary $e^{\pm}$ produce primary γ-rays through inverse

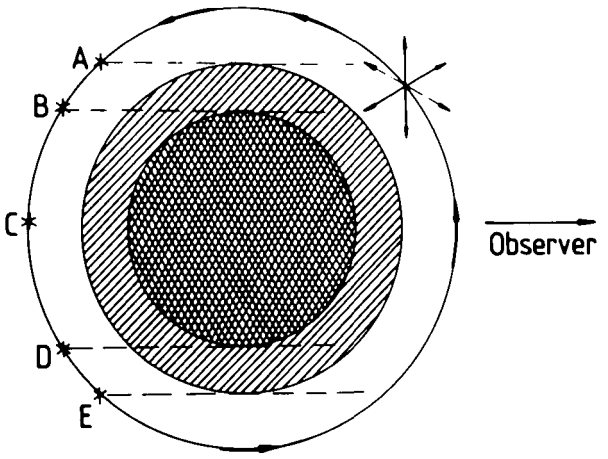

Figure 5.30. Schematic representation of how the UHEGR light curve can be generated from the Cygnus X-3 binary system (Vestrand and Eichler 1982). The cross-hatched region denotes the main body of the companion star, and the circumscribed shaded region denotes its atmosphere. The outer circle represents the pulsar orbit, and the dashed lines represent particle trajectories that produce γ-rays detectable at Earth. Pulses are produced when the pulsar is between A and B and between D and E. X-ray minimum occurs at position C.

Compton scattering on infra-red photons. These primary photons, in turn, produce secondary $e^{\pm}$ in collisions with the same infra-red photons. However, a small fraction of the photons can escape pair production in the collisions with the infra-red and X-ray photons and with the magnetic fields (already lower by several orders of magnitude than in the inner gaps) to emerge from the pulsar magnetosphere as detectable TeV γ-rays.

Hinata (1977) has pointed out that if UHEGR at $E_\gamma > 1$ TeV are produced at distances $\lesssim 36$ neutron star radii from the Crab pulsar through curvature radiation by electrons of $E_e \sim 10^{14}$ eV, the photons can escape pair production. The UHEGR intensities can be made to match those observed by the Mount Hopkins groups (Grindlay, Helmken and Weekes 1976). The author did not present details of how the electrons become accelerated to 10^{14} eV, however.

A number of authors (Milgrom and Pines 1978, Stepanian 1982, Vestrand and Eichler 1982, Eichler and Vestrand 1984, and Hillas 1984) have presented various scenarios of UHEGR production by Cygnus X-3. All the authors assumed that Cygnus X-3 is a binary system consisting of a neutron star and a normal stellar companion. High energy charged particles emitted by the neutron star (see Figure 5.30) interact with the atmosphere of the companion star, thus producing the UHEGR one sees in experiments. Since the generated photons are strongly beamed along the velocity vector of the incident particle, an observer detects only those photons that are produced when particles streaming towards him strike the intervening target, i.e. the stellar atmosphere. In this picture, the binary period ($\sim$4.8 h) is made to match the observed periodicity of the X-ray and UHEGR

signals from Cygnus X-3. The radiations are expected to populate two distinct phase regions separated by approximately $\Delta\phi = 0.5$. The problem of accelerating the charged particles is relegated to the neutron star. Charged particle beams could be produced in the environs of the neutron star in a pulsed mode as in the case of isolated pulsars. If the beam interacts with the material in the accretion disk or with the material surrounding the companion star, one can expect to see pulsed UHEGR. The Durham group (Chadwick *et al.* 1985*a*, Brazier *et al.* 1990*b*) have claimed to have detected 12.6 ms pulsed γ-rays at TeV energies from Cygnus X-3, but others failed to detect these, as outlined in Section 5.3.1D. Stephens and Verma (1984) have pointed out that, in the magnetic fields ~ 1330 G believed to exist near the companion star, UHEGR from Cygnus X-3 with $E_\gamma > 10^{16}$ eV will be attenuated by pair production, thus leading to a steepening of the UHEGR spectrum at this energy, as observed.

Chanmugam and Brecher (1985) have proposed a unipolar inductor model by which charged particles can be accelerated to very high energies in binary systems containing accreting magnetised neutron stars. In this model, the matter in the accretion disk surrounding the neutron star amplifies the ambient magnetic field and a potential difference is created between the inner and the outer edges of the accretion disk. Electrons and/or protons can be accelerated by this potential difference. UHEGR are then produced in the interactions of the beam particles with the matter in the accretion disk. Energy for acceleration is derived from the accretion process (i.e. gravitational energy). The potential difference is given by

$$V_{12} = 280 B_{12}^{-3/7} L_{38}^{5/7} \ln(r_2/r_1) \tag{5.16}$$

Here, V_{12} is the potential difference in units of 10^{12} V; B_{12} is the magnetic field in units of 10^{12} G; L_{38} is the accretion luminosity in units of 10^{38} erg s^{-1}; and r_1 and r_2 are the inner and outer radii, respectively, of the accretion disk. Considering Cygnus X-3 as an example, the authors used the values $B_{12} = 1.6 \times 10^{-4}$, $L_{38} = 3$, $r_1 = 10^6$ cm, and $r_2 = 10^{11}$ cm, to arrive at a value of 3×10^{17} V for the potential difference. An attractive feature of this model is that it works well at low magnetic fields, thus avoiding attenuation of UHEGR in the magnetic field by pair production.

We now consider the question of emission of UHEGR by Hercules X-1 with anomalous periodicity; observations were described in Section 5.3.1E. If the neutron star is accelerating protons by some mechanism, and if the target (to make γ-rays through production and decay of neutral pions) is either very firmly attached to the neutron star or is very far away from the binary system, one does expect the periodicity in UHEGR to be identical to that of the neutron star. Two models have been proposed to explain the discrepancy in the periods. The essential point in both the models is that the target is transient and can be considered to be semi-detached.

In the model of Slane and Fry (1989) γ-rays result from the interaction of a broad particle beam with target matter removed from the accretion disk by the instabilities at the disk–magnetosphere interface. The γ-rays are observed only when the target matter is between the neutron star and the observer; this explains

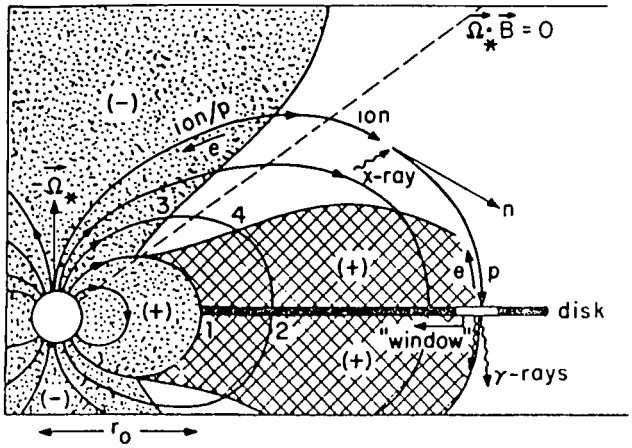

Figure 5.31. Model of K.S. Cheng and Ruderman (1989) for TeV γ-ray production in Hercules X-1. The proton beam accelerated in the neutron star's magnetosphere interacts with a thin window in the accretion disk producing γ-rays that emerge out of the accretion disk. Properties of the window are adjusted to fit the observational details of the burst of γ-rays with an anomalous period.

the episodal nature of the γ-ray signal. The γ-rays will be observed to be pulsed at the period of the Keplerian orbit of the target matter, which is slightly less than that of the neutron star. In the model of K.S. Cheng and Ruderman (1989), γ-rays arise as a result of interaction between the accelerated particle beam and the Keplerian accretion disk. Such γ-rays can escape the production region only when the target thickness is small, i.e. a window of $\sim 40\ \mathrm{g\ cm^{-2}}$ thick; see Figure 5.31. The burst duration is controlled by the size and the radial velocity of the window, and the period is determined by the appropriate Keplerian orbit of the window.

5.4.3 Implications of UHEGR

The existence of finite fluxes of UHEGR has some interesting implications in the fields of cosmic ray physics and X-ray astronomy.

Wdowczyk and Wolfendale (1983, 1984) have noted that, for sources such as the Crab pulsar/nebula and Cygnus X-3, the differential energy spectra of γ-rays seem to have flat exponents with $\gamma_d \sim -2$, whereas the cosmic ray differential spectrum has a steeper exponent of about -2.6 (up to a primary energy of $\sim 10^{15}$ eV). If all γ-ray sources in the Galaxy have $\gamma_d \sim -2$, then, normalising to the satellite γ-ray intensity from sources in the 100 MeV region, the γ-ray to cosmic ray proton ratio will increase with energy from about 3×10^{-6} at $E_\gamma \sim 100$ MeV to nearly 0.05 at 10^{15} eV; see Figure 5.32(*a*). The resulting admixture of UHEGR with primary cosmic rays at energies $> 10^{14}$ eV can then explain some of the hitherto inexplicable features of 'primary cosmic rays', which, in this picture, are not all charged particles.

In Figures 5.32(*b*) and (*c*) are shown the phase and the first harmonic of the primary cosmic ray anisotropy as a function of energy. It is clear that the phase

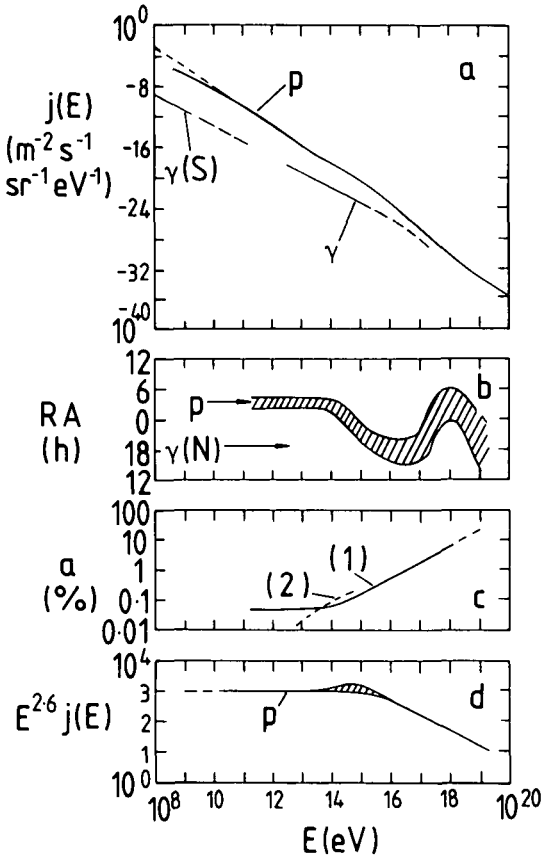

Figure 5.32. This figure, taken from Wdowczyk and Wolfendale (1983), shows in (*a*) the energy spectrum of cosmic-ray particles, denoted by p. $\gamma(S)$: 10% of the average γ-ray intensity with $|b| < 10°$ from satellite experiments. γ: the average γ-ray intensity with $|b| < 10°$ postulated by the authors. (*b*) Phase of first harmonic of cosmic-ray anisotropy for the Northern Hemisphere. *p* is the postulated phase for protons and $\gamma(N)$ is that expected for γ-rays. (*c*) Amplitudes of first and second harmonics for Northern Hemisphere anisotropies. (*d*) Proton spectrum. Note that the change of slope occurs at a higher energy than the changes in (*b*) and (*c*). The shaded area represents (a somewhat contentious) 'bump' in the spectrum.

of the harmonic changes direction from about R.A. ≈ 3 h to about 20 h in the energy range $10^{15\pm1}$ eV, and the amplitude starts increasing abruptly at $E = 10^{14}$ eV from its constant value of 0.07%. UHEGR then start to dominate the anisotropy for $E > 10^{14}$ eV in this model. In view of the fact that most of the cosmic ray experiments near 10^{14} eV are carried out at sea-level or mountain altitudes, where the nature of the primary is never identified, the model cannot yet be checked. If the γ/p ratio were to continue increasing with energy indefinitely then, above 10^{18} eV, γ-rays would predominate in the cosmic ray beam; however, based on the experience with Cygnus X-3, the γ-ray spectrum falls steeply above

10^{16} eV and a potential problem disappears. Wdowczyk and Wolfendale note that, if sources of the type of Cygnus X-3 emit 10^{15} eV protons with the same efficiency as 10^{15} eV γ-rays, only about 30 Cygnus X-3s are needed in the Galaxy to generate the required intensity of cosmic ray particles; if the γ-rays are secondary to protons, however, the number of Cygnus X-3s needed is reduced to one or two at any one time. This statement, however, is to be viewed with caution in the light of reduced flux levels from Cygnus X-3 as observed in the various experiments since 1983; see Section 5.3.1D.

Clay *et al.* (1984*a*) have looked for an excess of air showers in their Buckland Park air shower experiment from the Galactic Plane and Galactic Centre, which could be interpreted as due to UHEGR. Not finding any, the authors have placed an upper limit to the γ/p ratio at the 95% confidence level of about 2%. This upper limit is not in contradiction with the average value of $\sim 1\%$ for $|b| < 10°$ as suggested by Wdowczyk and Wolfendale (1983).

Rana *et al.* (1984) have looked at the consequences of γ-rays at $E_\gamma > 10^{15}$ eV propagating into the Galactic Halo. They argue that the UHEGR will interact with the 2.7 K microwave background photons, thereby producing electron–positron pairs, which in turn emit X-rays by synchrotron radiation in the Galactic magnetic field. This model predicts a flattening of the diffuse X-ray spectrum above 100 keV as measured at high Galactic latitudes, even for only one Cygnus X-3 type source in the Galaxy. A firm detection of these hard X-rays would provide evidence for the γ–γ interaction and also confirm that the microwave radiation extends to at least 10 kpc from the Galactic Plane.

5.5 Puzzles

As described in Section 5.3, most of the results, with a few exceptions, from UHEGR observations are not of high statistical significance. Some of the results have posed problems which are hard to understand on the basis of conventional physics.

The Whipple group (Weekes *et al.* 1989, Vacanti *et al.* 1991) have successfully demonstrated the usefulness of the Cerenkov imaging technique in rejecting a vast majority of the background cosmic ray showers, thus increasing the γ-ray signal-to-noise ratio. The same group (Lamb *et al.* 1988) detected a burst of pulsed TeV γ-rays from Hercules X-1 with an anomalous period; this was before making a cut on imaging. When the same data were subjected to the imaging cuts (Lewis *et al.* 1988), the evidence, instead of becoming stronger, vanished; see Figure 5.33. The imaging cut was designed on the basis of the signal being photonic in nature. Does this, then, indicate that the 'UHEGR' signal was not photonic in nature? Recently, the same group (Reynolds *et al.* 1991) have presented evidence, without making the imaging cut, that Hercules X-1 was perhaps emitting pulsed TeV γ-rays at very low intensity levels during the period 1984–7. However, when the imaging cut is made on the data, the evidence once again disappears; see Figure 5.34. This again raises doubts on the photonic nature of the signal.

At PeV energies too, the same puzzle seems to arise. In their discovery papers on Cygnus X-3, Samorski and Stamm (1983*c*) reported that, on the average, the

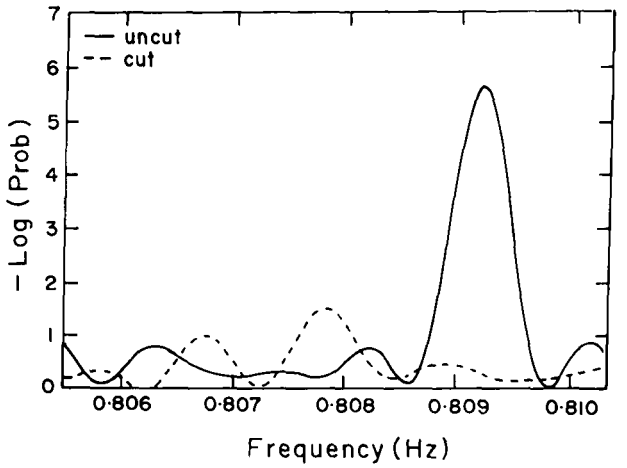

Figure 5.33. Probability of the burst of TeV γ-ray signal from Hercules X-1 on June 11, 1986, being due to chance fluctuations in the background versus trial frequency as deduced by the Whipple group (Lewis *et al.* 1988). The peak in the continuous line without the imaging cuts signifies that the signal is real, whereas the dashed line with the cuts does not show any signal.

muon density in the showers constituting the UHEGR signal is 0.77 ± 0.09 of that of the background cosmic ray showers. Dingus *et al.* (1988*b*) have also reported that the data of the two episodes of PeV γ-ray emission by Hercules X-1 on July 24, 1986, had shown that the muon content of the signal showers was the same as (or even greater than) that in the background showers. The KGF group (Acharya *et al.* 1990*a*) observed that the muon density in the signal showers in the episodal emission of PeV γ-rays by the Crab on February 23, 1989, was 0.93 ± 0.34 of that in the background showers. The expected density of muons on γ-ray initiated showers has been calculated by several authors on the basis of conventional physics to be of the order of $(10 \pm 5)\%$ of that in the background cosmic ray showers; see, for example, Stanev and Vankov (1985) and Stanev *et al.* (1985). One, therefore, cannot understand why the muon content was seen to be so much higher in the 'UHEGR' signals.

The above puzzle raises many questions. Are the 'signals' not genuine? In each of the claims of signal detection, the authors stated that the null hypothesis (i.e. that the observed result is only due to fluctuations in the background showers) was computed to have a very low probability and therefore was ruled out. If this is so, and the signal is real, is there some new physics in it? Is the signal not due to γ-rays but due to some other particles? Several papers have been published on these questions.

Photo-production cross sections, $\sigma_{\gamma N}$, have been measured at the accelerators and found to be small, $\sim 100\,\mu$b up to energies ~ 200 GeV; at higher energies there is no information. Drees and Halzen (1988) have suggested that, at extremely high energies, the photo-production cross section may increase by several orders

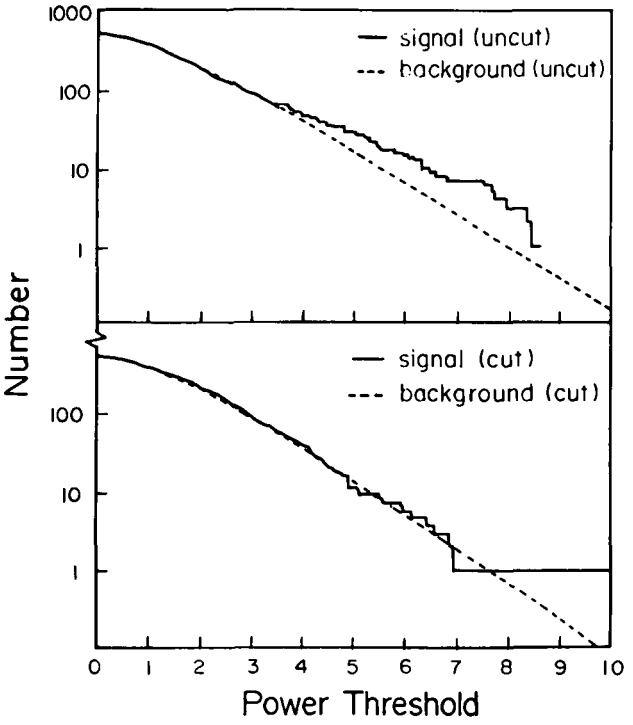

Figure 5.34. Cumulative Rayleigh power distributions of the event times of the Cerenkov flashes in the direction of Hercules X-1 in the data of the Whipple group (Reynolds *et al.* 1991) taken during 1984–7. Upper panel shows the uncut data in the source direction and in the background. Bottom panel shows the same after making the azwidth cut.

of magnitude depending on the low x behaviour of the structure functions of gluons and quarks. This increase, even if it were to happen, cannot, however, lead to increased muon densities in γ-ray showers; see Drees, Halzen and Hikasa (1989) and Gaisser *et al.* (1990). The point is that most of the muons result not from the first few collisions high in the atmosphere but from the more numerous collisions lower down, where the photon energies are in the range where the photoproduction cross sections have been measured to be low. Ochs and Stodolsky (1986) have suggested that $\sigma_{\gamma N}$ becomes huge at high energies, more rapid than that predicted by quantum chromodynamics. Halzen, Hikasa and Stanev (1986) have suggested that σ_{eN} might become large at high energies. There is yet another suggestion (Domokos and Nussinov 1987, Domokos and Kovesi-Domokos 1988) that $\sigma_{\nu N}$ becomes large at energies greater than 10^{12} eV and the primaries are neutrinos.

Jones (1990) has suggested that, at energies $\gtrsim 10^{18}$ eV, the primaries could be neutrons; the mean lifetime of neutrons at such energies could be 30 000 y. Although this suggestion is certainly important at energies of 10^{18} eV, where there

are some reports of emission from Cygnus X-3, it cannot explain the results at lower energies.

One may propose that the signal is not due to photons but to some other, hitherto unknown, neutral particles. The fact that the periodic nature of the signal is maintained, leading to a clearly discernible peak in the light curve, imposes an upper limit on the rest mass of such a particle. The time difference in the travel times from source to Earth for two neutral particles of energies E_1 and E_2 must obey the relation

$$\Delta t = \frac{DM^2}{2c}\left(\frac{1}{E_2^2} - \frac{1}{E_2^2}\right) \lesssim P/2 \tag{5.17}$$

Here, D is the distance from Earth to the source; M is the mass of the particle; and P is the pulsar period. Applying this condition to the case of Hercules X-1 ($P \approx 1.24$ s) and assuming $E_1 = 1$ TeV and $E_2 \gg E_1$, one finds that M must be less than 1.55 MeV/c^2. Any elementary particle of such a low mass enjoying a reasonably strong coupling with ordinary matter could not have escaped production and detection at accelerator experiments. The puzzle continues to remain unresolved.

There have been some other disconcerting features about some of the observations besides those already mentioned. Some authors detect a signal from Cygnus X-3 with a cut on muon numbers, i.e. selecting only those showers which are poor in muons, whereas Stamm and Samorski found that the showers were rich in muons. Some see the signal only when a cut is made on the age parameter; others without it. Some see both a DC excess and periodicity, while others see only the periodicity. Papers very critical of the observational situation have been published in the past by Bonnet-Bidaud and Chardin (1988) and Chardin and Gerbier (1989). Also, it was noted by Ramana Murthy (1987) that, in the vast majority of the reported results, the fluxes were so close to the experimental threshold as to make the luminosity of any arbitrary object lie close to the $L \propto D^2$ curve. This is clearly not to be expected, because one source does not 'know' what the others are doing. One has also witnessed that, in many observations, the statistical significance (signal-to-noise ratio) does not increase, as expected, as the square root of the exposure time. In the case of the episodal emissions, a group that first reports seeing an episode does not see any more of them, even though observations are carried out for much longer times.

One has to reflect on the fact that the Whipple group (Vacanti *et al.* 1991) saw a clear steady signal of unpulsed TeV γ-rays from the Crab; this could be understood in terms of the electron fluxes and magnetic fields that were deduced to exist within the nebula, *independently* of the UHEGR observations. As noted earlier, the 'signals' from Hercules X-1 vanished when the imaging cut was made. The authors observed more than a dozen other candidate sources, but did not see any UHEGR signal. There is, of course, no *independent* evidence that ultra high energy particle beams exist in these other candidate sources. One wonders, then, if the conclusion that the Crab is the only real source of UHEGR (and there are no others) is forced on us.

5.6 Summary

A number of observations have shown that UHEGR are emitted by pulsars, such as the Crab and Vela, by X-ray binaries, typified by Cygnus X-3, Hercules X-1 and Vela X-1, and by external galaxies such as M31 and Centaurus A. There have been also some upper limits in some cases. The details of the results are given in Section 5.3, and some of them are summarised in Tables 5.1–5.5. The situation can be summarised crudely in the following fashion. At $E_\gamma \sim 1$ TeV, time-averaged UHEGR fluxes are $\sim 10^{-11}\,\mathrm{cm}^{-2}\,\mathrm{s}^{-1}$ to within an order of magnitude from most objects. The time-averaged luminosities at $E_\gamma > 10^{12}$ eV for Galactic objects are $\sim 3 \times 10^{33}\,\mathrm{erg\,s}^{-1}$ to within a factor of four, except in the case of Cygnus X-3, for which the luminosity is $\sim 2 \times 10^{37}\,\mathrm{erg\,s}^{-1}$. Luminosities for the extragalactic objects M31 and Centaurus A are quoted by the authors to be 4×10^{40} and $2 \times 10^{41}\,\mathrm{erg\,s}^{-1}$, respectively. At $E_\gamma > 10^{15}$ eV, time-averaged UHEGR fluxes are in the region of $10^{-13}\,\mathrm{cm}^{-2}\,\mathrm{s}^{-1}$ to within a factor of five; time-averaged luminosities are $\sim 2.3 \times 10^{34}\,\mathrm{erg\,s}^{-1}$ in the case of Vela X-1 and $\sim 10^{37}\,\mathrm{erg\,s}^{-1}$ for the Crab pulsar and Cygnus X-3.

Most of the results published so far have two properties in common: poor statistics and time variability of source intensities. The detected signals, with a few exceptions, are seldom larger than 4 or 5σ above the background, and the calculated probabilities for chance fluctuations in the background are in most cases not much below 10^{-3}. The same groups of authors, using the same experimental set-ups, do not find signals every time, and therefore the conclusion must be that the source intensities vary with time, over time scales ranging from tens of milliseconds to years. Sceptics tend to deny the admissibility of the time-variability hypothesis and think that, whenever 'signals' are seen, they are probably due to chance fluctuations in the background. The sceptics imply that the improbability calculations made by the various authors probably did not take all the factors into account, and it must be admitted that such calculations are not easy to make.

Despite the sceptics' views, the present authors argue in favour of the experimenters in that, when they use a deliberately wrong period in a periodicity analysis, or when they look for excess counts from an uninteresting blank region in the sky, or for statistical fluctuations on the negative side (i.e. deficiencies of more than 4σ), signals are not seen. A fair summary of the situation, then, is that at least some of the experiments have already detected UHEGR from celestial sources, some with a high statistical significance and the rest at just above the detection threshold.

In future, efforts must be made to lower the detection thresholds both in terms of energy and flux levels. Also, whenever possible, experiments should be coordinated to view the same object simultaneously. It is clear that more and more detections relate to episodal emissions lasting for a few minutes to several tens of minutes, rather than steady emissions. The credibility of an episodal emissions rests, at the moment, entirely on the observations made and arguments presented by the single group reporting the episode. In a few examples in the past, there were simultaneous observations on an episode; for example, the Whipple

and the Durham groups on Hercules X-1 (Chadwick *et al.* 1987), two separated Cerenkov arrays operated by the Tata group (P.N. Bhat *et al.* 1986) on the Crab pulsar and the Baksan, and the KGF and the EAS–TOP arrays on the Crab (Acharya *et al.* 1990*a*). It would be extremely desirable if two or more arrays in the same longitudinal belt observed a given source simultaneously for episodal emissions. Simultaneous detection of an episode by more than one group goes a long way towards making the detection credible. Fortunately, several such groupings already exist. At TeV energies there are: the Narrabri, Adelaide, JANZOS and South Pole groups; the Potchefstroom and South Pole groups; and finally the two 10 m dishes at the Whipple Observatory. At PeV energies, the Los Alamos and the Utah–Michigan–Chicago collaborations, the KGF and Ooty groups, several groups in Japan and EAS–TOP, GREX and HEGRA arrays constitute such 'same longitudinal belt' groupings.

As mentioned in Section 5.1, the subject of UHEGR has a strong bearing on the problem of the origin of cosmic rays. Even after the whole sky is searched for UHEGR sources and mapped in a statistically significant way, many interesting problems remain. It will be necessary to decide whether the γ-rays come from the interactions of protons via π^0 decay or from electrons (or positrons) via synchrotron emission, bremsstrahlung and inverse Compton scattering processes; a deduction of the intensities of these charged particles in the source regions will then be necessary. Another problem will be to consider the leakage of charged high energy particles into interstellar space and whether the lifetimes and the numbers of sources are sufficient to account for the needed long term average input into cosmic radiation. Finally, it will be necessary to account for the charge composition, energy spectrum and the anisotropy of the cosmic radiation. The measurements described in this chapter are but a necessary first step towards solving the problem of the origin of the cosmic radiation.

Currently the EGRET detector aboard the GRO satellite is collecting data on γ-ray sources up to energies ~ 30 GeV. Prospects for locating more γ-ray sources are bright. Several ground-based arrays, both for TeV and PeV γ-ray observations, are in the process of being improved or are under operation. The Whipple collaboration (Akerlof *et al.* 1991) is about to commission a second 10 m diameter dish at Mount Hopkins, and the authors are confident that, by operating both the dishes simultaneously, they can reach angular resolutions of the order of 8 arc min in the source localisation. The array of the Utah–Michigan–Chicago collaboration described in Section 5.2.2 is the largest to go into operation for PeV γ-ray observations. In addition it has the largest muon detector array in operation. Observations with this array not only lead to establishing sources with the largest statistical significance but, in addition, will throw light on muon densities in γ-ray showers. One can, therefore, expect considerable progress in the field during the next decade.

5.7 Appendix: gamma-ray sources

See table on following page.

5.7 Appendix: gamma-ray sources

Object	Source direction RA h min	Decl. ° ′	l (degrees)	b (degrees)	Distance (kpc)	Radio	Optical	X-ray	γ-ray lines	Gamma-rays Medium high	(TeV)	(10^{15} eV)
Crab pulsar	05-32	+21-59	184.5	−5.8	2	○	○	○	○	○	○	○
Vela pulsar	08-34	−45-00	263.6	−2.5	0.5	○	○	○**		○	○	
Cygnus X-3	20-31	+40-47	79.9	+0.6	>11.4	○	×	○	×	○?	○	○*
Hercules X-1	16-56	+35-25	57.8	+37.7	5	×	○	○	○	×	○	○
Vela X-1	09-00	−40-21	263.0	+3.9	1.4	×	○	○		×	○	○
Geminga	6-34	+18-00	195	+4	≈0.1	×	○	○		○	○?	
SS433	19-09	+04-54	39.7	−2.2	5.5	○	○	○	○?		○?	
Galactic Centre	17-42	−28-54	0	0	≈10	○	○		○	○	○*	
M31 (Andromeda)	00-40	+41-00	121.4	−21.6	670		○				○?	
Centaurus A (NGC 5128)	13-22	−42-46	309.6	+19.4	6300	○	○	○		×	○	×
3C273	12-27	+02-20	289.3	+64.6	$\sim 9 \times 10^5$	○	○	○		○	×	×

○: observed at 4σ or higher significance
×: not seen
○?: claimed signals with less than 3.5σ effect; need confirmation
Blank: information not available
* decrease in intensity
** no periodicity

References

In the reference list we have listed single authors chronologically; authors with one other in alphabetical order of the second author; and works by three authors or more chronologically, irrespective of alphabetical ordering.

Chapter 1

Badhwar, G.D. and Stephens, S.A. (1977). *Proc. 15th Int. Cosmic Ray Conf.*, Plovdiv, **1**, 198.

Bedijn, P.J., Burger, J.J. and Swanenburg, B.N. (1973). *Proc. 13th Int. Cosmic Ray Conf.*, Denver, **5**, 3106.

Blandford, R.D. (1976). *Mon. Not. Roy. Astron. Soc.*, **176**, 465.

Chupp, E.L. (1976). *Gamma Ray Astronomy*, Reidel, Dordrecht.

Clayton, D.D., Colgate, S.A. and Fishman, D.J. (1969). *Astrophys. J.*, **155**, 75.

Dodds, D., Wolfendale, A. W. and Wdowczyk, J. (1976). *Mon. Not. Roy. Astron. Soc.*, **176**, 345.

Evans, R.D. (1955). *The Atomic Nucleus*, McGraw-Hill, New York.

Fisk, L.A. (1975). *Proc. 14th Int. Cosmic Ray Conf.*, Munich, **3**, 905.

Ginzburg, V.L. (1969). *Elementary Processes for Cosmic Ray Astrophysics*, Gordon and Breach, New York.

Ginzburg, V.L. and Syrovatskii, S.I. (1964). *The Origin of Cosmic Rays*, Pergamon Press, New York.

Hayakawa, S. (1969). *Cosmic Ray Physics*, Wiley-Interscience, New York.

Heitler, W. (1960). *The Quantum Theory of Radiation*, Oxford University Press.

Hillier, R. (1984). *Gamma Ray Astronomy*, Clarendon Press, Oxford.

Jauch, J.M. and Rohrlich, F. (1955). *The Theory of Photons and Electrons*, Addison-Wesley, Cambridge, MA.

Lamb, R.C., Ling, J.C., Mahoney, W.A., Riegler, G.R., Wheaton, W.A. and Jacobson, A.S. (1983). *Nature*, **305**, 37.

Lingenfelter, R.E., Higdon, J.C. and Ramaty, R. (1978). In *Gamma Ray Spectroscopy in Astrophysics* (Shen, B.S.P., ed.), p. 99, Benjamin, New York.

Lovelace, R.V.E. (1976) *Nature*, **262**, 649.

Manchester, R.N. and Taylor, J.H. (1977). *Pulsars*, Freeman, San Francisco.

Marmier, P. and Sheldon, E. (1969). *Physics of Nuclei and Particles*, vol. I, Academic Press, New York.

Meneguzzi, M. and Reeves, H. (1975). *Astron. Astrophys.*, **40**, 91.

Mihara, T., *et al.* (1990). *Nature*, **346**, 250.

Okeke, P.N. and Rees, M.J. (1980). *Astron. Astrophys.*, **81**, 263.

Ramaty, R. (1974). In *High Energy Particles and Quanta in Astrophysics* (McDonald, F.B. and Fichtel, C.E., eds), p. 122, MIT Press, Cambridge, MA.

Ramaty, R. and Lingenfelter, R.E. (1981). *Phil. Trans. Roy. Soc. Lond.*, **A301**, 671.
Ramaty, R., Kozlovsky, B. and Lingenfelter, R.E. (1979). *Astrophys. J. Suppl.*, **40**, 487.
Ramaty, R., Lingenfelter, R.E. and Kozlovsky, B. (1982). In *Gamma Ray Transients and Related Astrophysical Phenomena*, AIP Conf. Proc. 77 (Lingenfelter, R.E. *et al.*, eds), p. 211, AIP Press, New York.
Rossi, B. (1952). *High Energy Particles*, Prentice-Hall, Englewood Cliffs, NJ.
Stecker, F.W. (1971). *Cosmic Gamma Rays*, NASA SP-249, National Aeronautics and Space Administration, Washington, D.C.
Stecker, F.W. (1973). *Astrophys. & Space Sci.*, **20**, 47.
Stecker, F.W. (1975). In *Origin of Cosmic Rays* (Osborne, J.L. and Wolfendale, A.W., eds), p. 267, Reidel, Dordrecht.
Stephens, S.A. and Badhwar, G.D. (1981). *Astrophys. & Space Sci.*, **76**, 213.
Strong, A.W. and Wolfendale, A.W. (1981). *Phil. Trans. Roy. Soc. Lond.*, **A301**, 541.
Trumper, J., *et al.* (1978). *Astrophys. J. Lett.*, **219**, L105.
Wdowczyk, J., Thackzyk, W. and Wolfendale, A.W. (1972). *J. Phys.*, **A5**, 1419.
Wheaton, W., *et al.* (1979). *Nature*, **282**, 240.

Chapter 2

Abell, G.D. and Margon, B. (1979). *Nature*, **279**, 701.
Albernhe, F., Leborgne, J.F., Vedrenne, G., Boclet, D., Durochoux, P. and Da Coster, J.M. (1981). *Astron. Astrophys.*, **94**, 214.
Arnett, W.D. and Wefel, J.P. (1978). *Astrophys. J. Lett.*, **224**, L139.
Arnould, M., Norgaard, H., Thielemsn, F.-K. and Hillebrandt, W. (1980). *Astrophys. J.*, **237**, 931.
Baity, W.A., *et al.* (1981). *Astrophys. J.*, **244**, 429.
Begelman, M.C., Sarazin, C.L., Hatchett, S.P., McKee, C.F. and Arons, J. (1980). *Astrophys. J.*, **238**, 722.
Bhat, C.L., Houston, B.P., Issa, M.R., Mayer, C.J. and Wolfendale, A.W. (1985). *Nature*, **314**, 511.
Bhattacharya, D. and Gehrels, N. (1992). *Adv. Space Res.* In press.
Bussard, R.W., Ramaty, R. and Drachman, R.J. (1979). *Astrophys. J.*, **228**, 928.
Chupp, E.L. (1976). *Gamma Ray Astronomy*, Reidel, Dordrecht.
Clayton, D.D. (1973). In *Gamma-ray Astrophysics* (Stecker, F.W. and Trombka, J., eds), p. 263, NASA Spec. Publs. 339.
Clayton, D.D., Colgate, S.A. and Fishman, D.J. (1969). *Astrophys. J.*, **155**, 75.
Davidson, K. and McCray, R. (1980). *Astrophys. J.*, **241**, 1082.
Dean, A. J. and Ramsden, D. (1981). *Phil. Trans. Roy. Soc. Lond.*, **A301**, 577.
Dotani, T., *et al.* (1987). *Nature*, **330**, 230.
Fabian, A.C., Maccagni, D., Rees, M.J. and Stoeger, W.R. (1976). *Nature*, **260**, 683.
Gehrels, N., *et al.* (1984). *Astrophys. J.*, **278**, 122.
Gehrels, N., *et al.* (1987). *Astrophys. J.*, **322**, 215.
Gehrels, N., *et al.* (1992). *Astrophys. J. Lett.* In press.
Geldzahler, B.J., *et al.* (1985). *Proc. 19th Int. Cosmic Ray Conf.*, La Jolla, **1**, 187.
Graser, U. and Schonfelder, V. (1982). *Astrophys. J.*, **263**, 677.
Hall, R.D., Meegan, C.A., Walraven, G.D., Djuth, F.T. and Haymes, R.C. (1976). *Astrophys. J.*, **210**, 631.
Haymes, R.C., Walraven, G.D., Meegan, C.A., Hall, R.D., Djuth, F.T. and Shelton, D.M. (1976). *Astrophys. J.*, **210**, 593.
Hillebrandt, W. and Thielemann, F.-K. (1982). *Astrophys. J.*, **255**, 617.
Hillier, R. (1984). *Gamma-Ray Astronomy*, Clarendon Press, Oxford.

Johnson, W.N. and Haymes, R.C. (1973). *Astrophys. J.*, **184**, 103.
Koyama, K., *et al.* (1989). *Nature*, **339**, 603.
Lamb, R.C., Ling, J.C., Mahoney, W.A., Riegler, G.R., Wheaton, W.A. and Jacobson, A.S. (1983). *Nature*, **305**, 37.
Leventhal, M., MacCallum, C.J. and Watts, A.C. (1977). *Nature*, **266**, 696.
Leventhal, M., MacCallum, C.J. and Strong, P.D. (1978). *Astrophys. J. Lett.*, **225**, L11.
Leventhal, M., MacCallum, C.J., Huters, A.F. and Strong, P.D. (1980). *Astrophys. J.*, **240**, 338.
Leventhal, M., *et al.* (1989). *Nature*, **339**, 36.
Ling, J.C., Mahoney, W.A., Willett, J.B. and Jacobson, A.S. (1979). *Astrophys. J.*, **231**, 896.
Lingenfelter, R.E. and Ramaty, R. (1982). In *The Galactic Centre* (Riegler, G.R. and Blandford, R.D., eds), AIP Press, New York.
Lingenfelter, R.E. and Ramaty, R. (1985). *Proc. 19th Int. Cosmic Ray Conf.*, La Jolla, **9**, 19.
Lingenfelter, R.E. and Ramaty, R. (1989). *Astrophys. J.*, **343**, 686.
Lingenfelter, R.E., Higdon, J.C. and Ramaty, R. (1978). In *Gamma-Ray Spectroscopy in Astrophysics* (Cline, T.L. and Ramaty, R., eds), p. 252, NASA Tech. Mem. 79619.
MacCallum, C.J., *et al.* (1985). *Astrophys. J.*, **291**, 486.
Mahoney, W.A., Ling, J.C., Jacobson, A.S. and Tapphorn, R.M. (1980). *Nucl. Instr. Meth.*, **178**, 363.
Mahoney, W.A., Ling, J.C., Jacobson, A.S. and Lingenfelter, R.E. (1982). *Astrophys. J.*, **262**, 742.
Mahoney, W.A., Ling, J.C. and Jacobson, A.S. (1984*a*). *Astrophys. J.*, **278**, 784.
Mahoney, W.A., Ling, J.C., Wheaton, W.A. and Jacobson, A.S. (1984*b*). *Astrophys. J.*, **286**, 578.
Mallet, I., *et al.* (1992). In *Gamma Ray Line Astrophysics* (Durouchoux, Ph. and Prantzos, N., eds), AIP Press, New York. In press.
Margon, B. (1982). In *Accretion Driven Stellar X-Ray Sources* (Lewin, W.H.G. and Vanden Heuvel, E.P.T., eds), Cambridge University Press.
Marscher, A.P., Brecher, K., Wheaton, W.A., Ling, J.C., Mahoney, W.A. and Jacobson, A.S. (1984). *Astrophys. J.*, **281**, 566.
Matteson, J.L., Nolan, P.L. and Peterson, L.E. (1979). *X-Ray Astronomy*, p. 543, Pergamon Press, Oxford.
Matz, S.M., *et al.* (1988*a*). In *Nuclear Spectroscopy of Astrophysical Sources*, AIP Conf. Proc. 170 (Gehrels, N. and Share, G.H., eds), p. 51, AIP Press, New York.
Matz, S.M., *et al.* (1988*b*). *Nature*, **331**, 416.
Milgrom, M. (1979). *Astron. Astrophys. Lett.*, **76**, L3.
Owens, A. (1992). In *Gamma Ray Line Astrophysics* (Durouchoux, Ph. and Prantzos, N., eds), AIP Press, New York. In press.
Prantzos, N. (1992). In *Gamma Ray Line Astrophysics* (Durouchoux, Ph. and Prantzos, N., eds), AIP Press, New York. In press.
Ramaty, R. and Lingenfelter, R.E. (1979). *Nature*, **278**, 127.
Ramaty, R. and Lingenfelter, R.E. (1981). *Phil. Trans. Roy. Soc. Lond.*, **A301**, 671.
Ramaty, R. and Lingenfelter, R.E. (1992). In *Gamma Ray Line Astrophysics* (Durouchoux, Ph. and Prantzos, N., eds), AIP Press, New York. In press.
Ramaty, R. and Murphy, R.J. (1987). *Space Sci. Rev.*, **45**, 213.
Riegler, G.R., Ling, J.C., Mahoney, W.A., Wheaton, W.A., Willett, J.B., Jacobson, A.S. and Prince, T.A. (1981). *Astrophys. J. Lett.*, **248**, L13.

Riegler, G.R., Ling, J.C., Mahoney, W.A. and Jacobson, A.S. (1983). *J.P.L. Astrophys.* Preprint 54, California Institute of Technology.
Share, G.H., *et al.* (1985). *Astrophys. J. Lett.*, **292**, L61.
Share, G.H., *et al.* (1988). *Astrophys. J.*, **326**, 717.
Share, G.H., *et al.* (1990). *Astrophys. J.*, **358**, L45.
Strickman, M.S., Kurfess, J.D. and Johnson, W.N. (1982). *Astrophys. J. Lett.*, **253**, L23.
Sunayaev, R., *et al.* (1992). In *Proc. Texas/ESO–CERN Symposium on Relativistic Astrophysics, Cosmology and Fundamental Particle Physics*, Brighton, UK, 1991 (Barrows, J. and Thomas, P., eds), Cambridge University Press. In press.
Teegarden, B.J. (1991). *Adv. Space Res.* (In press).
Trombka, J.I. and Fichtel, C.E. (1982). NASA Tech. Mem. 84928.
Truran, J.W. and Cameron, A.G.W. (1978). *Astrophys. J.*, **219**, 226.
Von Ballmoos, P., *et al.* (1987). *Astrophys. J.*, **312**, 134.
Woosley, S.E. (1988*a*). *Astrophys. J.*, **324**, 466.
Woosley, S.E. (1988*b*). *Astrophys. J.*, **330**, 218.
Woosley, S.E. (1988*c*). *Astrophys. J.*, **331**, 101.
Woosley, S. (1992). In *Gamma Ray Line Astrophysics* (Durouchoux, Ph. and Prantzos, N., eds), AIP Press, New York. In press.
Woosley, S.E. and Weaver, T.A. (1980). *Astrophys. J.*, **238**, 1017.
Woosley, S.E., Axelrod, T.A. and Weaver, T.A. (1981). *Comments Nucl. Particle Phys.*, **9**, 185.

Chapter 3

Aharonian, F.A., Aloyan, A.M. and Sunyaev, R.A. (1980). *Yerevan Phys. Inst.*, preprint 432(39)-80.
Atteia, J.L., *et al.* (1987*a*). *Astrophys. J. Suppl.*, **64**, 305.
Atteia, J.L., *et al.* (1987*b*). *Astrophys. J. Lett.*, **320**, L105.
Babul, A., *et al.* (1987). *Astrophys. J. Lett.*, **316**, L49.
Baity, W.A., *et al.* (1984). In *High Energy Transients in Astrophysics*, AIP Conf. Proc. 115 (Woosley, S.E., ed.), p. 434, AIP Press, New York.
Barat, C., Chambon, G., Hurley, K., Niel, M., Vedrenne, G., Estulin, I.V., Kurt, V.G. and Zenchenko, V.M. (1979). *Astron. Astrophys. Lett.*, **79**, L24.
Barat, C., Chambon, G., Hurley, K., Niel, M., Vedrenne, G., Estulin, I.V., Kuznetsov, A.V. and Zenchenko, V.M. (1981). *Astrophys. & Space Sci.*, **75**, 83.
Barat, C., Hayles, R.I., Hurley, K., Niel, M., Vedrenne, G., Desai, U., Estulin, I.V., Kurt, V.G. and Zenchenko, V.M. (1983). *Astron. Astrophys.*, **126**, 400.
Barat, C., Hayles, R.J., Hurley, K., Niel, M., Vedrenne, G., Estulin, I.V. and Zenchenko, V.M. (1984*a*). *Astrophys. J.*, **285**, 791.
Barat, C., Hurley, K., Niel, M., Vedrenne, G., Evans, W.D., Fenimore, E.E., Klebesadel, R.W., Laros, J.G., Cline, T.L., Estulin, I.V., Zenchenko, V.M. and Kurt, V.G. (1984*b*). *Astrophys. J.*, **280**, 150.
Barat, C., Niel, M., Hayles, R.I., Hurley, K., Vedrenne, G., Mitrofanov, I.G., Estulin, I.V., Zenchenko, V.M. and Dolidze, V.S. (1984*c*). *Adv. Space Res.*, **3**, (10–12), 105.
Barat, C., Hurley, K., Niel, M., Vedrenne, G., Cline, T., Desai, U., Schaefer, B., Teegarden, B., Evans, W.D., Fenimore, E.E., Klebesadel, R., Laros, J.G., Estulin, I.V., Zenchenko, V.M., Kuznetsov, A.V., Kurt, V.G., Ilovaisky, S. and Motch, C. (1984*d*). *Astrophys. J. Lett.*, **286**, L5.
Beurle, K., Bewick, A., Mills, J.S. and Quenby, J.J. (1981). *Astrophys. & Space Sci.*, **77**, 201.

Bewick, A., Coe, M.J., Quenby, J.J. and Mills, J.S. (1975). *Nature*, **258**, 686.
Bhat, P.N., Gopalakrishnan, N.V., Gupta, S.K., Ramana Murthy, P.V., Sreekantan, B.V., Tonwar, S.C. and Viswanath, P.R. (1982). *Mon. Not. Roy. Astron. Soc.*, **199**, 1007.
Bisnovatyi-Kogan, G.S. (1987). In *The Origin and Evolution of Neutron Stars* (Helfand, D. and Huang, J.H., eds), p. 501, Reidel, Dordrecht.
Bisnovatyi-Kogan, G.S. and Chechetkin, V.M. (1981). *Sov. Astron.*, **25**, 320.
Boer, M., *et al.* (1986). *Adv. Space Res.*, **6** (4), 97.
Boer, M., *et al.* (1988). *Astron. Astrophys.*, **202**, 117.
Boer, M., *et al.* (1989). *Astron. Astrophys.*, **214**, 148.
Boer, M., *et al.* (1990). Preprint 174, Max-Planck Institut für Physik und Astrophysik, Institut für extraterrestriche Physik, Garching, Germany.
Boer, M., *et al.* (1992). In *Proc. Los Alamos Workshop on Gamma Ray Bursts*, Taos, New Mexico (Ho, C. and Fenimore, E., eds), Cambridge University Press.
Bonazzola, S., Hameury, J.M., Heyvaerts, J. and Lasota, J.P. (1984). *Astron. Astrophys.*, **136**, 89.
Brainerd, J.J. (1989). *Astrophys. J. Lett.*, **341**, L67.
Brainerd, J.J. and Lamb D.Q. (1987). *Astrophys. J.*, **313**, 231.
Brecher, K. (1982). In *Gamma Ray Transients and Related Astrophysical Phenomena*, AIP Conf. Proc. 77 (Lingenfelter, R.E., *et al.*, eds), p. 293, AIP Press, New York.
Bussard, R.W. and Lamb, F.K. (1982). In *Gamma Ray Transients and Related Astrophysical Phenomena*, AIP Conf. Proc. 77 (Lingenfelter, R.E., *et al.*, eds), p. 189, AIP Press, New York.
Cavallo, G. and Rees, M.J. (1978). *Mon. Not. Roy. Astron. Soc.*, **183**, 359.
Chambon, G. (1982). Doctoral Thesis 1045, UPS, Toulouse, France.
Cline, T.L. (1980). *Comments on Astrophys.*, **9**, 13.
Cline, T.L. (1982). In *Gamma Ray Transients and Related Astrophysical Phenomena*, AIP Conf. Proc. 77 (Lingenfelter, R.E., *et al.*, eds), p. 17, AIP Press, New York.
Cline, T.L. (1983). *Adv. Space Res.*, **3** (4), 175.
Cline, T.L. and Desai, U.D. (1974). *Proc. 9th ESLAB Symposium on the Context and Status of Gamma Ray Astronomy*, Noordwijk (Taylor, B., ed.), ESRO SP-106, p. 37.
Cline, T.L. and Desai, U.D. (1975). *Astrophys. J. Lett.*, **196**, L43.
Cline, T.L., Desai, U.D., Klebesadel, R.W. and Strong, I.B. (1973). *Astrophys. J. Lett.*, **185**, L1.
Cline, T.L., Desai, U.D., Schmidt, W.K.H. and Teegarden, B.J. (1977). *Nature*, **266**, 694.
Cline, T.L., Desai, U.D. and Teegarden, B.J. (1981*a*). *Astrophys. & Space Sci.*, **75**, 93.
Cline, T.L., Desai, U.D., Pizzichini, G., Teegarden, B.J., Evans, W.D., Klebesadel, R.W., Laros, J.G., Barat, C., Hurley, K., Niel, M., Vedrenne, G., Estulin, I.V., Mersov, G.A., Zenchenko, V.M. and Kurt, V.G. (1981*b*). *Astrophys. J. Lett.*, **246**, L133.
Cline, T.L., Desai, U.D., Teegarden, B.J., Evans, W.D., Klebesadel, R.W., Laros, J.G., Barat, C., Hurley, K., Niel, M., Vedrenne, G., Estulin, I.V., Kurt, V.G., Mersov, G.A., Zenchenko, V.M., Weisskopf, M.C. and Grindlay, J. (1982). *Astrophys. J. Lett.*, **255**, L45.
Colgate, S.A. (1968). *Can. J. Phys.*, **46**, S476.
Colgate, S.A. (1982). In *Gamma Ray Transients and Related Astronomical Phenomena*, AIP Conf. Proc. 77 (Lingenfelter, R.E., *et al.*, eds), p. 309, AIP Press, New York.

Colgate, S.A. and Petschek, A.G. (1981). *Astrophys. J.*, **248**, 771.
Daugherty, J.K. and Bussard, R.W. (1980). *Astrophys. J.*, **238**, 296.
Dennis, B.R., Frost, K.J., Kiplinger, A.L., Orwig, L.E., Desai, U. and Cline, T.L. (1982). In *Gamma Ray Transients and Related Astrophysical Phenomena*, AIP Conf. Proc. 77 (Lingenfelter, R.E., *et al.*, eds), p. 153, AIP Press, New York.
Dermer, C.D. (1989). *Astrophys. J. Lett.*, **347**, L13.
Downs, G.S. (1981). *Astrophys. J.*, **249**, 687.
Epstein, R.I. (1986). In *Radiation Hydrodynamics in Stars and Compact Objects* (Mihalas, D. and Winkler, D., eds), p. 305, Springer-Verlag, Berlin.
Epstein, R.I. (1989). In *Cosmic Gamma Rays, Neutrinos and Related Astrophysics* (Shapiro, M. and Wefel, E., eds), p. 381, Kluwer Academic Publishers, Dordrecht.
Evans, W.D., Belian, R.D. and Conner, J.P. (1976). *Astrophys. J. Lett.*, **207**, L91.
Evans, W.D., Klebesadel, R.W., Laros, J.G., Cline, T.L., Desai, U.D., Pizzichini, G., Teegarden, B.J., Hurley, K., Niel, M., Vedrenne, G., Estoolin, I.V., Kowznetsov, A.V., Zenchenko, V.M. and Kurt, V.G. (1980). *Astrophys. J. Lett.*, **237**, L7.
Evans, W.D., Fenimore, E.E., Klebesadel, R.W., Laros, J.G. and Terrell, N.J. (1981). *Astrophys. & Space Sci.*, **75**, 35.
Fabian, A.C., Icke, V. and Pringle, J.E. (1972). *Astrophys. & Space Sci.*, **42**, 77.
Felten, J.E. (1981). *Proc. 17th Int. Cosmic Ray Conf.*, Paris, **9**, 52.
Fenimore, E.E., Klebesadel, R.W., Laros, J.G. and Stockdale, R.E. (1982*a*). *Nature*, **297**, 665.
Fenimore, E.E., Laros, J.G., Klebesadel, R.W., Stockdale, R.E. and Kane, S.R. (1982*b*). In *Gamma Ray Transients and Related Astronomical Phenomena*, AIP Conf. Proc. 77 (Lingenfelter, R.E., *et al.*, eds), p. 201, AIP Press, New York.
Fenimore, E.E., *et al.* (1988). *Astrophys. J. Lett.*, **335**, L71.
Fishman, G.J. (1979). *Astrophys. J.*, **233**, 851.
Fishman, G.J. (1981). *Astrophys. & Space Sci.*, **75**, 125.
Fishman, G.J. (1988). In *Nuclear Spectroscopy of Astrophysical Sources*, AIP Conf. Proc. 170 (Gehrels, N. and Share, G., eds), p. 378, AIP Press, New York.
Fishman, G.J., Meegan, C.A., Watts, J.W. and Derrickson, J.H. (1978). *Astrophys. J. Lett.*, **233**, L13.
Fishman, G.J., *et al.* (1985). *Proc. 19th Int. Cosmic Ray Conf.*, La Jolla, **3**, 343.
Fishman, G.J., *et al.* (1989). *Proc. Gamma Ray Observatory Science Workshop* (Johnson, W.N., ed.), **2**, 39, NASA, Greenbert, MD.
Forrest, D.J., Chupp, E.L., Ryan, J.M., Cherry, M.L., Gleske, I.U., Reppin, C., Pinkau, K., Rieger, E., Kanbach, G., Kinzer, R.L., Share, G.H., Johnson, W.N. and Kurfess, J.D. (1980). *Solar Phys.*, **65**, 15.
Gilman, D., Metzer, A.E., Parker, R.H., Evans, L. and Trombka, J.I. (1980). *Astrophys. J.*, **236**, 951.
Golenetskii, S.V. (1988). *Adv. Space Res.*, **8** (2–3), p. 653.
Golenetskii, S.V., *et al.* (1979). *Sov. Astron. Lett.*, **5**, 340.
Golenetskii, S.V., Mazets, E.P., Aptekar, R.L. and Ilyinski, V.N. (1983). *Nature*, **306**, 451.
Golenetskii, S.V., Ilyinkskii, V.N. and Mazets, E.P. (1984). *Nature*, **307**, 41.
Golenetskii, S.V., *et al.* (1987*a*). Preprint 1119, Fiz. Tekh. Inst. Ioffe, Leningrad, Akad Nauk, USSR.
Golenetskii, S.V., *et al.* (1987*b*). *Sov. Astron. Lett.*, **13** (3), 166.
Grindlay, J.E., Wright, E.L. and McCrosky, R.E. (1974). *Astrophys. J. Lett.*, **192**, L113.

Grindlay, J.E., Cline, T., Desai, U.D., Teegarden, B.J., Pizzichini, G., Evans, W.D., Klebesadel, R.W., Laros, J.G., Hurley, K., Niel, M. and Vedrenne, G. (1982). *Nature*, **300**, 730.

Hartmann, D. and Blumenthal, G.R. (1989). *Astrophys. J.*, **342**, 521.

Hartmann, D. and Epstein, R.I. (1989). *Astrophys. J.*, **346**, 960.

Hartmann, D.H. and Woosley, S.F. (1988). In *Multiwavelength Astrophysics* (Cordova, F.A., ed.), p. 189, Cambridge University Press.

Harwit, M. and Salpeter, E.E. (1973). *Astrophys. J. Lett.*, **186**, L37.

Helfand, D.J. and Long, K.S. (1979). *Nature*, **282**, 589.

Helfand, D.J. and Vrtilek, S.D. (1983). *Nature*, **304**, 41.

Hewish, A., Bell, S.J., Pilkington, J.D.H., Scott, P.F. and Collins, R.A. (1968). *Nature*, **217**, 709.

Higdon, J.C. and Lingenfelter, R.E. (1984). In *High Energy Transients in Astrophysics*, AIP Conf. Proc. 115 (Woosley, S.E., ed.), p. 568, AIP Press, New York.

Higdon, J.C. and Lingenfelter, R.E. (1985). *Proc. 19th Int. Cosmic Ray Conf.*, La Jolla, **1**, 37.

Higdon, J.C. and Lingenfelter, R.E. (1990). *Ann. Rev. Astron. Astrophys.*, **28**, 401.

Higdon, J.C. and Schmidt, M. (1990). *Astrophys. J.*, **355**, 13.

Hjellming, R. and Ewald, S.P. (1981). *Astrophys. J. Lett.*, **246**, L137.

Ho, C. and Epstein, R. (1989). *Astrophys. J.*, **343**, 277.

Hudec, R., Ceplecha, Z., Ehrlich, J., Borovicka, J., Hurley, K., Atteia, J.L., Barat, C., Niel, M., Vedrenne, G., Estulin, I.V., Kuznetsov, A.K., Zenchenko, V.M., Cline, T.L., Desai, U., Evans, W.D., Fenimore, E., Klebesadel, R. and Laros, J. (1984). *Adv. Space. Res.*, **3** (10), 115.

Hudec, R., *et al.* (1990). *Astron. Astrophys.*, **235**, 174.

Hueter, G.J. (1987). Ph.D. Thesis, University of California, San Diego.

Hueter, G.J. and Gruber, D.E. (1982). In *Proc. Workshop on Accreting Neutron Stars* (Brinkmann, W. and Trumper, J., eds), Max Planck Institute Report 177, p. 213.

Hueter, G.J. and Lingenfelter, R.E. (1983). In *Positron-Electron Pairs in Astrophysics*, AIP Conf. Proc. 101 (Burns, M.L., Harding, A.K. and Ramaty, R., eds), p. 89, AIP Press, New York.

Hurley, K. (1982). In *Gamma Ray Transients and Related Astronomical Phenomena*, AIP Conf. Proc. 77 (Lingenfelter, R.E., *et al.*, eds), p. 85, AIP Press, New York.

Hurley, K. (1983*a*). *Adv. Space. Res.*, **3** (4), 163.

Hurley, K. (1983*b*). In *Positron-Electron Pairs in Astrophysics*, AIP Conf. Proc. 101 (Burns, M.L., Harding, A.K. and Ramaty, R., eds), p. 21, AIP Press, New York.

Hurley, K. (1983*c*). *Adv. Space Res.*, **3** (4), 203.

Hurley, K. (1984). In *High Energy Transients in Astrophysics*, AIP Conf. Proc. 115 (Woosley, S.E., ed.), p. 10, AIP Press, New York.

Hurley, K. (1989*a*). *Ann. New York Acad. Sci.*, **571**, 442.

Hurley, K. (1989*b*). In *Cosmic Gamma Rays, Neutrinos, and Related Astrophysics* (Shapiro, M. and Wefel, E., eds), p. 337, Kluwer Publishers, Dordrecht.

Jennings, M.C. (1982*a*). *Astrophys. J.*, **258**, 110.

Jennings, M.C. (1982*b*). In *Gamma Ray Transients and Related Astronomical Phenomena*, AIP Conf. Proc. 77 (Lingenfelter, R.E., *et al.*, eds), p. 107, AIP Press, New York.

Jennings, M.C. (1988). *Astrophys. J.*, **333**, 700.

Jennings, M.C. and White, R.S. (1980). *Astrophys. J.*, **238**, 110.

Joss, P.C. (1978). *Astrophys. J. Lett.*, **225**, L123.

Joss, P.C. (1979). *Comments Astrophys.*, **8**, 109.
Katoh, M., *et al.* (1984). In *High Energy Transients in Astrophysics*, AIP Conf. Proc. 115 (Woosley, S.E., ed.), p. 390, AIP Press, New York.
Katz, J.I. (1982). *Astrophys. J.*, **260**, 371.
Katz, J.I. (1983). In *Positron-Electron Pairs in Astrophysics*, AIP Conf. Proc. 101 (Burns, M.L., Harding, A.K. and Ramaty, R., eds), p. 65, AIP Press, New York.
Klebesadel, R.W. (1988). In *Physics of Neutron Stars and Black Holes* (Tanaka, Y., ed.), p. 387, University Academic Press, Tokyo.
Klebesadel, R.W., Strong, I.B. and Olson, R.A. (1973). *Astrophys. J. Lett.*, **182**, L85.
Klebesadel, R.W., Evans, W.D. and Laros, J.G. (1981). *Astrophys. & Space Sci.*, **75**, 5.
Klebesadel, R., *et al.* (1982). *Astrophys. J. Lett.*, **259**, L51.
Knight, F.K., Matteson, J.L. and Peterson, L.E. (1981). *Astrophys. & Space Sci.*, **75**, 21.
Kouveliotou, C., *et al.* (1987). *Astrophys. J. Lett.*, **322**, L21.
Kuznetsov, A.V., *et al.* (1987). *Sov. Astron. Lett.* **13** (6), 444.
Lamb, D.Q. (1982). In *Gamma Ray Transients and Related Astrophysical Phenomena*, AIP Conf. Proc. 77 (Lingenfelter, R.E., *et al.*, eds), p. 249, AIP Press, New York.
Lamb, D.Q. (1988). In *Nuclear Spectroscopy of Astrophysical Sources* (Gehrels, N. and Share, G.H., eds), p. 265, AIP Press, New York.
Lamb, D.Q., Lamb, F.K. and Pines, D. (1973). *Nature Phys. Sci.*, **246**, 52.
Laros, J.G. (1988). *Nature*, **333**, 124.
Laros, J.G., Evans, W.D., Fenimore, E.E., Klebesadel, R.W., Barat, C., Hurley, K., Niel, M., Vedrenne, G., Estulin, I.V., Zenchenko, V.M., and Mersov, G.A. (1981). *Astrophys. J. Lett.*, **245**, L63.
Laros, J.G., Evans, W.D., Fenimore, E.E. and Klebesadel, R.W. (1982). *Astrophys. & Space Sci.*, **88**, 243.
Laros, J.G., *et al.* (1985*a*). *Nature*, **318**, 448.
Laros, J.G., *et al.* (1985*b*). *Astrophys. J.*, **290**, 728.
Laros, J.G., *et al.* (1986). *Nature*, **322**, 152.
Laros, J.G., *et al.* (1987). *Astrophys. J. Lett.*, **320**, L111.
Lasota, J.P. and Belli, B.M. (1983). *Nature*, **304**, 139.
Lewin, W.G. and Joss, P.C. (1983). In *Accretion Drivers Stellar X-ray Sources* (Lewin, W.H.G. and Vanden Hewvel, E.P.J., eds), p. 41, Cambridge University Press.
Liang, E.P. (1981). *Nature*, **292**, 319.
Liang, E.P. (1982). *Nature*, **299**, 321.
Liang, E.P., Jerigan, T.E. and Rodrigues, R. (1983). *Astrophys. J.*, **271**, 766.
Ling, J.C., Mahoney, W.A., Willet, J.B. and Jacobson, A.S. (1982). In *Gamma Ray Transients and Related Astrophysical Phenomena*, AIP Conf. Proc. 77 (Lingenfelter, R.E., *et al.*, eds), p. 143, AIP Press, New York.
Lingenfelter, R.E., Higdon, J.C. and Ramaty, R. (1978). In *Gamma Ray Spectroscopy in Astrophysics* (Cline, T.L. and Ramaty, R., eds), p. 252, NASA Tech. Memo 79619.
London, R.A. and Cominsky, L.R. (1983). *Astrophys. J. Lett.*, **275**, L59.
Loznikov, V. and Kuznetsov, A.V. (1982). Preprint 743, Acad. Sci. USSR.
Mathewson, D.W. and Clark, J.N. (1973). *Astrophys. J.*, **180**, 725.
Mazets, E.P. (1985). *Proc. 19th Int. Cosmic Ray Conf.*, La Jolla, **9**, 415.
Mazets, E.P. (1988). *Adv. Space Res.*, **8** (2–3), 669.

Mazets, E.P. and Golenetskii, S.V. (1981*a*). *Astrophys. & Space Phys. Rev.*, **1**, 205.
Mazets, E.P. and Golenetskii, S.V. (1981*b*). *Astrophys. & Space Sci.*, **75**, 47.
Mazets, E.P. and Golenetskii, S.V. (1987). *Astronomia*, **32**, 16.
Mazets, E.P., Golenetskii, S.V., Ilinski, V.N., Aptekar, R.L. and Guryan, Y.A. (1979*a*). *Pisma Astron. Zh.*, **5**, 307 (*Sov. Astron. Lett.*, **5**, 163, 1980).
Mazets, E.P., Golenetskii, S.V., Ilinski, V.N., Aptekar, R.L. and Guryan, Y.A. (1979*b*). *Nature*, **282**, 587.
Mazets, E.P., Golenetskii, S.V., Aptekar, R.L., Guryan, Y.A. and Ilyinski, V.N. (1980). *Pisma Astron. Zh.*, **6**, 706.
Mazets, E.P., *et al.* (1981*a*). Preprint 738, A.F. Ioffe Physical-Technical Inst., Leningrad, USSR.
Mazets, E.P., Golenetskii, S.V., Ilyinskii, V.N., Panov, V.N., Aptekar, R.L., Guryan, Y.A., Proskura, M.P., Sokolov, I.A., Sokolova, Z.A. and Kharitonova, T.V. (1981*b*). *Astrophys. & Space Sci.*, **80**, pp. 3–83, 85–117, 119–43.
Mazets, E.P., *et al.* (1981*c*). Preprint 719, A.F. Ioffe Physical-Technical Inst., Leningrad, USSR.
Mazets, E.P., Golenetskii, S.V., Aptekar, R.L., Guryan, Y.A. and Ilyinskii, V.N. (1981*d*). *Nature*, **290**, 378.
Mazets, E.P., Golenetskii, S.V., Ilyninskii, V.N., Guryan, Y.A., Aptekar, R.L., Panov, V.N., Sokolov, I.A., Sokolova, Z.Y. and Kharitonova, T.V. (1982*a*). *Astrophys. & Space Sci.*, **82**, 261.
Mazets, E.P., Golenetskii, S.V., Guryan, Y.A. and Ilyinskii, V.N. (1982*b*). *Astrophys. & Space Sci.*, **84**, 173.
Mazets, E.P., Golenetskii, S.V., Guryan, Y.A., Aptekar, R.L., Ilyinskii, V.N. and Panov, V.N. (1983). In *Positron-Electron Pairs in Astrophysics*, AIP Conf. Proc. 101 (Burns, M.L., Harding, A.K. and Ramaty, R., eds), p. 36, AIP Press, New York.
Meegan, C.A., *et al.* (1985). *Astrophys. J.*, **291**, 479.
Metzger, A.E., Parker, R.H., Gilman, D., Peterson, L.E. and Trombka, J.I. (1974). *Astrophys. J. Lett.*, **194**, L19.
Mitrofanov, I.G., Estulin, I.V., Zenchenko, V.M., Dolidze, V.S., Barat, C., Niel, M., Hayles, R.I., Hurley, K. and Vedrenne, G. (1984). *Adv. Space Res.*, **3** (10–12), 119.
Mitrofanov, I.G., *et al.* (1989). Report PR-1497, Inst. Space Res., Moscow.
Moskalenko, E.I., *et al.* (1989). *Astron. Astrophys.*, **223**, 141.
Murakami, T. (1988). In *Physics of Neutron Stars and Black Holes* (Tanaka, Y., ed.), p. 405, University Academic Press, Tokyo.
Murakami, T. (1990). *Adv. Space Res.*, **10** (2), 63.
Murakami, T., *et al.* (1988). *Nature*, **335**, 234.
Murakami, T., *et al.* (1989). *Publ. Astron. Soc., Japan*, **41**, 405.
Murakami, T., *et al.* (1990). *Astron. Astrophys.*, **227**, 451.
Murakami, T., *et al.* (1991). *Nature*, **350**, 592.
Newman, M.J. and Cox, A.N. (1980). *Astrophys. J.*, **242**, 319.
Norris, J.P., Cline, T.L., Desai, U.D. and Teegarden, B.J. (1984). *Nature*, **308**, 434.
Paczynski, B. (1986). *Astrophys. J. Lett.*, **308**, L43.
Paczynski, B. (1987). *Astrophys. J. Lett.*, **317**, L51.
Paul, J., *et al.* (1990). *Proc. XXVIII COSPAR Meeting*, The Hague. In press.
Pedersen, H., Motch, C., Tarenghi, M., Danziger, J., Pizzichini, G. and Lewin, W.H.G. (1983). *Astrophys. J. Lett.*, **270**, L43.

Pedersen, H., Danziger, J., Hurley, K., Pizzichini, G., Motch, C., Ilovaisky, S., Gradmann, N., Brinkmann, W., Kanbach, G., Rieger, E., Reppin, C., Trumper, W. and Lund, N. (1984). *Nature*, **312**, 46.

Pedersen, H., *et al.* (1986). In *Gamma Ray Bursts*, AIP Conf. Proc. 141 (Liang, E.P. and Petrosian, V., eds), p. 39, AIP Press, New York.

Petrosian, V. (1981). *Astrophys. J.*, **251**, 727.

Pizzichini, G. (1981). *Astrophys. & Space Sci.*, **75**, 205.

Pizzichini, G., *et al.* (1986). *Astrophys. J.*, **301**, 641.

Prilutskii, O.P., Rozenthal, I. L. and Usov, V.V. (1975). *Usp. Fiz. Nauk.*, **116**, 517 (*Sov. Phys. Usp.*, **18**, 548, 1976).

Ramaty, R., Bonazzola, S., Cline, T.L., Kazanas, D., Metzaros, P., and Lingenfelter, R.E. (1980). *Nature*, **287**, 122.

Ramaty, R., Lingenfelter, R.E. and Bussard, R.W. (1981). *Astrophys. & Space Sci.*, **75**, 193.

Ramaty, R., McKinley, J.M. and Jones, F.C. (1982). In *Gamma Ray Transients and Related Astrophysical Phenomena*, AIP Conf. Proc. 77 (Lingenfelter, R.E., *et al.*, eds), p. 231, AIP Press, New York.

Ricker, G., *et al.* (1988). In *Nuclear Spectroscopy of Astrophysical Sources*, AIP Conf. Proc. 170 (Gehrels, N. and Share, G., eds), p. 407, AIP Press, New York.

Rieger, E., Reppin, C., Kanbach, G., Forrest, D.J., Chupp, E.L. and Share, G.H. (1982). In *Proc. Workshop on Accreting Neutron Stars* (Brinkmann, W. and Trumper, J., eds), Max Planck Inst. Report 177, p. 229.

Rothschild, R.E. and Lingenfelter, R.E. (1984). *Nature*, **312**, 737.

Ruderman, M. (1975). *Ann. N.Y. Acad. Sci.*, **262**, 164.

Ruderman, M. (1981). *Prog. Particle and Nucl. Phys.* **6**, 215 (Wilkinson, D., ed.), Pergamon Press, Oxford.

Schaefer, B.E. (1981). *Nature*, **294**, 722.

Schaefer, B.E. (1990). *Astrophys. J.*, **364**, 590.

Schaefer, B.E. and Desai, U.D. (1988). *Astron. Astrophys.*, **195**, 123.

Schaefer, B.E. and Ricker, G.R. (1983). *Nature*, **302**, 43.

Schaefer, B.E., Seitzer, P. and Bradt, H.V. (1983). *Astrophys. J. Lett.*, **270**, L49.

Schaefer, B.E., *et al.* (1984). *Astrophys. J. Lett.*, **286**, L1.

Schaefer, B.E., *et al.* (1987). *Astrophys. J.*, **313**, 226.

Schmidt, W.K.H. (1978). *Nature*, **271**, 525.

Schmidt, M., *et al.* (1988). *Astrophys. J. Lett.*, **329**, L85.

Strong, I.B. and Klebesadel, R.W. (1976). *Sci. Am.*, **235** (4), 66.

Taam, R.E. (1987). *Proc. 13th Texas Symp. Relativistic Astrophysics* (Ulmer, M., ed.), p. 546, World Scientific, Singapore.

Teegarden, B.J. (1982). In *Gamma Ray Transients and Related Astrophysical Phenomena*, AIP Conf. Proc. 77 (Lingenfelter, R.E., *et al.*, eds), p. 123, AIP Press, New York.

Teegarden, B.J. (1986). *Adv. Space Res.*, **6** (4), 93.

Teegarden, B.J. and Cline, T.L. (1980). *Astrophys. J. Lett.*, **236**, L67.

Teegarden, B.J. and Cline, T.L. (1981). *Astrophys. & Space Sci.*, **75**, 181.

Terrell, J., Evans, W.D., Klebesadel, R.W. and Laros, J.D. (1980). *Nature*, **285**, 383.

Terrell, J., Fenimore, E.E., Klebesadel, R.W. and Desai, U.D. (1982). *Astrophys. J.*, **254**, 279.

Trumper, J. (1978). In *Gamma Ray Spectroscopy in Astrophysics*, NASA Tech. Memo. 79619.

Tsygan, A.I. (1975). *Astrophys. & Space Sci.*, **44**, 21.

Tyson, J. and Jarvis, J. (1979). *Astrophys. J. Lett.*, **230**, L153.

Van Buren, D. (1982). In *Gamma Ray Transients and Related Astrophysical Phenomena*, AIP Conf. Proc. 77 (Lingenfelter, R.E., *et al.*, eds), p. 311, AIP Press, New York.
Van Horn, H.M. and Hansen, C.J. (1974). *Astrophys. J.*, **191**, 479.
Vedrenne, G. (1983). Paper presented at the Symposium on Problems of Collapse and Numerical Relativity, Toulouse, France.
Vedrenne, G. (1984). *Adv. Space Res.*, **3** (10), 97.
Vedrenne, G. and Chambon, G. (1983). *Space Sci. Rev.*, **36**, 319.
Ventura, J., Bonazzola, S., Hameury, J.M. and Heyvaerts, J. (1983). *Nature*, **301**, 491.
Vetter, F. (1982). *Phys. Rep.*, **81**, 293.
Wang, J.D., *et al.* (1989). *Phys. Rev. Lett.*, **63**, 1550.
Wood, K.S., Byram, E.T., Chubb, T.A., Friedman, H., Meekins, J.F., Share, G.H. and Yentis, J.A. (1981). *Astrophys. J.*, **247**, 632.
Woosley, S.E. (1982). In *Gamma Ray Transients and Related Astrophysical Phenomena*, AIP Conf. Proc. 77 (Lingenfelter, R.E., *et al.*, eds), p. 273, AIP Press, New York.
Woosley, S.E. and Wallace, R.K. (1982). *Astrophys. J.*, **258**, 716.
Yoshimori, M. (1978). *Austr. J. Phys.*, **31**, 189.
Zdziarski, A.A. (1987). *Proc. 13th Texas Symp. Relativistic Astrophysics* (Ulmer, M., ed.), p. 553, World Scientific, Singapore.
Zwicky, F. (1974). *Astrophys. Space Sci.*, **28**, 111.
Zytkow, A. (1990). *Astrophys. J.*, **359**, 138.

Chapter 4

Apparao, K.M. and Hoffman, J. (1970). *Astrophys. J.*, **5**, 25.
Baker, R.E., Bassani, L., Dean, A.J., Ramsden, D., Butler, R.C., di Cocco, G., Boella, G., Della Ventura, A., Perotti, F. and Villa, G. (1981). *Proc. 17th Int. Cosmic Ray Conf.*, Paris, **1**, 222.
Bania, T.M. (1977). *Astrophys. J.*, **216**, 381.
Bennett, K., Bignami, G.F., Boella, G., Buccheri, R., Burger, J.J., Cuccia, A., Hermsen, W., Higdon, J., Kanbach, G., Kock, L., Lichti, G.G., Masnou, J., Mayer-Hasselwander, H.A., Paul, J.A., Scarsi, L., Shukla, P.G., Swanenburg, B.N., Taylor, B.G. and Wills, R.D. (1976). *The Structure and Content of the Galaxy and Galactic Gamma Rays*, Goddard Space Flight Center X-662-76-154, p. 23.
Bennett, K., Bignami, G.F., Boella, G., Buccheri, R., Hermsen, W., Kanbach, G., Lichti, G.G., Masnou, J.L., Mayer-Hasselwander, H.A., Paul, J.A., Scarsi, L., Swanenburg, B.N., Taylor, B.G. and Wills, R.D. (1977). *Astron. Astrophys.*, **61**, 279.
Berkhuijsen, E.M., Haslam, C.G.T. and Salter, C.J. (1971). *Astron. Astrophys.*, **14**, 242.
Bertsch, D.L. *et al.* (1992). *Nature*, **357**, 306.
Bhat, C.L., Mayer, C.J. and Wolfendale, A.W. (1984*a*). *Astron. Astrophys.*, **140**, 284.
Bhat, C.L., Issa, M.R., Houston, B.P., Mayer, C.J. and Wolfendale, A.W. (1984*b*). *RAL Workshop on Astron. and Astrophys.*, RAL-84-101 (Gondhalekar, P.M., ed.), p. 39.
Bhat, C.L., Issa, M.R., Houston, B.P., Mayer, C.J. and Wolfendale, A.W. (1985*a*). *Nature*, **314**, 511.
Bhat, C.L., Issa, M.R., Mayer, C.J. and Wolfendale, A.W. (1985*b*). *Nature*, **314**, 515.
Bhat, C.L., Mayer, C.J. and Wolfendale, A.W. (1986). *Phil. Trans.*, **319**, 249.

Bignami, G.F. (1985). In *Cosmic Radiation in Contemporary Astrophysics*, International School of Cosmic Ray Astrophysics (Shapiro, M.M., ed.), Reidel, Dordrecht.

Bignami, G.F. and Caraveo, P.A. (1992). *Nature*, **357**, 287.

Bignami, G.F. and Hermsen, W. (1983). *Ann. Rev. Astron. Astrophys.*, **211**, 67.

Bignami, G.F., Fichtel, C.E., Hartman, R.C. and Thompson, D.J. (1979). *Astrophys. J.*, **232**, 649.

Bignami, G.F., Bennett, K., Buccheri, R., Caraveo, P.A., Hermsen, W., Kanbach, G.G., Lichti, G.G., Masnou, J.L., Mayer-Hasselwander, H.A., Paul, J.A., Sacco, B., Scarsi, L., Swanenburg, B.N. and Wills, R.D. (1981). *Astron. Astrophys.*, **93**, 71.

Bignami, G.F., Caraveo, P.A. and Paul, J.A. (1984). *Nature*, **310**, 464.

Bignami, G.F., *et al.* (1988). *Astron. Astrophys.*, **202**, L1.

Blandford, R.D. and Cowie, L.L. (1982). *Astrophys. J.*, **260**, 625.

Blitz, L. (1980). In *Giant Molecular Clouds in the Galaxy* (Solomon, P.M. and Edmunds, M.G., eds), Pergamon Press, Oxford.

Blitz, L. and Shu, F.H. (1980). *Astrophys. J.*, **238**, 148.

Bloemen, J.B.G.M. (1985). Ph.D. Thesis, University of Leiden.

Bloemen, J.B.G.M. (1987). *Astrophys. J.*, **317**, L15.

Bloemen, J.B.G.M., Bennett, K., Bignami, G.F., Blitz, L., Caraveo, P.A., Gottwald, M., Hermsen, W., Lebrun, F., Mayer-Hasselwander, H.A. and Strong, A.W. (1984*a*). *Astron. Astrophys.*, **135**, 12.

Bloemen, J.B.G.M., Caraveo, P.A., Hermsen, W., Lebrun, F., Maddalena, R.J., Strong, A.W. and Thaddeus, P. (1984*b*). *Astron. Astrophys.*, **139**, 37.

Bloemen, J.B.G.M., Strong, A.W., Blitz, L., Cohen, R.S., Dame, T.M., Grabelsky, D.A., Hermsen, W., Lebrun, F., Mayer-Hasselwander, H.A. and Thaddeus, P. (1986). *Astron. Astrophys.*, **154**, 25.

Bronfman, L., Cohen, R.S., Alvarez, H., May, J. and Thaddeus, P. (1988). *Astrophys. J.*, **324**, 248.

Brown, R.W. and Stecker, F.W. (1979). *Phys. Rev. Lett.*, **43**, 315.

Buccheri, R. (1980). *Advances in Space Exploration*, vol. 7, p. 17, Pergamon Press, Oxford.

Buccheri, R., Morini, M. and Sacco, B. (1981). *Phil. Trans. Roy. Soc. Lond.*, **A301**, 495.

Buccheri, R., *et al.* (1985). *Nature*, 316, 131.

Caraveo, P.A. (1981). *Phil. Trans. Roy. Soc. Lond.*, **A301**, 569.

Caraveo, P.A., Bennett, K., Bignami, G.F., Hermsen, W., Kanbach, G., Lebrun, F., Masnou, J.L., Mayer-Hasselwander, H.A., Paul, J.A., Sacco, B., Scarsi, L., Strong, A.W., Swanenburg, B.N. and Wills, R.D. (1980). *Astron. Astrophys. Lett.*, **91**, L3.

Caraveo, P.A., Bignami, G.F., Vigroux, L. and Paul, J.A. (1984). *Astrophys. J. Lett.*, **276**, L45.

Cavaliere, A., Morrison, P. and Pacini, F. (1970). *Astrophys. J. Lett.*, **162**, L133.

Chi, X. and Wolfendale, A.W. (1991). *J. Phys. G.*, **17**, 987.

Clark, G.W. (1971). *IAU Symp. 41* (La Buhn, F. and Lust, R., eds), p. 3, Reidel, Dordrecht.

Clark, G.W., Garmire, G.P. and Kraushaar, W.L. (1968). *Astrophys. J. Lett.*, **153**, L203.

Daugherty, J.K. and Harding, A. (1982). *Astrophys. J.*, **252**, 337.

Dean, A.J. and Ramsden, D. (1981). *Phil. Trans. Roy. Soc.*, **A301**, 577.

Derdeyn, S.M., Ehrmann, C.H., Fichtel, C.E., Kniffen, D.A. and Ross, R.W. (1972). *Nucl. Inst. & Meth.*, **98**, 557.

Dodds, D., Strong, A.W., Wolfendale, A.W. and Wdowczyk, J. (1974). *Nature*, **250**, 716.
Dodds, D., Strong, A.W. and Wolfendale, A.W. (1975). *Mon. Not. Roy. Astr. Soc.*, **171**, 569.
Fabian, A.C. and Nulsen, P.E.J. (1984). *Nature*, **312**, 48.
Fazio, G.G. (1970). *Nature*, **225**, 905.
Fazio, G.G. (1973). In *X-Ray and Gamma Ray Astronomy*, Proc. IAU Symp. 55, Madrid (Bradt, H. and Giacconi, R., eds), Reidel, Dordrecht.
Fichtel, C.E. (1981). *Phil. Trans. Roy. Soc. Lond.*, **A301**, 692.
Fichtel, C.E. (1982). NASA Tech. Memo. 83957.
Fichtel, C.E. (1983). In *Advances in Space Research* (Vedrenne, G. and Hurley, K., eds), vol. 3, no. 4, p. 5, Pergamon Press, Oxford.
Fichtel, C.E., Hartman, R.C., Kniffen, D.A. and Sommer, M. (1972). *Astrophys. J.*, **171**, 31.
Fichtel, C.E., Hartman, R.C., Kniffen, D.A., Thompson, D.J., Bignami, G.F., Ogelman, H., Ozel, M.E. and Turner, T. (1975). *Astrophys. J.*, **198**, 163.
Fichtel, C.E., Hartman, R.C., Kniffen, D.A., Thompson, D.J., Ogelman, H., Turner, T. and Ozel, M.E. (1978*a*). NASA Tech. Memo. 79650.
Fichtel, C.E., Simpson, G.A. and Thompson, D.J. (1978*b*). *Astrophys. J.*, **222**, 833.
Fichtel, C.E., *et al.* (1991). *Astrophys. J.*, **374**, 134.
Galper, A.M., Kirillov-Ugryumov, U.G., Kurochkin, A.V., Leikov, N.G., Luchkov, B.I., Hurkin, Uy.T., Fomin, V.P., Neshpor, Yu.I., Stepanian, A.A. and Vladimirsky, B.M. (1977). *Proc. 15th Int. Cosmic Ray Conf.*, Plovdiv, **1**, 131.
Ginzburg, V.L. (1968). *Astrophys. & Space Sci.*, **1**, 1.
Goned, A. (1981). *Proc. 17th Int. Cosmic Ray Conf.*, Paris, **1**, 210.
Gordon, M.A. and Burton, W.B. (1976). *Astrophys. J.*, **208**, 346.
Grenier, I.A., Hermsen, W. and Pollock, A.M.T. (1991). In AIP Conf. Proc. 220 (Matthews, J., ed.), p. 3, AIP Press, New York.
Halpern, J.P. and Holt, S.S. (1992). *Nature*, **357**, 22.
Harnden, F.R., *et al.* (1985). *Astrophys. J.*, **299**, 828.
Hartman, R.C., Fichtel, C.E., Kniffen, D.A., Lamb, R.C., Thompson, D.J., Bignami, G.F., Ogelman, H., Ozel, M. and Turner, T. (1976). *The Structure and Content of the Galaxy and Galactic Gamma Rays*, p. 12, Goddard Space Flight Center, X-662-76-154.
Haslam, C.G.T., Kearsey, S., Osborne, J.L., Phillips, S. and Stoffel, H. (1981). *Nature*, **289**, 470.
Hayakawa, S. (1952). *Prog. Theor. Phys.*, **8**, 517.
Heiligman, G.M. (1982). Ph.D. Thesis, Princeton University.
Henrichs, H.F. and Van den Heuvel, E.P.J. (1983). *Nature*, **303**, 213.
Hermsen, W. (1980). Ph.D. Thesis, University of Leiden.
Hermsen, W. (1981). *Phil. Trans. Roy. Soc. Lond.*, **A401**, 519.
Hermsen, W. and Bloemen, J.B.G.M. (1982). *Astrophysics and Space Science Library*, Reidel, Dordrecht.
Hermsen, W., *et al.* (1987). *Astron. Astrophys.*, **175**, 141.
Hess, V.F. (1912). *Phys. Z.*, **13**, 1084.
Houston, B.P. and Wolfendale, A.W. (1982). *Vistas, Astr.*, **26**, 107.
Houston, B.P. and Wolfendale, A.W. (1983). *Astron. Astrophys.*, **126**, 22.
Houston, B.P. and Wolfendale, A.W. (1984). *J. Phys. G*, **10**, 1587.
Houston, B.P. and Wolfendale, A.W. (1985). *J. Phys. G*, **11**, 407.
Houston, B.P., Riley, P.A. and Wolfendale, A.W. (1983). *Proc. 18th Int. Cosmic Ray Conf.*, Bangalore, **1**, 89.

Houston, B.P., Wolfendale, A.W. and Young, E.C.M. (1984). *J. Phys. G*, **10**, L147.
Hutchinson, G.W. (1952). *Phil. Mag.*, **43**, 847.
Issa, M.R. and Wolfendale, A.W. (1981*a*). *J. Phys. G*, **7**, L187.
Issa, M.R. and Wolfendale, A.W. (1981*b*). *Nature*, **292**, 430.
Issa, M.R., Strong, A.W. and Wolfendale, A.W. (1981*a*) *J. Phys. G*, **7**, 565.
Issa, M.R., Riley, P.A., Strong, A.W. and Wolfendale, A.W. (1981*b*). *J. Phys. G*, **7**, 973.
Khavtassi, J.Sh. (1960). *Atlas of Galactic Dark Nebulae*, Tiblisi, Abastumani Astrophysics Observatory.
Kniffen, D.A. and Fichtel, C.E. (1970). *Astrophys. J. Lett.*, **161**, L157.
Kniffen, D.A., Hartman, R.C., Thompson, D.J., Bignami, G.F., Fichtel, C.E., Ogelman, H. and Turner, T. (1974). *Nature*, **251**, 397.
Kniffen, D.A., Bertsch, D.L., Morris, D.L., Palmeira, R.A.R. and Rao, K.R. (1978). *Astrophys. J.*, **225**, 591.
Kniffen, D.A., Fichtel, C.E. and Hartman, R.C. (1983). *Proc. 18th Int. Cosmic Ray Conf.*, Bangalore, **1**, 165.
Knight, F.K. (1981). Ph.D. Thesis, University of San Diego.
Kraushaar, W.L., Clark, G.W., Garmire, G.P., Helmken, H., Higbie, P. and Agogino, M. (1965). *Astrophys. J.*, **141**, 845.
Kraushaar, W.L., Clark, G.W., Garmire, G.P., Borken, R., Higbie, P., Leong, C. and Thoros, J. (1972). *Astrophys. J.*, **177**, 341.
Kutner, M.L., Tucker, K.D., Chin, G. and Thaddeus, P. (1977). *Astrophys. J.*, **215**, 521.
Lamb, R.C., Fichtel, C.E., Hartman, R.C., Kniffen, D.A. and Thompson, D.J. (1977). *Astrophys. J. Lett.*, **212**, L63.
Lebrun, F. and Paul, J.A. (1983). *Astrophys. J.*, **266**, 276.
Li, T.P. and Wolfendale, A.W. (1981). *Astron. Astrophys. Lett.*, **100**, L26.
Li, T.P., Riley, P.A. and Wolfendale, A.W. (1983). *Mon. Not. Roy. Astron. Soc.*, **203**, 87.
Lichti, G.G., Buccheri, R., Caraveo, P., Gerardi, G., Hermsen, W., Kanbach, G., Masnou, J.L., Mayer-Hasselwander, H.A., Paul, J.A., Swanenburg, B.N. and Wills, R.D. (1980). *Advances in Space Exploration*, vol. 7, p. 49, Pergamon Press, Oxford.
Lyne, A.G., Manchester, R.N. and Taylor, J.H. (1985). *Mon. Not. Roy. Astron. Soc.*, **213**, 613.
Ma, Y. and Wolfendale, A.W. (1989). Proc. G.R.O. Science Workshop, Goddard Space Flight Center (Johnson, W.N., ed), NASA.
Masnou, J.L. (1977). *Proc. ESLAB Symp., Recent Advances in Gamma Ray Astronomy*, p. 33, ESA SP-124.
Masnou, J.L., *et al.* (1981). *Proc. 17th Int. Cosmic Ray Conf.*, Paris, **1**, 177.
Mayer-Hasselwander, H.A. (1983). In *Kinematics, Dynamics and Structure of the Milky Way* (Shuter, W.L.H., ed.), Reidel, Dordrecht.
Mayer-Hasselwander, H.A., Bennett, K., Bignami, G.F., Buccheri, R., Caraveo, P.A., Hermsen, W., Kanbach, G., Lebrun, F., Lichti, G.G., Masnou, J.L., Paul, J.A., Pinkau, K., Sacco, B., Scarsi, L., Swanenburg, B.N. and Wills, R.D. (1982). *Astron. Astrophys.*, **103**, 164.
Montmerle, Th. (1979). *Astrophys. J.*, **231**, 95.
Montmerle, Th. (1982). *Phil. Trans. Roy. Soc. Lond.*, **A301**, 505.
Morfill, G.E., Volk, H.J., Drury, L., Forman, M., Bignami, G.F. and Caraveo, P.A. (1981). *Astrophys. J.*, **246**, 810.
Ogelman, H.B., Fichtel, C.E., Kniffen, D.A. and Thompson, D.J. (1976). *Astrophys. J.*, **209**, 584.

Omnes, R. (1969). *Phys. Rev. Lett.*, **23**, 38.
Pagel, B.E.J. and Edmunds, M.G. (1981). *Ann. Rev. Astron. Astrophys. J.*, **276**, 182.
Parsignault, D.R., Gursky, H., Kellogg, E.M., Matilsky, T., Murray, S., Schreir, E., Tananbaum, H. and Giacconi, R. (1972). *Nature Phys. Sci.*, **239**, 123.
Pollock, A.M.T., Bignami, G.F., Hermsen, W., Kanbach, G., Lichti, G.G., Masnou, J.L., Swanenburg, B.N. and Wills, R.D. (1981). *Astron. Astrophys.*, **94**, 116.
Poon, C.B. (1983). Ph.D. Thesis, University of Hong Kong.
Protheroe, R.J., Strong, A.W. and Wolfendale, A.W. (1979). *Mon. Not. Roy. Astron. Soc.*, **188**, 863.
Rana, N.C., Sadzinska, M., Wdowczyk, J. and Wolfendale, A.W. (1984). *Astron. Astrophys.*, **141**, 394.
Rogers, M.J. and Wolfendale, A.W. (1987). *Proc. 20th Int. Cosmic Ray Conf.*, Moscow, **1**, 81.
Rogers, M.J., Sadzinska, M., Szabelski, J., van der Walt, D.J. and Wolfendale, A.W. (1988). *J. Phys. G*, **14**, 1147.
Sacher, W. and Schonfelder, V. (1984). *Astrophys. J.*, **279**, 817.
Said, S.S., Wolfendale, A.W., Giler, M. and Wdowczyk, J. (1982). *J. Phys. G*, **8**, 383.
Sanders, D.B., Solomon, P.M. and Scoville, N.Z. (1984). *Astrophys. J.*, **276**, 182.
Scarsi, L., Buccheri, R., Gerardi, G. and Sacco, B. (1981). *Origin of Cosmic Rays*, IAU Symp. 94, p. 279 (Setti, G., Spada, G. and Wolfendale, A.W., eds), Reidel, Dordrecht.
Schlickeiser, R. (1981). *Astron. Astrophys.*, **94**, 57.
Scoville, N.Z. and Solomon, P.M. (1973). *Astrophys. J.*, **180**, 31.
Scoville, N.Z., Solomon, P.M. and Jefferts, K. (1974). *Astrophys. J. Lett.*, **187**, L63.
Share, G.H. (1973). *Int. Symp. and Workshop on Gamma-Ray Astrophysics*, Goddard Space Flight Center, X-641-73-180.
Share, G.H., Kinzer, R.L. and Seeman, N. (1973). *X-rays and Gamma Ray Astronomy*, Proc. IAU Symp. 55, Madrid (Bradt, H. and Giacconi, R., eds), Reidel, Dordrecht.
Solomon, P.M. and Stecker, F.W. (1974). *Proc. ESLAB Gamma Ray Symp.*, Frascati, ESRO SP-106, p. 253.
Sreekumar, P. and Fichtel, C. (1992). *Astron. Astrophys.* In press.
Stecker, F.W. (1969). *Astrophys. J.*, **157**, 507.
Stecker, F.W. (1971). *Cosmic Gamma Rays*, Mono Book Corp., Baltimore.
Strong, A.W. and Bignami, G.F. (1983). *Astrophys. J.*, **274**, 549.
Strong, A.W. and Lebrun, F. (1982). *Astron. Astrophys.*, **105**, 159.
Strong, A.W., Wdowczyk, J. and Wolfendale, A.W. (1973). *Gamma Ray Astrophysics*, p. 259, NASA Spec. Publ. 339.
Strong, A.W., Wdowczyk, J. and Wolfendale, A.W. (1974). *J. Phys. A*, **7**, 120.
Strong, A.W., Wolfendale, A.W. and Worrall, D.M. (1976). *J. Phys. A*, **9**, 1553.
Strong, A.W., Bignami, G.F., Bloemen, J.B.G.M., Buccheri, R., Caraveo, P.A., Hermsen, W., Kanbach, G., Lebrun, F., Mayer-Hasselwander, H.A., Paul, J.A. and Wills, R.D. (1982). *Astron. Astrophys.*, **115**, 404.
Swanenburg, B.N., Bennett, K., Bignami, G.F., Buccheri, R., Caraveo, P., Hermsen, W., Kanbach, G., Lichti, G.G., Masnou, J.L., Mayer-Hasselwander, H.A., Paul, J.A., Sacco, B., Scarsi, L. and Wills, R.D. (1981). *Astrophys. J. Lett.*, **243**, L69.
Taylor, J.H. and Manchester, R.N. (1981). *Astr. J.*, **86**, 1953.
Thompson, D.J., Fichtel, C.E., Kniffen, D.A. and Ogelman, H.B. (1975). *Astrophys. J. Lett.*, **200**, L79.

Thompson, D.J., Fichtel, C.E., Hartman, R.C., Kniffen, D.A., Bignami, G.F., Lamb, R.C., Ogelman, H., Ozel, M.E. and Turner, T. (1976). *The Structure and Content of the Galaxy and Galactic Gamma Rays*, p. 1, Goddard Space Flight Center, X-662-76-154.

Thompson, D.J., Fichtel, C.E., Kniffen, D.A. and Ogelman, H.B. (1977). *Astrophys. J. Lett.*, **214**, L17.

Trombka, J.I. and Fichtel, C.E. (1982). NASA Tech. Memo. 84928, Goddard Space Flight Center, Maryland.

Trombka, J.I., Dyker, C.S., Evans, L.G., Bielefeld, H.M., Seltzer, S.M. and Metzger, A.E. (1977). *Astrophys. J.*, **212**, 925.

van der Walt, D.J. and Wolfendale, A.W. (1988). *Space Sci. Rev.*, **47**, 1.

Wills, R.D. (1981). *Phil. Trans. Roy. Soc. Lond.*, **A301**, 537.

Wills, R.D., Bennett, K., Bignami, G.F., Buccheri, R., Caraveo, P., D'Amino, N., Hermsen, W., Kanbach, G., Lichti, G.G., Masnou, J.L., Mayer-Hasselwander, H.A., Paul, J.A., Sacco, B. and Swanenburg, B.N. (1980). *Non-solar Gamma-Rays* (Cospar Symp.) (Cowsik, R. and Wills, R.D., eds), *Adv. Space Explor.*, **7**, 43.

Wolfendale, A.W. (1980). *Origin of Cosmic Rays, IAU Symp. 94*, p. 309, Reidel, Dordrecht.

Worrall, D.M. (1977). Ph.D. Thesis, University of Durham.

Wouterloot, J.G.A. (1981). Ph.D. Thesis, Leiden University.

Chapter 5

Acharya, B.S., *et al.* (1990*a*). *Nature*, **347**, 364.

Acharya, B.S. (1990*b*). *Astron. Astrophys.*, **232**, L5.

Acharya, B.S., Bhat, P.N., Gandhi, V.N., Ramana Murthy, P.V., Satyanarayana, G.P. and Viswanath, P.R. (1991). In AIP Conf. Proc. 220 (Matthews, J., ed.), p. 87, AIP Press, New York.

Aglietta, M., *et al.* (1991). *Europhys. Lett.*, **15**, 81.

Akerlof, C., DiMarco, J., Levy, H., Meyer, D., Radusewicz, P., Tschirhart, R., Yama, Z. and MacCallum, C. (1989). *Proc. GRO Workshop* (Johnson, W.N., ed.), p. 4, NASA/Goddard Space Flight Center, MD.

Akerlof, C., *et al.* (1991). *Astrophys. J. Lett.*, **377**, L97.

Alexeenko, V.V., *et al.* (1989). *Proc. Int. Workshop on Very High Energy Gamma Ray Astronomy*, Crimea (Stepanian, A.A., Fegan, D.J. and Cawley, M.F., eds), p. 187.

Baltrusaitis, R.M., Cassiday, G.L., Cooper, R., Elbert, J.W., Gerhardy, P.R., Loh, E.C., Mizumoto, Y., Sokolsky, P., Sommers, P. and Steck, D. (1985). *Astrophys. J. Lett.*, **293**, L69.

Battistoni, G., *et al.* (1985). *Phys. Rev. Lett. B*, **155**, 465.

Berezinsky, V.S. and Kudryavtsev, V.A. (1990). *Astrophys. J.*, **349**, 620.

Bhat, C.L., Sapru, M.L. and Razdan, H. (1986). *Astrophys. J.*, **306**, 587.

Bhat, C.L., *et al.* (1991). *Astrophys. J.*, **369**, 475.

Bhat, P.N., Gupta, S.K., Ramana Murthy, P.V., Sreekantan, B.V., Tonwar, S.C. and Viswanath, P.R. (1980). *Astron. Astrophys.*, **81**, L3.

Bhat, P.N., Gopalkrishnan, N.V., Gupta, S.K., Ramana Murthy, P.V., Sreekantan, B.V., Tonwar, S.C. and Viswanath, P.R. (1982). *Mon. Not. Roy. Astron. Soc.*, **199**, 1007.

Bhat, P.N., *et al.* (1985). *Proc. Workshop on Techniques in Ultra High Energy Gamma Ray Astronomy, La Jolla* (Protheroe, R.J. and Stephens, S.A., eds), p. 1.

Bhat, P.N., Ramana Murthy, P.V., Sreekantan, B.V. and Viswanath, P.R. (1986). *Nature*, **319**, 127.

Bhat, P.N., Gupta, S.K., Ramana Murthy, P.V., Sreekantan, B.V., Tonwar, S.C. and Vishwanath, P.R. (1987*a*). *Astron. Astrophys.*, **178**, 242.
Bhat, P.N., *et al.* (1987*b*). See the Rapporteur paper of Protheroe (1987).
Bhat, P.N., *et al.* (1987*c*). *Astron. Astrophys.*, **171**, 84.
Bhat, P.N., *et al.* (1988). *J. Astrophys. Astron.*, **9**, 155.
Bhat, P.N., *et al.* (1990*a*). *Proc. 21st Int. Cosmic Ray Conf.*, Adelaide, **2**, 148.
Bhat, P.N., Acharya, B.S., Gandhi, V.N., Ramana Murthy, P.V., Sathyanarayana, G.P. and Vishwanath, P.R. (1990*b*). *Astron. Astrophys.*, **236**, L1.
Blackett, P.M.S. (1948). Rep. Gassiot Committee 34, UK.
Bond, I.A., *et al.* (1988). *Phys. Rev. Lett.*, **61**, 2292.
Bond, I.A., *et al.* (1989). *Astrophys. J. Lett.*, **344**, L17.
Bond, I.A., *et al.* (1990). *Proc. 21st Int. Cosmic Ray Conf.*, Adelaide, **2**, 271.
Bonnet-Bidaud, J.M. and Chardin, G. (1988). *Phys. Rep.*, **170**, 325.
Boone, J., Cady, R., Cassiday, G.L., Elbert, J.W., Loh, E.C., Sokolsky, P., Steck, D. and Wasserbach, S. (1984). *Astrophys. J.*, **285**, 264.
Bowyer, C.S., Lampton, M., Mack, J. and De Mondonca, F. (1970). *Astrophys. J. Lett.*, **161**, L1.
Braun, O. and Sitte, K. (1965). *Proc. 9th Int. Cosmic Ray Conf.*, London, **2**, 712.
Brazier, K.T., *et al.* (1989). *Exptal. Astronomy*, **1**, 77.
Brazier, K.T.S., Carraminana, A., Chadwick, P.M., Dipper, N.A., Lincoln, E.W., Mannings, V.G., McComb, T.J.L., Orford, K.J., Rayner, S.M. and Turver, K.E. (1990*a*). *Proc. 21st Int. Cosmic Ray Conf.*, Adelaide, **2**, 304.
Brazier, K.T., *et al.* (1990*b*). *Astrophys. J.*, **350**, 745.
Brazier, K.T., *et al.* (1990*c*). *Proc. 21st Int. Cosmic Ray Conf.*, Adelaide, **2**, 292.
Brazier, K.T., *et al.* (1990*d*). *Proc. 21st Int. Cosmic Ray Conf.*, Adelaide, **2**, 296.
Brazier, K.T., *et al.* (1990*e*). *Nucl. Phys. B* (*Proc. Suppl.*), **14A**, 188.
Brazier, K.T., *et al.* (1990*f*). *Proc. 21st Int. Cosmic Ray Conf.*, Adelaide, **2**, 288.
Brink, C., *et al.* (1990). *Astrophys. J. Lett.*, **364**, L37.
Browning, R. and Turver, K.E. (1977). *Nuovo Cimento*, **38A**, 223.
Byrne, M.P., *et al.* (1990). *Proc. 21st Int. Cosmic Ray Conf.*, Adelaide, **2**, 395.
Carr, B.J. (1976). *Astrophys. J.*, **206**, 8.
Carraminana, A., Chadwick, P.M., Dipper, N.A., Lincoln, E.W., Mannings, V.G., McComb, T.J.L., Orford, K., Rayner, S.M., Turver, K.E. and Williams, D.G. (1989). *Astrophys. J.*, **346**, 967.
Cassiday, G., *et al.* (1989). *Phys. Rev. Lett.*, **62**, 383.
Cassiday, G., *et al.* (1990*a*). *Proc. 21st Int. Cosmic Ray Conf.*, Adelaide, **2**, 14.
Cassiday, G., *et al.* (1990*b*). *Proc. 21st Int. Cosmic Ray Conf.*, Adelaide, **2**, 60.
Castagnoli, C., *et al.* (1990). *Proc. 21st Int. Cosmic Ray Conf.*, Adelaide, **2**, 204.
Cawley, M.F. and Weekes, T.C. (1984). *Astron. Astrophys.*, **133**, 80.
Cawley, M.F., *et al.* (1985). *Proc. 19th Int. Cosmic Ray Conf.*, La Jolla, **1**, 264.
Cawley, M.F., *et al.* (1990). *Exptal. Astronomy*, **1**, 173.
Cawley, M.F., *et al.* (1991). *Astron. Astrophys.*, **243**, 143.
Chadwick, P.M., *et al.* (1985). *Nature*, **318**, 642.
Chadwick, P.M., *et al.* (1987). *Very High Energy Gamma Ray Astronomy* (Turver, K.E., ed.), p. 121, Reidel, Dordrecht.
Chadwick, P.M., *et al.* (1988). *Astrophys. J.*, **333**, L19.
Chadwick, P.M., McComb, T.J.L. and Turver, K.E. (1990). *J. Phys. G*, **16**, 1773.
Chanmugam, G. and Brecher, K. (1985). *Nature*, **313**, 767.
Chardin, G. and Gerbier, G. (1989). *Astron. Astrophys.*, **210**, 52.
Cheng, A., Ruderman, M. and Sutherland, P. (1976). *Astrophys. J.*, **203**, 209.
Cheng, K.S. and Ruderman, M. (1989). *Astrophys. J. Lett.*, **337**, L77.

Cheng, K.S., Ho, C. and Ruderman, M. (1986*a*). *Astrophys. J.*, **300**, 500.
Cheng, K.S., Ho, C. and Ruderman, M. (1986*b*). *Astrophys. J.*, **300**, 522.
Cheng, K.S., Cheung, T., Lau, M.M., Yu, K.N. and Kwok, P.W. (1990). *J. Phys. G*, **16**, 1115.
Chudakov, A.E. (1989). *Cosmic Gamma Rays, Neutrinos, and Related Astrophysics*, p. 163, Kluwer Academic Publishers, Dordrecht.
Chudakov, A.E., Zatsepin, V.I., Nesterova, N.M. and Dadykin, V.L. (1962). *J. Phys. Soc. Japan*, **17**, A-III, 106.
Chudakov, A.E., Dadykin, V.L., Zatsepin, V.I. and Nesterova, N.M. (1964). *Proc. Lebedev Physical Inst.*, **26**, 118.
Chudakov, A.E., Dadykin, V.L., Zatsepin, V.I. and Nesterova, N.M. (1965). *Trans. Consultants Bureau*, **26**, 99.
Chung, T. and MacKeown, P.K. (1988). *Il Nuowo Cimento*, **11c**, 193.
Ciampa, D., *et al.* (1988). *Astrophys. J. Lett.*, **326**, L9.
Ciampa, D., *et al.* (1990). *Proc. 21st Int. Cosmic Ray Conf.*, Adelaide, **2**, 35.
Clay, R.W., *et al.* (1984*a*). *Nature*, 309, 687.
Clay, R.W., *et al.* (1984*b*). *Aust. J. Phys.*, **37**, 91.
Cocconi, G. (1959). *Proc. Moscow Conf. on Cosmic Rays*, **2**, 309.
Cocke, W.J., Disney, M.J. and Taylor, D.J. (1969). *Nature*, **221**, 525.
Comella, J.M., Craft, H.D., Lovelace, R.V.E., Sutton, J.M. and Tyler, G.L. (1969). *Nature*, **221**, 453.
Corbato, S.C., Ciampa, D., Kolvdziejezak, J., Matthews, J., Nitz, D., Sinclair, D., Thornton, G. and van der Velde, J.C. (1990). *Proc. 21st Int. Cosmic Ray Conf.*, Adelaide, **2**, 159.
Danaher, S., Fegan, D.J., Porter, N.A. and Weekes, T.C. (1981). *Nature*, **289**, 568.
Dingus, B.L., *et al.* (1988*a*). *Phys. Rev. Lett.*, **60**, 1785.
Dingus, B.L., *et al.* (1988*b*). *Phys. Rev. Lett.*, **61**, 1906.
Domokos, G. and Nussinov, S. (1987). *Phys. Lett.*, **B187**, 372.
Domokos, G. and Kovesi-Domokos, S. (1988). *Phys. Rev.*, **D83**, 2833.
Dowthwaite, J.C., Gibson, A.I., Harrison, A.B., Kirkman, I.W., Lotts, A.P., Macrae, J.H., Orford, K.J., Turver, K.E. and Walmsley, M. (1983). *Astron. Astrophys.*, **126**, 1.
Dowthwaite, J.C., Harrison, A.B., Kirkman, I.W., Macrae, H.J., Orford, K.J., Turver, K.E. and Walmsley, M.S. (1984*a*). *Astron. Astrophys.*, **136**, L14.
Dowthwaite, J.C., Harrison, A.B., Kirkman, I.W., Macrae, H.J., Orford, K.J., Turver, K.E. and Walmsley, M.S. (1984*b*). *Astrophys. J. Lett.*, **286**, L35.
Dowthwaite, J.C., Harrison, A.B., Kirkman, I.W., Macrae, H.J., Orford, K.J., Turver, K.E. and Walmsley, M.S. (1984*c*). *Nature*, **309**, 691.
Dowthwaite, J.C., Harrison, A.B., Kirkman, I.W., Macrae, H.J., Orford, K.J., Turver, K.E. and Walmsley, M.S. (1985). *Astron. Astrophys.*, **142**, 55.
Drees, M. and Halzen, F. (1988). *Phys. Rev. Lett.*, **61**, 275.
Drees, M., Halzen, F. and Hikasa, K. (1989). *Phys. Rev.*, **D39**, 1310.
Dzikowski, T., Gawin, J., Grochalska, B. and Wdowczyk, J. (1983). *J. Phys. G*, **9**, 459.
Eichler, D. and Vestrand, W.T. (1984). *Nature*, **307**, 613.
Fazio, G.G. (1967). *Ann. Rev. Astron. and Astrophys.*, **5**, 481.
Fazio, G.G., Helmken, H.F., O'Mangain, E., Rieke, G.H. and Weekes, T.C. (1972). *Astrophys. J. Lett.*, **175**, L117.
Fegan, D.J. (1990). *Proc. 21st Int. Cosmic Ray Conf.*, Adelaide, **11**, 23.
Fegan, D.J., *et al.* (1989). *Astron. Astrophys.*, **211**, L1.
Felten, J.E. and Morrison, P. (1966). *Astrophys. J.*, **146**, 686.

Fomin, V.P., Vladimirsky, B.M. and Stepanian, A.A. (1977). *Proc. 15th Int. Cosmic Ray Conf.*, Plovdiv, **1**, 12.

Fritz, G., Henry, R.C., Meekins, J.F., Chubb, T.A. and Friedman, H. (1969). *Science*, **164**, 709.

Fruin, J.H., Jelley, J.V., Long, C.D., Porter, N.A. and Weekes, T.C. (1964). *Phys. Lett.*, **10**, 176.

Gaisser, T.K., *et al.* (1987). *Nature*, **329**, 314.

Gaisser, T.K., *et al.* (1989*a*). *Astrophys. J.*, **345**, 423.

Gaisser, T.K., *et al.* (1989*b*). *Phys. Rev. Lett.*, **62**, 1425.

Gaisser, T.K., Halzen, F., Stanev, T. and Zas, E. (1990). *Phys. Lett.*, **B243**, 444.

Galbraith, W. (1958). *Extensive Air Showers*, Butterworth, London.

Galbraith, W. and Jelley, J.V. (1953). *Nature*, **171**, 349.

Galbraith, W. and Jelley, J.V. (1955). *J. Atmos. Terr. Phys.*, **6**, 250.

Galper, A.M., Kirillov-Ugryumov, V.G., Kurochkin, A.V., Leikov, P.G., Luchkov, B.I., Urkin, U.L., Fomin, V.P., Neshpor, Y.I., Stepanian, A.A. and Vladimirsky, B.M. (1977). *Proc. 15th Int. Cosmic Ray Conf.*, Plovdiv, **1**, 131.

Giacconi, R., Gorenstein, P., Gursky, H. and Waters, J.R. (1967). *Astrophys. J. Lett.*, **148**, L119.

Gibson, A.I., Harrison, A.B., Kirkman, I.W., Lotts, A.P., Macrae, J.H., Orford, K.J., Turver, K.E. and Walmsley, M.S. (1982*a*). *Proc. Int. Workshop on Very High Energy Gamma Ray Astronomy*, Ootacamund (Ramana Murthy, P.V. and Weekes, T.C., eds), p. 97, Tata Inst. of Fundamental Research, Bombay.

Gibson, A.I., Harrison, A.B., Kirkman, I.W., Lotts, A.P., Macrae, J.H., Orford, K.J., Turver, K.E. and Walmsley, M. (1982*b*). *Nature*, **296**, 833.

Gillanders, G.H., Byrne, M.P., Fegan, D.J., Mackeown, P.K. and Weekes, T.C. (1990). *Proc. 21st Int. Cosmic Ray Conf.*, Adelaide, **2**, 23.

Ginzburg, V.L. and Syrovatskii, S.I. (1964). *The Origin of Cosmic Rays*, Pergamon Press, New York.

Goldreich, P. and Julian, W.H. (1969). *Astrophys. J.*, **157**, 869.

Goodman, J.A. (1990). *Nucl. Phys. B (Proc. Suppl.)*, **14A**, 84.

Gorham, P.W. and Learned, J.G. (1986). *Nature*, **323**, 422.

Gould, R.J. and Burbidge, G.R. (1965). *Ann. d'Astrophys.*, **28**, 171.

Gregory, A.A., Patterson, J.R., Roberts, M.D., Smith, N.I. and Thornton, G.J. (1990). *Astron. Astrophys.*, **237**, L5.

Greisen, K. (1960). *Ann. Rev. Nucl. Sci.*, **10**, 63.

Grindlay, J.E. (1971). *S.A.O. Special Report 334*, Smithsonian Astrophysical Observatory, USA.

Grindlay, J.E. (1982). *Proc. Int. Workshop on Very High Energy Gamma Ray Astronomy*, Ootacamund (Ramana Murthy, P.V. and Weekes, T.C., eds), p. 257, Tata Inst. of Fundamental Research, Bombay.

Grindlay, J.E., Helmken, H.F., Hanbury Brown, R., Davis, J. and Allen, L.R. (1975*a*). *Astrophys. J. Lett.*, **197**, L9.

Grindlay, J.E., Helmken, H.F., Hanbury Brown, R., Davis, J. and Allen, L.R. (1975*b*). *Astrophys. J.*, **201**, 82.

Grindlay, J.E., Helmken, H.F. and Weekes, T.C. (1976). *Astrophys. J.*, **209**, 592.

Gunn, J.E. and Ostriker, J.P. (1969). *Nature*, **221**, 454.

Gupta, S.K., Ramana Murthy, P.V., Sreekantan, B.V. and Tonwar, S.C. (1978). *Astrophys. J.*, **221**, 268.

Gupta, S.K., *et al.* (1990). *Astrophys. J. Lett.*, **354**, L13.

Gupta, S.K., *et al.* (1991*a*). *Astron. Astrophys.*, **241**, L21.

Gupta, S.K., *et al.* (1991*b*). *Astron. Astrophys.*, **245**, 141.

Halzen, F., Hikasa, K. and Stanev, T. (1986). *Phys. Rev.*, **D34**, 2061.
Helmken, H.F. and Weekes, T.C. (1979). *Astrophys. J.*, **228**, 531.
Hermsen, W., Benett, K., Bloemen, J.B.G.M., Buccheri, R., Jamsen, F.A., Mastichiadis, A., Mayer Hersselwander, H.A., Ozel, M.E., Pollock, A.M.T. and Strong, A.W. (1987). *Astron. Astrophys.*, **175**, 141.
Hewish, A., Bell, S.J., Pilkington, J.D.H., Scott, P.F. and Collins, R.A. (1968). *Nature*, **217**, 709.
Hillas, A.M. (1984). *Nature*, **312**, 50.
Hillas, A.M. (1985). *Proc. 19th Int. Cosmic Ray Conf.*, La Jolla, **3**, 445.
Hillas, A.M. (1987). *Proc. 20th Int. Cosmic Ray Conf.*, Moscow, **2**, 362.
Hillier, R.R., Jackson, W.R., Murray, A., Redfern, R.M. and Sale, R.G. (1970). *Astrophys. J.*, **206**, 282.
Hinata, S. (1977). *Astrophys. J.*, **216**, 101.
Jelley, J.V. (1967). *Prog. Elementary Particles and Cosmic Ray Physics* (Wilson, J.G. and Wouthuysen, S.A., eds), vol. 9, p. 41, North Holland Publishing Co., Amsterdam.
Jelley, J.V. and Porter, N.A. (1963). *Quart. J. Roy. Astron. Soc.*, **4**, 275.
Jones, L.W. (1990). *Proc. 21st Int. Cosmic Ray Conf.*, Adelaide, **2**, 75.
Kakimoto, F., *et al.* (1990). *Proc. 21st Int. Cosmic Ray Conf.*, Adelaide, **2**, 358.
Kanbach, G., Bennett, K., Bignami, G.F., Buccheri, R., Caraveo, P., D'Amico, N., Hermsen, W., Lichti, G.G., Masnou, J.L., Mayer-Hasselwander, H.A., Paul, J.A., Sacco, B., Swanenburg, B.N. and Wills, R.D. (1980). *Astron. Astrophys.*, **90**, 163.
Kaneko, T., *et al.* (1990). *Proc. 21st Int. Cosmic Ray Conf.*, Adelaide, **2**, 205.
Kaul, R.K., *et al.* (1989). *J. Phys. G*, **15**, 1333.
Kibble, T.W.B. (1976). *J. Phys.*, **A9**, 1387.
Kifune, T., *et al.* (1986). *Astrophys. J.*, **301**, 230.
Ko, S., Loh, E.C., Salamon, M.H., Sokolsky, P. and Sommers, P. (1990). *Proc. 21st Int. Cosmic Ray Conf.*, Adelaide, **2**, 131.
Lamb, R.C., Fichtel, C.E., Hartman, R.C., Kniffen, D.A. and Thompson, D.J. (1977). *Astrophys. J. Lett.*, **212**, L63.
Lamb, R.C., Godfrey, C.P., Wheaton, W.A. and Turner, T. (1982). *Nature*, **296**, 543.
Lamb, R.C., *et al.* (1988). *Astrophys. J. Lett.*, **328**, L13.
Lamb, R.C., *et al.* (1991). AIP Conf. Proc. 220 (Matthews, J., ed.), p. 47, AIP Press, New York.
Lawrence, M.A., *et al.* (1989). *Phys. Rev. Lett.*, **63**, 1121.
Lawrence, M.A., *et al.* (1990). *Proc. 21st Int. Cosmic Ray Conf.*, Adelaide, **2**, 67.
Leahy, D.A., Elsner, R.F. and Weisskopf, M.C. (1983). *Astrophys. J.*, **272**, 256.
Lewis, D.A. (1989). *Astron. Astrophys.*, **219**, 352.
Lewis, D.A., Cawley, M.F., Fegan, D.J., Hillas, A.M., Kwok, P.W., Lamb, R.C., McComb, D.J., Porter, N.A., Reynolds, P.T., Vancanti, G. and Weekes, T.C. (1988). *Proc. Workshop on Frontier Objects in Astrophysics and Particle Physics*, Volcano, USA.
Lewis, D.A., Lamb, R.C. and Biller, S.D. (1991). *Astrophys. J.*, **369**, 479.
Lichti, G.G., Buccheri, R., Caraveo, P., Gerardi, G., Hermsen, W., Kanbach, G., Masnou, J.L., Mayer-Hasselwander, H.A., Paul, J.A., Swanenburg, B.N. and Wills, R.D. (1980). In *Advances in Space Exploration* (Cowsik, R. and Wills, R.D., eds), vol. 7, p. 49, Pergamon Press, Oxford.
Lloyd-Evans, J., Coy, R.N., Lambert, A., Lapikens, J., Patel, M., Reid, R.J.O. and Watson, A.A. (1983*a*). *Nature*, **305**, 784.
Lloyd-Evans, J., Coy, R.N., Lambert, A., Lapikens, J., Patel, M., Reid, R.J.O. and Watson, A.A. (1983*b*). *Proc. 18th Int. Cosmic Ray Conf.*, Bangalore, **9**, 65.

Long, C.D., McBreen, B., Porter, N.A. and Weekes, T.C. (1965). *Proc. 9th Int. Cosmic Ray Conf.*, London, **1**, 318.
Lyne, A.G. (1987). *Nature*, **326**, 569.
Macomb, D.J., *et al.* (1991). *Astrophys. J.*, **376**, 738.
Manchester, R.N. and Taylor, J.H. (1977). *Pulsars*, p. 184, W.H. Freeman and Co., San Francisco.
Mardia, K.V. (1972). *Statistics of Directional Data*, Academic Press, New York.
Marshak, M.L., *et al.* (1985). *Phys. Rev. Lett.*, **55**, 1965.
Massaro, E. and Salvati, M. (1979). *Astron. Astrophys.*, **71**, 51.
Matano, T., *et al.* (1990). *Proc. 21st Int. Cosmic Ray Conf.*, Adelaide, **2**, 266.
Matthews, J., ed. (1991). AIP Conf. Proc. 220, AIP Press, New York.
Matthews, J., *et al.* (1992). *Astrophys. J.* In press.
Michel, F.C. (1982). *Rev. Mod. Phys.*, **54**, 1.
Milgrom, M. and Pines, D. (1978). *Astrophys. J.*, **220**, 272.
Mukanov, J.B. (1983). *Izv. Krimskol Astrophys. Observ.*, **67**, 55.
Muraki, Y., Shibata, S., Aoki, T., Mitsui, K., Okada, A., Ohashi, Y., Kobayakawa, K., Kojima, H., Kitamura, T., Kato, Y., Takahashi, T. and Nakamura, I. (1991). *Astrophys. J.*, **373**, 657.
Nagle, D.E., Gaisser, T.K. and Protheroe, R.J. (1988). *Ann. Rev. Nucl. Part. Sci.*, **38**, 609.
Neshpor, Y.I., Stepanian, A.A., Fomin, V.P., Gerasimov, S.A., Vladimirsky, B.M. and Ziskin, Y.L. (1979). *Astrophys. Space Sci.*, **61**, 349.
Nishimura, J. and Kamata, K. (1952). *Prog. Theor. Phys.*, **7**, 185.
North, A.R., Raubenheimer, B.C., De Jaeger, O.C., van Tonder, A.J. and van Urk, G. (1987). *Nature*, **326**, 567.
North, A.R., *et al.* (1990). *Proc. 21st Int. Cosmic Ray Conf.*, Adelaide, **2**, 275.
Ochs, W. and Stodolsky, L. (1986). *Phys. Rev.*, **D33**, 1247.
Ostriker, J.P. (1972). In *The Physics of Pulsars* (Lenchek, A.M., ed.), p. 159, Gordon and Breach, New York.
Ostriker, J.P., Thompson, C. and Witten, E. (1986). *Phys. Lett. B*, **180**, 231.
Oyama, Y., Arisaka, K., Kajita, T., Koshiba, M., Nakahata, M., Suzuki, A., Takita, M., Totsuka, Y., Kifune, T., Suda, T., Sato, N., Takahashi, K. and Myno, K. (1986). *Phys. Rev. Lett.*, **56**, 991.
Page, D.N. and Hawking, S.W. (1976). *Astrophys. J.*, **206**, 1.
Parsignault, D.R., Schreier, E., Grindlay, J. and Gursky, H. (1976). *Astrophys. J. Lett.*, **209**, L73.
Porter, N.A. (1983). *Proc. 18th Int. Cosmic Ray Conf.*, Bangalore, **12**, 435.
Porter, N.A. and Weekes, T.C. (1978). *S.A.O. Special Report 381*, Smithsonian Astrophysical Observatory, USA.
Porter, N.A. and Weekes, T.C. (1979). *Nature*, **277**, 199.
Protheroe, R.J. (1985*a*). *Proc. Workshop on Techniques in UHEGR Astronomy*, La Jolla (Protheroe, R.J. and Stephens, S.A., eds), p. 91, Dept. of Physics, University of Adelaide, Australia.
Protheroe, R.J. (1985*b*). *Astron. Express*, **1**, 33.
Protheroe, R.J. (1987). *Proc. 20th Int. Cosmic Ray Conf.*, Moscow, **8**, 21.
Protheroe, R.J. and Clay, R.W. (1985). *Nature*, **315**, 205.
Protheroe, R.J., Clay, R.W. and Gerhardy, P.R. (1984). *Astrophys. J. Lett.*, **280**, L47.
Ramana Murthy, P.V. (1980). *Non-Solar Gamma-Rays (COSPAR)* (Cowsik, R. and Wills, R.D., eds), p. 71, Pergamon Press, Oxford.

Ramana Murthy, P.V. (1987). *Very High Energy Gamma Ray Astronomy* (Turver, K.E., ed.), p. 39, Reidel, Dordrecht.
Ramana Murthy, P.V. (1990). *Nucl. Phys. B (Proc. Suppl.)*, **14A**, 73.
Ramana Murthy, P.V. and Weekes, T.C., eds. (1982). *Proc. Int. Workshop on Very High Energy Gamma Ray Astronomy*, Ootacamund, Tata Inst. of Fundamental Research, Bombay.
Rana, N.C., Sadzinska, M., Wdowczyk, J. and Wolfendale, A.W. (1984). *Astron. Astrophys.*, **141**, 394.
Raubenheimer, B.C., *et al.* (1988). *Astron. Astrophys.*, **193**, L11.
Raubenheimer, B.C., North, A.R., De Jaeger, O.C. and Nel, H.I. (1989). *Astrophys. J.*, **336**, 394.
Resvanis, L., *et al.* (1987*a*). *Very High Energy Gamma Ray Astronomy* (Turver, K.E., ed.), p. 105, Reidel, Dordrecht.
Resvanis, L., *et al.* (1987*b*). *Very High Energy Gamma Ray Astronomy* (Turver, K.E., ed.), p. 135, Reidel, Dordrecht.
Resvanis, L.K., *et al.* (1988). *Astrophys. J. Lett.*, **328**, L9.
Reynolds, P.T., *et al.* (1987). *Very High Energy Gamma Ray Astronomy* (Turver, K.E., ed.), p. 169, Reidel, Dordrecht.
Reynolds, P.T., *et al.* (1990). *Proc. 21st Int. Cosmic Ray Conf.*, Adelaide, **2**, 383.
Reynolds, P.T., *et al.* (1991). *Astrophys. J.*, **382**, 640.
Rieke, G.H. and Weekes, T.C. (1969). *Astrophys. J.*, **155**, 429.
Rosenberg, L.J. (1991). AIP Conf. Proc. 220 (Matthews, J., ed.), p. 220, AIP Press, New York.
Ruderman, M.A. and Sutherland, P.G. (1975). *Astrophys. J.*, **196**, 51.
Samorski, M. (1992). *Proc. 22nd Int. Cosmic Ray Conf.*, Dublin. In press.
Samorski, M. and Stamm, W. (1983*a*). *Astrophys. J. Lett.*, **268**, L17.
Samorski, M. and Stamm, W. (1983*b*). *Proc. 18th Int. Cosmic Ray Conf.*, Bangalore, **1**, 135.
Samorski, M. and Stamm, W. (1983*c*). *Proc. 18th Int. Cosmic Ray Conf.*, Bangalore, **11**, 244.
Samorski, M. and Stamm, W. (1985). *Proc. Workshop on Techniques in UHEGR Astronomy*, La Jolla (Protheroe, R.J. and Stephens, S.A., eds), p. 85, Dept. of Physics, University of Adelaide, Australia.
Shabad, A.E. and Usov, V.V. (1982). *Nature*, **295**, 215.
Shklovskii, I.S. (1953). *Dokl. Akad. Nauk SSR*, **90**, 983.
Sinha, S., *et al.* (1990). *Proc. 21st Int. Cosmic Ray Conf.*, Adelaide, **2**, 370.
Slane, P. and Fry, W.F. (1989). *Astrophys. J.*, **342**, 1129.
Smith, F.G. (1977). *Pulsars*, Cambridge University Press.
Staelin, D.H. and Reifenstein, E.C. (1968). *Science*, **162**, 1481.
Stamm, W. and Samorski, M. (1983). *Proc. 18th Int. Cosmic Ray Conf.*, Bangalore, **1**, 131.
Stanev, T. and Vankov, Ch.P. (1985). *Phys. Lett.*, **158B**, 75.
Stanev, T., Gaisser, T.K. and Halzen, F. (1985). *Phys. Rev.*, **D32**, 1244.
Stecker, F.W. (1971). *Cosmic Gamma Rays*, NASA Publication SP 249, USA.
Stepanian, A.A. (1982). *Astrophys. & Space Sci.*, **84**, 347.
Stepanian, A.A., Fomin, V.P., Neshpor, Y.I., Vladimirsky, B.M. and Zyskin, Y.L. (1982). *Proc. Int. Workshop on Very High Energy Gamma Ray Astronomy*, Ootacamund (Ramana Murthy, P.V. and Weekes, T.C.), p. 43, Tata Inst. of Fundamental Research, Bombay.
Stephens, S.A. and Verma, R.P. (1984). *Nature*, **308**, 828.
Sturrock, P.A. (1971). *Astrophys. J.*, **164**, 529.

Suga, K., *et al.* (1987). *Proc. 20th Int. Cosmic Ray Conf.*, Moscow, **1**, 277.
Sunyaev, R., *et al.* (1990). *Proc. 21st Int. Cosmic Ray Conf.*, Adelaide, **12**, 39.
Swanenburg, B.N., Bennett, K., Bignami, G.F., Buccheri, R., Caraveo, P., Hermsen, W., Kanbach, G., Lichti, G.G., Masnou, J.L., Mayer-Hasselwander, H.A., Paul, J.A., Sacco, B., Scarsi, L. and Wills, R.D. (1981). *Astrophys. J. Lett.*, **243**, L69.
Tanaka, Y. (1989). In *Physics of Neutron Stars and Black Holes* (Tanaka, Y., ed.), p. 431, Universal Academy Press, Tokyo.
Tanimori, T. (1990). *Nucl. Phys. B (Proc. Suppl.)*, **14A**, 183.
Tannanbaum, H., *et al.* (1972). *Astrophys. J. Lett.*, **174**, L143.
Teshima, M., Nagano, M., Hara, T., Hayashida, N., Honda, M., Kamata, K., Kifune, T. and Ohoka, H. (1990). *Phys. Rev. Lett.*, **64**, 1628.
Tonwar, S.C., *et al.* (1988). *Astrophys. J. Lett.*, **330**, L107.
Tonwar, S.C., *et al.* (1990). *Nucl. Phys. B (Proc. Suppl.)*, **14A**, 226.
Trumper, J., *et al.* (1978). *Astrophys. J. Lett.*, **219**, L105.
Tumer, O.T., *et al.* (1985). *Proc. 19th Int. Cosmic Ray Conf.*, La Jolla, **1**, 139.
Tumer, O.T., Hammond, J.S., Zych, A.D. and MacCallum, C. (1990). *Nucl. Phys. B (Proc. Suppl.)*, **14A**, 176.
Turver, K.E., ed. (1987). *Very High Energy Gamma Ray Astronomy*, Reidel, Dordrecht.
Turver, K.E. and Weekes, T.C. (1978). *Nuovo Cim.*, **45B**, 99.
Vacanti, G., *et al.* (1990). *Proc. 21st Int. Cosmic Ray Conf.*, Adelaide, **2**, 329.
Vacanti, G., *et al.* (1991). *Astrophys. J.*, **377**, 467.
van der Klis, M. and Bonnet-Bidaud, J.M. (1981). *Astron. Astrophys.*, **95**, L5.
van der Klis, M. and Bonnet-Bidaud, J.M. (1989). *Astron. Astrophys.*, **214**, 203.
Vestrand, W.T. and Eichler, D. (1982). *Astrophys. J.*, **261**, 251.
Villenkin, A. (1988). *Nature*, **332**, 610.
Vishwanath, P.R. (1982). *Proc. Int. Workshop on Very High Energy Gamma Ray Astronomy*, Ootacamund (Ramana Murthy, P.V. and Weekes, T.C.), p. 21, Tata Inst. of Fundamental Research, Bombay.
Vishwanath, P.R., *et al.* (1989). *Astrophys. J.*, **342**, 489.
Vladimirsky, B.M., Stepanian, A.A. and Fomin, V.P. (1973). *Proc. 13th Int. Cosmic Ray Conf.*, Denver, **1**, 456.
Wdowczyk, J. (1965). *Proc. 9th Int. Cosmic Ray Conf.*, London, **2**, 691.
Wdowczyk, J. and Wolfendale, A.W. (1983). *Nature*, **305**, 609.
Wdowczyk, J. and Wolfendale, A.W. (1984). *J. Phys. G*, **10**, 1599.
Witten, E. (1985). *Nucl. Phys. B*, **249**, 557.
Weekes, T.C. (1988). *Phys. Reports*, **160**, 1–121.
Weekes, T.C. (1992). *Proc. 15th Texas Conf. on Relativistic Astrophysics* (Barrows, J. and Thomas, P., eds), Cambridge University Press.
Weekes, T.C. and Helmken, H.F. (1977). *Recent Adv. Gamma Ray Astron.*, ESA, Frascati, p. 39.
Weekes, T.C., Fazio, G.G., Helmken, H.F., O'Mongain, E.P. and Rieke, G.H. (1972). *Astrophys. J.*, **174**, 165.
Weekes, T.C., Helmken, H.F. and Grindlay, J.E. (1979). *Proc. 16th Int. Cosmic Ray Conf.*, Kyoto, **1**, 132.
Weekes, T.C., *et al.* (1989). *Astrophys. J.*, **342**, 379.
Yamada, Y., *et al.* (1988). *Prog. Theor. Phys.*, **79**, 416.

Yodh, G.B. (1989). *Cosmic Gamma Rays, Neutrinos and Related Astrophysics* (Shapiro, M.M. and Wefel, J.P., eds), p. 183, Kluwer Academic Publishers, Dordrecht.

Yodh, G.B., Wold, D.C. and Kropp, W.R., eds. (1990). *Nucl. Phys. B (Proc. Suppl.)*, **14A**.

Zyskin, Y.L. and Mukanov, D.B. (1983). *Proc. 18th Int. Cosmic Ray Conf.*, Bangalore, **1**, 122.

Index